HELMHOLTZ
Centre for Environmental Research

Lin Qian

Degradation of Perfluoroalkyl Acids using Zeolite

PHD DISSERTATION 12|2021
Helmholtz Centre for Environmental Research – UFZ
Department of Environmental Engineering

Degradation of Perfluoroalkyl Acids using Zeolites

Der Fakultät für Chemie und Mineralogie

der Universität Leipzig

vorgelegte

DISSERTATION

zur Erlangung des akademischen Grades

DOCTOR RERUM NATURALIUM

(Dr. rer. nat.)

von M. Sc. Lin Qian

geboren am 21.12.1990 in Shengzhou, China

Leipzig, den 30.03.2021

The present thesis was conducted in the period from January 2018 to March 2021 at the Department of Environmental Engineering, Helmholtz Centre for Environmental Research – UFZ under the supervision of Dr. Anett Georgi and Prof. Dr. Frank-Dieter Kopinke.

Bibliographic description

Lin Qian

Degradation of Perfluoroalkyl Acids using Zeolites

University of Leipzig, Doctoral Thesis

157 Pages, 62 Figures, 22 Tables, 229 References

Abstract

The present thesis is aiming at developing novel techniques for treating perfluoroalkyl acids (PFAAs) in water. It is a huge challenge to treat PFAAs in aqueous environment due to their low concentrations (ng L^{-1} to μg L^{-1}) and high resistance to biological and chemical degradation. To tackle this challenge, combining pre-enrichment and degradation processes can provide promising solutions. Three different pathways were studied in the present thesis to treat PFAAs after pre-enrichment on zeolites. A novel photochemical degradation approach of perfluorooctanoic acid (PFOA) under UV-A irradiation after adsorption on Fe-doped zeolites with molecular oxygen as the terminal oxidant has been established for the first time. Zeolite-bound iron species were proposed to offer catalytic sites for carboxylate-to-metal charge transfer activated by UV-A as initial step of PFOA degradation. The Fe-zeolite photocatalytic system was further applied for the even more resistant perfluorooctanesulfonic acid (PFOS). After adsorption on Fe-zeolite, UV-C irradiation was required to trigger its photochemical degradation and fully mineralize the short-chain byproducts after introduction of sodium persulfate. The activation of sodium persulfate can be alternatively achieved by heat to treat PFOA pre-loaded on BEA zeolites. A complete PFOA mineralization was realized in the presence of zeolites. The effects of reaction conditions, such as reaction pH and coexisting inorganic ions were investigated for all three established systems as well as the long-term stability. The Fe-zeolite photocatalytic system designed for PFOS and heat-activated persulfate/zeolite system for PFOA were successfully applied to real ground water samples containing trace-level PFAAs. These findings of the thesis provide efficient strategies for treatment of water containing highly recalcitrant trace amounts of PFAAs, which can inspire remediation techniques for water contaminated by other micropollutants as well.

Bibliographische Beschreibung

Lin Qian

Abbau von Perfluoralkylsäuren unter Verwendung von Zeolithen

Universität Leipzig, Dissertation

157 Seiten, 62 Abbildungen, 22 Tabellen, 229 Referenzen

Kurzreferat

Die vorliegende Arbeit zielt darauf ab, neuartige Techniken zur Entfernung von Perfluoralkylsäuren (PFAAs) aus Wasser zu entwickeln. Die Behandlung von PFAA-Kontaminationen in Wasser stellt aufgrund ihrer geringen Konzentrationen (ng l^{-1} bis µg l^{-1}) und ihrer hohen Resistenz gegenüber biologischem und chemischem Abbau eine große Herausforderung dar. Eine vielversprechende Lösung bietet die Kombination aus Voranreicherungs- und Abbauprozessen. In der vorliegenden Arbeit wurden drei verschiedene Wege zur Behandlung von PFAAs nach Adsorption in Zeolithen untersucht. Ein neuartiger photochemischer Ansatz zum Abbau von Perfluoroctansäure (PFOA) unter UV-A-Bestrahlung, nach Adsorption an Fe-dotierten Zeolithen, mit molekularem Sauerstoff als terminalem Oxidationsmittel wurde erstmals etabliert. Die vorliegenden Ergebnisse weisen darauf hin, dass Zeolith-gebundene Eisenspezies katalytische Zentren für den durch UV-A aktivierten Carboxylat-zu-Metall-Ladungstransfer bieten, welcher für den PFOA-Abbau verantwortlich ist. Des Weiteren wurde das photokatalytische System aus Fe-Zeolithen auch für die noch persistentere Perfluoroctansulfonsäure (PFOS) angewendet. Um den photochemischen Abbau nach der Adsorption an Fe-Zeolithen, zu initiieren, war eine UV-C-Bestrahlung erforderlich, sowie die Einführung von Natriumpersulfat, um die kurzkettigen Nebenprodukte vollständig zu mineralisieren. Die Aktivierung von Natriumpersulfat kann alternativ auch thermisch erreicht werden. Eine vollständige PFOA-Mineralisierung wurde in Gegenwart von Zeolithen realisiert. Die Auswirkungen der Reaktionsbedingungen, wie pH-Wert und vorliegende anorganische Ionen, wurden für alle drei etablierten Systeme untersucht, ebenso wie die Langzeitstabilität. Das für PFOS entwickelte Fe-Zeolith-Photokatalysatorsystem und das durch Hitze aktivierte Persulfat/Zeolith-System für PFOA wurden erfolgreich auf reale Grundwasserproben angewendet, die PFAAs im Spurenbereich enthielten. Die Ergebnisse dieser Arbeit liefern effiziente Strategien für die Behandlung von Wasser, das geringe Mengen von hochgradig persistenten PFAAs enthält, und können als Inspiration für Sanierungsverfahren für Wasser dienen, das auch mit anderen Mikroverunreinigungen kontaminiert ist.

Contents

1 Introduction

Water is essential for all life on earth. Only 2.5% of all water sources on earth can be regarded as freshwater, whose majority exists in form of ice and permanent snow and thus is not available for direct use. Currently, only 0.3% of freshwater is easily accessible by human beings [1]. With the development of production activity of humankind, industrial wastewater and sanitary sewage are discharged into natural water, causing serious environmental pollution. The discharged pollutants are ranged from traditional persistent organic pollutants (POPs), e.g., polychlorinated biphenyls (PCBs), to emerging contaminants in the categories of pesticides, pharmaceuticals, surfactants, and personal care products. Per- and polyfluoroalkyl substances (PFAS) are among the emerging POPs which have drawn much attention in last decades as they are frequently detected in groundwaters, sediments, animals and even human beings globally [2-4]. Recent studies show that the exposure of PFAS at certain levels may cause adverse effects on human health. Even though production and application of PFAS was currently restricted, the risk of human exposure due to accumulation in marine systems and contaminations in groundwater used for drinking water production will continue to exist for decades [5].

The PFAS are reported to slip through the wastewater treatment plants and end up in the treated water [2]. Treatment of PFAS in the environment is a huge challenge due to the following reasons. Firstly, the PFAS are resistant to most conventional reduction and oxidation processes as well as biological degradation due to the strong C-F bonds [6]. For instance, PFAS are practically inert to hydroxyl radicals as they do not contain C-H bonds available for H abstraction [7] so that many ·OH-based advanced oxidation strategies fail to degrade PFAS. Secondly, PFAS concentrations in the water bodies are rather low, i.e., usually at the ng L^{-1} to µg L^{-1} level [8]. Treating trace amount of PFAS in complex water matrices is particularly difficult. Thus, there is an urgent need for development of novel technologies which can i) enrich trace-level PFAS from complex water matrices; ii) degrade PFAS efficiently and cost-effectively.

Extensive research within the last two decades focused on various strategies for PFAS degradation which in general require harsh conditions. Reductive degradation has been investigated for PFAS treatment in recent years. During various reductive processes, active reducing species are typically yielded, e.g., hydrated electrons from UV photolysis of iodide, sulfite, and indole acetic acid [9]. The hydrated electrons can directly interact with C-F bonds yielding fluoride ions. Electrochemical degradation is another technique for PFAS treatment receiving growing research interest recently, in which PFAS can be directly oxidized on various types of anodes [10, 11]. These PFAS degradation technologies can fully or partially degrade PFAS within acceptable time, showing promising results. Nevertheless, such technologies still face certain practical limitations: i) relatively high energy demands and/or operation costs; ii) low space-time yield, in particular for low concentrations in large water fluxes.

The proper materials assisting PFAS treatment should: i) possess high adsorption affinity towards PFAS to effectively enrich it from complex water matrix; ii) be stable during a regeneration process and allow *in-situ* PFAS degradation. For instance, activated carbon and carbon nanotubes are typical adsorbents used in PFAS treatment [12, 13]. Yet the stability of carbon-based adsorbents remains uncertain during various degradation/regeneration processes, e.g., hydrated electron-based reductive processes, activated persulfate processes, and electrochemical processes. Except carbon-based material, zeolites, i.e., microporous minerals with certain framework structures, are also commonly applied as adsorbents and/or catalysts. In recent years, zeolites are frequently being utilized in wastewater treatment, e.g., for adsorptive removal of PFAS. But the catalytic properties of certain types of zeolite for PFAS degradation have not yet been investigated.

Perfluoroalkyl acids (PFAAs) are a subgroup of PFAS. PFAAs such as perfluorooctanoic acid (PFOA) and perfluorooctanesulfonic acid (PFOS) draw much attention recently as they were frequently detected in the environment. The present thesis is aiming at contributing to the field of PFAAs removal/degradation techniques based on trap & treat principle. We use zeolite as both adsorbent and catalyst, which opens the design of novel approaches for PFAAs treatment. A feasible process scheme typically consists of the following steps: in the first step, PFAAs is removed from water by adsorption to zeolite fixed bed or dispersed zeolite that can then be separated by microfiltration. In the second step, the loaded zeolite particles can be regenerated *in situ* by various techniques: UV-A / UV-C irradiation for PFOA and PFOS degradation (Fe-zeolite); Heat-activated persulfate for PFOA degradation (Beta zeolite). Overall, a combination of PFAAs adsorptive enrichment and degradation by applying related types of zeolite can be realized, which is promising for the treatment of this highly recalcitrant trace level contaminant.

2 Background

2.1 Introduction to PFAAs

PFAAs are emerging persistent organic pollutants (POPs), which have drawn much attention in last decades as they are reported to be not eliminated in wastewater treatment plants [14]. The increasing interests in PFAAs in the environment can be seen from the number of published papers from 1997 to 2020 provided by Web of Science index in Figure 1.

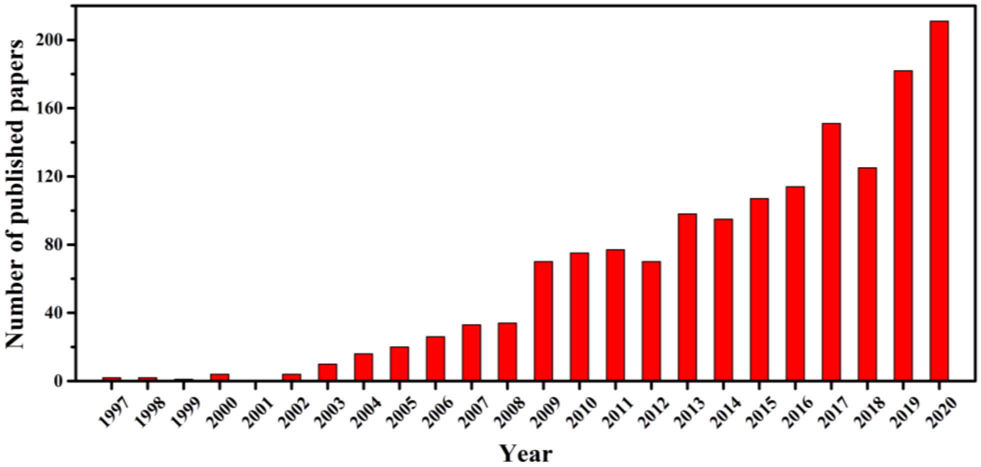

Figure 1. Number of published papers by searching key words “environmental” and “perfluorinated” in Web of Science (01.02.2021).

PFAAs are a family of synthetic chemicals, initially developed by the 3M Company. One characteristic of PFAAs is that all of hydrogen atoms in PFAAs are replaced by fluorine atoms. The common chemical state of fluorine in the environment is in metal salts, e.g., cryolite (Na_2AlF_6), fluorspar (CaF_2), and fluorapatite ($Ca_5F(PO_4)_3$) [15] or in dissolved state as fluoride (F^-). The natural fluorination of hydrocarbons rarely happens in the environment, as the formation of carbon fluorine bonds in biological systems needs extremely high energy input. Hence, all the PFAAs and other organic chemicals found in the environment that contain carbon fluorine bonds are of anthropogenic origin [16].

The carbon fluorine bond has a high bond energy and polarity. In addition, the carbon fluorine bond is getting stronger with the increasing fluorination degree as shown in Table 1 [13]. When all the hydrogen atoms are replaced by fluorine atoms in the hydrocarbon, these carbon fluorine bonds will contribute to the high chemical and thermal stabilities of molecules.

Table 1. Carbon fluorine bond length and strength in various fluorocarbon structures [13].

	Bond Length (Å)	**Bond Strength (kJ mol^{-1})**
H_3C-H	1.11	422
H_3C-F	1.385	448
H_2FC-F	1.358	458
HF_2C-F	1.332	479
F_3C-F	1.317	485

The molecular weight, boiling point, heat of vaporization, and surface tension comparison of perfluoroalkane with its hydrocarbon alkane is shown in Table 2 [13]. Fluorine has a small atomic van der Waal radius (1.35 Å), a high ionization potential (1680 kJ mol^{-1}), and low polarizability, which leads to weak inter- and intramolecular interaction [13]. This explains the low boiling points of perfluoroalkanes relative to their molecular weights, and their low refractive indexes as well as low surface tensions.

Table 2. Physical properties of n-perfluorooctane compared to n-octane [13].

	C_8F_{18}	**C_8H_{18}**
Molecular weight (g mol^{-1})	438	114
Boiling point (°C)	97	125
Heat of vaporization (kJ kg^{-1})	84	363
Refractive index (n_D^{20})	1.280	1.398
Surface tension (mN m^{-1})	15	22

Usually, PFAAs contain one or several functional groups connected to the fluorocarbon chain according to their applications. This functional group commonly mediates a certain water solubility of the compound. For instance, in the perfluorooctanoic acid (PFOA) a reactive, charged and hydrophilic carboxylic headgroup provides the molecule the desired application properties [17].

2.1.1 Introduction to PFOA and PFOS

Perfluorooctanoic acid (PFOA) and perfluorooctane sulfonate (PFOS) are two representative PFAAs which have been extensively detected in the environment among various kinds of PFAAs.

Some physical and chemical properties of PFOA and PFOS are presented in Table 3. Note, that free acids are usually not met in aqueous environments. The properties of the corresponding anions are more relevant.

Table 3. Some physical and chemical properties of PFOA and PFOS [18-21].

	PFOA	**PFOS**
CAS number	335-67-1	1763-23-1
Chemical formula	$C_8HF_{15}O_2$	$C_8HF_{17}O_3S$
Molecule weight (g mol^{-1})	414.07	500.13
Structure	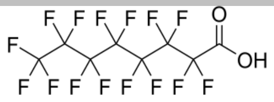	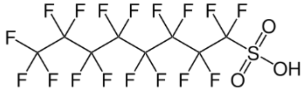
Solubility in water at 25°C (mg L^{-1})	3400	570 (potassium salt)
Melting point (°C)	54.3	54
Boiling point (°C)	192	258 – 260
pK_a	-0.5	-6.0 – -2.6
Vapor pressure at 25°C (mm Hg)	0.526	0.002
Critical micelle concentration (M)	$10^{-2.04}$	$10^{-2.97}$

There are two main industrial production processes used for synthesizing PFOA and PFOS, i.e., electrochemical fluorination and telomerization. The electrochemical fluorination process has been applied for synthesizing perfluorinated compounds (PFCs) since the 1960s [22]. The electrochemical fluorination process produces a mixture of branched and linear isomers. For instance, an organic raw material (e.g., $C_8H_{17}SO_2F$) will go through electrolysis in anhydrous HF, which leads to the replacement of all the hydrogen atoms by fluorine atoms. The radical nature of the process results in the breakage of carbon chains and their rearrangement, which leads to the production of a mixture of branched and linear isomers [23]. The proportion of branched to linear carbon chains during the electrochemical fluorination depends on the introduced chemicals and processes conditions. For PFOA and PFOS, the average content of branched isomers is 20% to 30% [24]. Dupont firstly applied telomerization method into production of PFOA [25]. The PFOA produced by the telomerization process is almost completely linear. Because the telomerization method is able to produce more pure linear products than electrochemical fluorination, it has been used for producing reagent and analytical grade of PFOA and PFOS standards.

Historically, PFOA, PFOS and their related substances have been extensively used in the manufacture of various industrial and commercial products, such as fire-fighting foams, paper and packing protective coatings, leather, carpets, inert surfactants, household cleaning products, pesticides, insecticides, thermally stable lubricants etc. [26, 27].

2.1.2 Distribution of PFOA and PFOS

The overall estimated historical worldwide production of perfluorooctane sulfonyl fluoride (POSF), an intermediate for PFOS production, was 96,000 – 122,500 tons from 1970 to 2002. The estimated release is about 45,250 tons POSF to the environment globally from direct (production and consumer products) and indirect sources (precursors and impurities) between 1970 – 2012 [28]. Although 3M had ceased the production of POSF in 2002 and a reduction has been observed in some compartments, the remaining sectors where POSF and its related substances are still used, e.g., existing fire-fighting foam stock, photolithography and semiconductors, and hydraulic fluids and metal plating [29]. The future environmental exposure is determined by emission routes and transportation. The PFOA and PFOS are two predominant PFAAs representatives which are frequently detected in the environment. The properties of PFOA and PFOS, e.g., low vapor pressure and high water solubility, indicate that they are present dominantly in the hydrosphere, e.g., oceans, lakes, rivers, groundwater and related sediments [30]. A global survey of PFAAs concentrations in oceans showed that PFOA and PFOS are the predominant PFAAs contaminants at the surface and deep (4000 – 4400 m) water in Pacific and Atlantic Oceans, with a concentration range of 15 – 192,000 pg L^{-1} for PFOA and 1.1 – 57,000 pg L^{-1} for PFOS [8]. The total PFOA inventory in ocean water is estimated to be in the range of 110 to 10,000 tons [31]. For PFOS the range is 235 to 1,770 tons [28]. From a global distribution model, the estimated total inventory of perfluorooctanoate (PFO) were 4 – 800 tons in freshwater and 3 – 340 tons in sediments [31, 32].

2.1.3 Bioaccumulation and toxicity of PFOA and PFOS

More and more studies suggest that PFOA and PFOS can bioaccumulate in food chains, they are commonly found in the tissues of wild animals all over the world, indicating the bioaccumulation of PFOA and PFOS occurs globally. As far as in the North Pacific Ocean, the

PFOA and PFOS were detected from the blood sera samples from seals, Laysan and black footed albatrosses [33]. The PFOA and PFOS can be related or contacted with living organisms through many pathways. But the clearances of PFOA and PFOS were reported to be almost negligible in humans [34]. According to investigation on retired fluorochemical production workers, the elimination half-lives in serum were 3.5 years for PFOA and 4.8 years for PFOS, respectively [35]. Several studies suggest that the exposure to PFOA and PFOS over certain levels may result in harmful health effects in humans and animals, i.e., liver and kidney toxicity, cardiotoxicity, reproductive toxicity and neurotoxicity [36-39].

2.2 Strategies for PFAAs treatment

Most wastewater plants are not designed to process PFAAs. As a consequence, any PFAAs that come into the wastewater plant usually end up in the treated water through the plant. PFAAs are resistant to most conventional oxidation and reduction processes due to the strong C-F bonds. For instance, it is practically inert to hydroxyl radicals because PFAAs do not contain C-H bonds available for H abstraction. Recently, several PFAAs removal/degradation technologies have been reported, including adsorption, hydrated electron-based degradation, sulfate radical-based degradation, electrochemical degradation, photochemical and photocatalytic degradation [40].

2.2.1 Adsorption

Adsorption is one of the most important wastewater treatment techniques which has been widely used for removing various kinds of pollutants from water over the last decades. The most widely applied adsorbents at technical scale for PFAAs treatment are activated carbon and ion-exchange resins.

Ochoa-Herrera et al. [41] evaluated different adsorbents towards PFOS, i.e., active carbon, high-silica zeolite NaY, anaerobic sludge. Active carbon showed the highest adsorption affinity to PFOS among these adsorbents. In addition, they investigated the adsorption of PFOS, PFOA and perfluorobutanesulfonate (PFBS) on activated carbon. They found the adsorption affinity of PFOS onto activated carbon was stronger than PFOA and PFBS, which indicated the substitution of sulfonic group by carboxylic group and decreasing fluorocarbon chain length led to a weaker adsorption of the PFCs on activated carbon. Saeidi et al. [13] investigated the adsorption of PFOA and PFOS on activated carbon felts (ACFs). They found the particularly high adsorption affinity of surface-defunctionalized ACF towards PFAAs due to the joint effect of hydrophobic interactions and electrostatic attraction between positively charged adsorbent surface sites and PFAAs anions. They claimed PFAAs adsorption behaviors on various ACFs were significantly affected by the surface chemistry of ACFs in terms of their anion/cation exchange capacity, point of zero net proton charge and oxygen content.

The adsorption technique is widely used for treatment of wastewater. It benefits from its simple facilities, easy operation, and cost-effectiveness. However, the pollutants enriched solids after adsorption are produced and needed to be further treated. Taking the activated carbon as an example, the common way to treat the exhausted activated carbon is incineration at high temperature. That is, extra efforts are needed after adsorption step, and attention should be paid for a secondary pollution during these treatments.

2.2.2 Reductive degradation with hydrated electrons

Reductive degradation has been investigated for wastewater treatment in recent years. The characteristics of reductive processes are yielding active reducing species, i.e., hydrated electrons and hydrogen atoms, when combing with certain activation methods e.g., UV light, ultrasound, and electron beam irradiation in presence of certain reducing reagents such as iodide, sulfite, and indole acetic acid. Because the produced active reducing species, e.g., hydrated electrons, are able to donate an unpaired electron to the target compound and reduce it chemically, the reductive degradation processes are particularly promising towards certain hardly degradable contaminants in water, e.g., chlorinated and fluorinated organic compounds, and inorganic pollutants (bromate and perchlorate).

Park et al. [42] investigated the PFOA and PFOS degradation by iodide photolysis under UV-C irradiation. The photolysis of iodide under UV-C irradiation produces iodine radical and hydrated electron (eq.1).

$$I^- + h\upsilon \longrightarrow I\cdot + e^-_{aq} \qquad (1)$$

The degradation kinetics of PFOA and PFOS were found dependent on perfluorocarbon chain length, headgroups, iodide concentration, and initial PFOA and PFOS concentration, but not affected by pH. One limitation of iodide-mediated hydrated electron generation by photolysis is that the produced hydrated electrons will be scavenged by the intermediates triiodide.

Besides iodide, sulfite was also used as a reductant to generate hydrated electrons upon photolysis (eq.2).

$$SO_3^{2-} + h\upsilon \xrightarrow{\qquad} SO_3^{-}\cdot + e_{aq}^{-} \qquad (2)$$

Bentel et al. [43] studied the structure-reactivity relationships with 34 typical PFAS with hydrated electrons generated by UV irradiation of sodium sulfite. They found the perfluorinated carboxylic acids (PFCAs) with different perfluorocarbon chain length (from 2 to 10 carbon numbers) showed a similar degradation and defluorination rate. In contrast, the perfluorinated sulfonic acids (PFSAs) exhibited an apparent relationship between reactivity and chain length. Combining with theoretical calculations on carbon fluorine bond dissociation energies, they found several reaction pathways of PFAS degradation caused by hydrated electrons. They are: H/F exchange, terminal function group dissociation, HF elimination and hydrolysis triggered by decarboxylation. Huang et al. [44] reported the reactivity of hydrated electrons towards a series of perfluorinated carboxylates by laser flash photolysis. At ionic strength of 0.01 M $NaClO_4$, the second-order rate constants for the reactions of hydrated electrons with PFOA, perfluorobutanoic acid (PFBA) and trifluoroacetic acid (TFA) were estimated to be $(1.7 \pm 0.5) \times 10^7\ M^{-1}s^{-1}$, $(8.8 \pm 0.2) \times 10^6\ M^{-1}s^{-1}$ and $(2.3 \pm 0.2) \times 10^6\ M^{-1}s^{-1}$, respectively. The rate constant appeared to increase with the increasing fluorocarbon chain lengths. In addition, the second-order rate constants for hydrated electrons with PFOS (in the form of tetraethylammonium salt) was reported to be $7.3 \times 10^7\ M^{-1}s^{-1}$ [45]. However, hydrated electrons can easily be quenched by some coexisted scavengers in wastewater as shown in Table 4. Therefore, great care must be paid to these coexisted scavengers before applying hydrated electron-based treatment into PFAAs degradation.

Reduction degradation processes that utilize hydrated electrons for efficient PFAAs degradation and defluorination have been investigated and proved. Nevertheless, most researchers conducted their experiments in artificially simulated water. These processes usually require certain conditions, e.g., Milli-Q or deionized water, alkaline pH, anaerobic environment, and high reagent dosages. Considering the high reactivity of hydrated electrons towards some coexisted scavengers in wastewater, the effectiveness and efficiency of hydrated electron-based processes for PFAAs treatment in natural water matrices still need to be evaluated.

Table 4. Rate constants for reaction of hydrated electrons with some solutes [46, 47].

solute	k ($M^{-1} s^{-1}$)
H^+	$(2.4 \pm 0.2) \times 10^{10}$
$\cdot OH$	$\sim 3 \times 10^{10}$
CO_2	$(7.7 \pm 1.1) \times 10^9$
O_2	$(1.9 \pm 0.2) \times 10^{10}$
NO_3^-	$(1.1 \pm 0.1) \times 10^{10}$
Cl^-	$<10^6$
SO_4^{2-}	$<10^6$
CO_3^{2-}	$<10^6$

2.2.3 Oxidative degradation with sulfate radicals

Sulfate radical-based advanced oxidation processes (AOPs) have been successfully used in wastewater treatment. Comparing with hydroxyl radicals (another reactive species in AOPs), the sulfate radicals have even higher redox potential (E_0 = 2.5 – 3.1 V vs. NHE) than hydroxyl radicals (E_0 = 1.8 – 2.7 V vs. NHE) [48]. The typical ways to generate sulfate radicals are thermal activation and UV irradiation of some oxidants, e.g., peroxymonosulfate (PMS) and persulfate (PS). One limitation of applying sulfate radical-based processes in PFAAs treatment is that sulfate radicals are not able to degrade perfluorinated sulfonic acid, e.g., PFOS.

Hori et al. [49, 50] were the pioneers who applied sulfate radicals in treatment of perfluorocarboxylic acids (PFCAs), including PFOA. They tried both strategies to generate sulfate radicals, i.e., photolysis of PS with UV-visible light and thermal activation of PS at elevated temperature (80 °C). They claimed the produced sulfate radicals will attack PFCAs via one-electron transfer (eq.3). After decarboxylation, subsequent several radical reactions and hydrolysis processes, a complete mineralization of PFCAs can be achieved.

$$C_nF_{2n+1}COO^- + SO_4^{-}\cdot \longrightarrow C_nF_{2n+1}COO\cdot + SO_4^{2-} \qquad (3)$$

Several researchers investigated the reaction rate constants for sulfate radicals with PFCAs by experiments and model simulations. Lutze et al. [51] reported that the second-order rate constants for sulfate radicals with different PFCAs (C4 to C8) are in the range of $1.7 - 4.4 \times 10^4$ $M^{-1}s^{-1}$. The difference in the relative reaction rate constants are not related to the chain length of different PFCAs but can rather be considered as experimental errors. Kutsuna et al. [52] also provided the similar second-order rate constants of sulfate radicals and PFCAs (1.3×10^4 $M^{-1}s^{-1}$ for PFBA, 1.4×10^4 $M^{-1}s^{-1}$ for PFPrA). However, Qian et al. [53] reported different rate constants between sulfate radicals and PFCAs. They derived these constants by fitting model data with experimental data of PFOA degradation and shorter-chain PFCAs formation (PFHpA, PFHxA, PFPeA, PFBA, and PFPrA) on the basis of a stepwise degradation of PFCAs (Table 5).

Table 5. Rate constants for reaction of sulfate radicals with PFCAs from model simulations [53].

PFCAs	**k (M^{-1} s^{-1})**
PFOA ($C_8HF_{15}O_2$)	2.59×10^5
PFHpA ($C_7HF_{13}O_2$)	2.68×10^5
PFHeA ($C_6HF_{11}O_2$)	7.02×10^5
PFPeA ($C_5HF_9O_2$)	1.26×10^6
PFBA ($C_4HF_7O_2$)	1.05×10^7
PFPrA ($C_3HF_5O_2$)	9.31×10^7

It is indicated that the rate constants between sulfate radicals and PFCAs are related to the carbon chain lengths (rate constants increases with a decreasing carbon chain lengths). However, the competition of PFOA and shorter-chain PFCA products for sulfate radicals can be ignored only under circumstances of very high degradation rates for all products and very low yields of shorter-chain PFCA products. Therefore, these derived rate constants by model simulations are not very convincing. Besides, sulfate radicals can also be quenched by certain coexisted scavengers in wastewater as shown in Table 6.

Table 6. Rate constants for reaction of sulfate radicals with some solutes [54-58].

solute	k ($M^{-1} s^{-1}$)
$SO_4^{-}\cdot$	4.4×10^{10}
OH^-	1.4×10^7
$S_2O_8^{2-}$	6.3×10^5
CO_3^{2-}	4.1×10^6
HCO_3^-	9.1×10^6
Cl^-	2.7×10^8

The reported second-order rate constants for reactions between sulfate radicals and different PFCAs are much smaller compared with reactions between hydrated electrons and PFCAs. Yet, sulfate radical-based techniques have some advantages over hydrated electron-based techniques on PFCAs degradation from these aspects:

i) The half-life of sulfate radicals (30 – 40 μs) [59] is three order of magnitude longer than hydrated electrons (< 60 ns) [60], which enables sulfate radicals to survive the mass transfer more easily and better contact with target compounds than hydrated electrons;

ii) Sulfate radical-based techniques are supposed to be less vulnerable and more suitable in the real water matrix. Apart from lower reaction rates with certain coexisted scavengers, sulfate radical-based techniques do not require anaerobic conditions.

iii) More activation strategies can be performed in sulfate radical-based techniques, e.g., thermal, UV light, and transition metal based catalysts/reagents [61]. In contrast, the ways to generate hydrated electrons are relatively limited. The most reported methods are activation of certain reducing reagents by UV light, γ -irradiation and electron beam, which usually require high energy [62, 63].

2.2.4 Electrochemical degradation

Electrochemical degradation has been receiving growing interest recently for wastewater treatment, because it is able to completely mineralize a wide range of recalcitrant organic compounds into water, carbon dioxide and inorganic ions. There are two major strategies during electrochemical degradation: (1) Direct oxidation: direct oxidation of organic pollutants on the anode surface; (2) Indirect oxidation: the formation of radical species that attack pollutants. The strategies of direction oxidation of PFAAs on the various types of anodes have been widely investigated.

Carter et al. [10] first reported the oxidative degradation of PFOS using boron-doped diamond (BDD) film electrodes. The degradation of PFOS yielded fluoride, sulfate, carbon dioxide, and traces of shorter-chain PFCAs. They used a flow-through reactor to monitor the PFOS reaction rate and found the overall PFOS reaction was mass transfer limited. The density functional theory (DFT) simulation indicated the rate-limiting step for PFOS oxidation was most likely the direct electron transfer from PFOS to BDD electrode (eq. 4).

$$C_8F_{17}SO_3^- \longrightarrow C_8F_{17}SO_3\cdot + e^- \tag{4}$$

Lin et al. [11] compared the activities of Ti/SnO_2–Sb/PbO_2, Ti/SnO_2–Sb, and Ti/SnO_2–Sb/MnO_2 anodes on degradation of PFOA. The Ti/SnO_2–Sb/PbO_2 and Ti/SnO_2–Sb showed better PFOA degradation and defluorination efficiencies. The main influential factors on electrochemical degradation of PFOA on Ti/SnO_2–Sb anode were investigated, i.e., initial pH values, current density, initial PFOA concentrations and electrode distance. Based on the intermediate products (shorter-chain PFCAs and fluoride) during the electrochemical degradation of PFOA, they proposed a PFOA degradation mechanism including several steps of direct electron transfer, decarboxylation, radical reaction, and hydrolysis. A complete mineralization of PFOA can be achieved at the end.

The electrochemical degradation of PFAAs turns out to be a promising solution. However, electrochemical degradation processes usually have relatively low efficiency of electrical energy usage but high operational cost, especially when the concentrations of the target pollutants are low.

2.2.5 Photochemical degradation

Photochemical degradation technique utilizes the UV or visible light to degrade the pollutants directly. It is acknowledged that solar energy is the most abundant energy resource on earth. The solar energy is environmentally friendly, as there are no emissions, no greenhouse gases, and no fossil fuels during the utilization. But currently, only limited UV range can be used for PFAAs degradation.

Chen et al. [64] found PFOA degrades very slowly by direct photolysis under 254 nm UV light, and the direct photolysis of PFOA can be considerably accelerated under 185 nm UV light. As PFOA has strong absorption from 190 nm to 220 nm (Figure 2), which makes the decarboxylation easier under 185 nm UV light.

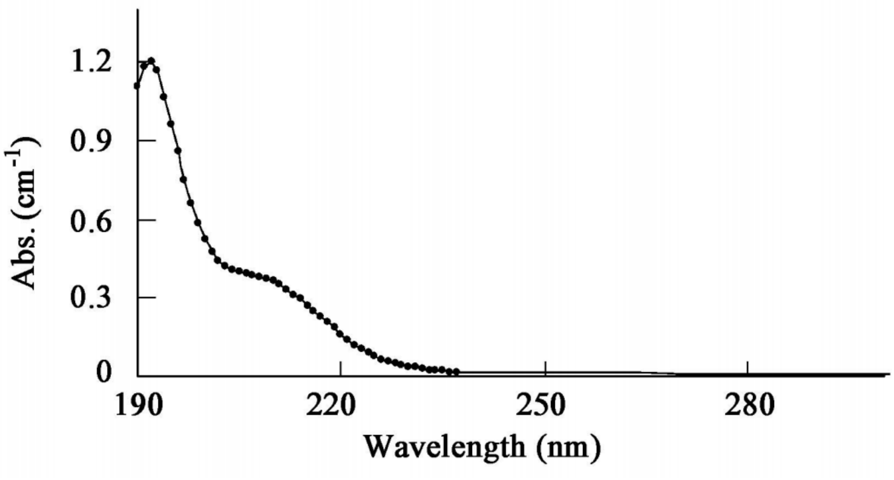

Figure 2. UV absorption of 50 mg L^{-1} aqueous PFOA solution [64]

Jin et al. [65] reported a rapid degradation of PFOS under anaerobic alkaline conditions with 185 nm UV irradiation. They found the photochemical degradation of PFOS was more favored at anaerobic alkaline conditions compared with aerobic neutral conditions. The decomposition rates of branched PFOS isomers were much faster than the linear PFOS, which indicated hydrated electrons might be the active species for PFOS degradation [65]. Besides, very limited fluorinated intermediates were detected and quantified suggesting the defluorination process was relatively complete. Direct photodegradation usually takes place under UV ranges, and shows a better degradation efficiency at vacuum UV range (185 nm), which is not applicable when utilizing the solar energy. Researchers tried to introduce reactive reagents during the photodegradation, so that a higher degradation efficiency and broader adsorption band can be achieved. Hori et al. [66] improved the photochemical degradation of PFCAs under 254 nm UV light by introducing trace amounts of ferric ions. The reaction constants of PFCAs degradation with ferric ion addition were 3.6 – 5.3 times higher than those with photochemical degradation alone. The improved PFCAs photodegradation efficiency could be explained by photoredox reactions between ferric/ferrous ions, oxygen and PFCAs via the complexation between PFCAs and ferric ions (eqs.5 - 8).

$$C_nF_{2n+1}COO^- + Fe^{3+} \longrightarrow [C_nF_{2n+1}COO\text{-}Fe]^{2+} \tag{5}$$

$$[C_nF_{2n+1}COO\text{-}Fe]^{2+} \xrightarrow{\text{254 nm UV}} Fe^{2+} + C_nF_{2n+1}COO\cdot \tag{6}$$

$$Fe^{2+} + O_2 \rightarrow Fe^{3+} + \cdot O_2^- \tag{7}$$

$$Fe^{2+} + \cdot OH \rightarrow Fe^{3+} + OH^- \tag{8}$$

Wang et al. [67] also applied these photoredox reactions to PFOA photochemical degradation. They investigated the influence of different initial ferric ion concentrations on PFOA degradation under 254 nm UV irradiation. Besides the ferric ions, they tried to introduce other metal ions during the photodegradation of PFOA, e.g., cupric ions, magnesium ions, zinc ions, manganese ions, etc. They found the introduction of cupric ions and zinc ions can also slightly improve the reaction rate in photochemical degradation of PFOA. Jin et al. [68] found that the addition of ferric ions could greatly enhance the degradation rate of PFOS under 254 nm UV irradiation. The degradation rate constant of PFOS photodecomposition in the presence of ferric ions was 50 times higher than that with direct photolysis. From scavenger experiments, they found molecule oxygen might involve in PFOS defluorination processes in the absence of hydroxyl radicals. In addition, although hydroxyl radicals are inert to PFOS decomposition, they can promote the defluorination processes. They finally suggested the ligand-to-metal charge transfer was the key step during PFOS photodecomposition (eqs.9 and 10).

$$C_8F_{17}SO_3^- + Fe^{3+} \longleftrightarrow [C_8F_{17}SO_3\text{-}Fe]^{2+} \tag{9}$$

$$[C_8F_{17}SO_3\text{-}Fe]^{2+} \xrightarrow{\text{UV- C}} C_8F_{17}SO_3\cdot + Fe^{2+} \tag{10}$$

Photochemical degradation is an environmentally friendly technique for PFAAs degradation. Yet, high energy demand (185 or 254 nm UV light) and relatively low PFAAs degradation rates will limit the application of this technique.

2.2.6 Photocatalytic degradation

Similar to the technique of photochemical degradation, the photocatalytic degradation also utilizes UV or visible light to degrade the pollutants. The difference is that photocatalytic degradation achieves pollutant degradation via using catalysts. The most common active species produced during photocatalytic degradation are hydroxyl radicals, superoxide radicals, electrons and oxidative holes in metal oxides.

Panchangam et al. [69] reported photocatalytic degradation of various PFCAs by TiO_2 under 254 nm UV irradiation. They claimed the oxidative holes in excited TiO_2 generated during UV irradiation were the oxidation sites for PFCAs. They proposed the degradation of PFCAs started with TiO_2 excitation under UV irradiation, which would produce excited TiO_2 species with electron-hole pair (eq.11). The excited TiO_2 can accept electrons from PFCAs anions to produce PFCAs radicals.

$$\mathrm{TiO_2} + h\upsilon \longrightarrow \mathrm{TiO_2^*} \tag{11}$$

Li et al. [70] compared the catalytic degradation of PFOA with TiO_2 and In_2O_3 as photocatalysts under 254 nm UV light, and they found In_2O_3 possesses much higher activity for PFOA decomposition. They claimed that the PFOA terminal carboxylate group can tightly coordinate to In_2O_3 surface with bridging or bidentate configuration, which is helpful for PFOA to be decomposed directly by reactions with photogenerated holes in In_2O_3 (Figure 3). In contrast, PFOA coordinated to TiO_2 surface through a monodentate configuration, and photogenerated holes in TiO_2 will transform to hydroxyl radicals preferentially, which are inert to PFOA degradation.

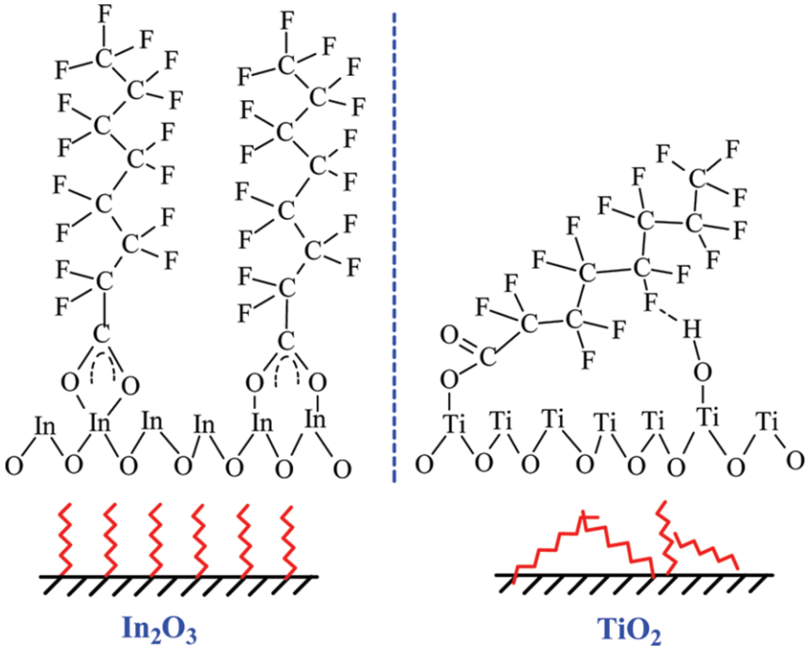

Figure 3. Schematic diagram of PFOA configurations adsorbed on In_2O_3 and TiO_2 [70].

Zhao et al. [71] reported a wide band gap photocatalyst (β-Ga_2O_3) for photocatalytic decomposition of PFOA under 254 nm UV light. The decomposition of PFOA with β-Ga_2O_3 followed the pseudo-first-order kinetics. They claimed that the electron photogenerated by exciting the catalyst surface can react with water to produce hydrated electrons, which were the main reactive species for PFOA decomposition. Alternatively, the surface adsorbed PFOA molecules can also be directly degraded by photogenerated electrons from β-Ga_2O_3 conduction band upon irradiation.

Photocatalytic degradation of PFAAs is a promising technology which is capable of decomposing a wide range of organic pollutants. A significant amount of research has been focused on TiO_2 based photocatalysts at a laboratory scale, but certain limitations e.g., low quantum yields, less reactivity and narrow-band absorption, need to be addressed before industrial scale application.

2.2.7 Other PFAAs degradation techniques

Besides the PFAAs removal/degradation technologies discussed above, other PFAAs degradation techniques were also reported, e.g., ultrasonic degradation, biodegradation and mechanochemical degradation. The degradation of PFAAs through ultrasonication is mainly through pyrolysis in cavitation bubbles at very high temperature [72, 73], which is less energy efficient. On the other hand, only very limited microorganisms can be applied for biodegradation of PFAAs [74-76]. Mechanochemical processes were reported to be effective on PFAAs decomposition. For instance, the mechanical agitation can generate high transient temperature which initiates the reactions between the reagents (e.g. potassium hydroxide) and PFAAs [77].

2.3 PFOA and PFOS degradation pathways

2.3.1 Oxidative degradation pathway

In most of oxidative PFOA degradation processes as discussed in chapter 2.2.3 (e.g., sulfate radical-based degradation, BDD electrode-based electrochemical degradation, ferric ion mediated photochemical degradation and TiO_2 mediated photocatalytic degradation), the degradation of PFOA was reported to start with an attack of the reactive species at its carboxylic headgroup [49, 67, 69]. After losing one electron from PFOA headgroup, $C_7F_{15}COO\bullet$ will be produced (eq. 12). The radical $C_7F_{15}COO\bullet$ undergoes Kolbe decarboxylation reaction to form $\bullet C_7F_{15}$ (eq. 13) which is supposed to react further with (i) molecule oxygen, (ii) hydroxyl radicals, (iii) water and (iv) can recombine with other (perfluorinated) radicals. In the (i) case, •C_7F_{15} can react with oxygen to produce perfluoroalkylperoxyl radicals which undergo a bimolecular radical-radical reaction and yield two perfluoroalkoxy radicals •OC_7F_{15} (eqs. 14-16) [51, 52]. •OC_7F_{15} will abstract H from HSO_4^- (in sulfate radical-based processes) or from water to form perfluoroalkyl alcohol ($C_7F_{15}OH$) (eqs. 17 and 18). It eliminates rapidly one HF and forms $C_6F_{13}COF$ then hydrolyzed to $C_6F_{13}COOH$. $C_6F_{13}COOH$ will follow a similar degradation pathway as for PFOA (eqs. 19 and 20). Finally, a complete degradation/defluorination of PFOA can be achieved. In the (ii) case, •C_7F_{15} may react with •OH to produce $C_7F_{15}OH$ (eq. 21) [78] then further degraded as described in (i). In addition, some researcher also claimed the •C_7F_{15} can directly react with water (the (iii) case) to form $C_7F_{15}OH$ and •H [79, 80]. This mechanism is however suspicious because •H is much more reactive than • C_7F_{15}.

$$C_7F_{15}COO^- \xrightarrow{in\ various\ oxidative\ processes} C_7F_{15}COO\bullet \quad (12)$$

$$C_7F_{15}COO\bullet \rightarrow \bullet C_7F_{15} + CO_2 \quad (13)$$

$$\bullet C_7F_{15} + O_2 \rightarrow C_7F_{15}OO\bullet \quad (14)$$

$$2C_7F_{15}OO\bullet \rightarrow C_7F_{15}OOOOC_7F_{15} \quad (15)$$

$$C_7F_{15}OOOOC_7F_{15} \rightarrow 2C_7F_{15}O\bullet + O_2 \quad (16)$$

$$C_7F_{15}O\bullet + HSO_4^- \rightarrow C_7F_{15}OH + SO_4^-\bullet \quad (17)$$

$$C_7F_{15}O\bullet + H_2O \rightarrow C_7F_{15}OH + \bullet OH \quad (18)$$

$$C_7F_{15}OH \rightarrow C_7F_{13}OF + HF \quad (19)$$

$$C_7F_{13}OF + H_2O \rightarrow C_6F_{13}COOH + HF \quad (20)$$

$$\bullet C_7F_{15} + \bullet OH \rightarrow C_7F_{15}OH \quad (21)$$

The recombination of fluorinated radicals ($\bullet C_nF_{2n+1} + \bullet C_mF_{2m+1} \rightarrow C_{n+m}F_{2(n+m+1)}$) yields perfluoroalkanes which are volatile and may escape from the aqueous solution. This maybe the reason that they are not considered in many reaction schemes. Applied on peroxyl radicals recombination can yield peroxides (R_F-OO•+ •R_F'→ R_F-O-O-R_F') which have been postulated by Lutze et al. [51] but not identified so far.

Similarly, the degradation of PFOS was also initiated from the attack of oxidizing species at its sulfonate headgroup in oxidative degradation processes (BDD electrode-based electrochemical degradation and ferric ion mediated photochemical degradation) [10, 68]. After losing one electron from PFOS headgroup, $C_8F_{17}SO_3$• will be produced (eq. 22). The loss of one electron leads to the stretching of the C-S bond, thus easing the desulfurization when reacting with water, yielding perfluorinated alkyl radicals (•C_8F_{17}) and sulfate anions (eq. 23). The •C_8F_{17} will follow the reaction pathway as •C_7F_{15} does and be converted to PFOA.

$$C_8F_{17}SO_3^- \xrightarrow{in\ various\ oxidative\ processes} C_8F_{17}SO_3\bullet \tag{22}$$

$$C_8F_{17}SO_3\bullet + H_2O \rightarrow \bullet C_8F_{17} + SO_4^{2-} + 2H^+ \tag{23}$$

2.3.2 Reductive degradation pathway

The reported mechanisms of reductive PFOA and PFOS degradation processes (mainly hydrated electron-based) were more controversial. There were two major pathways for PFOA or PFOS degradation, i.e., H/F exchange and decarboxylation/desulfurization [81]. In the former case, the hydrated electron attacks the carbon preferentially on the α-position of PFOA or PFOS. Two H/F exchanges on the α-position take place sequentially and yield the relatively stable $C_6F_{13}CH_2COO^-$ (eqs. 24-29) or $C_7F_{15}CH_2SO_3^-$ (eqs. 30-35) [81, 82]. It is also possible that additional H/F exchange takes place at the middle –CF_2– groups. But complete defluorination of PFOA and PFOS cannot be achieved by this degradation pathway [81]. Some researchers claimed the intermediate $C_6F_{13}CH_2COO^-$ and $C_7F_{15}CH_2SO_3^-$ will be further transformed to $C_6F_{13}COO^-$ and $C_7F_{15}SO_3^-$ /$C_7F_{15}COO^-$ respectively, via reactions 36-39 [82-84], which seemed, however, rather unlikely.

In addition, it is reported that decarboxylation and desulfurization of PFOA and PFOS can occur when their headgroups are attacked by hydrated electrons [81, 85-87]. After subsequent radical reactions and hydrolysis, the shorter-chain PFCAs with one CF_2 unit less are produced. Various reaction pathways were proposed but remained suspicious. The electronic state of the postulated intermediate dianion $C_7F_{15}COO^{2-}$• is not clear. In addition, the availability of free H radicals for reductive saturation of fluorinated radicals in aqueous solution remains suspicious.

$$C_7F_{15}COO^- + e_{aq}^- \rightarrow C_7F_{15}COO^{2-}\bullet \tag{24}$$

$$C_7F_{15}COO^{2-}\bullet \rightarrow C_6F_{13}C\bullet FCOO^- + F^- \tag{25}$$

$$C_6F_{13}C\bullet FCOO^- + H\bullet \rightarrow C_6F_{13}CHFCOO^- \tag{26}$$

$$C_6F_{13}CHFCOO^- + e_{aq}^- \rightarrow C_6F_{13}CHFCOO^{2-}\bullet \tag{27}$$

$$C_6F_{13}CHFCOO^{2-}\bullet \rightarrow C_6F_{13}C\bullet HCOO^- + F^- \tag{28}$$

$$C_6F_{13}C\bullet HCOO^- + H\bullet \rightarrow C_6F_{13}CH_2COO^- \tag{29}$$

$$C_8F_{17}SO_3^- + e_{aq}^- \rightarrow C_8F_{17}SO_3^{2-}\bullet \tag{30}$$

$$C_8F_{17}SO_3^{2-}\bullet \rightarrow C_7F_{15}C\bullet FSO_3^- + F^- \tag{31}$$

$$C_7F_{15}C\bullet FSO_3^- + H\bullet \rightarrow C_7F_{15}CHFSO_3^- \tag{32}$$

$$C_7F_{15}CHFSO_3^- + e_{aq}^- \rightarrow C_7F_{15}CHFSO_3^{2-}\bullet \tag{33}$$

$$C_7F_{15}CHFSO_3^{2-}\bullet \rightarrow C_7F_{15}C\bullet HSO_3^- + F^- \tag{34}$$

$$C_7F_{15}C\bullet HSO_3^- + H\bullet \rightarrow C_7F_{15}CH_2SO_3^- \tag{35}$$

$$C_6F_{13}CH_2COOH \rightarrow \bullet C_6F_{13} + :CH_2 + \bullet COOH \tag{36}$$

$$\bullet C_6F_{13} + \bullet COOH \rightarrow C_6F_{13}COOH \tag{37}$$

$$C_7F_{15}CH_2SO_3^- \rightarrow \bullet C_7F_{15} + :CH_2 + SO_3^-\bullet \tag{38}$$

$$\bullet C_7F_{15} + SO_3^-\bullet \rightarrow C_7F_{15}SO_3^- \tag{39}$$

2.4 Zeolites

2.4.1 Introduction of zeolites

Zeolites are crystalline aluminosilicates with macromolecular inorganic frameworks and microporous inner structure, which can be found in metamorphic, sedimentary, and volcanic rocks [88]. The structure of zeolites can be described by a general formula:

$$M_{x/z}[(AlO_2)_x(SiO_2)_y] \cdot n\,H_2O$$

in which M stands for mono- or divalent cations with the positive charge z. The zeolite framework consists of negatively charged $[AlO_{4/2}]^-$- and neutral $SiO_{4/2}$-tetrahedra which share bridge oxygen atoms [89]. The density of negative charges on zeolite framework is dependent on its aluminum content, which is compensated by positively charged cations, e.g., protons and metal ions. This enables zeolites possess ion exchange property. For instance, zeolites can be loaded with iron ions by simple ion exchange procedures [90]. To remove any leachable iron in the zeolites, a competitive exchange by potassium ions can be performed under acidic conditions [91]. Theoretically, increasing aluminum content leads to an increasing number of negatively charged sites, i.e., a higher cation exchange capacity. On the other hand, increasing silicon content leads to an increasing hydrophobicity of zeolite surface. Moreover, the additional species (e.g., water) inside the pores of zeolites can be removed, so that the void space can be utilized for selective hosting of certain guest species of specific shape, size and polarity. On top of that, the catalytically active sites in zeolite frameworks coupled with the spatial confinement of zeolite pores provides zeolites with shape-selective catalysis [92].

Depending on synthesis conditions, zeolites can possess various types of framework structures. The framework structure defines i) pore volume and distribution; ii) pore opening shape and size; iii) channels and cages arrangement. Different types of zeolites are defined with three-letter codes by International Zeolite Association according to their framework structures, e.g., beta-BEA, faujasite-FAU, mordenite-MOR, and pentasil-MFI, etc. To describe a zeolite precisely, the molar ratio of SiO_2/Al_2O_3 will be stated after its three-letter code, e.g., BEA35 is a Beta structure type zeolite with a 35-molar ratio of SiO_2/Al_2O_3.

2.4.2 Zeolites application in water treatment

Zeolites have been widely used as catalysts, adsorbents and ion exchangers in industrial processes (e.g., in traditional petrochemical industries). In the past few decades, zeolites were also applied in the field of wastewater treatment thanks to its remarkable adsorption and ion-exchange capability [92]. For instance, zeolites can be fabricated as membranes for reverse osmosis due to its molecular-sieving properties. Spilled oil or salt removal from water can be achieved by zeolite membranes with water permeation and high oil/salt rejection properties [93]. Recently, an all-silica zeolite Beta was investigated for selective removal of PFOA [94]. It is claimed that the adsorption of PFOA is driven by favorable steric factors and a negative adsorption enthalpy, i.e., the helical conformation of the perfluorocarbon chains positioned in a tight packing with a maximal sterical capacity. These properties from all-silica zeolite Beta type zeolite allow a high adsorption affinity and selectivity toward PFOA and other similar perfluorinated compounds. Moreover, with its superior ion-exchange property, zeolite impregnated with various metal ions can be realized, which has been widely used in micropollutants treatment *in situ* with trap & treat principle.

Besides zeolites, some carbonaceous materials, e.g., activated carbon, graphene, and carbon nanotubes, have been frequently used as adsorbents for micropollutants removal from water. Carbonaceous materials usually possess high specific surface area and strong adsorption affinities to varieties of micropollutants. However, if a combined adsorption and degradation processes were considered, carbonaceous materials often encounter challenges by strong oxidative species, e.g., hydroxyl radicals or ozone, in the regeneration step. For instance, Valdes et al. [95] studied a combined process of ozone and activated carbon in wastewater treatment. They claimed the ozone will generate oxygen-containing functional groups, e.g., anhydride, lactones, and carboxylic groups, on activated carbon surface and decrease its specific surface area, which led to a decline in the adsorption capacity of the activated carbon to micropollutants. However, zeolites are relatively stable thanks to their composition and inherent properties, which are not subject to oxidation. Zeolites are thereby suitable candidate as long-lived recyclable catalysts, which can adsorb recalcitrant pollutants but maintain the adsorption capacity during the regeneration process in the presence of strong oxidants. For instance, Gonzales-Olmos et al. [96] designed a combined adsorption/reaction strategy for methyl tert-butyl ether (MTBE) treatment with Fe-doped zeolites. After Fe species are immobilized on zeolite, a heterogeneous Fenton-like reaction in the presence of H_2O_2 enables an efficient degradation of MTBE after its adsorption. The calcined Fe-doped zeolites showed no significant loss in catalytic reactivity after 6 reaction cycles. In addition, this kind of two-step strategy makes a large-scale application possible when column setups and fixed-bed reactors are considered.

Reference

[1] D.o.P.I.V. International Atomic Energy Agency, All about water, IAEA Bulletin (Online), 53 (2011) 17-20.

[2] L. Ahrens, Z. Xie, R. Ebinghaus, Distribution of perfluoroalkyl compounds in seawater from northern europe, atlantic ocean, and southern ocean, Chemosphere, 78 (2010) 1011-1016.

[3] C.P. Higgins, R.G. Luthy, Sorption of perfluorinated surfactants on sediments, Environmental Science & Technology, 40 (2006) 7251-7256.

[4] J.A. Björklund, K. Thuresson, C.A. de Wit, Perfluoroalkyl compounds (PFCs) in indoor dust: concentrations, human exposure estimates, and sources, Environmental Science & Technology, 43 (2009) 2276-2281.

[5] E.M. Sunderland, X.C. Hu, C. Dassuncao, A.K. Tokranov, C.C. Wagner, J.G. Allen, A review of the pathways of human exposure to poly- and perfluoroalkyl substances (PFASs) and present understanding of health effects, Journal of Exposure Science & Environmental Epidemiology, 29 (2019) 131-147.

[6] B.D. Key, R.D. Howell, C.S. Criddle, Fluorinated organics in the biosphere, Environmental Science & Technology, 31 (1997) 2445-2454.

[7] C.K.O. da Silva-Rackov, W.A. Lawal, P.A. Nfodzo, M.M.G.R. Vianna, C.A.O. do Nascimento, H. Choi, Degradation of PFOA by hydrogen peroxide and persulfate activated by iron-modified diatomite, Applied Catalysis B: Environmental, 192 (2016) 253-259.

[8] N. Yamashita, K. Kannan, S. Taniyasu, Y. Horii, G. Petrick, T. Gamo, A global survey of perfluorinated acids in oceans, Marine Pollution Bulletin, 51 (2005) 658-668.

[9] H. Tian, J. Gao, H. Li, S.A. Boyd, C. Gu, Complete defluorination of perfluorinated compounds by hydrated electrons generated from 3-indole-acetic-acid in organomodified montmorillonite, Scientific Reports, 6 (2016) 32949.

[10] K.E. Carter, J. Farrell, Oxidative destruction of perfluorooctane sulfonate using boron-doped diamond film electrodes, Environmental Science & Technology, 42 (2008) 6111-6115.

[11] H. Lin, J. Niu, S. Ding, L. Zhang, Electrochemical degradation of perfluorooctanoic acid (PFOA) by Ti/SnO2–Sb, Ti/SnO2–Sb/PbO2 and Ti/SnO2–Sb/MnO2 anodes, Water Research, 46 (2012) 2281-2289.

[12] C.J.A.F. Kwadijk, I. Velzeboer, A.A. Koelmans, Sorption of perfluorooctane sulfonate to carbon nanotubes in aquatic sediments, Chemosphere, 90 (2013) 1631-1636.

[13] N. Saeidi, F.-D. Kopinke, A. Georgi, Understanding the effect of carbon surface chemistry on adsorption of perfluorinated alkyl substances, Chemical Engineering Journal, 381 (2020) 122689.

[14] F. Xiao, T.R. Halbach, M.F. Simcik, J.S. Gulliver, Input characterization of perfluoroalkyl substances in wastewater treatment plants: Source discrimination by exploratory data analysis, Water Research, 46 (2012) 3101-3109.

[15] V. Rokade, Integrated study of geochemistry and health, Medical Geology.

[16] K.Y. Kwok, E. Yamazaki, N. Yamashita, S. Taniyasu, M.B. Murphy, Y. Horii, G. Petrick, R. Kallerborn, K. Kannan, K. Murano, P.K.S. Lam, Transport of perfluoroalkyl substances (PFAS) from an arctic glacier to downstream locations: implications for sources, Science of The Total Environment, 447 (2013) 46-55.

[17] R. Renner, Growing concern over perfluorinated chemicals, Environmental Science & Technology, 35 (2001) 154A-160A.

[18] M. Cooke, Technical fact sheet–perfluorooctane sulfonate (PFOS) and perfluorooctanoic acid (PFOA), Emergency, O. o. L. a., ed., United States Envrionmental Protection Agency, (2017).

[19] B. Bhhatarai, P. Gramatica, Prediction of aqueous solubility, vapor pressure and critical micelle concentration for aquatic partitioning of perfluorinated chemicals, Environmental Science & Technology, 45 (2011) 8120-8128.

[20] U.E.P. Agency., Revised draft hazard assessment of perfluorooctanoic acid and its salts, (2002).

[21] K.-U. Goss, The pKa values of PFOA and other highly fluorinated carboxylic acids, Environmental Science & Technology, 42 (2008) 456-458.

[22] Q. Ma, L. Liu, W. Cui, R. Li, T. Song, Z. Cui, Electrochemical degradation of perfluorooctanoic acid (PFOA) by Yb-doped Ti/SnO2–Sb/PbO2 anodes and determination of the optimal conditions, RSC Advances, 5 (2015) 84856-84864.

[23] Y. Alsmeyer, W. Childs, R. Flynn, G. Moore, J. Smeltzer, Electrochemical fluorination and its applications, Organofluorine Chemistry, Springer1994, pp. 121-143.

[24] W. Reagen, K. Lindstrom, C. Jacoby, R. Purcell, T. Kestner, R. Payfer, J. Miller, Environmental characterization of 3M electrochemical fluorination derived perfluorooctanoate and perfluorooctanesulfonate, Society of Environmental Toxicology and Chemistry North America 28th Annual Meeting, 2007, pp. 11-15.

[25] P.M. Savu, Fluorinated higher carboxylic acids, Kirk‐Othmer Encyclopedia of Chemical Technology.

[26] H.-J. Lehmler, Synthesis of environmentally relevant fluorinated surfactants—a review, Chemosphere, 58 (2005) 1471-1496.

[27] A.B. Lindstrom, M.J. Strynar, E.L. Libelo, Polyfluorinated compounds: past, present, and future, Environmental Science & Technology, 45 (2011) 7954-7961.

[28] A.G. Paul, K.C. Jones, A.J. Sweetman, A first global production, emission, and environmental inventory for perfluorooctane sulfonate, Environmental Science & Technology, 43 (2009) 386-392.

[29] T. Seppälä, Guidance on preparing inventories of perfluorooctane sulfonic acid (PFOS), its salts and perfluorooctane sulfonyl fluoride (PFOSF) listed under the Stockholm Convention on Persistent Organic Pollutants.

[30] X. Zhang, R. Lohmann, E.M. Sunderland, Poly- and perfluoroalkyl substances in seawater and plankton from the northwestern atlantic margin, Environmental science & technology, 53 (2019) 12348-12356.

[31] K. Prevedouros, I.T. Cousins, R.C. Buck, S.H. Korzeniowski, Sources, fate and transport of perfluorocarboxylates, Environmental Science & Technology, 40 (2006) 32-44.

[32] F. Wania, D. Mackay, A global distribution model for persistent organic chemicals, Science of The Total Environment, 160-161 (1995) 211-232.

[33] J.P.G.a.K. Kannan, Peer reviewed: perfluorochemical surfactants in the environment, Environmental Science & Technology, 36 (2002) 146A-152A.

[34] K. Harada, K. Inoue, A. Morikawa, T. Yoshinaga, N. Saito, A. Koizumi, Renal clearance of perfluorooctane sulfonate and perfluorooctanoate in humans and their species-specific excretion, Environmental Research, 99 (2005) 253-261.

[35] G.W. Olsen, J.M. Burris, D.J. Ehresman, J.W. Froehlich, A.M. Seacat, J.L. Butenhoff, L.R. Zobel, Half-life of serum elimination of perfluorooctanesulfonate, perfluorohexanesulfonate, and perfluorooctanoate in retired fluorochemical production workers, Environmental health perspectives, 115 (2007) 1298-1305.

[36] C. Fei, J.K. McLaughlin, L. Lipworth, J. Olsen, Maternal levels of perfluorinated chemicals and subfecundity, Human Reproduction, 24 (2009) 1200-1205.

[37] K.T. Eriksen, O. Raaschou-Nielsen, M. Sørensen, M. Roursgaard, S. Loft, P. Møller, Genotoxic potential of the perfluorinated chemicals PFOA, PFOS, PFBS, PFNA and PFHxA in human HepG2 cells, Mutation Research/Genetic Toxicology and Environmental Mutagenesis, 700 (2010) 39-43.

[38] K. Harada, F. Xu, K. Ono, T. Iijima, A. Koizumi, Effects of PFOS and PFOA on L-type Ca2+ currents in guinea-pig ventricular myocytes, Biochemical and Biophysical Research Communications, 329 (2005) 487-494.

[39] N. Johansson, A. Fredriksson, P. Eriksson, Neonatal exposure to perfluorooctane sulfonate (PFOS) and perfluorooctanoic acid (PFOA) causes neurobehavioural defects in adult mice, Neurotoxicology, 29 (2008) 160-169.

[40] M. Trojanowicz, A. Bojanowska-Czajka, I. Bartosiewicz, K. Kulisa, Advanced oxidation/reduction processes treatment for aqueous perfluorooctanoate (PFOA) and perfluorooctanesulfonate (PFOS) – a review of recent advances, Chemical Engineering Journal, 336 (2018) 170-199.

[41] V. Ochoa-Herrera, R. Sierra-Alvarez, Removal of perfluorinated surfactants by sorption onto granular activated carbon, zeolite and sludge, Chemosphere, 72 (2008) 1588-1593.
[42] H. Park, C.D. Vecitis, J. Cheng, N.F. Dalleska, B.T. Mader, M.R. Hoffmann, Reductive degradation of perfluoroalkyl compounds with aquated electrons generated from iodide photolysis at 254 nm, Photochemical & Photobiological Sciences, 10 (2011) 1945-1953.
[43] M.J. Bentel, Y. Yu, L. Xu, Z. Li, B.M. Wong, Y. Men, J. Liu, Defluorination of per-and polyfluoroalkyl substances (PFASs) with hydrated electrons: structural dependence and implications to PFAS remediation and management, Environmental science & technology, 53 (2019) 3718-3728.
[44] L. Huang, W. Dong, H. Hou, Investigation of the reactivity of hydrated electron toward perfluorinated carboxylates by laser flash photolysis, Chemical Physics Letters, 436 (2007) 124-128.
[45] E. Szajdzinska-Pietek, J.L. Gebicki, Pulse radiolytic investigation of perfluorinated surfactants in aqueous solutions, Research on Chemical Intermediates, 26 (2000) 897-912.
[46] S. Gordon, E. Hart, M.S. Matheson, J. Rabani, J. Thomas, Reactions of the hydrated electron, Discussions of the Faraday Society, 36 (1963) 193-205.
[47] J. Thomas, S. Gordon, E.J. Hart, The Rates of Reaction of the Hydrated Electron in Aqueous Inorganic Solutions1, The Journal of Physical Chemistry, 68 (1964) 1524-1527.
[48] J. Li, R. Li, L. Zou, X. Liu, Efficient degradation of norfloxacin and simultaneous electricity generation in a persulfate-photocatalytic fuel cell system, Catalysts, 9 (2019) 835.
[49] H. Hori, A. Yamamoto, E. Hayakawa, S. Taniyasu, N. Yamashita, S. Kutsuna, H. Kiatagawa, R. Arakawa, Efficient decomposition of environmentally persistent perfluorocarboxylic acids by use of persulfate as a photochemical oxidant, Environmental Science & Technology, 39 (2005) 2383-2388.
[50] H. Hori, Y. Nagaoka, M. Murayama, S. Kutsuna, Efficient decomposition of perfluorocarboxylic acids and alternative fluorochemical surfactants in hot water, Environmental Science & Technology, 42 (2008) 7438-7443.
[51] H.V. Lutze, J. Brekenfeld, S. Naumov, C. von Sonntag, T.C. Schmidt, Degradation of perfluorinated compounds by sulfate radicals – new mechanistic aspects and economical considerations, Water Research, 129 (2018) 509-519.
[52] S. Kutsuna, H. Hori, Rate constants for aqueous-phase reactions of SO4− with C2F5C(O)O− and C3F7C(O)O− at 298 K, International Journal of Chemical Kinetics, 39 (2007) 276-288.
[53] Y. Qian, X. Guo, Y. Zhang, Y. Peng, P. Sun, C.-H. Huang, J. Niu, X. Zhou, J.C. Crittenden, Perfluorooctanoic acid degradation using UV–persulfate process: modeling of the degradation and chlorate formation, Environmental Science & Technology, 50 (2016) 772-781.
[54] C. George, J.-M. Chovelon, A laser flash photolysis study of the decay of SO4− and Cl2− radical anions in the presence of Cl− in aqueous solutions, Chemosphere, 47 (2002) 385-393.
[55] R.E. Huie, C.L. Clifton, Kinetics of the self-reaction of hydroxymethylperoxyl radicals, Chemical Physics Letters, 205 (1993) 163-167.
[56] S. Padmaja, P. Neta, R.E. Huie, Rate constants for some reactions of inorganic radicals with inorganic ions. Temperature and solvent dependence, International Journal of Chemical Kinetics, 25 (1993) 445-455.
[57] L. Dogliotti, E. Hayon, Flash photolysis of per [oxydi] sulfate ions in aqueous solutions. The sulfate and ozonide radical anions, The Journal of Physical Chemistry, 71 (1967) 2511-2516.
[58] H. Herrmann, A. Reese, R. Zellner, Time-resolved UV/VIS diode array absorption spectroscopy of SOx−(x=3, 4, 5) radical anions in aqueous solution, Journal of Molecular Structure, 348 (1995) 183-186.
[59] F. Ghanbari, M. Moradi, Application of peroxymonosulfate and its activation methods for degradation of environmental organic pollutants: review, Chemical Engineering Journal, 310 (2017) 41-62.
[60] L. Dharmarathne, M. Ashokkumar, F. Grieser, On the generation of the hydrated electron during the sonolysis of aqueous solutions, The Journal of Physical Chemistry A, 117 (2013) 2409-2414.
[61] J. Wang, S. Wang, Activation of persulfate (PS) and peroxymonosulfate (PMS) and application for the degradation of emerging contaminants, Chemical Engineering Journal, 334 (2018) 1502-1517.

[62] B.B. Bhanu Prakash Vellanki, and Ahmed Abdel-Wahab, Advanced reduction processes: a new class of treatment processes, Environmental Engineering Science, 30 (2013) 264-271.

[63] Z. Zhang, J.-J. Chen, X.-J. Lyu, H. Yin, G.-P. Sheng, Complete mineralization of perfluorooctanoic acid (PFOA) by γ-irradiation in aqueous solution, Scientific Reports, 4 (2014) 7418.

[64] J. Chen, P.-y. Zhang, J. Liu, Photodegradation of perfluorooctanoic acid by 185 nm vacuum ultraviolet light, Journal of Environmental Sciences, 19 (2007) 387-390.

[65] L. Jin, P. Zhang, Photochemical decomposition of perfluorooctane sulfonate (PFOS) in an anoxic alkaline solution by 185nm vacuum ultraviolet, Chemical Engineering Journal, 280 (2015) 241-247.

[66] H. Hori, A. Yamamoto, K. Koike, S. Kutsuna, I. Osaka, R. Arakawa, Photochemical decomposition of environmentally persistent short-chain perfluorocarboxylic acids in water mediated by iron(II)/(III) redox reactions, Chemosphere, 68 (2007) 572-578.

[67] Y. Wang, P. Zhang, G. Pan, H. Chen, Ferric ion mediated photochemical decomposition of perfluorooctanoic acid (PFOA) by 254 nm UV light, Journal of Hazardous Materials, 160 (2008) 181-186.

[68] L. Jin, P. Zhang, T. Shao, S. Zhao, Ferric ion mediated photodecomposition of aqueous perfluorooctane sulfonate (PFOS) under UV irradiation and its mechanism, Journal of Hazardous Materials, 271 (2014) 9-15.

[69] S.C. Panchangam, A.Y.-C. Lin, K.L. Shaik, C.-F. Lin, Decomposition of perfluorocarboxylic acids (PFCAs) by heterogeneous photocatalysis in acidic aqueous medium, Chemosphere, 77 (2009) 242-248.

[70] X. Li, P. Zhang, L. Jin, T. Shao, Z. Li, J. Cao, Efficient photocatalytic decomposition of perfluorooctanoic acid by indium oxide and its mechanism, Environmental science & technology, 46 (2012) 5528-5534.

[71] B. Zhao, P. Zhang, Photocatalytic decomposition of perfluorooctanoic acid with β-Ga2O3 wide bandgap photocatalyst, Catalysis Communications, 10 (2009) 1184-1187.

[72] H. Moriwaki, Y. Takagi, M. Tanaka, K. Tsuruho, K. Okitsu, Y. Maeda, Sonochemical decomposition of perfluorooctane sulfonate and perfluorooctanoic acid, Environmental Science & Technology, 39 (2005) 3388-3392.

[73] L. Rodriguez-Freire, R. Balachandran, R. Sierra-Alvarez, M. Keswani, Effect of sound frequency and initial concentration on the sonochemical degradation of perfluorooctane sulfonate (PFOS), Journal of Hazardous Materials, 300 (2015) 662-669.

[74] B.D. Key, R.D. Howell, C.S. Criddle, Defluorination of organofluorine sulfur compounds by pseudomonas sp. strain D2, Environmental Science & Technology, 32 (1998) 2283-2287.

[75] M.J.A. Dinglasan, Y. Ye, E.A. Edwards, S.A. Mabury, Fluorotelomer alcohol biodegradation yields poly- and perfluorinated acids, Environmental Science & Technology, 38 (2004) 2857-2864.

[76] B.G. Kwon, H.-J. Lim, S.-H. Na, B.-I. Choi, D.-S. Shin, S.-Y. Chung, Biodegradation of perfluorooctanesulfonate (PFOS) as an emerging contaminant, Chemosphere, 109 (2014) 221-225.

[77] K. Zhang, J. Huang, G. Yu, Q. Zhang, S. Deng, B. Wang, Destruction of perfluorooctane sulfonate (PFOS) and perfluorooctanoic acid (PFOA) by ball milling, Environmental Science & Technology, 47 (2013) 6471-6477.

[78] T. Ochiai, Y. Iizuka, K. Nakata, T. Murakami, D.A. Tryk, Y. Koide, Y. Morito, A. Fujishima, Efficient decomposition of perfluorocarboxylic acids in aqueous suspensions of a TiO2 photocatalyst with medium-pressure ultraviolet lamp irradiation under atmospheric pressure, Industrial & Engineering Chemistry Research, 50 (2011) 10943-10947.

[79] B. Zhao, M. Lv, L. Zhou, Photocatalytic degradation of perfluorooctanoic acid with β-Ga2O3 in anoxic aqueous solution, Journal of Environmental Sciences, 24 (2012) 774-780.

[80] N. Takeuchi, R. Oishi, Y. Kitagawa, K. Yasuoka, Adsorption and efficient decomposition of perfluoro compounds at plasma–water interface, IEEE Transactions on Plasma Science, 39 (2011) 3358-3363.

[81] M.J. Bentel, Y. Yu, L. Xu, Z. Li, B.M. Wong, Y. Men, J. Liu, Defluorination of Per- and Polyfluoroalkyl Substances (PFASs) with Hydrated Electrons: Structural Dependence and Implications to PFAS Remediation and Management, Environmental Science & Technology, 53 (2019) 3718-3728.

[82] S.-H. Ma, M.-H. Wu, L. Tang, R. Sun, C. Zang, J.-J. Xiang, X.-X. Yang, X. Li, G. Xu, EB degradation of perfluorooctanoic acid and perfluorooctane sulfonate in aqueous solution, Nuclear Science and Techniques, 28 (2017) 137.
[83] W. Wang, Y. Chen, G. Li, W. Gu, T. An, Photocatalytic reductive defluorination of perfluorooctanoic acid in water under visible light irradiation: the role of electron donor, Environmental Science: Water Research & Technology, 6 (2020) 1638-1648.
[84] Z. Song, H. Tang, N. Wang, L. Zhu, Reductive defluorination of perfluorooctanoic acid by hydrated electrons in a sulfite-mediated UV photochemical system, Journal of Hazardous Materials, 262 (2013) 332-338.
[85] Y. Gu, W. Dong, C. Luo, T. Liu, Efficient reductive decomposition of perfluorooctanesulfonate in a high photon flux UV/sulfite system, Environmental Science & Technology, 50 (2016) 10554-10561.
[86] Y. Wang, P. Zhang, Photocatalytic decomposition of perfluorooctanoic acid (PFOA) by TiO2 in the presence of oxalic acid, Journal of Hazardous Materials, 192 (2011) 1869-1875.
[87] M. Trojanowicz, I. Bartosiewicz, A. Bojanowska-Czajka, T. Szreder, K. Bobrowski, G. Nałęcz-Jawecki, S. Męczyńska-Wielgosz, H. Nichipor, Application of ionizing radiation in decomposition of perfluorooctane sulfonate (PFOS) in aqueous solutions, Chemical Engineering Journal, 379 (2020) 122303.
[88] R. Rinaldi, Zeolites, Mineralogy, Springer US, Boston, MA, 1983, pp. 522-532.
[89] R. Gläser, J. Weitkamp, The application of zeolites in catalysis, in: M. Baerns (Ed.) Basic Principles in Applied Catalysis, Springer Berlin Heidelberg, Berlin, Heidelberg, 2004, pp. 159-212.
[90] S. Navalon, M. Alvaro, H. Garcia, Heterogeneous fenton catalysts based on clays, silicas and zeolites, Applied Catalysis B: Environmental, 99 (2010) 1-26.
[91] R. Gonzalez-Olmos, U. Roland, H. Toufar, F.D. Kopinke, A. Georgi, Fe-zeolites as catalysts for chemical oxidation of MTBE in water with H2O2, Applied Catalysis B: Environmental, 89 (2009) 356-364.
[92] Y. Li, L. Li, J. Yu, Applications of zeolites in sustainable chemistry, Chem, 3 (2017) 928-949.
[93] S. Daer, J. Kharraz, A. Giwa, S.W. Hasan, Recent applications of nanomaterials in water desalination: a critical review and future opportunities, Desalination, 367 (2015) 37-48.
[94] M. Van den Bergh, A. Krajnc, S. Voorspoels, S.R. Tavares, S. Mullens, I. Beurroies, G. Maurin, G. Mali, D.E. De Vos, Highly selective removal of perfluorinated contaminants by adsorption on all-silica zeolite beta, Angewandte Chemie International Edition, 59 (2020) 14086-14090.
[95] H. Valdés, M. Sánchez-Polo, J. Rivera-Utrilla, C.A. Zaror, Effect of ozone treatment on surface properties of activated carbon, Langmuir, 18 (2002) 2111-2116.
[96] R. Gonzalez-Olmos, F.-D. Kopinke, K. Mackenzie, A. Georgi, Hydrophobic fe-zeolites for removal of MTBE from water by combination of adsorption and oxidation, Environmental Science & Technology, 47 (2013) 2353-2360.

3 Overview of the following manuscripts

In the manuscript 3.1 “Degradation of perfluorooctanoic acid adsorbed on Fe-zeolites with molecular oxygen as oxidant under UV-A irradiation”, we established for the first time the photochemical degradation of PFOA under UV-A irradiation after adsorption on Fe-doped zeolites. We investigated the effects of reaction pH, adsorption of PFCAs, coexisted inorganic ions, atmosphere, and long-term reusability. We finally proposed a photochemical PFOA degradation mechanism with zeolite-bound iron species as catalytic sites for carboxylate-to-metal charge transfer. It offers a novel approach for the removal of the highly recalcitrant PFOA from contaminated waters. Using Fe-zeolites as both adsorbent and photocatalyst could provide guidance in the design of new technological approaches for degradation of PFOA.

In the manuscript 3.2 “Photodegradation of perfluorooctanesulfonic acid on Fe-zeolites in water”, we applied Fe-zeolites photocatalytic system from perfluorinated *carboxylates*, i.e., PFOA, now to perfluorinated *sulfonates*, i.e., PFOS. PFOS is known as highly resistant towards electron-transfer reactions with, e.g., sulfate radicals (whereas PFOA reacts). The photochemical degradation of PFOS after adsorption on Fe-zeolites was triggered under UV-C irradiation. The resulting byproducts, i.e., short-chain PFCAs, are desorbed into the aqueous phase. Their complete mineralization can be achieved in the regeneration solution by combination with UV activation of sodium persulfate. It is indicated that PFOS photochemical degradation is initiated by electron transfer from sulfonate to iron. Additionally, we successfully applied the Fe-zeolites photocatalytic system to real ground water samples where trace PFOS was present.

In the manuscript 3 “Enhanced degradation of perfluorooctanoic acid by heat-activated persulfate in the presence of zeolite”, we developed an innovative treatment strategy for PFOA using heat-activated persulfate in the presence of zeolite (BEA35). BEA35 zeolite can not only remove PFOA by adsorption, but also facilitate the degradation of PFOA by means of heat-activated persulfate until a complete mineralization is achieved. The effects of reaction pH, zeolites dosages and types on PFOA degradation performances were studied. We applied the heat-activated persulfate/BEA35 system to ground water samples that contained trace PFOA. We also tried to provide a first estimation of the costs for treatment of PFOA-contaminated water in a realistic application scenario, i.e., zeolite-based fixed-bed adsorber. These findings provide an effective and efficient strategy for treatment of water containing traces of PFOA which can also inspire the development of remediation technologies for water contaminated by other micropollutants.

3.1 Degradation of perfluorooctanoic acid adsorbed on Fe-zeolites with molecular oxygen as oxidant under UV-A irradiation

Lin Qian[a], Anett Georgi[a], Rafael Gonzalez-Olmos[b] and Frank-Dieter Kopinke[a]*

[a] Helmholtz Centre for Environmental Research – UFZ, Department of Environmental Engineering, Permoserstrasse 15, D-04318 Leipzig, Germany

[b] IQS School of Engineering, Universitat Ramon Llull, Via Augusta 390, 08017 Barcelona, Spain

Abstract

Perfluorooctanoic acid (PFOA) is of emerging concern owing to its global distribution and environmental persistence. Efficient degradation approaches are so far limited. Herein, we demonstrate for the first time the photochemical degradation of PFOA under UV-A irradiation after adsorption on Fe-doped zeolites with molecular oxygen as the terminal oxidant. In a system containing 1 g L^{-1} PFOA-loaded Fe-zeolites, outstanding PFOA decomposition (> 99%) was achieved within 24 h under slightly acidic conditions ($pH \leq 5.5$). Short-chain perfluorinated carboxylic acids (PFCAs) are the main intermediates, beside fluoride and CO_2. No PFOA degradation occurs with Fe-free zeolites or dissolved ferric ions. Furthermore, we investigated the effects of pH, inorganic ions and gas atmospheres on PFOA degradation. A photochemical degradation mechanism with zeolite-bound iron species as catalytic sites for carboxylate-to-metal charge transfer is proposed. The presented study offers a novel approach for the removal of the highly recalcitrant PFOA from contaminated waters.

Keywords: Fe-zeolites; Degradation; UV-A; Heterogeneous photochemistry; Perfluorooctanoic acid

1. Introduction

Perfluorooctanoic acid (PFOA) is one of the most important perfluorinated organic compounds: it possesses unique physicochemical properties and has been widely used in industrial and consumer applications [1-3]. Recently, PFOA has received much attention because it is extremely persistent in the environment and is detected in groundwaters [4], sediments [5] and human beings worldwide [6]. In addition, PFOA is resistant to most conventional reduction and oxidation processes as well as biological degradation, due to the strong C-F bond [7-9]. It is practically inert to hydroxyl radicals (•OH) as it does not contain C-H bonds available for H abstraction [10].

Extensive research within the last two decades identified various reductive and oxidative pathways for PFOA degradation which in general require long reaction times and/or harsh conditions [11]. Reductive defluorination of PFOA requires solvated electrons that can be generated e.g., from the UV photolysis of iodide [12]. With respect to PFOA oxidation, it has been reported that electrochemical and photocatalytic treatments are efficient tools for degrading PFOA [13, 14]. Zhuo et al. used a Ti/SnO_2-Sb-Bi electrode for electrochemical decomposition of PFOA and claimed that the oxidation of PFOA was initiated through a direct one-electron transfer from the carboxylate group to the anode [15]. Li et al. used indium oxide for the photocatalytic degradation of PFOA, where PFOA is decomposed directly by photogenerated holes of indium oxide under UV-C irradiation [16]. Alternatively, sulfate radicals produced by the thermolysis or photolysis of peroxydisulfate ($S_2O_8^{2-}$) can decompose PFOA via the electron transfer from its carboxylate group to the sulfate radical [17, 18]. However, the efficiency of persulfates is rather low because the second-order rate constant for the reaction between sulfate radicals and PFOA ($k_{SO4-\bullet} = (1.7\text{-}4.4) \times 10^4\ M^{-1}s^{-1}$) is much lower than those for typical water matrix components (e.g., chloride or carbonate) [19].

PFOA itself can hardly be degraded by direct photolysis, as it has a very weak light absorbance in the UV range [20, 21]. Nevertheless, by adding a certain amount of ferric ions to the system under acidic conditions (pH ≤ 3.0), PFOA degradation is promoted. It has been suggested that under these conditions $[PFOA\text{-}Fe]^{2+}$ complexes are formed (reaction 1) and react under vacuum UV (V-UV, 185 nm) or UV-C (254 nm) irradiation to produce ferrous ions and carboxyl radicals via a ligand-to-metal charge transfer (reaction 2) [20, 22, 23]:

$$C_7F_{15}COO^- + Fe^{3+} \xrightarrow{pH\leq 3} [C_7F_{15}COO\text{-}Fe]^{2+} \qquad (1)$$

$$[C_7F_{15}COO\text{-}Fe]^{2+} \xrightarrow{\text{V-UV or UV-C}} Fe^{2+} + C_7F_{15}COO\bullet \tag{2}$$

Decarboxylation of $C_7F_{15}COO\bullet$ yields perfluorinated alkyl radicals $C_7F_{15}\bullet$. They may combine with molecular oxygen or hydroxyl radicals, or react with water to be decomposed further [24, 25]. In the presence of oxygen, ferrous ion can be re-oxidized to ferric ion, thus closing the catalytic iron cycle [23].

However, light with longer wavelength is unable to trigger such a ligand-to-metal charge transfer. Furthermore, the restricted operation pH range ($pH \leq 3.0$), low reaction rates and the production of iron sludge in this homogeneous photochemical system will limit its applications in practical wastewater treatment.

Although the principle of ligand-to-metal charge transfer is known for PFOA degradation in solution, it has not been tested and reported in a heterogeneous system. In the present study, we found out that by adding Fe-loaded zeolites instead of aqueous ferric ions, the photochemical degradation of PFOA can already occur under UV-A irradiation ($300\ nm < \lambda < 400\ nm$) instead of UV-C (e.g., at $\lambda \approx 254\ nm$). Furthermore, as the zeolite acts as adsorbent for PFOA, a combination of adsorptive enrichment and photochemical degradation can be achieved. The separable heterogeneous catalyst and adsorbent can be used to concentrate PFOA from typical trace level polluted water streams and facilitates degradation under well-controllable conditions. These potential advantages are significant for application and justify a detailed mechanistic and optimization study.

Zeolites can be loaded with iron ions by simple ion exchange procedures. It has been shown in several studies that Fe-loaded zeolites are active as heterogeneous Fenton-like catalysts for the degradation of various organic contaminants by hydrogen peroxide [26, 27]. Isolated mononuclear and binuclear iron species attached to acidic sites at the inner zeolite surfaces are generally attributed to high redox reactivity [28, 29]. In addition, Gonzalez-Olmos et al. observed an acceleration of dissolved organic carbon (DOC) removal in phenol degradation using Fe-loaded zeolites as catalysts, and ascribed this effect to a photo-Fenton reaction at the iron sites inside the zeolite pores improving the degradation of carboxylic acid intermediates [30].

The present study makes use of specific colloidal µm-sized Fe-zeolites: Trap-Ox®, a material designed for groundwater treatment. The applied synthetic zeolites are of BEA framework type and were selected based upon an initial screening of PFOA adsorption to various zeolite types

[31]. Degradation of PFOA adsorbed to the Fe-zeolite under UV-A irradiation yields short-chain PFCAs as intermediates. Complete mass balances were obtained by means of an exhaustive extraction approach. The effects of pH, inorganic ions and gas atmospheres were investigated. Moreover, a degradation mechanism with molecular oxygen (O_2) as the final oxidant is proposed.

2. Experimental Section

2.1. Chemicals and Materials.

All chemicals were in reagent grade and used without further purification, where not otherwise stated. Deionized water was used for the preparation of all solutions and suspensions. The Trap-Ox® zeolites BEA35 and Fe-BEA35 were provided by Clariant Produkte GmbH (Germany) and INTRAPORE GmbH (Germany), respectively. The number 35 represents the molar ratio of SiO_2/Al_2O_3 for both zeolites. The BEA framework type is characterized by channels with 12 T atoms (T = Si or Al) having diameters of around 6.6-6.7 Å for the larger straight channels and 5.6-5.7 Å for the smaller zig-zag channels [32, 33]. Iron(III) oxide nanopowder (<50 nm particle size), PFOA ($C_7F_{15}COOH$, 96% purity) and heptafluorobutyric acid (HFBA, C_3F_7COOH, 98% purity) were obtained from Sigma Aldrich. Perfluorohexanoic acid (PFHeA, $C_5F_{11}COOH$, 98% purity), perfluoropentanoic acid (PFPeA, C_4F_9COOH, 97% purity) and perfluoropropionic acid (PFPrA, C_2F_5COOH, 97% purity) were obtained from J&K Scientific. Perfluoroheptanoic acid (PFHpA, $C_6F_{13}COOH$, 97% purity) was obtained from Alfa Aesar. Trifluoroacetic acid (TFA, CF_3COOH, 99% purity) was obtained from Fluka.

2.2. Catalyst Pre-treatment.

In this study, commercially available Fe-BEA35 was used as adsorbent and catalyst. Preliminary experiments showed that the original Fe-BEA35 contains a certain amount of labile iron which is potentially leached during the reaction. Therefore, a pretreatment procedure was applied in order to stabilize iron as Fe^{3+} and remove any leachable iron by competitive exchange with potassium ions under acidic conditions [34]: 4 g of Fe-BEA35 in a 50 mL plastic centrifuge vial was mixed with 40 mL of 0.1 M KNO_3 (pH = 3.0) and 100 µL of 30 wt-% H_2O_2 solution. The suspension was shaken overnight, centrifuged at 2500 rpm for 5 min and the supernatant was removed. This washing procedure was repeated a second time (2 h contact), after which the solid was washed twice with 20 mL deionized water (1 h contact). Finally, the Fe-BEA35 was dried in an oven at 80 °C.

2.3. Photochemical Procedures and Reusability Test.

Where not otherwise stated, an aqueous PFOA solution (100 mL, 48 µM) was mixed with 0.1 g of Fe-BEA35 in a 200 mL glass bottle followed by shaking for 24 h in order to obtain a homogeneous suspension. The calculated concentrations of total iron in Fe-BEA35 and PFOA under these conditions are 2.32×10^{-4} M and 4.83×10^{-5} M, respectively. In one set of experiments, the PFOA concentration was increased by a factor of 10. 0.1 M HCl and 0.1 M NaOH were used to adjust pH values. 30 mL suspension was taken to a 40 mL quartz bottle equipped with a Mininert^{TM} valve. The suspension was purged with oxygen or nitrogen gas for 10 min shortly before UV irradiation. The quartz bottle was shaken during the degradation process with 240 rpm to ensure a good dispersion of the zeolite particles (see Figure S1, Supporting Information (SI)). The reactions under nitrogen atmosphere were performed in a nitrogen-filled glovebox in order to preclude penetration of oxygen into the reaction vessels. For irradiation, a mercury lamp (either 4 W, UV-A, central wavelength 365 nm, or 4 W, UV-C, central wavelengths 254 nm, both from Herolab GmbH Laborgeräte, Germany) was placed beneath the plane reactor basal face, which was made from quartz glass. The photon flux was determined by means of ferrioxalate actinometry to be 4.47×10^{-6} mol s^{-1} under UV-A and 4.54×10^{-6} mol s^{-1} under UV-C, respectively. The spectral curves of these two UV lamps are shown in Figure S2. The distance between the UV lamp screen and the bottom of the reactor was 20 mm. Details of the reactor setup are shown in Figure S1.

Samples of the reaction suspension were taken at certain time intervals. In order to determine the total amounts of PFOA and byproducts (including adsorbed fractions), an exhaustive extraction approach was used as follows: 100 µL aliquots of suspension were taken and sulfuric acid was used to adjust the suspension to pH 2, and then extracted with 2 mL acetonitrile for 24 h. The suspension was centrifuged at 2500 rpm for 5 min, and the clear supernatant was taken for LC-MS analysis. The applied extraction method was developed in preliminary tests where acetonitrile extraction at various pH values was studied. Acidic conditions showed the highest PFOA recovery. Fluoride and the freely dissolved acid concentrations in the aqueous phase were determined by IC and LC-MS analysis, using the clear supernatants obtained by centrifugation of 1 mL suspension aliquots (2500 rpm for 5 min).

UV-A irradiation leads to degradation of PFOA into short-chain PFCAs which are released into the aqueous phase thus regenerating the adsorbent. For a complete mineralization of these degradation products, the aqueous phase of the suspension in one experiment was subsequently treated by UV-C activation of sodium persulfate as follows: the UV-A irradiated suspension was centrifuged at 2500 rpm for 5 min to separate the zeolite particles which were practically free of residual PFCAs. The clear supernatant was taken and 8.4 mM sodium persulfate was added once every 2 hours, followed by UV-C irradiation until all of the short-chain PFCAs were decomposed.

For catalyst reusability tests (1 g L^{-1} Fe-BEA35, $C_{0,\mathrm{PFOA}}$ = 48 μM, pH_0 = 5.5, oxygen purged), after every irradiation period the supernatant was removed and replaced by the same volume of fresh aqueous PFOA solution. After shaking for 1 day for adsorption equilibration, the suspension was ready for the next irradiation run.

2.4. Analysis.

PFOA and its degradation products PFHpA (C7), PFHeA (C6), PFPeA (C5), and PFBA (C4) were measured by means of a HPLC system coupled to a single-stage quadrupole mass spectrometer with electrospray ionization (LCMS-2020; SHIMADZU Corp.). Aliquots of 3 μL of the solution containing the target compounds were injected by an auto-sampler into a 100 mm × 2 mm Gemini C6-Phenyl column (110 Å pore and 3 μm particle size, Phenomenex) at 40 °C. The mobile phase was a combination of 30 vol-% solvent A (10 mM ammonium acetate dissolved in 90 vol-% deionized water and 10 vol-% methanol) and 70 vol-% solvent B (10 mM ammonium acetate dissolved in 90 vol-% methanol and 10 vol-% deionized water), delivered at a flow rate of 0.3 mL min^{-1} with a total run time of 33 min. The correlation coefficients (R^2) of the calibration curves for PFOA and the other acids were ≥ 0.99 for sample concentrations ≤ 1 mg L^{-1}. PFPrA (C3), TFA (C2). Fluoride concentrations were analyzed by means of an IC DX 500 ion chromatograph (Dionex) equipped with an anion suppressor (ASRS300), conductivity detector (IC 25) and an IonPac AS11-HC column (250 mm × 4 mm) using a flow rate of 1 mL min^{-1} and the following eluent gradient: 1 mM KOH from 0 to 8 min, increased linearly to 30 mM KOH over 20 min and held at 30 mM KOH for 2 min. In this study, the defluorination ratio (d_{F^-}) is calculated as follows:

$$d_{F^-} = \frac{C_{\mathrm{F}^-}}{15 \times C_0} \times 100\% \qquad (3)$$

where C_{F^-} is the fluoride concentration (μM) and C_0 is the initial concentration of PFOA (μM). The factor 15 represents the number of fluorine atoms in one PFOA molecule. Complete defluorination of PFOA results in d_{F^-} = 100%.

The analysis of gas phase intermediates was conducted on a GC/MS (GCMS-QP2010, SHIMADZU Corp.) by means of headspace sampling (25 µL gas) after 24 h irradiation. The GC separation column was a 30 m DB1 (0.32 mm inner diameter, 0.25 µm film thickness). The MS was operated in the SCAN-mode (m/z = 41-500 amu). The injector temperature was set at 150 °C, and the GC oven program was isothermal at 35 °C.

A Zetasizer Nano ZS (Malvern Instruments Ltd, U.K.) was used for dynamic light scattering (DLS) and zeta potential measurements. Scanning electron microscopy images were recorded with a Zeiss Merlin VP scanning electron microscope (Zeiss, Germany). X-ray photoelectron spectroscopy (XPS) measurements were performed on an Axis Ultra photoelectron spectrometer (Kratos, Manchester, UK) using monochromatized Al Kα radiation (*hv* = 1486.6 eV). X-ray powder diffraction (XRD) patterns were obtained on a Bruker D8-Advance diffractometer. For details of XPS and XRD measurements see SI part.

UV–vis diffuse reflectance spectra (DRS) of zeolite samples were obtained for the 10 g L^{-1} zeolite suspensions using a Varian Cary 3 spectrophotometer with a diffuse reflectance accessory in the 190–600 nm range. $BaSO_4$ powder was used as a non-absorbing reference standard. The spectra were converted according to the Kubelka–Munk function and deconvoluted into sub-bands with Gaussian peak shape using Origin 2018 [31]. Spectra were interpreted by comparing the positions of the resulting peaks with literature data [31, 35, 36].

3. Results and Discussion

3.1. Catalyst characterization

As shown in Figure 1, Fe-BEA35 zeolites comprise joined spherical particles without sharp edges. According to the SEM images, the diameter of primary particles is around 0.5 µm. Table S1 shows the particle size distribution of Fe-BEA35 in suspension, which was determined by means of dynamic light scattering revealing a mean diameter of 0.86 µm. It was in good accordance with the particle size determined by laser diffraction for the dry Fe-BEA35 powder samples. The XRD pattern was in good agreement with the BEA framework type as shown in Figure S3 [37]. The iron content of the Fe-BEA35 was measured to be 1.3 wt-% by X-ray fluorescence analysis. In addition, the peak at binding energy of 711.2 eV in Fe 2p 3/2 XPS spectra of Fe-BEA35 indicates the existence of Iron (III) (Figure S4) [38]. A BET surface area of 600

m^2 g^{-1} and a total pore volume of 0.42 cm^3 g^{-1} were determined from N_2 adsorption/desorption measurements (for details see SI part).

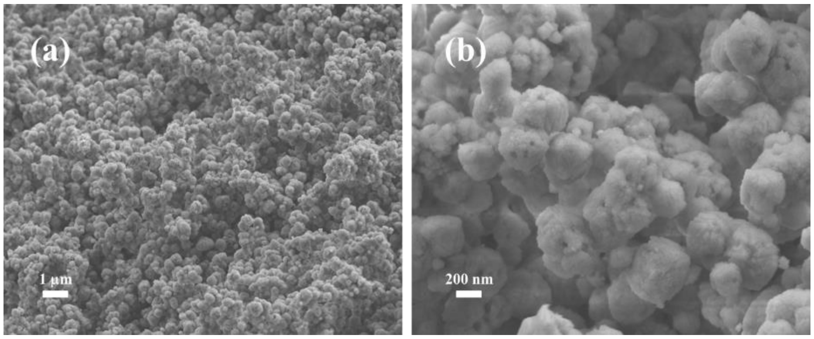

Figure 1. Scanning electron microscope (SEM) images of Fe-BEA35.

3.2. Photochemical degradation of PFOA in the presence of Fe-BEA35 under UV-A irradiation.

From the point of view of application, UV-A has a number of advantages over shorter wavelengths, including potential use of solar irradiation or LEDs and less demands on material selection for reactor design. A typical reaction suspension contained 1 g L^{-1} Fe-BEA35 and $C_{0,\mathrm{PFOA}}$ = 48 µM with $pH_0 = 5.5$. Under these conditions, PFOA was predominantly in the adsorbed state, as only 16% of the initially added PFOA was detected in the aqueous phase after the pre-equilibration period of 24 h, i.e., before start of the irradiation period. Thus, the initial loading of PFOA on the zeolite was 16.8 mg g^{-1}. In order to follow the total concentrations, residual PFOA and intermediates were extracted from the zeolite into the liquid phase by adding sulfuric acid to adjust pH to 2, and then introducing 95 vol% acetonitrile for extraction. The recovery of PFOA in this procedure (before irradiation) was nearly complete, i.e. (94 ± 3)%.

In order to elucidate the photochemical degradation mechanism, control experiments were carried out under the same conditions in the presence of non-Fe-doped BEA35 and in the absence of zeolite but presence of ferric ions (pH_0 = 3.0 and 5.5, Figure 2(a)). As revealed by previous studies, PFOA has almost no absorption in the UV-A range and the direct photolysis of PFOA does not take place in relevant time scales [20, 21]. In addition, PFOA degradation within 24 h is also insignificant in the presence of 200 µM Fe^{III} at pH = 3.0 (dissolved Fe) and 5.5 (colloidal Fe) under UV-A irradiation, as indicated by the two control experiments. No PFOA degradation was also observed with BEA35 (no iron). However, in the presence of Fe-BEA35, up to 90% of the initial PFOA was decomposed after 6 h of UV-A irradiation, and complete degradation (> 99%) with d_{F^-} = 38% was achieved within 24 h. When applying a high-surface area iron oxide, i.e., iron (III) oxide nanoparticles (Figure S5), almost no PFOA degradation was observed within 24 h. Thus, only the combination of UV-A irradiation and Fe-BEA35 effected a significant PFOA degradation and the Fe speciation within the zeolite obviously plays an important role.

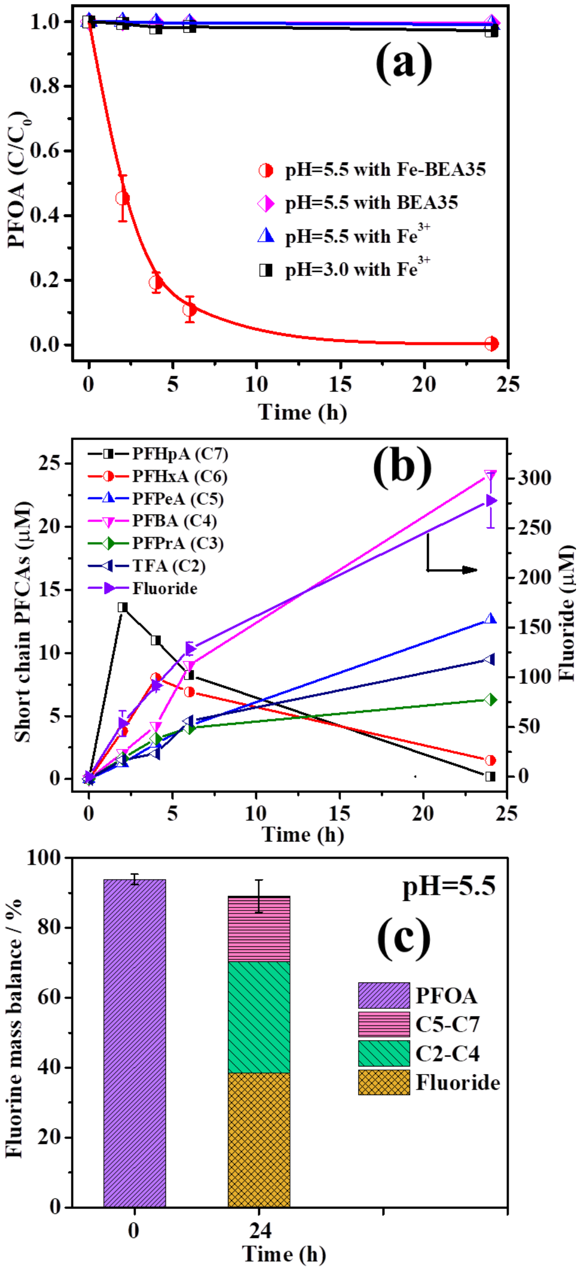

Figure 2. Degradation of PFOA under UV-A irradiation ($C_{0,\mathrm{PFOA}}$ = 48 µM, oxygen atmosphere, 1 g L^{-1} (Fe-)BEA35 and $C_{0,\mathrm{Fe}^{3+}}$ = 200 µM, where applied). (a) Comparison of degradation in presence of ferric ions, Fe-BEA35 and BEA35 (pH$_0$ = 3 and pH$_0$ = 5.5). (b) Formation of short-chain intermediates and fluoride in the presence of Fe-BEA35 (1 g L^{-1}, pH$_0$ = 5.5). (c) Mass balance of fluorine for the above experiment. Mass balance at 0 h represents F detected as PFOA in ACN extract of zeolite suspension before start of reaction, and at 24 h is composed of fluorine detected as C2-C4 PFCAs and fluoride in aqueous phase of suspension as well as C5 to C7 PFCAs in ACN extract of suspension. Error ranges represent average deviations of single values from the mean of triplicate assays in Figures 1(a) and (b). Error bars for individual PFCAs were omitted for the sake of clarity but are exemplarily shown for PFPeA. The cumulative error is shown in Figure 1(c). Lines are added to guide the eye.

In spite of its almost complete degradation, only a partial defluorination of PFOA was achieved within 24 h. We found six shorter-chain perfluorinated carboxylic acids (PFCAs) with 2 to 7 carbon atoms. They were identified and quantified by LC/MS (C7 to C4) and IC (C3 and C2) analysis. Their concentration time profiles, shown in Figure 2(b), indicate that the longer-chain PFCAs are decomposed stepwise towards shorter-chain PFCAs during the irradiation. The possible reason for steadily increasing concentrations of C5 to C2 PFCAs was further investigated by means of adsorption experiments.

X_{sorb} and X_{free} as the fractions of adsorbed and freely dissolved PFCA, respectively, were calculated according to eqs. 4 and 5, where $C_{\mathrm{PFCA,free}}$ and $C_{\mathrm{PFCA,total}}$ are the freely dissolved and total PFCA concentrations added, respectively.

$$X_{\mathrm{sorb}} = 1 - X_{\mathrm{free}} \tag{4}$$

$$X_{\mathrm{free}} = C_{\mathrm{PFCA,free}} \,/\, C_{\mathrm{PFCA,total}} \tag{5}$$

As shown in Figure 3, X_{sorb} decreases with decreasing chain lengths, e.g., the distribution between X_{sorb} and X_{free} in 1 g L^{-1} zeolite suspensions changes from 84:16 for PFOA to 10:90 for PFBA. This may explain why the shorter-chain PFCAs are accumulated in irradiated zeolite suspensions: they are preferably released from the zeolite phase where the photochemical reaction takes place.

It can be hypothesized that complex formation is a pre-requisite for photochemical degradation of PFCAs according to eqs. 6 and 7:

$$\mathrm{C_nF_{2n+1}COO^-} + \mathrm{Fe^{3+}}\text{-zeolite} \longleftrightarrow [\mathrm{C_nF_{2n+1}COO\text{-}Fe}]^{2+}\text{-zeolite} \tag{6}$$

$$[\mathrm{C_nF_{2n+1}COO\text{-}Fe}]^{2+}\text{-zeolite} \xrightarrow{\text{UV-A}} \mathrm{C_nF_{2n+1}COO}\cdot + \mathrm{Fe^{2+}}\text{-zeolite} \tag{7}$$

Based on this mechanism, a simplified rate equation (8) can be derived:

$$\frac{\mathrm{d[PFCA]}}{\mathrm{dt}} = -k \cdot C_{[\mathrm{C_nF_{2n+1}COO\text{-}Fe}]^{2+}\text{-zeolite}} = -k \cdot X_{\text{complex}} \cdot C_{\text{PFCA, total}} \tag{8}$$

where X_{complex} (with $0 \leq X \leq 1$) is the fraction of PFCA in reactive complexes. To better illustrate the PFCAs complex formation, a schematic diagram of PFOA adsorbed on Fe-BEA35 was displayed in Figure 4. Two adsorptive states of PFOA are presented on the zeolite: complexed PFOA (i.e. specifically adsorbed PFOA at ferric ions) and non-specifically adsorbed PFOA. The complexed PFOA is signified by its carboxylic group in the close vicinity to the ferric ions, which enables the carboxylate-to-metal charge transfer upon irradiation, while the non-specifically adsorbed PFOA has less or no chance to allow the charge transfer as its carboxylic group is not able to reach the ferric ions. While X_{complex} cannot be easily determined, the overall degree of adsorption (X_{sorb}) is obtained experimentally (eqs. 4 and 5). Thus, using lumped rate coefficients k' and k''

$$k' = k \cdot X_{\text{complex}}/X_{\text{sorb}} \tag{9}$$

$$k'' = k' \cdot X_{\text{sorb}} \tag{10}$$

eq. 8 can be simplified to a pseudo-first-order rate law:

$$\frac{\mathrm{d[PFCA]}}{\mathrm{dt}} = -k' \cdot X_{\text{sorb}} \cdot C_{\text{PFCA, total}} = -k'' \cdot C_{\text{PFCA, total}} \tag{11}$$

The X values and the ratio $X_{\text{complex}}/X_{\text{sorb}}$ are related to compound properties such as chain lengths of PFCAs, which determine their hydrophobicity and thus their tendency for non-specific adsorption into the zeolite. The composition of the aqueous phase, e.g., pH value and concentrations of competing inorganic ions as well as other factors, can also affect $X_{\text{complex}}/X_{\text{sorb}}$, which will be discussed in the following chapters. In addition, it is worth noting that pseudo-first-order kinetics cannot describe the whole degradation curve according to the experiment, but gives satisfying fitting within the initial reaction period (0 – 6 h) (Figure S6).

The fluorine mass balance during Fe-zeolite-catalyzed photo-degradation of PFOA is shown in Figure 2(c). The fluorine in the suspension is grouped into four contributions: the remaining PFOA, C5 to C7 PFCAs, C2 to C4 PFCAs and fluoride. The initial recovery by acetonitrile extraction is around (94 ± 3)% after 24 h adsorption. The final recovery of fluorine in the form of the various products related to total PFOA initially added is (89 ± 5)% after 24 h of irradiation. Some highly volatile fluorinated alkanes, i.e., C_nHF_{2n+1} were formed as detected by GC/MS headspace analysis (see Table S2) but only in trace amounts (<0.1 mol-% of initial PFOA).

It should be pointed out that the remaining shorter-chain products desorb from the zeolite and accumulate in the aqueous phase. Thus, the process can be exploited in terms of regeneration of the adsorbent for PFOA adsorption. Comparing with PFOA, the toxicity of these shorter-chain products is lower [39-41]. Nevertheless, the aqueous phase containing shorter-chain products is a concentrated regeneration solution which can be subject to further degradation, e.g., by oxidation with sulfate radicals produced from UV activation of persulfate [17, 19]. To test whether a complete mineralization of PFOA by a UV/persulfate post-treatment of the regeneration solution is feasible, the aqueous phase of the 24 h-UV-A irradiated PFOA/zeolite suspension was further treated by UV-C activation in the presence of sodium persulfate. A certain amount of sodium persulfate was added portion-wise every two hours to minimize the self-scavenging effect otherwise would occur when a large amount of sodium persulfate is added at a time. As shown in Figure S7, the shorter-chain PFCAs (C2, C3, C4, C5 and C6) were nearly completely decomposed within 10 h. Thus, a nearly complete defluorination (86±4 %) and mineralization of PFOA was achieved by the combined process (Figure S8). It is worth noting that the degradation of PFCAs by sulfate radicals is strongly suppressed by typical water matrix components such as chloride [19]. Thus, it is obvious that for future design of a technical process, the sequence of steps is the key to improved efficiency, i.e., I) PFOA adsorption out of e.g., contaminated groundwater into zeolite particles, II) separation of particles and III) PFOA photodegradation inside the zeolite releasing shorter-chain acids into a controllable regeneration solution (water largely free of chloride, carbonate and natural organic matter as typical radical scavengers) which can be IV) post-treated by UV/persulfate.

3.3. Effect of the adsorption of PFCAs on the photochemical degradation of PFOA.

One of the driving forces of PFCAs adsorption on zeolites is the hydrophobic effect, as the hydrophobic perfluoroalkyl chains of PFCAs find a suitable environment in the narrow zeolite channels. The electrostatic repulsion between terminal aluminol groups (internal surface) and silanol groups (external surface) of Fe-BEA35 and carboxylate head groups of PFCAs counteracts the adsorption [42]. As the Al content in the zeolite is low (1 Al atom per 17 Si atoms) it can be assumed that zeolite-bound Fe^{3+} ions cannot be not coordinatively saturated by sufficient negatively charged aluminol groups in close proximity but need further ligands, e.g., OH^- or H_2O and can also bind PFCA anions. As can be seen from Figure 3, adsorption affinity of PFCAs decreases with decreasing chain length and thus decreasing hydrophobicity. Thus, the complexing ability of the zeolite-bound Fe^{3+} for PFCAs is obviously not strong, instead one can assume a synergistic effect of electrostatic interactions between $R–COO^-$ and Fe^{3+} sites together with hydrophobic interactions of the perfluoroalkyl chain in the zeolite channels.

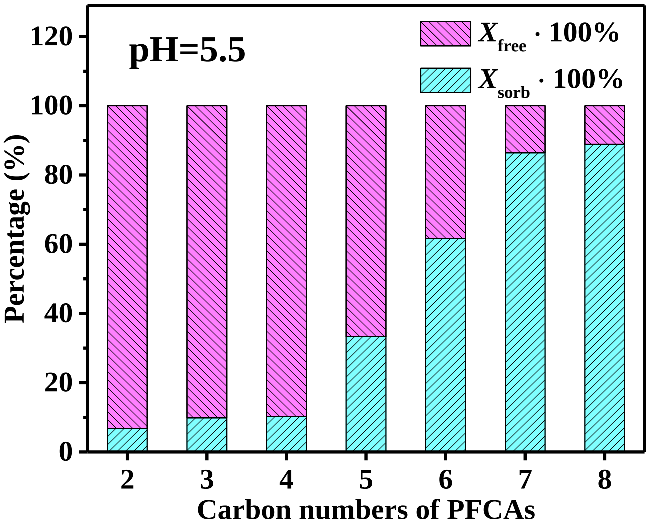

Figure 3. Results of adsorption experiments: distribution of PFCAs with various chain lengths between zeolite Fe-BEA35 (X_{sorb}) and the aqueous phase (X_{free}) after 4 days shaking. $C_{Fe\text{-}BEA35}$ = 1 g L^{-1}, $C_{0,PFCAs}$ = 48 μM and pH_0 = 5.5.

It is considered that the performance of the photochemical degradation of PFCAs is dependent on two steps: i) the adsorption of PFCAs into the zeolites, and ii) the formation of the complex between PFCAs and ferric ions. Since the pK_a values of the C2 and C8 PFCAs are comparably low, i.e., close to 0 [43], it is reasonable to speculate that the complexing abilities should not differ greatly in the series of PFCAs. The effect on the photochemical degradation of PFCAs caused by different complexing abilities of PFCAs can thus be neglected.

In order to understand the impact of adsorption on the photochemical degradation of PFCAs, the degradation of PFOA and PFBA as PFCAs with different perfluoroalkyl chain lengths, was investigated and compared in Figure 5. By fitting the degradation curves using pseudo-first-order kinetics in accordance with eq. 11, it was found that $k_{\mathrm{obs,PFOA}}$ is by a factor of 10 higher than $k_{\mathrm{obs,PFBA}}$. This is in line with a factor of 8.4 in X_{sorb} for PFOA compared to PFBA. Thus, it can be concluded that the hydrophobic interactions provided by the zeolite channels for the perfluoroalkyl chains of PFCAs play an important role in the iron-catalyzed photodegradation process. Indeed, a lower X_{sorb} value indicates a smaller possibility of PFBA to be adsorbed and complexed, resulting in an accumulation of PFBA up to the end of the 24 h irradiation time (Figure 2(b)).

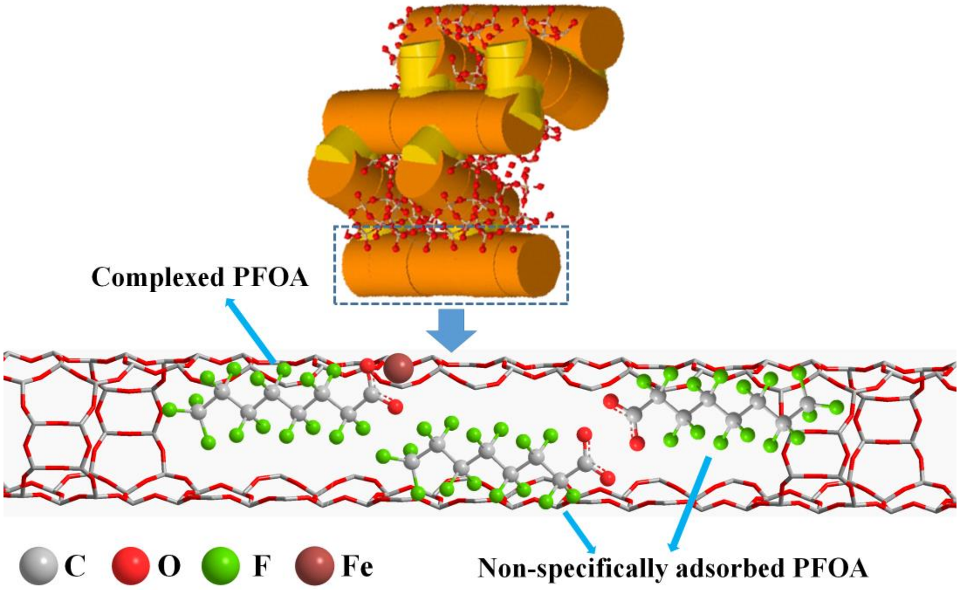

Figure 4. Scheme of PFOA configurations on Fe-BEA35 with and without specific adsorption. Up: Cutaway of BEA framework with 2-1-1 unit cells; Down: Zoom-in of a single channel. The complexed PFOA means the specifically adsorbed PFOA at ferric ions.

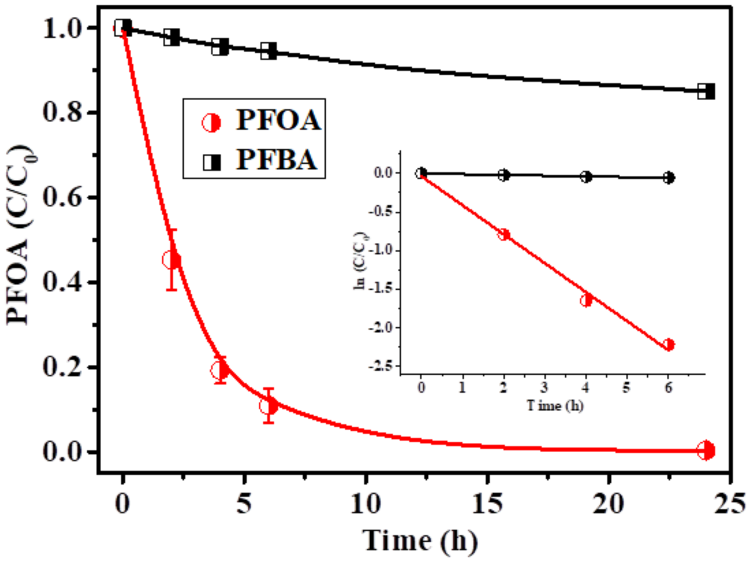

Figure 5. The comparison of PFOA and PFBA degradation in the presence of Fe-BEA35 (1 g L^{-1}) under UV-A irradiation. $C_{0,\mathrm{PFCAs}}$ = 48 µM, pH$_0$ = 5.5, oxygen atmosphere. Error bars represent standard deviations of triplicate assays. Lines are added to guide the eye.

3.4. Effect of pH on the photochemical degradation of PFOA.

Figure 6(a) and (b) show the degradation and defluorination behaviors of PFOA within 24 h UV-A irradiation at various initial pH conditions. The distribution of PFOA between zeolite and aqueous solution at various initial pH values is shown in Table 1. The zeta potential of Fe-BEA35 at different pH values is shown in Table S3. The zeta potential of Fe-BEA35 becomes more negative with increasing pH values. However, it should be noticed that zeta potential reflects the charge at the external particle surface only whereas the inner surfaces provide the highest contribution to specific surface area and adsorption. The initially adsorbed fractions of PFOA (X_{sorb}) on Fe-BEA35 are 98% and 84% at pH 3.0 and 5.5, respectively. The extents of PFOA degradation and the corresponding d_{F^-} are identical for the reactions under these acidic conditions (pH$_0$ = 3.0 or 5.5). However, under neutral and alkaline conditions (pH$_0$ = 7.0 and 9.0), PFOA degradation is significantly inhibited, although about 70% is still in an adsorbed state (Table 1). More precisely, increasing pH from 5.5 to 7.0 and 9.0 results in only 16% and 18% reduction in X_{sorb} but in 21 and 35 times higher PFOA half-life, respectively. This points to significant changes in PFOA speciation within the zeolite when pH changes. When pH increases, though the majority of PFOA remains adsorbed, a fraction of complexed PFOA is likely shifted to non-specifically adsorbed sites as is shown in Figure 4. The possible reason for this PFOA speciation variation is the change of ligand environment within the zeolite when pH is increasing. The ferric ions can complex with other ions, e.g., they have a strong affinity to hydroxide ions [44]. As a consequence of pH increasing, more hydroxide ions will compete with the complexed PFOA at the ferric ions and push the latter to non-specifically adsorption sites. Similar effect is assumed for the shorter chains PFCAs as well. In short, the negative influence of pH increasing on PFOA photochemical degradation is attributed to a lower fraction of complexed PFOA (PFOA-Fe^{3+}) in favor of its non-specifically adsorbed fraction caused by a change in the ligand environment: replacement of H_2O by OH^- ligands at the iron. As mentioned in the previous section, the adsorption of PFOA on zeolites is a precondition, but the specific complexation between PFOA and ferric ions in the zeolite is the key factor for its photochemical degradation. Additionally, the pH value also influences the PFCAs adsorption. When the pH value decreases, the density of negative surface charges is reduced. The electrostatic repulsion between PFOA and zeolite becomes weaker, which promotes the adsorption. To sum up, acidic or slightly acidic conditions are optimal for this system.

Table 1. Adsorbed fraction (X_{sorb}, in %) and loading of PFOA on zeolite (in mg g^{-1}) after 24 h shaking at various initial pH values in aqueous suspension. $C_{0,\text{PFOA}} = 48$ µM and $C_{\text{Fe-BEA35}} = 1$ g L^{-1}

	pH = 3.0	**pH = 5.5**	**pH = 7.0**	**pH = 9.0**
X_{sorb} (%)	98	84	68	66
Loading of PFOA on zeolite (mg g^{-1})	20	17	14	13

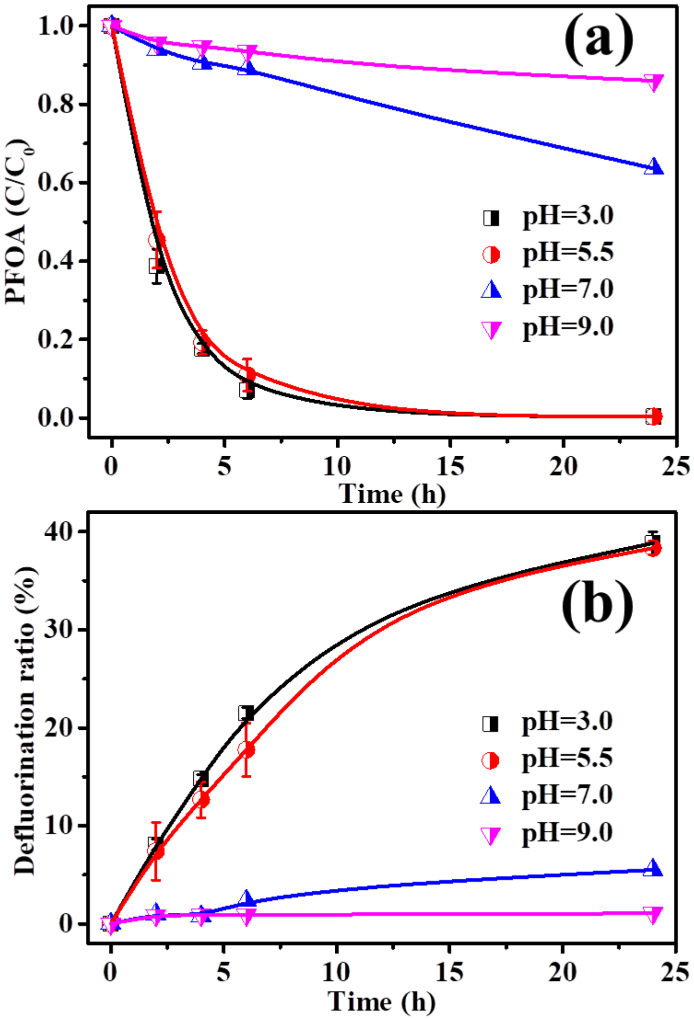

Figure 6. Degradation of PFOA under UV-A irradiation in the presence of Fe-BEA35 (1 g L^{-1}) at various initial pH values. Time course of (a) residual PFOA concentration and (b) defluorination ratios (d_{F^-}). $C_{0,\mathrm{PFOA}}$ = 48 µM, oxygen atmosphere. Error ranges represent average deviations of single values from the mean of triplicate assays. Lines are added to guide the eye.

3.5. Effect of inorganic ions and atmosphere on photochemical degradation of PFOA.

The influence of four inorganic anions, i.e., sulfate (SO_4^{2-}), nitrate (NO_3^-), chloride (Cl^-) and perchlorate (ClO_4^-), on PFOA degradation is presented in Figure 7(a) and Table 2. Apart from SO_4^{2-}, the addition of other anions has very limited or almost no influence on PFOA degradation kinetics and defluorination. Two possible effects can be considered as negative impacts: (i) competitive complexation with ferric ions;[44] and (ii) capture of hydroxyl radicals (•OH) which are formed by the photolysis of ferric species and water under UV-A irradiation (eq. 12) [45].

$$\text{Fe}^{3+}\text{-zeolite} + \text{H}_2\text{O} \xrightarrow{\text{UV- A}} \text{Fe}^{2+}\text{-zeolite} + \bullet\text{OH} + \text{H}^+ \quad (12)$$

A significant inhibiting effect on PFOA degradation and defluorination is observed in the presence of SO_4^{2-}. In fact, SO_4^{2-} rarely reacts with •OH, but it has the potential to coordinate with ferric ions in Fe-BEA35. The affinity for interaction between ferric ions and the anions follows the order of $OH^- > SO_4^{2-} > Cl^- > NO_3^- > ClO_4^-$ [44]. As a consequence, SO_4^{2-} may interfere most strongly with the complexation between PFOA and ferric ions, and thus reduce $k_{\text{obs,PFOA}}$ and d_{F^-}. The introduction of Cl^- has only a slight influence on $k_{\text{obs,PFOA}}$ and d_{F^-}, which may also be caused by the competitive complexation of ferric ions. Alternatively, Cl^- will react with •OH. Although •OH itself cannot attack PFOA, it can promote the re-oxidation of ferrous ions and may be involved in the conversion of intermediates, thus playing a significant role during defluorination of PFOA. Nevertheless, the presence of NO_3^- and ClO_4^- has practically no negative effect on $k_{\text{obs,PFOA}}$ and d_{F^-}, compared with the reference case where no salts were added.

Table 2. Defluorination ratios (d_{F^-}), pseudo-first-order degradation rate constants ($k_{\text{obs,PFOA}}$) for initial reaction period (6 h) and half-lives of PFOA degradation with Fe-BEA35 and UV-A irradiation under various reaction conditions. $C_{0,\text{PFOA}}$ = 48 μM and $C_{\text{Fe-BEA35}}$ = 1 g L^{-1}, inorganic salts were added (only where stated) at a concentration of 10 mM.

	pH = 3.0[a]	**pH = 5.5**[a]	**pH = 7.0**[a]	**pH = 9.0**[a]	**N_2**[b]	**Na_2SO_4**[c]	**NaCl**[c]	**$NaClO_4$**[c]	**$NaNO_3$**[c]
d_{F^-} after 24 h (%)	39 ± 1[d]	38 ± 1	5.5 ± 0.2	1.1 ± 0.1	12.0 ± 0.5	28 ± 1	32 ± 1	36 ± 1	33 ± 1
$k_{\text{obs,PFOA}}$ (h^{-1})	0.44 ± 0.02	0.38 ± 0.04	0.019 ± 0.005	0.011 ± 0.007	0.059 ± 0.016	0.063 ± 0.007	0.32 ± 0.06	0.35 ± 0.08	0.39 ± 0.10
PFOA $t_{1/2}$ (h)	1.6 ± 0.1	1.8 ± 0.2	37 ± 8	63 ± 25	12 ± 2	11 ± 1	2.2 ± 0.3	2.0 ± 0.4	1.8 ± 0.4

[a] The suspensions were initially purged with oxygen. pH values are initial values.

[b] The initial pH of suspension was 5.5 and the suspension was initially purged with N_2.

[c] The suspensions were initially purged with oxygen. The initial pH of suspensions was 5.5. C_{salt} = 10 mM

[d] Error ranges represent average deviations of single values from the mean of triplicate assays.

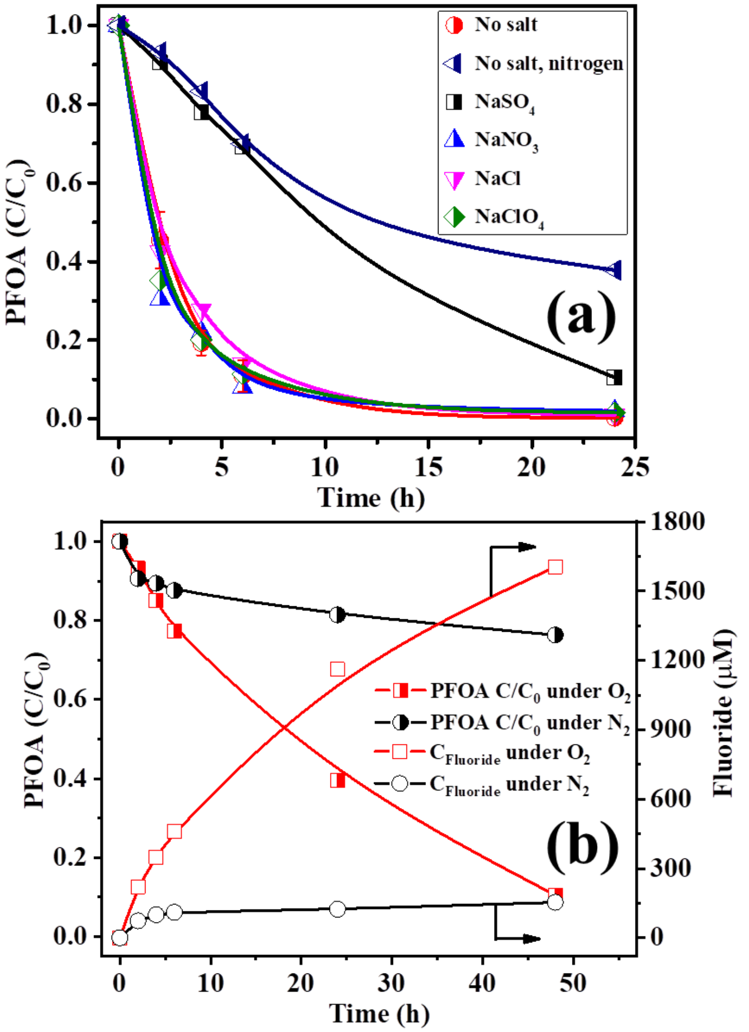

Figure 7. Effect of inorganic ions and gas atmosphere on photochemical degradation of PFOA in the presence of Fe-zeolite under UV-A light. $C_{0,\mathrm{PFOA}}$ = 48 μM or 480 μM, 1 g L^{-1} Fe-BEA35, 10 mM SO_4^{2-}, Cl^-, NO_3^-, and ClO_4^- were added where applied, pH_0 = 5.5 and oxygen atmosphere where not otherwise stated. (a) Influence of inorganic ions and atmosphere at $C_{0,\mathrm{PFOA}}$ = 48 μM. (b) Influence of atmosphere (O_2 or N_2) at $C_{0,\mathrm{PFOA}}$ = 480 μM. Lines are added to guide the eye.

In order to understand the mechanism of the photochemical degradation of PFOA better, the influence of dissolved oxygen on PFOA degradation and defluorination was investigated. Where not otherwise stated, reactions were conducted in closed vessels with a certain headspace volume of pure oxygen (10 mL O_2 per 30 mL of aqueous phase). The system was not purged with oxygen continuously because the amount of oxygen (446 μmol) in the headspace was sufficient for accepting all electrons released in total mineralization of PFOA (1.45 μmol). When the reaction was carried out under nitrogen atmosphere, the photochemical degradation of PFOA was strongly inhibited (Table 2 and Figure 7(a)). The d_{F^-} after 24 h irradiation decreased from 38% to 12%, and the $k_{\mathrm{obs,PFOA}}$ decreased from 0.23 h^{-1} to 0.040 h^{-1}. The role of oxygen in photochemical degradation of PFOA becomes even more obvious when a 10 times higher initial PFOA concentration (480 μM) was introduced. As seen in Table S4 and Figure 7(b), the d_{F^-} after 48 h irradiation time was 22.1% and 2.1%, and the $k_{\mathrm{obs,PFOA}}$ was 0.046 h^{-1} and 0.0045 h^{-1}, under oxygen and nitrogen atmospheres, respectively. These results clearly show that oxygen plays an important role in the photochemical degradation of PFOA. Molecular oxygen may be involved in at least three reactions: (i) it is the source for reactive species such as •OH and $•O_2H$, which may also promote the re-oxidation step as well as facilitate the mineralization of PFOA intermediates [25], (ii) it facilitates the re-oxidation of ferrous iron to ferric iron and thus closes the catalytic cycle as also discussed by Hori et al. [23], and (iii) O_2 is directly involved in the complex radical chemistry of PFCA degradation (eq. (16)).

3.6. Photochemical properties of Fe-BEA35.

In order to characterize the photochemical properties of Fe-BEA35, UV-vis-DRS values were measured. This technique is able to distinguish between different isolated iron species and iron oxide clusters. The spectra of Fe-BEA35 and BEA35 zeolites as well as the deconvolution of the spectrum of Fe-BEA35 are shown in Figure 8. The spectrum of Fe-BEA35 shows strong and broad absorption bands in the ultraviolet and visible range. Its deconvolution reveals five peaks. Based on literature sources [31, 35, 36], the absorption bands below 220 nm and around 280 nm are ascribed to Fe^{3+} ions in tetrahedral and octahedral coordination, respectively. The absorption band around 350 nm is ascribed to octahedral Fe^{3+} ions in small oligomeric iron oxide clusters. The absorption bands around 400 nm and above 450 nm are ascribed to larger iron-oxide particles. In various redox reactions catalyzed by Fe-zeolites, isolated iron sites are assumed to be more active than the iron oxide clusters [28]. In the present study, the photochemical degradation of PFOA on Fe-BEA zeolites takes place under UV-A irradiation. The overlap between the UV-A emission (320 to 380 nm, see Figure S2) and the absorption bands of isolated Fe^{3+} ions (especially those in octahedral coordination, 200 to 340 nm, see Figure 8) is in accordance with the hypothesis that these sites are involved in the carboxylate-to-metal charge transfer ($Fe^{3+} \leftarrow O$) under UV-A irradiation [36, 46]. Part of the adsorbed PFOA is assumed to be complexed with Fe^{3+} ions at such positions, so these PFOA-Fe^{3+}-zeolite complexes can be excited by UV-A irradiation and finally decomposed by decarboxylation. The distribution of iron species shown by the deconvolution also fits to the observation presented in Figure 8: not all the iron species in Fe-BEA35 are active in photochemical degradation of PFOA. In the absence of dissolved oxygen (i.e., without recycling of ferric iron), only 24% of 480 μM PFOA was converted after 48 h irradiation. This amount corresponds to 114 μM redox-active Fe^{3+} species of approx. 232 μM total iron content in 1 g L^{-1} Fe-BEA35. In other words, only about 50% of the Fe^{3+} present in the zeolite Fe-BEA35 is available as electron acceptor. Compared with Fe-BEA35, the UV-vis-DR spectrum of BEA35 exhibits no strong absorption bands, due to the absence of iron (Figure 8). In addition, we investigated the UV-vis-DR spectra of Fe-BEA35 with and without PFOA loading (Figure S9). Surprisingly, the two spectra are almost identical. As discussed above, the ferric ions have a strong affinity to hydroxide ions, so it can be speculated that only a small fraction of the adsorbed PFOA is actually in a complexed state. In this case, the absorption spectra of PFOA-Fe^{3+} complexes cannot be well characterized by UV-vis-DRS.

According to the UV–vis-DR spectrum of Fe-BEA35, it may be possible to improve the photochemical efficiency by shifting the irradiation to shorter wavelengths. As is shown in Figure 9, the degradation and defluorination behavior of PFOA is considerably enhanced under UV-C irradiation with 254 nm. The d_{F^-} after 24 h under UV-C irradiation was increased from 38% to 49%, and the $k_{\mathrm{obs,PFOA}}$ increased from 0.38 h^{-1} to 0.82 h^{-1}. The improvement in photochemical degradation of PFOA is reasonable, because the absorption band around 280 nm, referring to $Fe^{3+} \leftarrow O$ charge transfer in isolated Fe^{3+} ions, is the strongest sub-band. From the application point of view, however, UV-A irradiation has significant advantages over UV-C irradiation with respect to reactor equipment and potential use of LED lamps or even natural sunlight. Further optimization potential for the Fe-BEA35 catalyst lies in decreasing the proportion of iron oxide clusters and large iron-oxide particles, because their absorption bands around 350 nm and 400 nm compete for photons from UV-A irradiation and thus decrease the photochemical efficiency of this redox-catalyst.

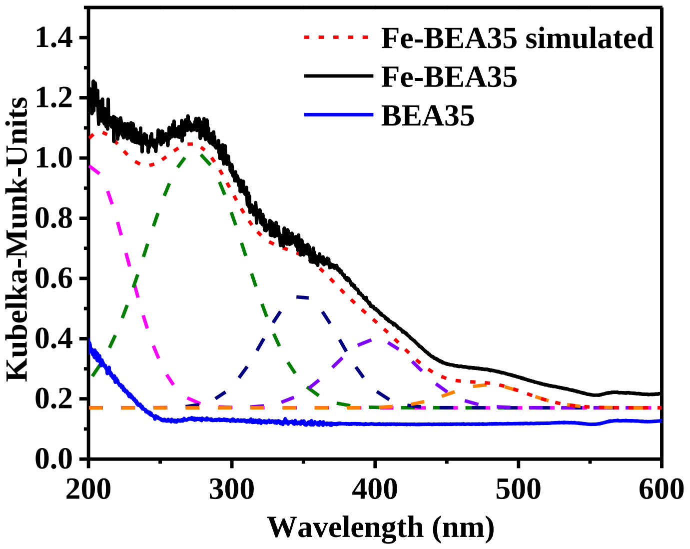

Figure 8. UV-vis-DR spectra of 10 g L^{-1} Fe-BEA35 suspension (black line) and 10 g L^{-1} BEA35 suspension (blue line), simulated deconvolution curves for UV-vis-DR spectra of Fe-BEA35 suspension (dashed lines).

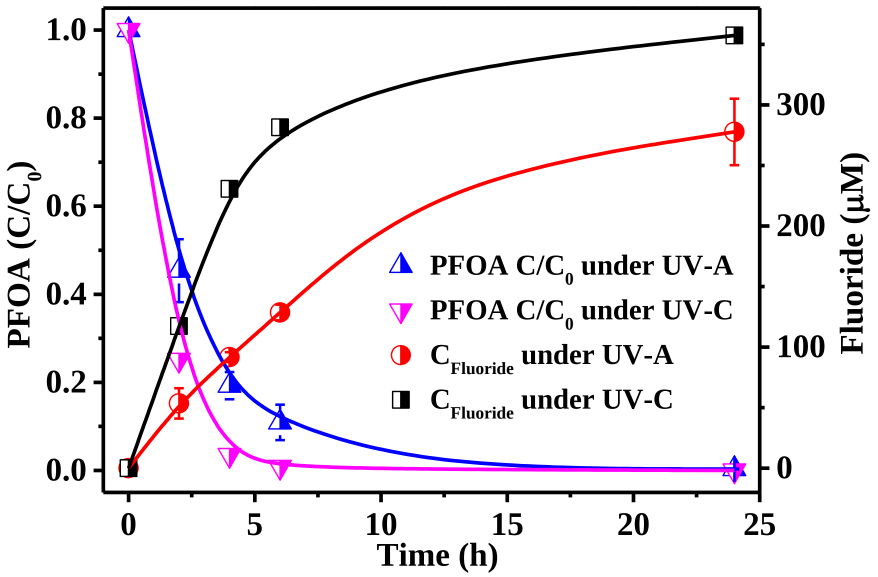

Figure 9. Degradation of PFOA in the presence of Fe-BEA35 (1 g L^{-1}) under UV-A and UV-C irradiation. $C_{0,PFOA}$ = 48 µM , pH_0 = 5.5, oxygen atmosphere. Error bars represent standard deviations of triplicate assays. Lines are added to guide the eye.

3.7. Reusability Test.

Figure 10 shows degradation and defluorination behaviors of PFOA in a recycling experiment. The catalyst activity showed a slightly decreasing tendency, but maintained about 80% of its initial activity in the sixth consecutive run. Two reasons can be considered to explain the observed apparent decrease in catalytic performance: (i) unavoidable mass losses of the catalyst during the recycling process, and (ii) some carry-over of adsorbed PFOA and its reaction products between the runs. Neither phenomenon affects the inherent catalyst activity. These results demonstrate that Fe-BEA35 is relatively stable and has a promising potential for practical application.

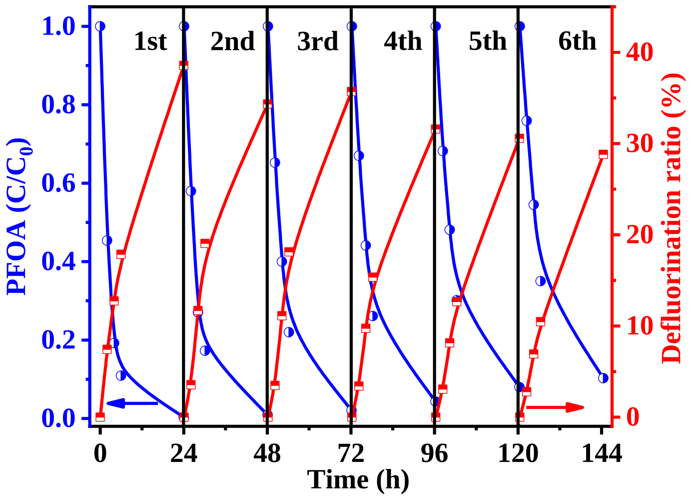

Figure 10. PFOA degradation and defluorination in consecutive batch runs with Fe-BEA35 (1 g L^{-1}) under UV-A light. $C_{0,\mathrm{PFOA}}$ = 48 μM each, pH_0 = 5.5, oxygen atmosphere. Lines are added to guide the eye.

3.8. Possible pathways of photochemical degradation of PFOA.

Based on the presented results, a reaction mechanism is proposed in Scheme 1. It is similar to suggested schemes for PFOA photo-degradation in homogeneous iron-containing solutions from the literature [19, 20, 25, 47]. First, the adsorbed PFOA is complexed with isolated Fe^{3+} ions in tetrahedral and octahedral coordination to form PFOA-Fe^{3+} complexes. After the excitation under UV-A irradiation, complexed PFOA is oxidized via a ligand-to-metal charge transfer process (eq. 14) [20, 22, 23]. The resulting carboxyl radicals decarboxylate, yielding perfluorinated alkyl radicals ($\bullet C_7F_{15}$) (eq. 15) [48]. The $\bullet C_7F_{15}$ can then react further, preferentially with dissolved oxygen (eq. 16). The subsequent radical and hydrolysis reactions are proposed in the literature [19, 47] but remain speculative (eqs. 18-22). In particular, radical-radical reactions such as (17) and (18) are less likely in the zeolite pores. The shorter-chain PFCAs follow a similar degradation pathway as PFOA. In order to close the photocatalytic cycle, reduced iron sites must be re-oxidized either by molecular oxygen or by •OH radicals (eqs. 23 and 24).

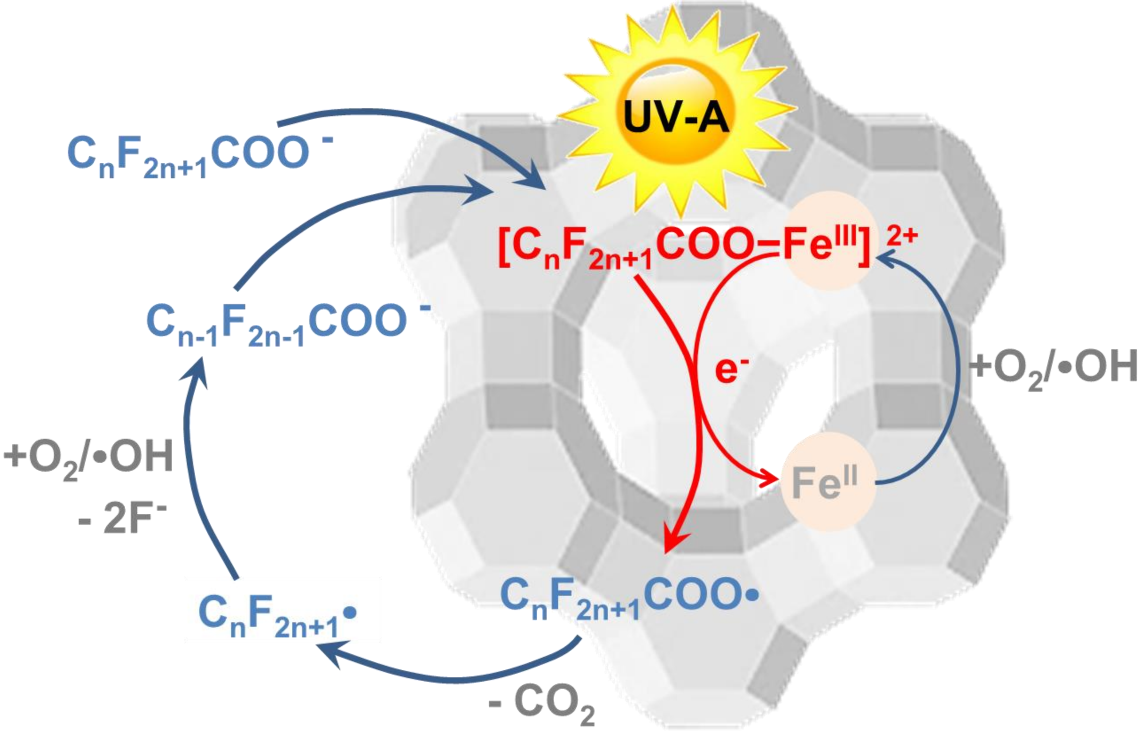

Scheme 1. Hypothetical reaction mechanism for the photochemical degradation of PFOA on Fe-BEA35.

$$C_7F_{15}COO^- + Fe^{3+}\text{-zeolite} \longleftrightarrow [C_7F_{15}COO\text{-}Fe]^{2+}\text{-zeolite} \qquad (13)$$

$$[C_7F_{15}COO\text{-}Fe]^{2+}\text{-zeolite} \xrightarrow{\text{UV-A}} C_7F_{15}COO\bullet + Fe^{2+}\text{-zeolite} \qquad (14)$$

$$C_7F_{15}COO\bullet \rightarrow C_7F_{15}\bullet + CO_2 \qquad (15)$$

$$C_7F_{15}\bullet + O_2 \rightarrow C_7F_{15}OO\bullet \qquad (16)$$

$$C_7F_{15}\bullet + \bullet OH \rightarrow C_7F_{15}OH \qquad (17)$$

$$2C_7F_{15}OO\bullet \rightarrow C_7F_{15}OOOOC_7F_{15} \quad (18)$$

$$C_7F_{15}OOOOC_7F_{15} \rightarrow 2C_7F_{15}O\bullet + O_2 \quad (19)$$

$$C_7F_{15}O\bullet + H_2O \rightarrow C_7F_{15}OH + \bullet OH \quad (20)$$

$$C_7F_{15}OH \rightarrow C_7F_{13}OF + HF \quad (21)$$

$$C_7F_{13}OF + H_2O \rightarrow C_6F_{13}COOH + HF \quad (22)$$

$$Fe^{2+}\text{-zeolite} + O_2 \rightarrow Fe^{3+}\text{-zeolite} + \bullet O_2^- \quad (23)$$

$$Fe^{2+}\text{-zeolite} + \bullet OH \rightarrow Fe^{3+}\text{-zeolite} + OH^- \quad (24)$$

Perfluorinated alkyl radicals ($\bullet C_nF_{2n+1}$) are key intermediates in the supposed reaction pathway. In the absence of dissolved oxygen (nitrogen atmosphere), they were expected to stabilize by bimolecular reactions such as recombination or disproportionation or by H-abstraction from water. Indeed, trace amounts of corresponding 1H-perfluoroalkanes ($C_nF_{2n+1}H$) were detected in the gas phase as shown in Table S2. However, even in the presence of reactive H-donors such as methanol (1 vol-%), $C_7F_{15}H$ was detected only at a trace level (<0.1 mol-% of converted PFOA). The corresponding experiments took carefully into account the volatility of these compounds. Therefore, the supposed reaction mechanism in the absence of O_2 must be considered as a hypothesis requiring additional proof. Understanding the fate of perfluoroalkyl radicals is not only an academic question: reactions with O_2 and •OH (eqs. 16 and 17) result in shorter-chain PFCAs, which have to be chemically degraded further. Other radical stabilization reactions, such as H-abstraction from appropriate H-donors (or water), would produce highly volatile compounds (e.g. $C_nF_{2n+1}H$) which are easily removed from the aqueous phase. Hence, controlling the fate of the key intermediate $\bullet C_nF_{2n+1}$ would provide a tool to make the entire treatment process more efficient.

In addition, methanol can also work as an effective •OH quencher. As seen in Figure S10, the addition of methanol (1 vol-%) has almost no effect on PFOA degradation and defluorination, which indicates that •OH does not play a key role in the rate-determining steps of the photochemical degradation of PFOA.

4. Conclusions

In this study, a novel, efficient degradation approach of PFOA under UV-A irradiation after adsorption on Fe-zeolites with molecular oxygen being the terminal oxidant was established. Experimental results show i) Fe-zeolites based photochemical system exhibits a better PFOA degradation performance under irradiation (a wider range from UV-C to UV-A) compared to the homogeneous ferric ions system. ii) Slightly acidic conditions are optimal in terms of PFOA adsorption and complexation. iii) Molecular oxygen works as the terminal oxidant and is involved in re-oxidization of ferrous ions to ferric ions, producing reactive species and facilitating further mineralization of PFOA. iv) Except for SO_4^{2-}, the presence of other commonly present inorganic anions has a negligible impact on PFOA degradation. v) The isolated Fe^{3+} ions in octahedral coordination are involved in the carboxylate-to-metal charge transfer, which plays the major role in the process of PFOA degradation. Using Fe-zeolites as both adsorbent and photocatalyst opens up the design of new technological approaches for degradation of PFOA. A feasible process scheme could consist of the following steps: in the first step, PFOA is removed from water by adsorption to the Fe-zeolites that can then be separated by microfiltration. In the second step, the loaded zeolite particles can be regenerated *in situ* by photochemical degradation under optimal reaction conditions with UV-A irradiation (300 nm > λ > 400 nm), i.e., a solar light fraction. Post-treatment of the regeneration solution by UV-C/persulfate can be used for complete mineralization of released shorter-chain PFCAs. Overall, a combination of PFOA adsorptive enrichment and photochemical degradation by applying Fe-zeolites can be realized, which is promising for the treatment of this highly recalcitrant trace-level contaminant.

Acknowledgments

We thank Mireia Arqué Hernández for technical support in experimental design, Dr. Roberto Köferstein (Martin-Luther-Univeristät Halle-Wittenberg, Germany) for the XRD analysis. L.Q. acknowledges financial support by China Scholarship Council.

References

[1] H.-J. Lehmler, Synthesis of environmentally relevant fluorinated surfactants - a review, Chemosphere 58 (2005) 1471-1496.

[2] A.B. Lindstrom, M.J. Strynar, E.L. Libelo, Polyfluorinated compounds: Past, present, and future, Environ. Sci. Technol. 45 (2011) 7954-7961.

[3] C. Baduel, C.J. Paxman, J.F. Mueller, Perfluoroalkyl substances in a firefighting training ground (FTG), distribution and potential future release, J. Hazard. Mater. 296 (2015) 46-53.

[4] C.A. Moody, J.A. Field, Perfluorinated surfactants and the environmental implications of their use in fire-fighting foams, Environ. Sci. Technol. 34 (2000) 3864-3870.

[5] C.P. Higgins, R.G. Luthy, Sorption of perfluorinated surfactants on sediments, Environ. Sci. Technol. 40 (2006) 7251-7256.

[6] J.A. Björklund, K. Thuresson, C.A. De Wit, Perfluoroalkyl compounds (PFCs) in indoor dust: concentrations, human exposure estimates, and sources, Environ. Sci. Technol. 43 (2009) 2276-2281.

[7] J. Hollingsworth, R. Sierra-Alvarez, M. Zhou, K.L. Ogden, J.A. Field, Anaerobic biodegradability and methanogenic toxicity of key constituents in copper chemical mechanical planarization effluents of the semiconductor industry, Chemosphere 59 (2005) 1219-1228.

[8] B.D. Key, R.D. Howell, C.S. Criddle, Fluorinated organics in the biosphere, Environ. Sci. Technol. 31 (1997) 2445-2454.

[9] M.M. Schultz, C.P. Higgins, C.A. Huset, R.G. Luthy, D.F. Barofsky, J.A. Field, Fluorochemical mass flows in a municipal wastewater treatment facility, Environ. Sci. Technol. 40 (2006) 7350-7357.

[10] C.K.O. da Silva-Rackov, W.A. Lawal, P.A. Nfodzo, M. Vianna, C.A.O. do Nascimento, H. Choi, Degradation of PFOA by hydrogen peroxide and persulfate activated by iron-modified diatomite, Appl. Catal. B Environ. 192 (2016) 253-259.

[11] K.H. Kucharzyk, R. Darlington, M. Benotti, R. Deeb, E. Hawley, Novel treatment technologies for PFAS compounds: A critical review, Journal of environmental management 204 (2017) 757-764.

[12] H. Park, C.D. Vecitis, J. Cheng, N.F. Dalleska, B.T. Mader, M.R. Hoffmann, Reductive degradation of perfluoroalkyl compounds with aquated electrons generated from iodide photolysis at 254 nm, Photochem. Photobiol. Sci. 10 (2011) 1945-1953.

[13] H. Hori, A. Yamamoto, K. Koike, S. Kutsuna, M. Murayama, A. Yoshimoto, R. Arakawa, Photocatalytic decomposition of a perfluoroether carboxylic acid by tungstic heteropolyacids in water, Appl. Catal. B Environ. 82 (2008) 58-66.

[14] H. Zhao, J. Gao, G. Zhao, J. Fan, Y. Wang, Y. Wang, Fabrication of novel SnO_2-Sb/carbon aerogel electrode for ultrasonic electrochemical oxidation of perfluorooctanoate with high catalytic efficiency, Appl. Catal. B Environ. 136 (2013) 278-286.

[15] Q. Zhuo, S. Deng, B. Yang, J. Huang, G. Yu, Efficient electrochemical oxidation of perfluorooctanoate using a Ti/SnO2-Sb-Bi anode, Environ. Sci. Technol. 45 (2011) 2973-2979.

[16] Z. Li, P. Zhang, T. Shao, X. Li, In2O3 nanoporous nanosphere: a highly efficient photocatalyst for decomposition of perfluorooctanoic acid, Appl. Catal. B Environ. 125 (2012) 350-357.

[17] H. Hori, A. Yamamoto, E. Hayakawa, S. Taniyasu, N. Yamashita, S. Kutsuna, H. Kiatagawa, R. Arakawa, Efficient decomposition of environmentally persistent perfluorocarboxylic acids by use of persulfate as a photochemical oxidant, Environ. Sci. Technol. 39 (2005) 2383-2388.

[18] H. Hori, Y. Nagaoka, M. Murayama, S. Kutsuna, Efficient decomposition of perfluorocarboxylic acids and alternative fluorochemical surfactants in hot water, Environ. Sci. Technol. 42 (2008) 7438-7443.

[19] H.V. Lutze, J. Brekenfeld, S. Naumov, C. von Sonntag, T.C. Schmidt, Degradation of perfluorinated compounds by sulfate radicals–New mechanistic aspects and economical considerations, Water Res. 129 (2018) 509-519.

[20] Y. Wang, P. Zhang, G. Pan, H. Chen, Ferric ion mediated photochemical decomposition of perfluorooctanoic acid (PFOA) by 254 nm UV light, J. Hazard. Mater. 160 (2008) 181-186.

[21] Y. Qu, C. Zhang, F. Li, J. Chen, Q. Zhou, Photo-reductive defluorination of perfluorooctanoic acid in water, Water Res. 44 (2010) 2939-2947.

[22] H. Tang, Q. Xiang, M. Lei, J. Yan, L. Zhu, J. Zou, Efficient degradation of perfluorooctanoic acid by UV–Fenton process, Chem. Eng. J. 184 (2012) 156-162.
[23] H. Hori, A. Yamamoto, K. Koike, S. Kutsuna, I. Osaka, R. Arakawa, Photochemical decomposition of environmentally persistent short-chain perfluorocarboxylic acids in water mediated by iron (II)/(III) redox reactions, Chemosphere 68 (2007) 572-578.
[24] J.-h. Cheng, X.-y. Liang, S.-w. Yang, Y.-y. Hu, Photochemical defluorination of aqueous perfluorooctanoic acid (PFOA) by VUV/Fe3+ system, Chem. Eng. J. 239 (2014) 242-249.
[25] L. Jin, P. Zhang, T. Shao, S. Zhao, Ferric ion mediated photodecomposition of aqueous perfluorooctane sulfonate (PFOS) under UV irradiation and its mechanism, J. Hazard. Mater. 271 (2014) 9-15.
[26] S. Navalon, M. Alvaro, H. Garcia, Heterogeneous Fenton catalysts based on clays, silicas and zeolites, Appl. Catal. B Environ. 99 (2010) 1-26.
[27] M. Hartmann, S. Kullmann, H. Keller, Wastewater treatment with heterogeneous Fenton-type catalysts based on porous materials, J. Mater. Chem. 20 (2010) 9002-9017.
[28] R. Gonzalez-Olmos, F.-D. Kopinke, K. Mackenzie, A. Georgi, Hydrophobic Fe-zeolites for removal of MTBE from water by combination of adsorption and oxidation, Environ. Sci. Technol. 47 (2013) 2353-2360.
[29] A. Zecchina, M. Rivallan, G. Berlier, C. Lamberti, G. Ricchiardi, Structure and nuclearity of active sites in Fe-zeolites: comparison with iron sites in enzymes and homogeneous catalysts, Phys. Chem. Chem. Phys. 9 (2007) 3483-3499.
[30] R. Gonzalez-Olmos, M.J. Martin, A. Georgi, F.-D. Kopinke, I. Oller, S. Malato, Fe-zeolites as heterogeneous catalysts in solar Fenton-like reactions at neutral pH, Appl. Catal. B Environ. 125 (2012) 51-58.
[31] G. Gillies, R. Raj, F.-D. Kopinke, A. Georgi, Suspension stability and mobility of Trap-Ox Fe-zeolites for in-situ nanoremediation, J. Colloid Interface Sci. 501 (2017) 311-320.
[32] A.L. Allred, Electronegativity values from thermochemical data, J. Inorg. Nuclear Chem. 17 (1961) 215-221.
[33] Database of Zeolite Structures., http://www.iza-structure.org/IZA-SC/framework_3d.php?STC=BEA
[34] R. Gonzalez-Olmos, U. Roland, H. Toufar, F.-D. Kopinke, A. Georgi, Fe-zeolites as catalysts for chemical oxidation of MTBE in water with H2O2, Appl. Catal. B Environ. 89 (2009) 356-364.
[35] L. Čapek, V. Kreibich, J. Dědeček, T. Grygar, B. Wichterlova, Z. Sobalik, J. Martens, R. Brosius, V. Tokarova, Analysis of Fe species in zeolites by UV–VIS–NIR, IR spectra and voltammetry. Effect of preparation, Fe loading and zeolite type, Micropor. Mesopor. Mater. 80 (2005) 279-289.
[36] G.D. Pirngruber, P.K. Roy, R. Prins, On determining the nuclearity of iron sites in Fe-ZSM-5—a critical evaluation, Phys. Chem. Chem. Phys. 8 (2006) 3939-3950.
[37] J.B. Higgins, R.B. LaPierre, J.L. Schlenker, A.C. Rohrman, J.D. Wood, G.T. Kerr, W.J. Rohrbaugh, The framework topology of zeolite beta, Zeolites 8 (1988) 446-452.
[38] S. Shwan, R. Nedyalkova, J. Jansson, J. Korsgren, L. Olsson, M. Skoglundh, Hydrothermal stability of Fe–BEA as an NH3-SCR catalyst, Industrial & engineering chemistry research 51 (2012) 12762-12772.
[39] A. Hagenaars, L. Vergauwen, W. De Coen, D. Knapen, Structure–activity relationship assessment of four perfluorinated chemicals using a prolonged zebrafish early life stage test, Chemosphere 82 (2011) 764-772.
[40] M.-J. Lopez-Espinosa, T. Fletcher, B. Armstrong, B. Genser, K. Dhatariya, D. Mondal, A. Ducatman, G. Leonardi, Association of perfluorooctanoic acid (PFOA) and perfluorooctane sulfonate (PFOS) with age of puberty among children living near a chemical plant, Environmental science & technology 45 (2011) 8160-8166.
[41] K. Kleszczyński, A.C. Składanowski, Mechanism of cytotoxic action of perfluorinated acids. III. Disturbance in Ca2+ homeostasis, Toxicology and applied pharmacology 251 (2011) 163-168.
[42] U. Shafique, V. Dorn, A. Paschke, G. Schuurmann, Adsorption of perfluorocarboxylic acids at the silica surface, Chem. Commun. 53 (2017) 589-592.

[43] K.-U. Goss, The pKa Values of PFOA and other highly fluorinated carboxylic acids, Environ. Sci. Technol. 42 (2008) 456-458.

[44] E. Hogfeldt, Stability constants of metal-ion complexes. Part A Inorganic ligands. International Union of Pure and Applied Chemists., Pergamon Press, New York, 1982.

[45] H.J. Benkelberg, P. Warneck, Photodecomposition of iron(III) hydroxo and sulfato complexes in aqueous solution: Wavelength dependence of OH and SO_4-quantum yields, J. Phys. Chem. 99 (1995) 5214-5221.

[46] M. Schwidder, M.S. Kumar, K. Klementiev, M.M. Pohl, A. Bruckner, W. Gruenert, Selective reduction of NO with Fe-ZSM-5 catalysts of low Fe content - I. Relations between active site structure and catalytic performance, J. Catal. 231 (2005) 314-330.

[47] S. Kutsuna, H. Hori, Rate constants for aqueous-phase reactions of SO_4- with $C_2F_5C(O)O$- and $C_3F_7C(O)O$- at 298 K, Int. J. Chem. Kinet. 39 (2007) 276-288.

[48] D.V. Avila, K.U. Ingold, J. Lusztyk, W.R. Dolbier, H.Q. Pan, M. Muir, Absolute rate constants for some reactions of perfluoro-n-alkyl radicals in solution, J. Am. Chem. Soc. 116 (1994) 99-104.

Supporting information

Experimental procedures

N_2 adsorption/desorption measurements were performed on a BELSORP-miniII instrument (Bel, Japan) at -196 °C. Each sample was degassed at 100 °C before measurement. Structural parameters (specific surface area, pore volume, pore diameter and pore size distribution) were calculated using Brunauer–Emmett–Teller (BET) and Barrett-Joyner-Halenda (BJH) methods by means of BELSORP-miniII analysis software.

Major elements (MgO, Al_2O_3, SiO_2, P_2O_5, K_2O, CaO, MnO, Fe_2O_3) were determined by means of wavelength-dispersive X-ray fluorescence analysis (WDXRF) using a WDXRF-spectrometer S4 PIONEER (Bruker-AXS) equipped with a 4 kW-Rh X-ray tube (75 µm Be window), 60 kV generator and an eight-position crystal changer. Aliquots of the sample powder were diluted with $Li_2B_4O_7$ (1 g sample + 7 g $Li_2B_4O_7$) in order to prepare glass discs by fusion at 1200 °C in a 95% platinum-5% gold crucible for 20 min. The spectrometer operating conditions were vacuum, 34 mm collimator mask and 0.23° collimator in conjunction with the analyzing crystals OVO 55, Ge, LIF 100 and LIF 110. The calibration functions for the individual analytes were based on relationships between certified concentration data and the measured response provided by the analysis of reference materials: CANMET-LKSD1-LKSD4 (lake sediments), CANMET-STSD1-STSD4 and GBW07309-11 (stream sediments), NIST-SRM2689 and NIST-SRM2691 (coal fly ashes). The measurement process and data collecting were controlled by the software package SPECTRA^{plus}.

XPS spectra were recorded on an Axis Ultra photoelectron spectrometer (Kratos, Manchester, UK) using monochromatized Al Kα radiation (hν=1486.6 eV). Pass energies of 160 eV and 40 eV were set for measuring the survey and the high-resolution spectra, respectively. The main component of the C 1s signal was set as reference at 284.8 eV for binding energy determination.

X-ray powder diffraction patterns were recorded at room temperature on a Bruker D8-Advance diffractometer, equipped with a one-dimensional silicon strip detector (LynxEye) using Cu-K radiation and a counting time of 1 s per data point.

Table S1. Particle sizes of dry Fe-BEA35 powders and particle size distribution in Fe-BEA35 suspension.

	Fe-BEA35
Particle size as $d_{10}/d_{50}/d_{90}$ (μm) [a]	0.4/1.0/2.1
d_{DLS} (μm) [b]	0.86

[a] Determined by laser diffraction for dry powder with HELOS. Particle size distribution d_{10}, d_{50}, and d_{90} corresponding to the percentages 10%, 50%, and 90% of particles under the reported particle size.

[b] DLS analysis (intensity-based harmonic mean of particle diameter). A zeolite concentration of 1 g L^{-1} in 10 mM KNO_3 was applied.

Table S2. Identified gas phase products by headspace GC/MS measurement after 24 h irradiation of PFOA in 1 g L^{-1} Fe-BEA35 suspension. GC/MS conditions see main part.

Retention time (min)	**Formula**	**Chemical Structure (GC/MS Library)**
0.89	C_2HF_5	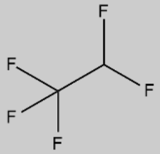
0.97	C_3HF_7	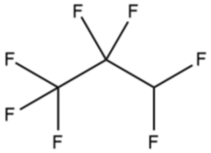
1.14	C_4HF_9	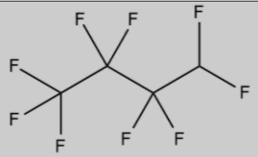
1.45	C_5HF_{11}	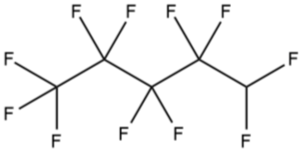

2.01	C_6HF_{13}	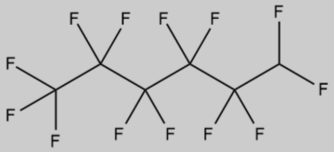
3.08	C_7HF_{15}	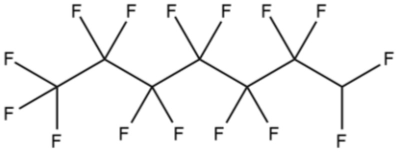

The terminal position of the H atoms in the molecules was derived tentatively from the EI-fragmentation pattern.

Table S3. Zeta potential of Fe-BEA35 determined at different pH values in Fe-BEA35 (1 g L^{-1}) suspension in 10 mM KNO_3.

	pH=3.0	**pH=5.5**	**pH=7.0**	**pH=9.0**
Zeta potential (mV)	-21	-26	-29	-34

Table S4. Degradation rate constants ($k_{obs,PFOA}$), defluorination ratios (d_{F^-}) and half-lives ($t_{1/2}$, calculated from $k_{obs,PFOA}$) of PFOA in the presence of Fe-BEA35 (1 g L^{-1}) and initial pH = 5.5 under various reaction conditions.

	O_2 [a]	**N_2** [a]	**UV-A** [b]	**UV-C** [b]
d_{F^-} after 24 h (%)	16	1.7	38±0.70 [c]	49
d_{F^-} after 48 h (%)	22	2.1	- [d]	-
$k_{obs,PFOA}$ (h^{-1})	0.046 ± 0.004	0.0045 ± 0.0022	0.38 ± 0.04	0.82 ± 0.08

[a] $C_{0,PFOA}$ = 480 µM, UV-A irradiation

[b] $C_{0,PFOA}$ = 48 µM, oxygen atmosphere.

[c] Error ranges represent average deviations of single values from the mean of triplicate assays.

[d] Not available.

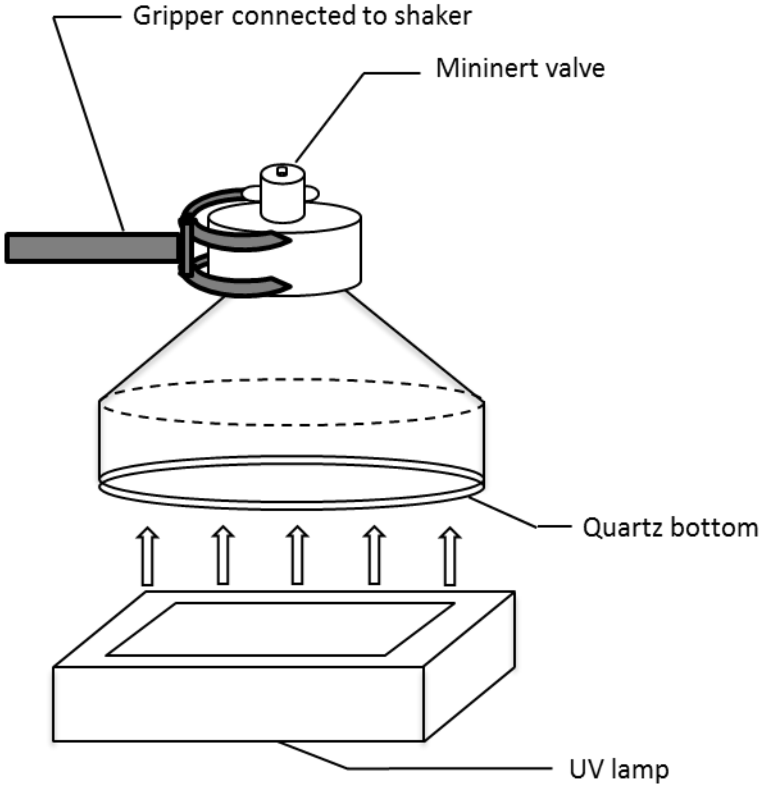

Figure S1. Schematic of the experimental setup for photochemical experiments.

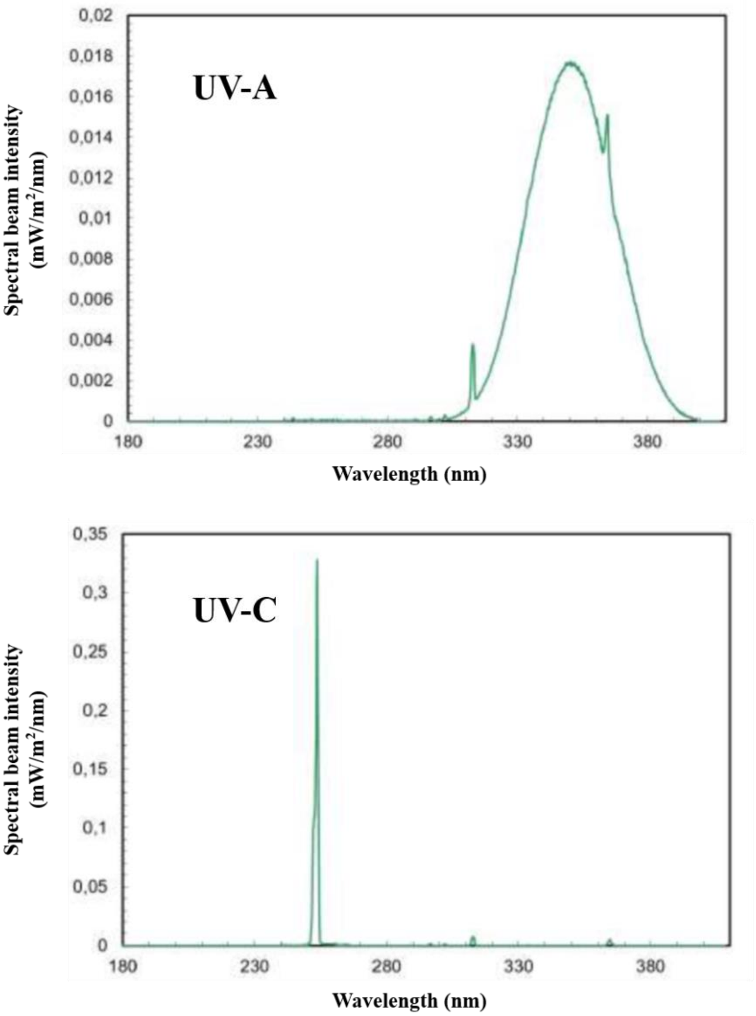

Figure S2. Spectral emission curves of UV lamps used (UV-A and UV-C). The intensity varies according to power of the lamp. The spectral curves were obtained from the website of the UV lamp provider (https://www.herolab.de).

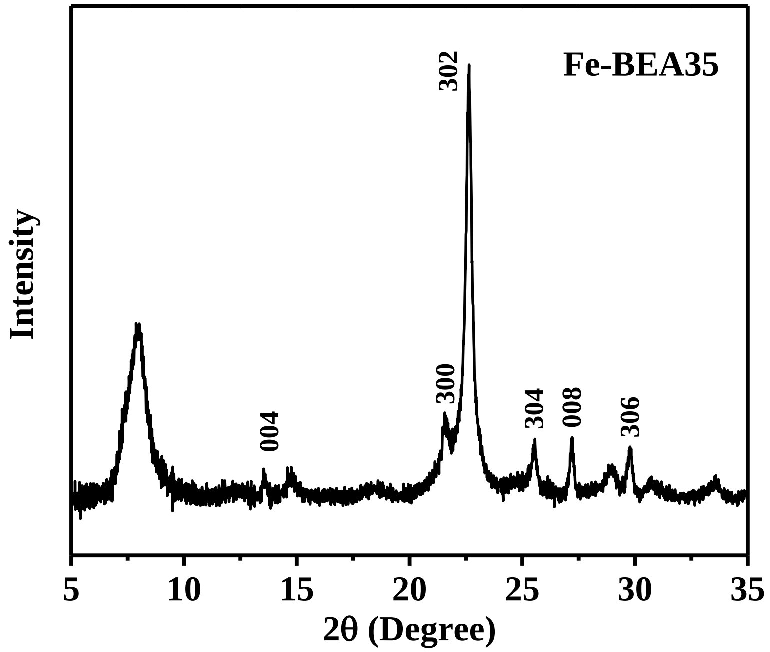

Figure S3. The X-ray powder diffraction pattern of Fe-BEA35.

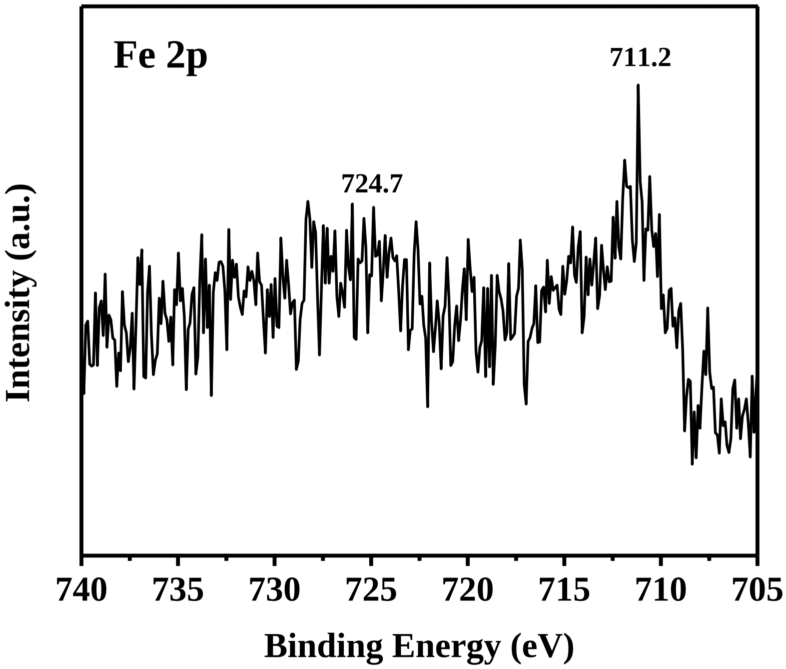

Figure S4. Fe 2p XPS spectra of Fe-BEA35.

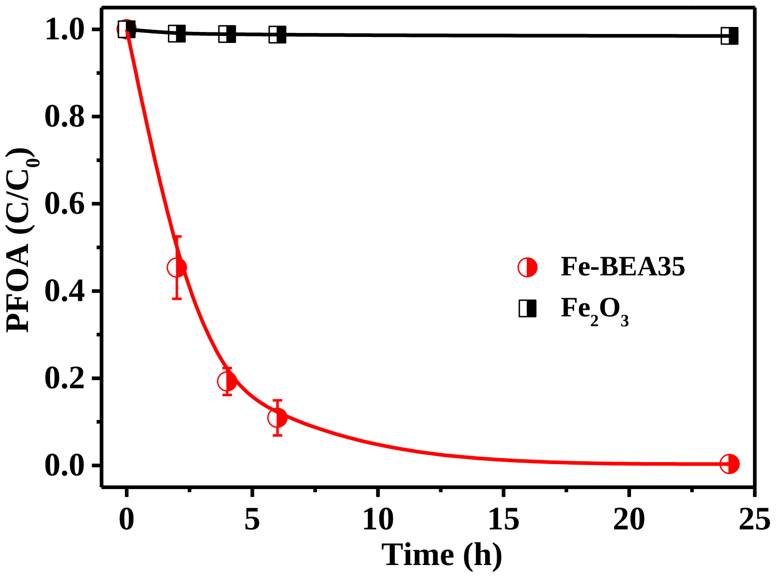

Figure S5. Comparison of PFOA degradation kinetics in the presence of iron(III) oxide nanoparticles and BEA35. $C_{\text{Fe-BEA35}}$ = 1 g L^{-1}, $C_{\text{iron(III) oxide}}$ = 0.1 g L^{-1}, $C_{0,\text{PFOA}}$ = 48 µM and pH$_0$ = 5.5. Error bars represent standard deviations of triplicate assays. Lines are added to guide the eye.

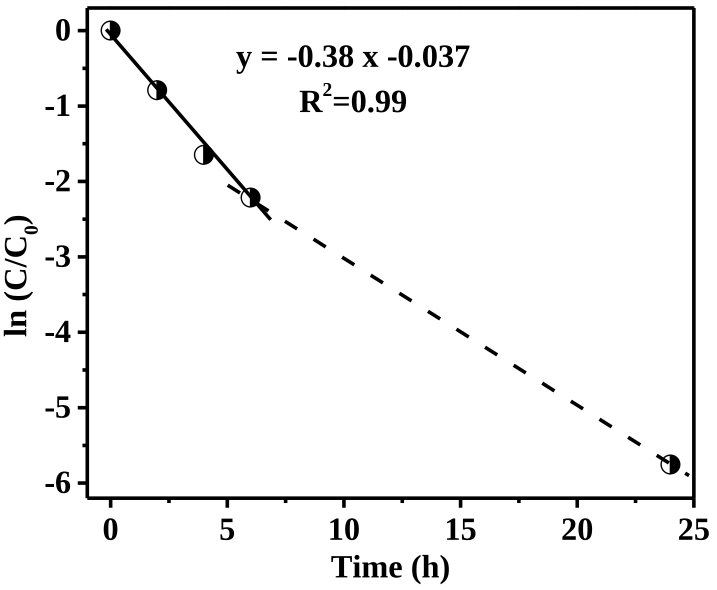

Figure S6. First-order-kinetics plot of PFOA degradation, ln(C/C$_0$) versus irradiation time. $C_{\text{Fe-BEA35}}$ = 1 g L^{-1}, $C_{0,\text{PFOA}}$ = 48 µM and pH$_0$ = 5.5. Pseudo-first-order kinetics can describe well PFOA degradation within the initial period of 0-6 h corresponding to ≤ 90% turnover. The reaction slows down slightly for higher turnover.

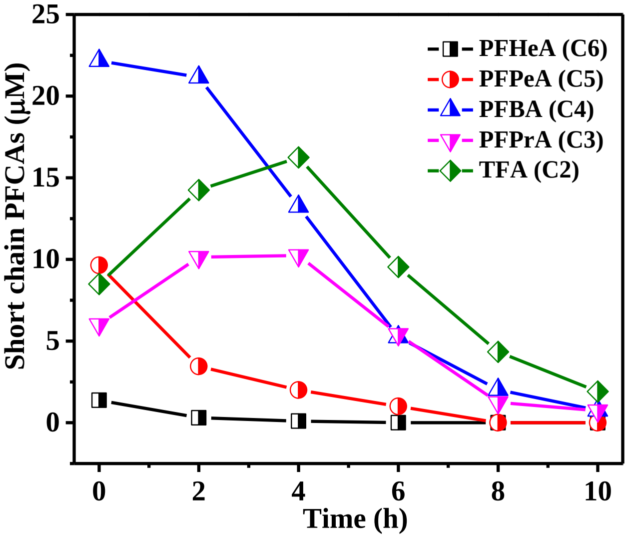

Figure S7. Degradation of short-chain perfluorinated carboxylic acids by UV-C activation of sodium persulfate. During the reaction, 8.4 mM sodium persulfate was added every 2 h.

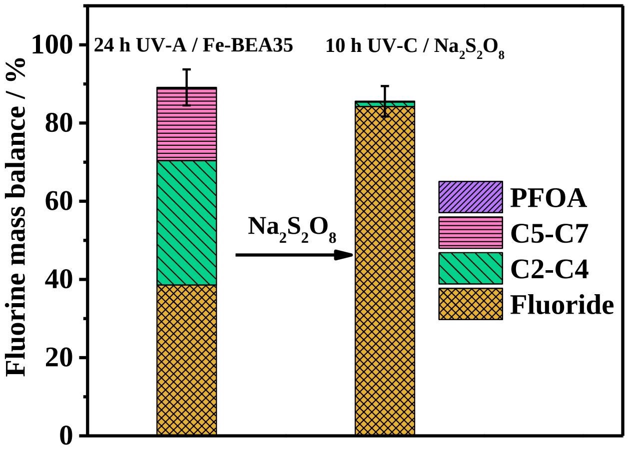

Figure S8. Mass balance of fluorine before and after UV-C activation of sodium persulfate.

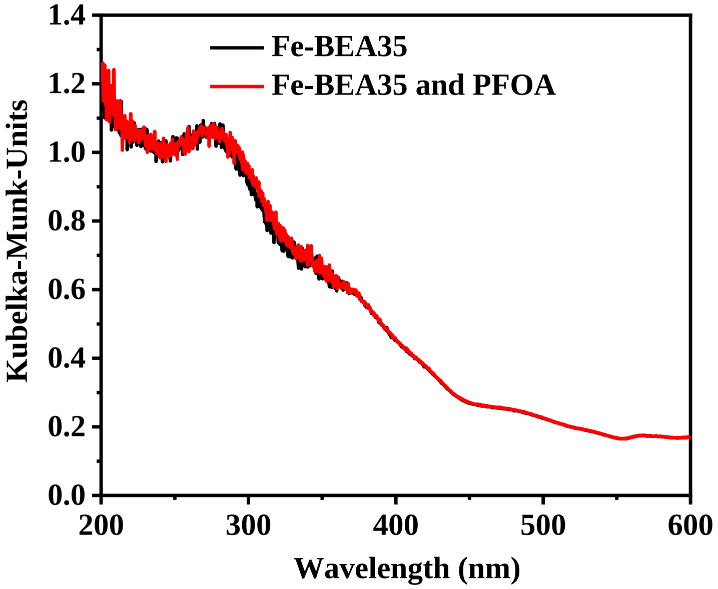

Figure S9. UV-vis-DR spectra of 10 g L^{-1} Fe-BEA35 suspension in the absence and in the presence of 1.92 mM adsorbed PFOA.

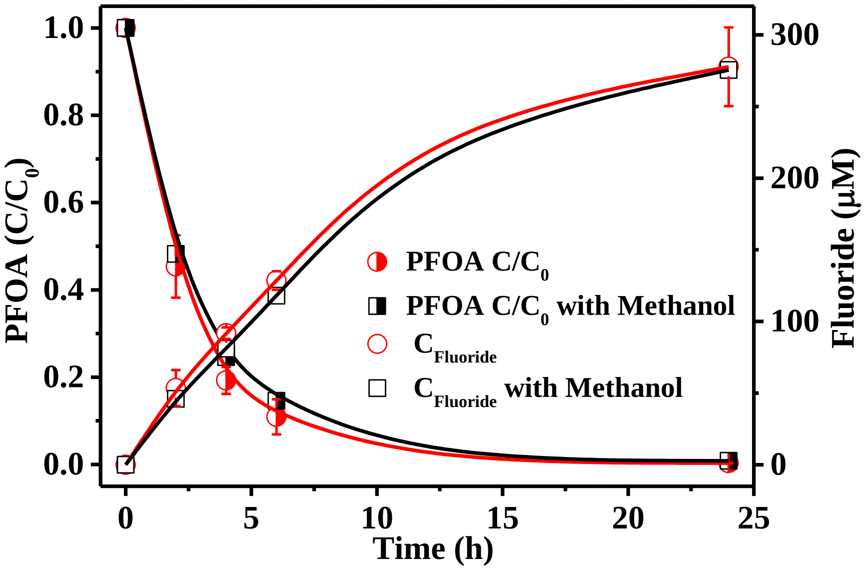

Figure S10. Degradation of PFOA in the presence of Fe-BEA35 (1 g L^{-1}) with and without (1 vol-%) methanol addition. $C_{0,\mathrm{PFOA}}$ = 48 µM, pH_0 = 5.5, oxygen atmosphere. Error bars represent standard deviations of triplicate assays. Lines are added to guide the eye.

3.2 Photodegradation of perfluorooctanesulfonic acid on Fe-zeolites in water

*Lin Qian, Frank-Dieter Kopinke and Anett Georgi**

Helmholtz Centre for Environmental Research – UFZ, Department of Environmental
Engineering, Permoserstrasse 15, D-04318 Leipzig, Germany

ABSTRACT: Perfluorooctanesulfonic acid (PFOS) decomposition in aqueous environment remains a huge challenge because of its extreme chemical and biological inertness even when compared with other per- and polyfluoroalkyl substances (PFAS). In this work, we demonstrate for the first time a successful photochemical PFOS degradation by irradiation with 254 nm ultraviolet (UV) light after adsorption on μm-sized Fe(III)-loaded zeolites under ambient conditions with oxygen (O_2) as the terminal oxidant. 20 μM PFOS loaded on 0.5 g L^{-1} Fe-zeolites in aqueous suspension was degraded up to 99% within 96 h under acidic conditions ($pH \leq 5.5$) in the presence of oxygen. Beside fluoride and sulfate, short-chain perfluorinated carboxylic acids (PFCAs) were identified and quantified as products. In addition, the effects of initial pH, catalyst dosages and operation temperature on the degradation of PFOS were investigated. We also successfully applied the system to real ground water samples where trace PFOS was present. Our results indicate that PFOS degradation is initiated by electron transfer from sulfonate to iron. The presented experimental study offers an option for a novel water remediation technology, comprising first a zeolite-based adsorption step followed by a step for photochemical regeneration of the adsorbent.

1. INTRODUCTION

Perfluorooctanesulfonic acid (PFOS) is one of the most important per- and polyfluoroalkyl substances (PFAS) being widely used in manufacturing industrial and consumer products [1], such as fire retardants, high-temperature lubricants, waterproof textiles and Teflon-related products [2]. PFOS has been found to be globally distributed in aquatic and terrestrial environments [3], also in many organisms [4, 5]. Several studies suggest that the exposure to PFOS over certain levels may result in harmful health effects in humans and animals, i.e., liver and kidney toxicity, cardiotoxicity, reproductive toxicity and neurotoxicity [6-9]. Even though production and use of the extremely persistent PFOS was phased out after the compound was added to Annex B of Stockholm convention, the risk of human exposure due to accumulation in marine systems and contaminations in groundwater used for drinking water production will continue to exist for decades [10].

PFOS is resistant to most of the conventional reduction/oxidation processes and biological degradation due to its strong C-F bonds [11]. Advanced oxidation processes (AOPs) are ineffective as PFAS have negligible reactivity with hydroxyl radicals [12], the main reactant in AOPs [13]. Destruction of perfluorinated *carboxylic* acids (PFCAs) was achieved in persulfate systems activated by heat or UV irradiation, but PFOS was found inert to such approaches [14]. Although there is substantial published research on the degradation of PFCAs, e.g., perfluorooctanoic acid (PFOA), studies on the degradation of PFOS remain rather limited. The reason is that degradation of PFOS is an even greater challenge than that of PFCAs.

There are two major approaches reported to be effective in the degradation of PFOS. Firstly, the reductive pathway using hydrated electrons (e_{aq}^-) as reactive species, generated by UV photolysis of potassium iodide [15], sodium sulfite [16] or indole acetic acid [17]. However, the generation of hydrated electrons requires alkaline and anaerobic conditions, and furthermore, the produced by-products have the potential to contaminate the treated water. Alternatively, PFOS can be degraded electrochemically, e.g. at boron-doped diamond (BDD) electrodes. It has been reported that the oxidation of PFOS is initiated by direct electron transfer from PFOS to the anode [18], after which a sequence of radical and hydrolysis reactions can take place. However, a significant shortcoming of this process is its low space-time-yield, in particular for highly diluted water fluxes. In summary, there is an urgent need to develop a method for decomposing PFOS ecologically and economically under feasible and practically available conditions.

Nowadays, UV irradiation is becoming more and more widespread as a method for disinfecting drinking, waste, and feed waters [19]. Unfortunately, PFOS has almost no absorbance in the UV range and cannot be directly photolyzed by UV light [20]. This obstacle can be overcome using coordination complexes which interact with photons of artificial UV or solar light giving rise to their photodecomposition. For instance, it has been reported that PFOS can be complexed with ferric ions to form $[PFOS\text{-}Fe]^{2+}$ (eq. 1). The complex can be excited under vacuum-ultraviolet (VUV, 185 nm) or ultraviolet-C (UV-C, 254 nm) irradiation to produce ferrous ions and $C_8F_{17}SO_3\cdot$ via ligand-to-metal electron transfer (eq. 2) [21].

$$C_8F_{17}SO_3^- + Fe^{3+} \longleftrightarrow [C_8F_{17}SO_3\text{-}Fe]^{2+} \tag{1}$$

$$[C_8F_{17}SO_3\text{-}Fe]^{2+} \xrightarrow{\text{UV- C}} C_8F_{17}SO_3\cdot + Fe^{2+} \tag{2}$$

Desulfurization of $C_8F_{17}SO_3\cdot$ yields perfluorinated alkyl radicals, which may react with oxygen or hydroxyl radicals to be further decomposed. However, the shortcomings of this ferric-ion-mediated photodecomposition of PFOS in homogeneous systems are obvious: (i) the operational pH range is restricted to pH ≤ 3, (ii) reaction rates are low, and (iii) the reaction is probably vulnerable to the real water matrix [22] so an additional pre-enrichment of PFOS is desirable.

In the present study, a complementary combination of efficient PFOS adsorption on commercially available µm-sized Fe(III)-loaded BEA-type zeolite particles (Fe-BEA35, details see SI) and photo-oxidation under UV-C irradiation is proposed. This overcomes several issues of the existing PFOS degradation techniques. The Fe-BEA35 zeolite was characterized in detail and firstly applied for photochemical degradation of PFOA using UV-A light in our previous study [23]. Nevertheless, PFOS is known as more persistent than perfluorocarboxylic acids as it is e.g., unreactive in e-transfer by sulfate radicals. In this study we show for the first time that PFOS is degraded using these microscale Fe-zeolite particles when irradiated with UV-C light and identify the operation steps and conditions for its complete mineralization. Thanks to the high adsorption affinity towards PFOS, Fe-BEA35 can act as efficient adsorbent for this contaminant, whereby the ferric ions embedded in the zeolites possess desirable coordination and catalytic abilities while being much less vulnerable to the surrounding water matrix. Furthermore, the effects of pH, zeolite dosages and operation temperature on degradation of PFOS are investigated in this work. Our study shows for the first time that this heterogeneous system works successfully in real ground water. Furthermore, it can be operated in a wider pH range (up to pH 5.5) than the homogeneous process. The findings in this study offer a promising new strategy for remediation of water containing low concentrations of PFOS.

2. EXPERIMENTAL SECTION

Detailed information on chemicals, materials, photochemical procedures and analyses are described in Supporting Information (SI). For a typical photochemical PFOS degradation, a 350 mL reaction suspension containing certain amounts of Fe-zeolites and PFOS was loaded in a closed-system reactor. A low-pressure mercury lamp (254 nm, 20 W) was used for all reactions. Details about the reactor setup and the groundwater sample treatment are shown in Figures S1 and S2. In this study, the desulfurization ratio ($d_{\mathrm{SO_4^{2-}}}$) and defluorination ratio ($d_{\mathrm{F^-}}$) are calculated as follows:

$$d_{\mathrm{SO_4^{2-}}} = \frac{C_{\mathrm{SO_4^{2-}}}}{C_0} \times 100\% \tag{3}$$

$$d_{\mathrm{F^-}} = \frac{C_{\mathrm{F^-}}}{17 \times C_0} \times 100\% \tag{4}$$

where $C_{\mathrm{SO_4^{2-}}}$ is the sulfate concentration (μM), $C_{\mathrm{F^-}}$ is the fluoride concentration (μM), and C_0 is the initial concentration of PFOS (μM). The factor 17 is the number of fluorine atoms in one PFOS molecule. A complete desulfonation and defluorination of PFOS would yield $d_{\mathrm{SO_4^{2-}}}$ and $d_{\mathrm{F^-}}$ of 100%, respectively.

3. RESULTS AND DISCUSSION

3.1. Degradation of PFOS by UV. A typical reaction suspension contained 0.5 g L^{-1} Fe-BEA35 and $C_{0,\mathrm{PFOS}}$ = 20 μM with initial pH_0 = 3.0. Under these conditions, after 24 h equilibration PFOS was predominantly in the adsorbed state (98%) before start of the irradiation. Thus, the initial loading of PFOS on the zeolite was 19.6 mg g^{-1} (Table S1). In order to follow the total concentration of PFOS (including adsorbed and freely dissolved fraction), an extraction step was performed as described in SI. After 96 h UV-C irradiation, up to 99% of total initial PFOS was decomposed with $d_{\mathrm{F^-}}$ = 69% and $d_{\mathrm{SO_4^{2-}}}$= 99% (Figure 1).

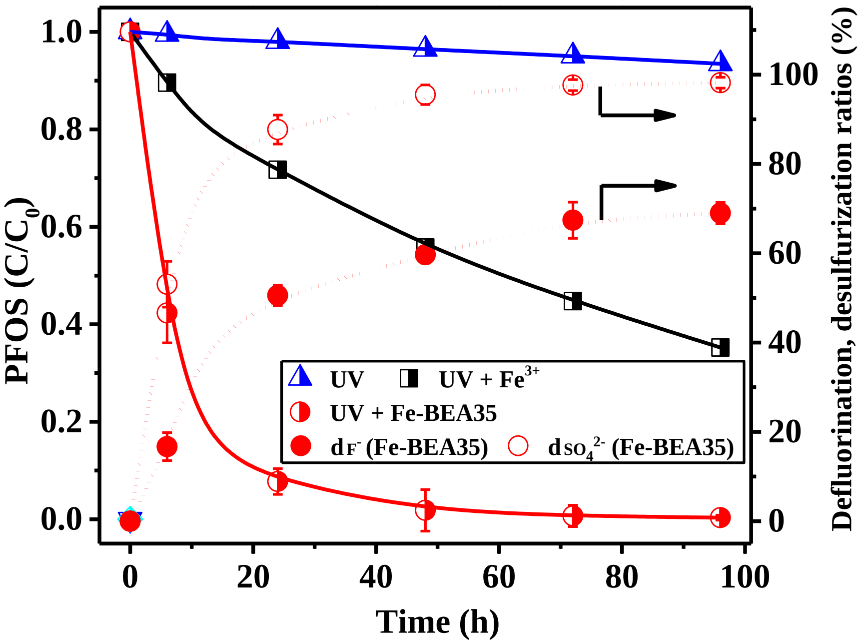

Figure 1. Comparison of PFOS degradation and product formation in three experiments: (i) UV alone, (ii) UV and ferric ions, (iii) UV and Fe-BEA35. $C_{0,\mathrm{PFOS}}$ = 20 µM, pH_0 = 3.0, oxygen atmosphere, 0.5 g L^{-1} Fe-BEA35 (1.3 wt-% Fe in zeolites) and $C_{0,\mathrm{Fe}^{3+}}$ = 200 µM, where applied. Error ranges stand for the standard deviations of the results from triplicate assays. Lines serve as guides for the eye.

In order to reveal the key factor causing the high degradation degree in the system, control experiments under the same conditions with (i) neither Fe-BEA35 nor other iron sources, and (ii) dissolved ferric ions but no zeolites, were performed. As shown in Figure 1, only little degradation of PFOS (6%) occurred after 96 h UV-C irradiation in the systems in the absence of zeolites and in the absence of iron sources, indicating almost no direct photolysis of PFOS. This is not unexpected, as previous studies confirmed that PFOS exhibits no significant adsorption in the UV-C range [20]. Therefore, significant PFOS degradation due to direct photolysis can be ruled out. In the second control experiment, the PFOS degradation performance in a homogenous system containing 200 µM dissolved ferric ions at pH 3.0 was tested. It is known that PFOS can form complexes with ferric ions in aqueous solution (PFOS-Fe^{3+}), which can then be decomposed under UV-C irradiation and contribute to PFOS degradation [21]. With dissolved ferric ions, 69% of the initial PFOS was decomposed and $d_{\mathrm{F^-}}$ = 18% was achieved within 96 h. The lower PFOS degradation (69% in 96 h vs. 92% in 24 h) in the homogeneous system strongly suggests that the presence of Fe-BEA35 was responsible for the high PFOS degradation performance in the heterogeneous system. We assume that the adsorption of PFOS to the zeolite is a pre-condition for photochemical degradation. The fractions of adsorbed PFOS (X_{sorb}) and freely dissolved PFOS (X_{free}) can be described as follows:

$$X_{\mathrm{sorb}} = 1 - X_{\mathrm{free}} \qquad (5)$$

$$X_{\mathrm{free}} = C_{\mathrm{PFOS,free}} / C_{\mathrm{PFOS,total}} \qquad (6)$$

where $C_{\mathrm{PFOS,free}}$ and $C_{\mathrm{PFOS,total}}$ are the freely dissolved PFOS and total extractable PFOS concentrations, respectively. Similar to our previous study [23], it is reasonable to hypothesize the complex formation as a prerequisite for photochemical PFOS degradation according to eqs. 7 and 8:

$$\mathrm{C_8F_{17}SO_3^-} + \mathrm{Fe^{3+}\text{-zeolite}} \longleftrightarrow \mathrm{[C_8F_{17}SO_3\text{-}Fe]^{2+}\text{-zeolite}} \qquad (7)$$

$$\mathrm{[C_8F_{17}SO_3\text{-}Fe]^{2+}\text{-zeolite}} \xrightarrow{\text{UV- C}} \mathrm{C_8F_{17}SO_3\cdot} + \mathrm{Fe^{2+}\text{-zeolite}} \qquad (8)$$

Based upon this mechanism, a first-order rate equation can be derived:

$$\frac{\mathrm{d}C_{\mathrm{PFOS}}}{\mathrm{dt}} = -k \cdot C_{\mathrm{[C_8F_{17}SO_3\text{-}Fe]^{2+}\text{-zeolite}}} = -k \cdot X_{\mathrm{complex}} \cdot C_{\mathrm{PFOS,total}} = -k_{\mathrm{obs,PFOS}} \cdot C_{\mathrm{PFOS,total}} \qquad (9)$$

where X_{complex} is the fraction of PFOS in reactive complexes. While the overall degree of sorption X_{sorb} is experimentally obtained, X_{complex} cannot be easily determined. Hence, we integrate it in the observable rate coefficient $k_{\mathrm{obs,PFOS}} = k \cdot X_{\mathrm{complex}}$. The initial reaction period (0 – 24 h) can be well fitted by a first-order kinetics (Figure S3). However, the reaction slows down at high turnover (>92% at t >24 h). The influence of PFOS concentration on the rate coefficients together with possible reasons are discussed in detail in Section 3.3.

In order to understand the PFOS photochemical degradation pathways and underlying mechanisms better, intermediate products were investigated. No sulfur-containing compounds other than PFOS and sulfate were detected and almost full sulfur mass recovery (98%) was obtained, suggesting that the C-S bond of the PFOS anion was cut and sulfate was subsequently produced. Apart from fluoride and sulfate, seven perfluorinated carboxylic acids (PFCAs) with 2 to 8 carbon atoms (named C2 to C8, respectively) were detected and quantified by LC/MS and IC analysis.

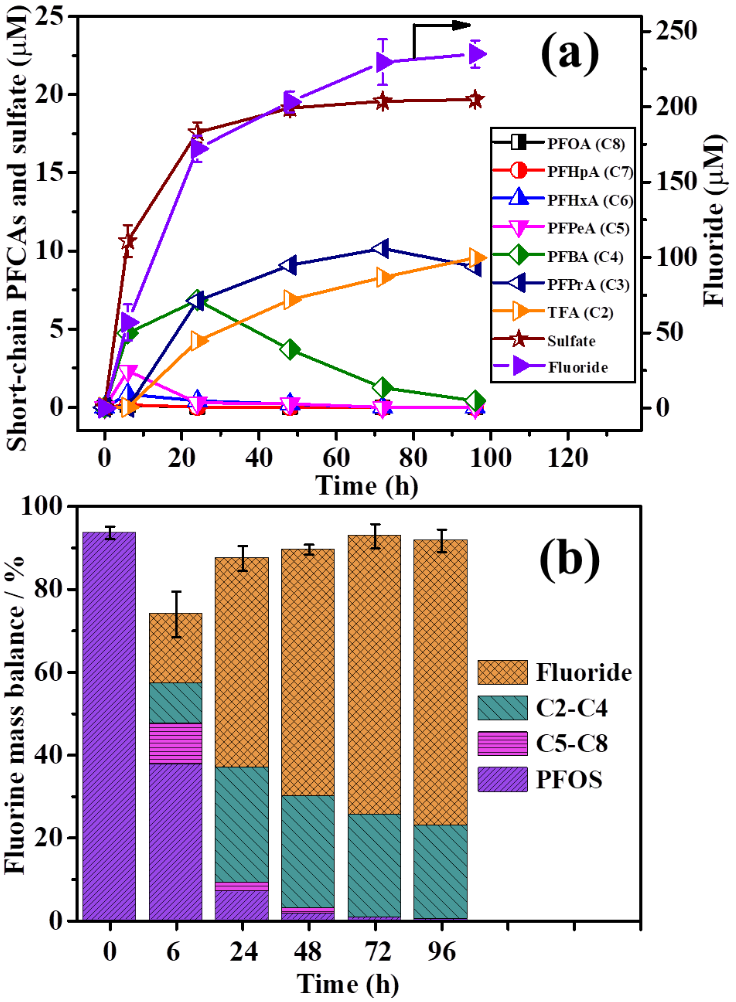

Figure 2. (a) Formation of short-chain PFCA intermediates, fluoride and sulfate during photochemical degradation of PFOS; (b) Fluorine mass balance during photochemical degradation of PFOS. The 0 h mass balance represents fluorine detected as PFOS in zeolite suspension by ACN extraction before start of irradiation. The 96 h mass balance represents fluorine detected as fluoride and C2 to C4 PFCAs in aqueous phase, and C5 to C8 PFCAs and PFOS by ACN extraction. 0.5 g L^{-1} Fe-BEA35, $C_{0,\mathrm{PFOS}} = 20$ µM, $\mathrm{pH}_0 = 3.0$, oxygen atmosphere. Error ranges stand for the standard deviations of the results from triplicate assays in Figures 2(a). The cumulative error is shown in Figure 1 (b). Lines serve as guides for the eye.

The concentration profiles of the PFOS intermediates along the reaction time are shown in Figure 2 (a). The concentrations of C5, C4 and C3 passed maxima at 6 h, 24 h and 72 h, respectively, and decreased subsequently, while the concentration of C2 increased continuously over the whole reaction time. In addition, the early reaction stages (0 to 6 h) were investigated in more detail (Figure S4). It is worth noting that the concentrations of the initially produced C8, C7, C6 and C5 were relatively low, indicating that the reactivity of carboxylates with longer chains (≥C5) is higher than that of PFOS in the presence of Fe-BEA35. Taking the two C8 compounds, sulfonate vs. carboxylate, as an example, two batch experiments were performed containing PFOA and PFOS separately (Figure S5). By fitting the degradation curves using first-order kinetics (eq. 9), around 8-times higher k_{obs} of PFOA than that of PFOS was observed under the same conditions. Overall, the reaction pattern indicates that cleavage of the C-S bond in the PFOS molecule yields PFOA, which is decomposed stepwise towards shorter-chain PFCAs. The possible reason for the continuous increase of C2 is that this very polar compound is not likely to be adsorbed by zeolites, but rather to be released from the zeolites instead, as shown in Figure S6 and also discussed in the next section.

Figure 2 (b) shows the fluorine mass balance during the degradation of PFOS. The fluorine sources are grouped into four categories: the remaining PFOS, C5 to C8 PFCAs, C2 to C4 PFCAs and fluoride. After 24 h adsorption, a total fluorine (i.e. PFOS) recovery of (94 ± 2)% was achieved by acetonitrile (ACN) extraction (see SI part). The small but significant deficit of (6 ± 2)% points to strong or partially irreversible bonding between Fe-BEA35 and PFOS. After irradiation for 96 h, the final recovery of fluorine in the form of various fluorine-containing products was (92 ± 3)%, which indicates a largely complete PFOS conversion. Nevertheless, the incomplete fluorine mass balance during the reaction (at 6 h, 24 h and 48 h) indicates: (i) formation of some undetected fluorine-containing intermediates, which finally were converted to PFCAs and fluoride (at 72 h and 96 h), and (ii) formation of some strongly bound intermediates, which cannot be thoroughly extracted but remained reactive. In addition, traces (<0.1% of the converted PFOS) of highly volatile 1H-perfluoroalkanes ($C_nF_{2n+1}H$) were detected in the gas phase (Table S2).

In spite of the almost complete PFOS degradation (99%), $d_{\mathrm{F}^-} = 69\%$ indicates an only partial mineralization, whereas some short-chain PFCAs survived. This is in accordance with our previous findings on PFOA degradation in the Fe-zeolite/UV system [23]. Shorter-chain PFCAs (≤4 C) show a low adsorption degree at the applied zeolite concentration, i.e. they desorb into the solution phase instead of being further degraded. To confirm that a complete mineralization of PFOS can finally be obtained, the solution phase of the 96 h UV irradiated Fe-zeolite suspension was further treated by UV activation of sodium persulfate ($Na_2S_2O_8$), which was added in five steps (8.4 mM each) every two hours. As shown in Figure S7, the remaining short-chain PFCAs were nearly completely decomposed (C2 >93%, C3 and C4 >98% removal degree) after 10 h. A nearly complete defluorination (d_{F^-} = 89%) of PFOS was achieved (Figure S8). To sum up, a complete PFOS degradation and defluorination can be achieved in three steps: (i) in the first step, PFOS is removed from water by adsorption on the separable zeolite adsorbent, (ii) the adsorbed (and thus enriched) PFOS can be photochemically degraded on Fe-zeolites and the adsorbent is 'reactively regenerated', and (iii) in the third step, UV/persulfate is applied in order to generate sulfate radicals ($SO_4^{-}\cdot$), which are nonreactive towards PFOS but are able to degrade the remaining PFCAs [14]. This three-step approach is promising for the treatment of PFOS when aiming at its complete mineralization.

3.2. Effect of pH on photochemical degradation of PFOS. As discussed above, the addition of Fe-BEA35 can greatly enhance the photochemical degradation of PFOS. For practical wastewater treatment, further influential factors of the water matrix must be considered, e.g., the pH value. Therefore, we investigated the photochemical degradation of PFOS at various initial pH conditions, i.e. pH_0 = 3.0, 5.5 and 7.0, as shown in Figures 3 (a), (b) and (c). Compared to pH 5.5 (the native pH value of the 0.5 g L^{-1} zeolite suspension with 20 μM PFOS), degradation rate, defluorination and desulfurization efficiencies were notably improved at pH 3.0. The $k_{\text{obs,PFOS}}$ increased from 0.033 h^{-1} to 0.10 h^{-1}, and the half-life was shortened from 21 h to 7 h (Table S1). Within 96 h irradiation, nearly complete PFOS degradation could be achieved at both pH values of 3.0 and 5.5, but a higher d_{F^-} was obtained at pH 3.0 (69%) compared to that at pH 5.5 (56%). The lower defluorination ratio at pH 5.5 is due to lower reaction rates of the formed PFCA intermediates. Their concentration profile along the reaction time at pH_0 = 5.5 is presented in Figure S9. Under these conditions, the concentration of C4 plateaued at t ≥ 72 h, whereas the concentration of C3 and C2 increased continuously over the whole reaction time.

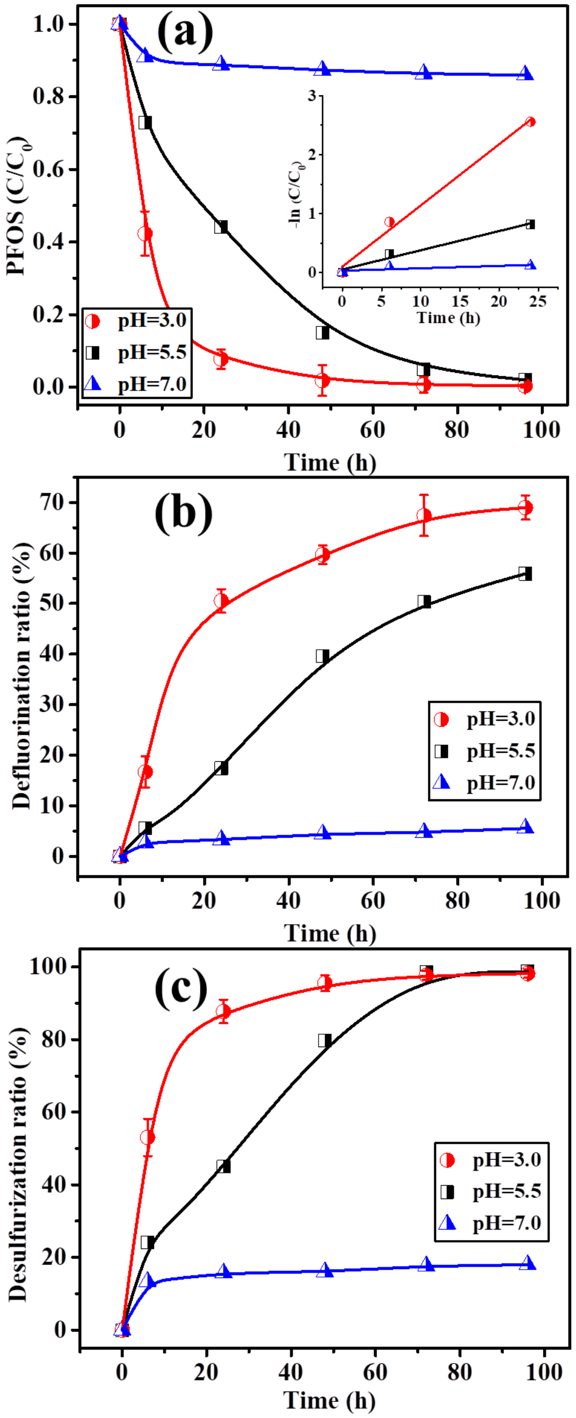

Figure 3. Degradation of PFOS under UV-C irradiation at various initial pH values. Time course of (a) residual PFOS concentration; (b) defluorination ratios (d_{F^-}) and (c) desulfurization ratios ($d_{\mathrm{SO}_4^{2-}}$). 0.5 g L^{-1} Fe-BEA35, $C_{0,\mathrm{PFOS}}$ = 20 μM, oxygen atmosphere. Error ranges stand for the standard deviations of the results from triplicate assays. Lines serve as guides for the eye.

In contrast, at $pH_0 = 3.0$, the concentrations of both C4 and C3 decreased after they passed their maxima (Figure 2(a)). One possible reason for the observed pH effect is that the acidic conditions (pH = 3.0) can promote the adsorption of the PFAS on zeolite, as already observed and discussed in our previous study [23]. Table S1 shows the percentages of the PFOS fraction adsorbed on the zeolite (X_{sorb}) at pH 3.0 and pH 5.5, which are 98% and 84%, corresponding to PFOS loadings on the zeolite of 19.6 mg g^{-1} and 16.8 mg g^{-1}, respectively. A similar pattern was observed in PFCAs adsorption on zeolite, as shown in Figure S6. At both pH values, decreasing X_{sorb} was found for PFCAs with decreasing chain lengths, but still higher X_{sorb} was achieved at pH 3.0 for all PFCAs. In fact, PFOS is nearly exclusively present in its anionic form under all relevant pH conditions due to its very low pK_a value (<0) [24]. It is reasonable to assume that the adsorption of PFOS on zeolites is regulated by the combined effect of hydrophobic interactions between the zeolite surface and the perfluoroalkyl chain, and electrostatic interactions [25-27]. The latter comprise interactions of the terminal $R\text{-}SO_3^-$ group, which are repulsive with silanol or $Si\text{-}O\text{-}Al^-$ groups of the zeolite surface and attractive with Fe^{3+} bound to ion-exchange sites of the zeolite. When pH decreases from 5.5 to 3.0, the density of negative surface charges on zeolites causing repulsive interactions is diminished and adsorption of PFOS is promoted.

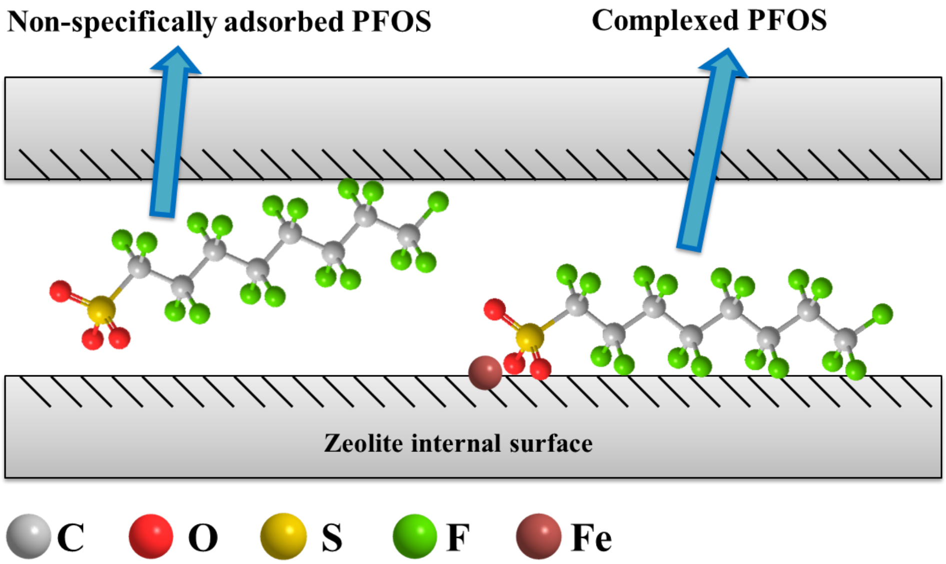

Figure 4. Schematic diagram of PFOS configurations on Fe-BEA35 with and without specific adsorption. The term “complexed PFOS” means the specifically adsorbed PFOS at ferric ions.

When the pH was further increased to 7, the degradation, defluorination and desulfurization efficiencies were strongly inhibited (Figure 3). However, the adsorption of PFOS on zeolites did not decrease significantly (see Table S1) in the range of pH 5.5 to 7. We therefore relate the reduced PFOS degradation efficiency at pH 7 to the altered $X_{\mathrm{complex}}/X_{\mathrm{sorb}}$, i.e. the fraction of complexed (reactive) PFOS related to total adsorbed PFOS on the zeolite. As illustrated in Figure 4, the adsorbed PFOS on Fe-BEA35 can be classified into two categories: the non-specifically adsorbed PFOS and the complexed PFOS (specifically adsorbed PFOS). Upon irradiation, the sulfonate-to-metal charge transfer takes place on the complexed PFOS with its sulfonic group very close to the ferric ions, whereas this charge transfer is hindered on the non-specifically adsorbed PFOS due to the larger gap between its sulfonic group and the ferric ions. As ferric ions have a high affinity to hydroxide ions [28], a lower fraction of the complexed PFOS or a higher non-specifically adsorbed fraction of PFOS can be expected when pH increases. To sum up, a hampered PFOS photochemical degradation upon pH increase was caused by a decreased fraction of complexed PFOS (PFOS-Fe^{3+}) and/or a possibly altered ligand environment at the ferric sites where OH^- ligands replace H_2O.

3.3. Effect of zeolite dosage and PFOS concentration. When the proportion of the Fe-BEA35 dosage and initial PFOS concentration was kept constant, $k_{\mathrm{obs,PFOS}}$ and $d_{\mathrm{F^-}}$ both remained nearly the same with Fe-BEA35 dosages from 0.25 g L^{-1} to 1.0 g L^{-1} and initial PFOA concentrations from 10 μM to 40 μM (Figure 5 and Table 1).

With a constant Fe-BEA35 dosage of 0.5 g L^{-1}, the $k_{\mathrm{obs,PFOS}}$ and $d_{\mathrm{F^-}}$ underwent only a minor decrease when the initial PFOS concentration was reduced from 20 μM to 10 μM. However, when considering PFOS concentrations in the range of real contaminated water (46 nM total PFOS, corresponding to $C_{\mathrm{PFOS,free}}$ = 0.25 nM), a significant decline in $k_{\mathrm{obs,PFOS}}$ was observed, approximately by a factor of 7 (Table 1). In fact, a deceleration of the reaction and 0.4 μM total remaining PFOS was found in the system with initially 20 μM PFOS after 96 h irradiation, also suggesting that a lower $k_{\mathrm{obs,\ PFOS}}$ would appear when low PFOS concentrations are reached. The possible reason is that even if Fe-BEA35 dosage is constant and a similar X_{sorb} is achieved at different PFOS concentrations, the PFOS loading on the zeolite (q_{PFOS}) is strongly decreased at lower PFOS concentration, and a much higher single-point sorption coefficient ($K_{\mathrm{d}} = q_{\mathrm{PFOS}}/C_{\mathrm{PFOS,free}}$) is observed (Table 1).

Table 1. Adsorption and kinetic data on PFOS degradation with varying initial PFOS and zeolite concentrations (at $pH_0 = 3.0$, oxygen atmosphere, T = 25°C if not otherwise noted)

	0.25 g L^{-1} zeolite 10 µM PFOS	**0.5 g L^{-1} zeolite 20 µM PFOS**	**1.0 g L^{-1} zeolite 40 µM PFOS**	**0.5 g L^{-1} zeolite 10 µM PFOS**	**0.5 g L^{-1} zeolite 0.046 µM PFOS**	**0.5 g L^{-1} zeolite 0.046 µM PFOS in real water**	**0.5 g L^{-1} zeolite 20 µM PFOS at 80 °C**
$X_{Sorb, PFOS}$ (%)	96.6	98.6	99.2	98.9	99.6	99.5	98.8
$C_{PFOS, free}$ (µM)	0.34	0.28	0.33	0.11	0.00019	0.00025	0.25
q_{PFOS} (wt%) [a]	1.92	1.96	1.98	0.99	0.0046	0.0046	1.96
K_d (L kg^{-1}) [b]	11×10^4	14×10^4	12×10^4	19×10^4	47×10^4	36×10^4	15×10^4
d_{F^-} after 96 h (%)	60	69	70	66	-[c]	-	72
$k_{obs,PFOS}$ (h^{-1})	0.067±0.013[d]	0.10±0.019	0.13±0.016	0.095±0.024	0.013±0.002	0.020±0.002	0.13±0.048
PFOS $t_{1/2}$ (h)	10±2	7±1	5±1	7±1	54±6	34±5	5±1

[a] Sorbent loading.

[b] Single point adsorption coefficient K_d (L kg^{-1}) = q_{PFOS} (µmol kg^{-1})/$C_{PFOS,free}$ (µmol L^{-1}).

[c] Not available.

[d] The error ranges are derived from the regression analysis of the data.

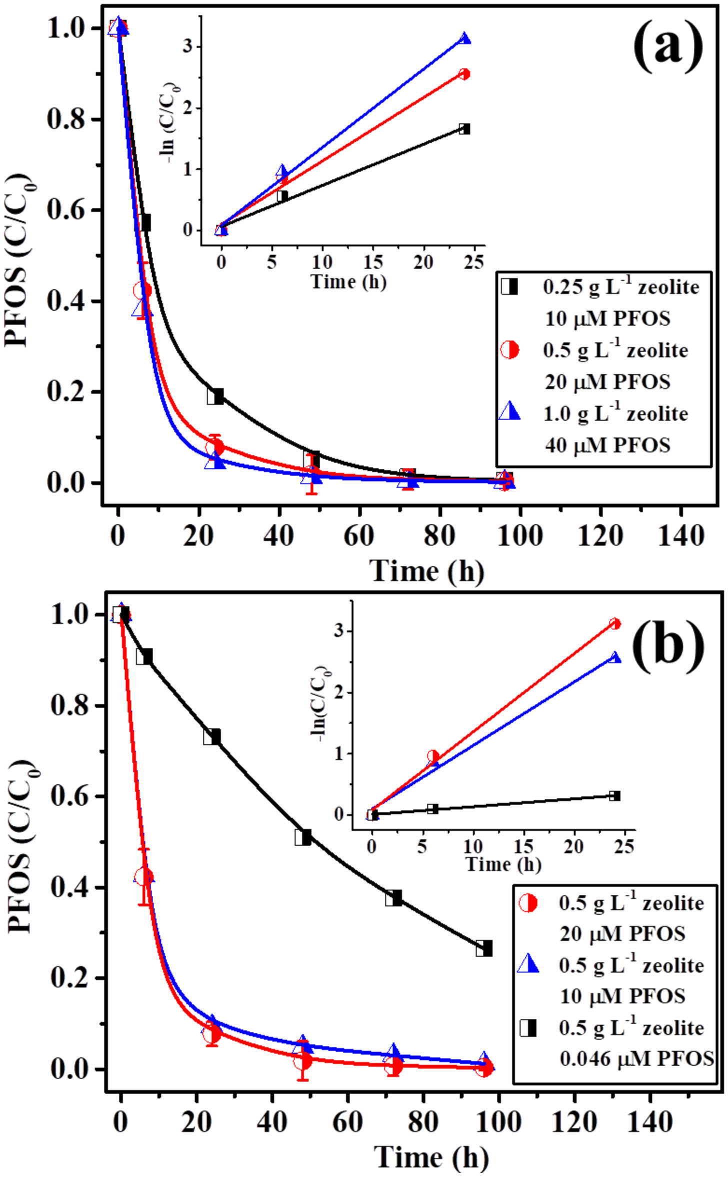

Figure 5. Degradation of PFOS under UV-C irradiation: (a) in the presence of various zeolite dosages; (b) with various initial PFOS concentrations. $pH_0 = 3.0$, oxygen atmosphere. Error ranges stand for the standard deviations of the results from triplicate assays. Lines serve as guides for the eye.

As a result, a lower $X_{\text{complex}}/X_{\text{sorb}}$ ratio is likely expected with a lower PFOS concentration due to the increase of some strongly but non-Fe bonded adsorbates (non-specifically adsorbed PFOS).

That is to say, the $X_{\mathrm{complex}}/X_{\mathrm{sorb}}$ apparently decreases not only with increasing pH (as discussed in Section 3.2) but also at lower PFOS concentrations.

To sum up, increasing the zeolite concentration to a certain extent while keeping the ratio of zeolite dosage to PFOS initial concentration constant will not influence the reaction rate, making it possible to modify the zeolite concentration for application. The overall reaction rate decreases at very low initial PFOS concentration. In practice, a preconcentration of PFOS should be provided in order to make the best use of the established Fe-BEA35/UV system with a high PFOS degradation rate.

3.4. Effect of operation temperature. Increasing temperature would improve chemical reaction rates in most cases, but enhanced temperatures are rarely practical in wastewater treatment due to energy efficiency considerations [29]. Nevertheless, there is a potential to apply photochemical degradation of PFOS under solar light where the UV fraction of solar light can be utilized for driving the photochemical reaction and the higher wavelength fractions for heating up the suspension. The main purposes of performing this experiment with elevated temperatures are to: (i) test whether PFOS photochemical degradation and defluorination can be significantly enhanced at higher temperatures, and (ii) shed light on the mechanistic aspect of the photochemical degradation process. As seen in Figure 6 (a) and Table 1, both $k_{\mathrm{obs,PFOS}}$ and defluorination ratio were only slightly enhanced when reaction temperature was increased from 25 °C to 80 °C (by factor 1.3 in $k_{\mathrm{obs,PFOS}}$). We also observed that the initial PFOS adsorption on zeolite is identical at both temperatures. This is most likely a response to various superimposing effects. Briefly, elevated temperatures in the scale tested do not strongly facilitate the photochemical degradation of PFOS. Such results are in accordance with the photon efficiency of the excitation of the PFOS-Fe^{3+} complex as the rate-limiting factor for the photochemical degradation of PFOS.

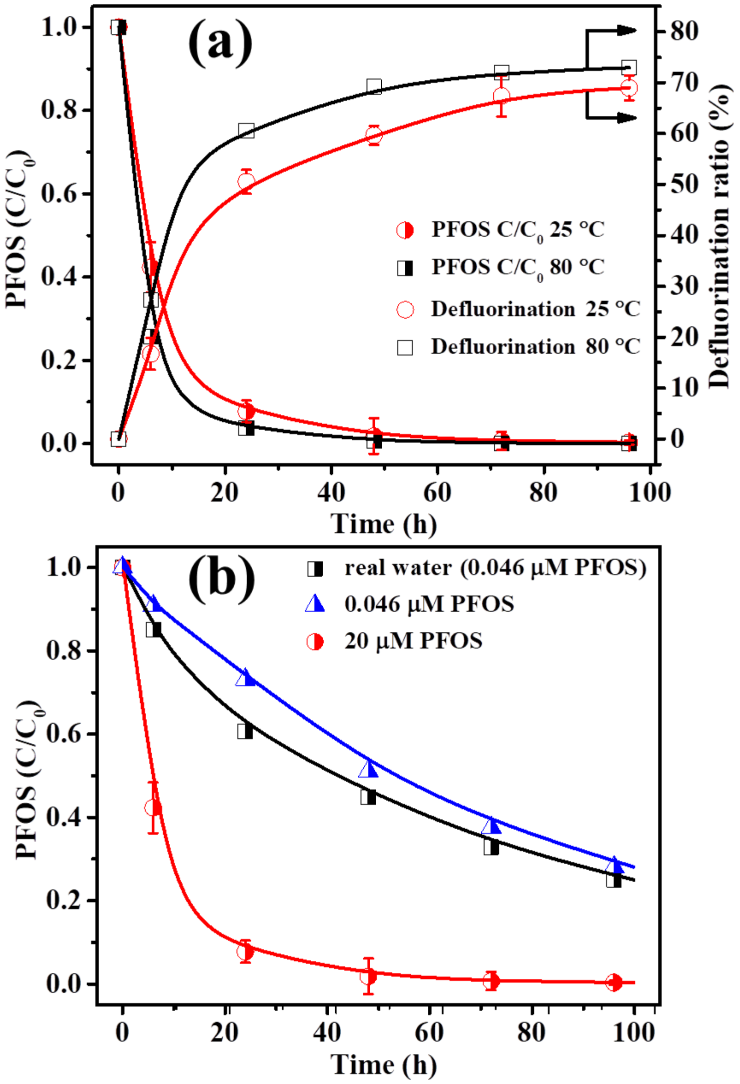

Figure 6. Degradation of PFOS under UV-C irradiation: (a) at different operation temperatures, $C_{0,\mathrm{PFOS}}$ = 20 µM; (b) in a real groundwater sample and synthetic water samples with various initial PFOS concentrations. 0.5 g L^{-1} Fe-BEA35, pH_0 = 3.0, oxygen atmosphere. Error ranges stand for the standard deviations of the results from triplicate assays. Lines serve as guides for the eye.

3.5. Real water test. We have demonstrated a successful and efficient photochemical PFOS degradation by UV-C irradiation after adsorption on Fe-doped zeolites in simple reactors. However, for complex matrices of water containing PFOS, like real ground and surface waters, the degradation behavior of PFOS is unknown and thus worthy of investigation. In this study, a groundwater sample was taken from a well located in Leuna, Germany, for testing. Leuna is a former refinery site near Merseburg in the eastern part of Germany. The groundwater sample contains 9.2 nM of PFOS. In addition, other organic compounds, e.g., methyl *tert*-butyl ether (1.9 mg L^{-1}) and benzene (3.5 mg L^{-1}), were detected in the sample. The detailed chemical composition is presented in Table S3. Due to the very low PFOS concentration in the groundwater sample, preconcentration by zeolite adsorption as described in SI was performed prior to the reaction. The initial total concentration of PFOS in the zeolite suspension was 46 nM after preconcentration. For comparison, a synthetic water sample with the same PFOS concentration (46 nM) was prepared. Apart from the decreased $k_{\mathrm{obs,PFOS}}$ caused by the lower PFOS concentration as discussed in the previous section, the results in Figure 6 (b) and Table 1 show that the degradation performance of PFOS in the groundwater sample is comparable to that in the synthetic water sample with the identical initial PFOS concentration, or even slightly better. Nevertheless, a further preconcentration of PFOS concentration is feasible for the improvement of the degradation behavior. Our previous study about the effect of inorganic ions on PFOA photochemical degradation indicates that sulfate may interfere with the complexation between PFOA and ferric ions, and thus reducing the reaction rate [23]. Such an inhibiting effect was not observed in the groundwater sample even though inorganic ions including sulfate were present ($C_{\mathrm{SO_4^{2-}}}$= 5.6 mM). Overall, a certain PFOS enrichment by Fe-BEA35 from a groundwater sample was achieved, and the photochemical PFOS degradation process established seems applicable to a real water matrix.

3.6. Reusability test. From the perspective of practical applications, catalyst stability and reusability are important issues that must be considered. The stability test of Fe-zeolites was evaluated by degrading PFOS in a recycling experimental set-up as described in the SI. As shown in Figure S10, the catalyst activity showed a slightly decreasing tendency, but around 90% of its initial activity was maintained with respect to the remaining PFOS percentage in the fourth consecutive run. Two reasons are plausible for the observed decrease in the catalytic performance: (i) hardly avoidable mass losses of the catalyst particles during the reusability test, and (ii) a certain carry-over of adsorbed PFOS as well as its degradation products during the runs. Nevertheless, the inherent catalyst activity will not be affected for either of these two reasons. The results of the recycling test demonstrate the good stability of Fe-BEA35, and the potential for application.

3.7. Considerations of energy demand. In terms of practical application, energy demand is an important issue that must be considered. The specific energy consumption (SEC) for 90% PFOS degradation in contaminated water without an enrichment step was calculated to be 468 kWh m^{-3} based on the fluence rate of the photochemical reactor with a 1.1 cm optical path length [30].

Comparing our system with other PFOS *degradation* processes, e.g., the BDD-based electrochemical system, the SEC for 90% PFOS degradation was reported as 20 kWh m^{-3} [31]. Apparently, the Fe-zeolite-based photocatalytic system is a highly energy demanding PFOS treatment method. However, thanks to Fe-zeolites' high adsorption affinity towards PFOS, most water can be discharged after desired PFOS depletion. In such a two-step system the contribution of SEC for the photocatalytic PFOS destruction as main driver for energy consumption would be much lower (approx. 47 or 4.7 kWh m^{-3} treated water by assuming a 90 or 99% water disposal). Nevertheless, this energy demand alone corresponds to a contribution of ≥ 1 €/m^3 to total operation costs. For the currently prevailing large-scale PFAS *removal* technologies, i.e. activated carbon adsorption, ion exchange and reverse osmosis, full operation treatment costs in the range of 0.5 – 0.9 € m^{-3}, 0.8 – 1.7 € m^{-3} and 1.7 – 2.2 € m^{-3} were reported for the example of groundwater pump-and-treat units.[32] This comparison illustrates that further material and process optimization is required for the Fe-zeolite-based photocatalysis system in order to improve energy-efficiency and expected operation costs. The present study should be understood as a proof-of-principle for a combined adsorption/photocatalysis approach that not only removes PFAS from water but facilitates their on-site destruction and adsorbent regeneration. More detailed discussion about energy demand and practical application can be found in the SI part.

3.8. Possible pathways of photochemical degradation of PFOS. Several reaction pathways of photochemical degradation of PFOS have been investigated in the literature [21, 23, 33-36]. Based on the literature study and our experimental results, a possible reaction mechanism is proposed in Scheme 1. First, PFOS is specifically adsorbed on Fe^{3+} sites, forming PFOS-Fe^{3+} complexes (eq. 7). After the excitation under UV irradiation, the Fe^{3+} complexes are oxidized via a sulfonate-to-metal electron transfer process to produce $C_8F_{17}SO_3\cdot$ (eq. 8) [21]. A similar electron transfer step is proposed in ferric ion mediated photo-decomposition and electrochemical oxidation of PFOS in previous studies [21, 37]. The loss of one electron leads to a stretching of the C-S bond, thus easing the desulfurization when reacting with water, yielding perfluorinated alkyl radicals ($\bullet C_8F_{17}$) and sulfate anions (eq. 10).

$$C_8F_{17}SO_3\cdot + H_2O \longrightarrow C_8F_{17}\cdot + SO_4^{2-} + 2H^+ \qquad (10)$$

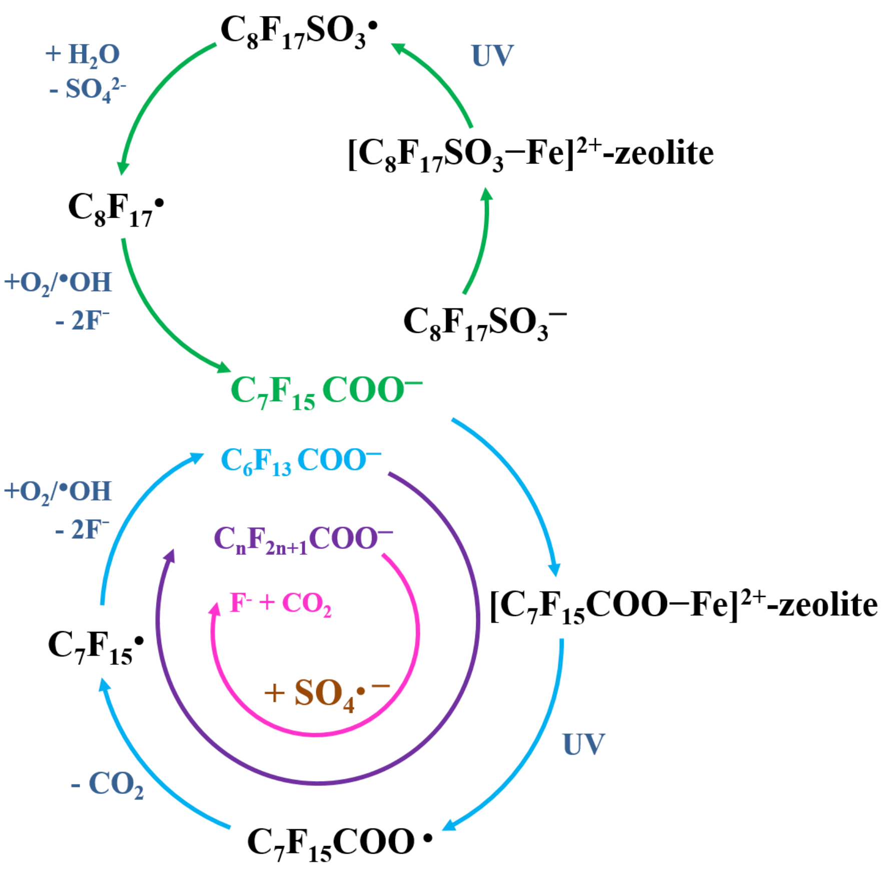

Scheme 1. Proposed reaction mechanism for PFOS photochemical degradation on Fe-BEA35. Detailed radical reactions and hydrolysis steps are presented in SI.

The fate of the $\bullet C_8F_{17}$ radical is determined by a number of radical reactions and hydrolysis steps, further detailed in the SI part. They are the same for PFOS and PFOA decomposition, regardless of the initial head group. In addition, the reduced iron sites (Fe^{2+}) will be re-oxidized by oxygen or hydroxyl radicals in order to close the photocatalytic cycle (eqs. 11-12). Hydroxyl radicals may be formed during the photolysis of water and ferric species under UV irradiation (eq. 13) [38].

$$Fe^{2+}\text{-zeolite} + O_2 \longrightarrow Fe^{3+}\text{-zeolite} + \cdot O_2^- \qquad (11)$$

$$Fe^{2+}\text{-zeolite} + \cdot OH \longrightarrow Fe^{3+}\text{-zeolite} + OH^- \qquad (12)$$

$$Fe^{3+}\text{-zeolite} + H_2O \xrightarrow{UV} Fe^{2+}\text{-zeolite} + \cdot OH + H^+ \qquad (13)$$

4. ENVIRONMENTAL IMPLICATIONS.

The idea of using Fe-zeolites as both adsorbent and photocatalyst enables an efficient technological approach for PFOS removal and degradation as well as on-site sorbent regeneration.

In the first step, PFOS is removed from the large volume of incoming water by adsorption onto the Fe-zeolites, which can be separated e.g. by filtration. In the second step, the concentrate of the loaded zeolite particles can be regenerated *in situ* by photochemical degradation with UV-C irradiation. The resulting byproducts, i.e. short-chain PFCAs, are desorbed into the aqueous phase. Their complete mineralization can be achieved in the regeneration solution (third step) by combination with UV activation of sodium persulfate. The Fe-zeolite, as a separable adsorbent, is able to catalyze not only PFOS but also PFOA degradation in the adsorbed state. Thus, our findings are relevant for: (i) the development of adsorptive PFAS removal technologies combined with on-site adsorbent regeneration; (ii) inspiring PFAS removal approaches based on other Fe-loaded catalysts; (iii) providing suggestions for future studies on material optimization, reactor and process design.

ACKNOWLEDGMENTS

We thank Jieying Zhou for useful discussion and proof reading. Lin Qian acknowledges financial support by China Scholarship Council.

REFERENCES

[1] A. Pistocchi, R. Loos, A map of European emissions and concentrations of PFOS and PFOA, Environ. Sci. Technol., 43 (2009) 9237-9244.
[2] R. Arrieta-Cortes, P. Farias, C. Hoyo-Vadillo, M. Kleiche-Dray, Carcinogenic risk of emerging persistent organic pollutant perfluorooctane sulfonate (PFOS): A proposal of classification, Regul. Toxicol. Pharmacol., 83 (2017) 66-80.
[3] L. Ahrens, Z. Xie, R. Ebinghaus, Distribution of perfluoroalkyl compounds in seawater from Northern Europe, Atlantic Ocean, and Southern Ocean, Chemosphere, 78 (2010) 1011-1016.
[4] U. Eriksson, A. Roos, Y. Lind, K. Hope, A. Ekblad, A. Kärrman, Comparison of PFASs contamination in the freshwater and terrestrial environments by analysis of eggs from osprey (Pandion haliaetus), tawny owl (Strix aluco), and common kestrel (Falco tinnunculus), Environ. Res., 149 (2016) 40-47.
[5] M. González-Doncel, C. Fernández Torija, M.V. Pablos, P. García Hortigüela, M. López Arévalo, E.M. Beltrán, The role of PFOS on triclosan toxicity to two model freshwater organisms, Environ. Pollut., 263 (2020) 114604.
[6] K.T. Eriksen, O. Raaschou-Nielsen, M. Sørensen, M. Roursgaard, S. Loft, P. Møller, Genotoxic potential of the perfluorinated chemicals PFOA, PFOS, PFBS, PFNA and PFHxA in human HepG2 cells, Mutat. Res.-Gen. Tox. En., 700 (2010) 39-43.
[7] K. Harada, F. Xu, K. Ono, T. Iijima, A. Koizumi, Effects of PFOS and PFOA on L-type Ca2+ currents in guinea-pig ventricular myocytes, Biochem. Biophys. Res., 329 (2005) 487-494.

[8] C. Fei, J.K. McLaughlin, L. Lipworth, J. Olsen, Maternal levels of perfluorinated chemicals and subfecundity, Hum. Reprod., 24 (2009) 1200-1205.
[9] N. Johansson, A. Fredriksson, P. Eriksson, Neonatal exposure to perfluorooctane sulfonate (PFOS) and perfluorooctanoic acid (PFOA) causes neurobehavioural defects in adult mice, Neurotoxicology, 29 (2008) 160-169.
[10] E.M. Sunderland, X.C. Hu, C. Dassuncao, A.K. Tokranov, C.C. Wagner, J.G. Allen, A review of the pathways of human exposure to poly- and perfluoroalkyl substances (PFASs) and present understanding of health effects, J. Exposure Sci. Environ. Epidemiol., 29 (2019) 131-147.
[11] K. Sekiguchi, T. Kudo, K. Sankoda, Combined sonochemical and short-wavelength UV degradation of hydrophobic perfluorinated compounds, Ultrason. Sonochem., 39 (2017) 87-92.
[12] H. Javed, C. Lyu, R. Sun, D. Zhang, P.J.J. Alvarez, Discerning the inefficacy of hydroxyl radicals during perfluorooctanoic acid degradation, Chemosphere, 247 (2020) 125883.
[13] M. Trojanowicz, A. Bojanowska-Czajka, I. Bartosiewicz, K. Kulisa, Advanced Oxidation/Reduction Processes treatment for aqueous perfluorooctanoate (PFOA) and perfluorooctanesulfonate (PFOS) – A review of recent advances, Chem. Eng. J., 336 (2018) 170-199.
[14] T.A. Bruton, D.L. Sedlak, Treatment of perfluoroalkyl acids by heat-activated persulfate under conditions representative of in situ chemical oxidation, Chemosphere, 206 (2018) 457-464.
[15] H. Park, C.D. Vecitis, J. Cheng, N.F. Dalleska, B.T. Mader, M.R. Hoffmann, Reductive degradation of perfluoroalkyl compounds with aquated electrons generated from iodide photolysis at 254 nm, Photochem. Photobiol. Sci., 10 (2011) 1945-1953.
[16] M.J. Bentel, Y. Yu, L. Xu, Z. Li, B.M. Wong, Y. Men, J. Liu, Defluorination of per- and polyfluoroalkyl substances (PFASs) with hydrated electrons: Structural dependence and implications to PFAS remediation and management, Environ. Sci. Technol., 53 (2019) 3718-3728.
[17] H. Tian, J. Gao, H. Li, S.A. Boyd, C. Gu, Complete defluorination of perfluorinated compounds by hydrated electrons generated from 3-indole-acetic-acid in organomodified Montmorillonite, Sci. Rep., 6 (2016) 32949.
[18] K.E. Carter, J. Farrell, Oxidative destruction of perfluorooctane sulfonate using boron-doped diamond film electrodes, Environ. Sci. Technol., 42 (2008) 6111-6115.
[19] I. Grčić, G. Li Puma, Photocatalytic degradation of water contaminants in multiple photoreactors and evaluation of reaction kinetic constants independent of photon absorption, irradiance, reactor geometry, and hydrodynamics, Environ. Sci. Technol., 47 (2013) 13702-13711.
[20] Z. Sun, C. Zhang, P. Chen, Q. Zhou, M.R. Hoffmann, Impact of humic acid on the photoreductive degradation of perfluorooctane sulfonate (PFOS) by UV/iodide process, Water Res., 127 (2017) 50-58.
[21] L. Jin, P. Zhang, T. Shao, S. Zhao, Ferric ion mediated photodecomposition of aqueous perfluorooctane sulfonate (PFOS) under UV irradiation and its mechanism, J. Hazard. Mater., 271 (2014) 9-15.
[22] X. Liang, J. Cheng, C. Yang, S. Yang, Factors influencing aqueous perfluorooctanoic acid (PFOA) photodecomposition by VUV irradiation in the presence of ferric ions, Chem. Eng. J., 298 (2016) 291-299.
[23] L. Qian, A. Georgi, R. Gonzalez-Olmos, F.-D. Kopinke, Degradation of perfluorooctanoic acid adsorbed on Fe-zeolites with molecular oxygen as oxidant under UV-A irradiation, Appl. Cat. B: Environ., 278 (2020) 119283.
[24] D. Brooke, A. Footitt, T. Nwaogu, Environmental risk evaluation report: Perfluorooctanesulphonate (PFOS), Environment Agency, UK, 2004.
[25] U. Shafique, V. Dorn, A. Paschke, G. Schuurmann, Adsorption of perfluorocarboxylic acids at the silica surface, Chem. Commun., 53 (2017) 589-592.
[26] P. Punyapalakul, K. Suksomboon, P. Prarat, S. Khaodhiar, Effects of surface functional groups and porous structures on adsorption and recovery of perfluorinated compounds by inorganic porous silicas, Sep. Sci. Technol., 48 (2013) 775-788.

[27] V. Ochoa-Herrera, R. Sierra-Alvarez, Removal of perfluorinated surfactants by sorption onto granular activated carbon, zeolite and sludge, Chemosphere, 72 (2008) 1588-1593.
[28] E. Hogfeldt, Stability constants of metal-ion complexes. Part A Inorganic ligands. International Union of Pure and Applied Chemists., Pergamon Press, New York, 1982.
[29] B. Tang, L. Yu, S. Huang, J. Luo, Y. Zhuo, Energy efficiency of pre-treating excess sewage sludge with microwave irradiation, Bioresour. Technol., 101 (2010) 5092-5097.
[30] I.A. Katsoyiannis, S. Canonica, U. von Gunten, Efficiency and energy requirements for the transformation of organic micropollutants by ozone, O3/H2O2 and UV/H2O2, Water Res., 45 (2011) 3811-3822.
[31] L. Wang, J. Lu, L. Li, Y. Wang, Q. Huang, Effects of chloride on electrochemical degradation of perfluorooctanesulfonate by Magnéli phase Ti4O7 and boron doped diamond anodes, Water Res., 170 (2020) 115254.
[32] Züblin Umwelttechnik GmbH Website; .
[33] S. Wang, Q. Yang, F. Chen, J. Sun, K. Luo, F. Yao, X. Wang, D. Wang, X. Li, G. Zeng, Photocatalytic degradation of perfluorooctanoic acid and perfluorooctane sulfonate in water: A critical review, Chem. Eng. J., 328 (2017) 927-942.
[34] H. Hori, A. Yamamoto, K. Koike, S. Kutsuna, I. Osaka, R. Arakawa, Photochemical decomposition of environmentally persistent short-chain perfluorocarboxylic acids in water mediated by iron (II)/(III) redox reactions, Chemosphere, 68 (2007) 572-578.
[35] H.V. Lutze, J. Brekenfeld, S. Naumov, C. von Sonntag, T.C. Schmidt, Degradation of perfluorinated compounds by sulfate radicals–New mechanistic aspects and economical considerations, Water Res., 129 (2018) 509-519.
[36] D. Liu, Z. Xiu, F. Liu, G. Wu, D. Adamson, C. Newell, P. Vikesland, A.-L. Tsai, P.J. Alvarez, Perfluorooctanoic acid degradation in the presence of Fe(III) under natural sunlight, J. Hazard. Mater., 262 (2013) 456-463.
[37] Q. Zhuo, M. Luo, Q. Guo, G. Yu, S. Deng, Z. Xu, B. Yang, X. Liang, Electrochemical oxidation of environmentally persistent perfluorooctane sulfonate by a novel lead dioxide anode, Electrochim. Acta, 213 (2016) 358-367.
[38] H.-J. Benkelberg, P. Warneck, Photodecomposition of iron(III) hydroxo and sulfato complexes in aqueous solution: wavelength dependence of OH and SO4- quantum yields, J. Phys. Chem., 99 (1995) 5214-5221.

Supporting information

Detailed information on Experimental Section

Chemicals and Materials. All chemicals were of reagent grade purity and used without purification. Deionized water was used in this work for solution preparation. The Trap-Ox® zeolite Fe-BEA35 was obtained from INTRAPORE GmbH (Germany). The molar ratio of SiO_2/Al_2O_3 in this zeolite is 35. The BEA framework consists of two types of channels with 12 atoms (Si or Al), i.e. Ø 5.6 – 5.7 Å, zig-zag form, and Ø 6.6 – 6.7 Å, straight form, respectively. The characterization of Fe-BEA35 including morphology, zeolite framework type, iron species, etc., were described in our previous work [1]. In this study, the Fe-BEA35 is used as adsorbent and catalyst. The pretreatment of Fe-BEA35 was applied in order to stabilize iron ions in the form of Fe^{3+} and to remove any leachable iron species by competitive exchange with potassium ions under acidic conditions (pH = 3.0) [2]. The iron content in Fe-BEA35 after pretreatment was 1.3 wt-% measured by X-ray fluorescence analysis. After 96 h reaction under acidic conditions (pH = 3.0), the concentration of the total leached iron was 0.11 mg L^{-1} as determined photometrically. This value is even below the permitted iron concentration (0.2 mg L^{-1}) for drinking water according to German Environment Agency (UBA) in Germany. The particle size of Fe-BEA35 in suspension was measured by dynamic light scattering indicating a mean diameter of 860 nm. PFOS potassium salt ($C_8F_{17}SO_3K$, 98%), heptafluorobutyric acid (HFBA, C_3F_7COOH, 98%), perfluorooctanoic acid (PFOA, $C_7F_{15}COOH$, 96%) and sodium persulfate ($Na_2S_2O_8$, 98%) were purchased from Sigma Aldrich. Perfluoroheptanoic acid (PFHpA, $C_6F_{13}COOH$, 97%) was purchased from Alfa Aesar. Perfluorohexanoic acid (PFHeA, $C_5F_{11}COOH$, 98%), Perfluoropropionic acid (PFPrA, C_2F_5COOH, 97%) and perfluoropentanoic acid (PFPeA, C_4F_9COOH, 97%) were purchased from J&K Scientific. Trifluoroacetic acid (TFA, CF_3COOH, 99%) was purchased from Fluka.

Photochemical Procedures. The photochemical experiments were conducted in a 450 mL cylindrical reactor. Details about the reactor setup are shown in Figure S1. The outer and inner diameters of the reactor were 60 mm and 38 mm, respectively. A low-pressure mercury lamp (20 W, Peschl Ultraviolet GmbH, Germany) covered with an immersion quartz tube (8) was placed in the center of the reactor, emitting 254 nm UV light. The photon flux was determined by ferrioxalate actinometry to be 1.46×10^{-5} mol s^{-1} [3]. Where not otherwise stated, an aqueous PFOS solution (350 mL, 40 µM) was mixed with 0.175 g of Fe-BEA35 in a 500 mL bottle followed by shaking for 24 h to establish adsorption equilibrium. The initial pH values were adjusted by HCl or NaOH. The 350 mL suspension was added to the reactor and purged with oxygen gas from inlet gas port (6) for 30 min shortly before UV irradiation. Reactions were performed in the closed reactor with a certain headspace volume of oxygen (100 mL oxygen per 350 mL of suspension). The reaction temperature was maintained at 25 °C or 80 °C, accordingly, by a circulating cooling or heating system from inlet water port (3) to outlet water port (4). This cylindrical reactor is equipped with an integrated magnetic drive circulation bar (9), which provides the mixing of zeolites suspension when used together with a lateral riser bypass (5) as indicated with arrows. Samples of the reaction suspension were taken from sampling port (2) at certain time intervals.

In order to obtain the total concentration (including adsorbed and freely dissolved fraction), residual PFOS and byproducts were extracted from the zeolite into a liquid phase by adjusting suspension pH to 2, followed by addition of 95 vol-% acetonitrile for extraction. Based on preliminary tests, the PFOS recovery (before irradiation) by this procedure was supported by the addition of the acid and was almost complete, i.e. (94 ± 2) %. In order to obtain the total fluoride, sulfate and freely dissolved acid concentrations in the aqueous phase, 1 mL aliquots of the suspension were taken and subsequently centrifuged for 5 min at 2500 rpm. The clear supernatant was subjected to LC-MS and IC analysis.

In order to achieve a complete mineralization of PFOS and its degradation products, the UV-irradiated suspension was further treated with UV/$Na_2S_2O_8$ in the following way: the irradiated suspension was centrifuged for 5 min at 2500 rpm to remove the zeolite particles (containing almost no PFOS and its degradation products, as shorter-chain PFCAs desorb into the water phase). The supernatant (about 340 mL) was taken and sodium persulfate was added in five steps (8.4 mM each) every two hours, under UV irradiation, until all PFCAs were degraded.

The investigated real groundwater sample contained PFOS in very low concentration (9.2 nM). For the purpose of improving the degradation reaction rate and the utilization of UV light, the PFOS concentration was enriched from the water sample on the Fe-BEA35 zeolite with high adsorption affinity towards PFOS. Figure S2 shows a scheme of the groundwater sample treatment prior to irradiation. 1.75 L of real groundwater was filtered by 0.45 μm filter paper in a Buchner funnel in order to remove large particles and aggregates. The filtered water sample (chemical composition shown in Table S3) was then mixed with 0.175 g Fe-BEA35 and shaken for 24 h. After 24 h, the majority (≥90%) of PFOS was adsorbed on zeolites. The concentration of dissolved

PFOS was below the detection limit (<1 nM) of the LC-MS method when directly injected. Thus, it was preconcentrated by evaporation of 90% of the water at 60°C in an oven. The suspension was then kept unstirred for another 48 h, after which 80% of clear supernatant was removed. The remaining PFOS-containing zeolite particles were re-suspended and the suspension (350 mL) was collected for further photochemical treatment.

In the reusability test, after each irradiation period, the irradiated suspension was centrifuged for 5 min at 2500 rpm to remove the supernatant. The remaining zeolites contained almost no PFOS and its degradation products, as shorter-chain PFCAs and fluoride desorbed into the aqueous phase. The zeolite particles were re-suspended after adding the same amount of fresh aqueous PFOS solution. The suspension was ready for the next irradiation run after 1-day adsorption.

Analyses. PFOS and its C4-C8 degradation intermediates, i.e. PFBA, PFPeA, PFHeA, PFHpA and PFOA, were determined with an HPLC-MS system (SHIMADZU Corporation; LCMS-2020). The mobile phase consisted of solvents A and B: solvent A was composed of 20 mM ammonium acetate in 10 vol-% methanol and 90 vol-% deionized water and solvent B was composed of 20 mM ammonium acetate in 10 vol-% deionized water and 90 vol-% methanol. A combination of 65 vol-% of solvent B and 35 vol-% of solvent A was pumped with a flow rate of 0.25 mL min^{-1}. The run time of each measurement was 28 min. The PFOS reagent contained linear and branched isomers, whereby the linear PFOS was the major component. In this study, we focused on the properties of linear PFOS. Beside fluoride and sulfate, PFPrA (C3) and TFA (C2) concentrations were measured with an IC DX 500 ion chromatograph (Thermo Fisher) equipped with conductivity detector (IC 25), anion suppressor (ASRS300) and an IonPac AS11-HC column.

The analysis of gas-phase intermediates produced during PFOS photodegradation was performed on a GC/MS (SHIMADZU Corp., GCMS-QP2010) through headspace sampling and injection of gaseous samples (25 µL) after irradiation. A 30 m DB1 (0.25 µm film thickness, 0.32 mm inner diameter) was used as GC separation column. The MS was operated in the SCAN mode (m/z = 41-250 amu). The GC oven was kept isothermal at 35°C, and the injector temperature was set at 150 °C.

Tables S1 to S3 Referred in the Main Text

Table S1. PFOS adsorption, defluorination ratios (d_{F^-}), pseudo-first-order degradation rate constants ($k_{\mathrm{obs,PFOS}}$) and half-lives of PFOS degradation at different initial pH values in aqueous suspension. 0.5 g L^{-1} Fe-BEA35, $C_{0,\mathrm{PFOS}}$ = 20 µM, oxygen atmosphere.

	pH = 3.0	**pH = 5.5**	**pH = 7.0**
Percentage on zeolite [a]	98	84	88
Loading of PFOS on zeolite (mg g^{-1})	19.6	16.8	17.6
d_{F^-} after 96 h (%)	69	56	6
$k_{\mathrm{obs,PFO}S}$ (h^{-1}) [b]	0.10 ± 0.019	0.033 ± 0.010	0.0041 ± 0.0059
PFOS $t_{1/2}$ (h) [b]	7 ± 1	21 ± 5	169 ± 99

[a] after 24 h adsorption.

[b] Error ranges are derived from the regression analysis of the data and correspond to one standard deviation.

Table S2. Gas-phase products identified by GC/MS headspace analysis after 96 h irradiation. 0.5 g L^{-1} Fe-BEA35, $C_{0,\mathrm{PFOS}}$ = 20 µM, pH$_0$ = 3.0 and oxygen atmosphere. GC/MS conditions see Experimental section.

Retention time (min)	**Formula**	**Chemical Structure (GC/MS Library)**
0.89	C_2HF_5	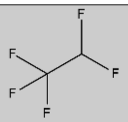
0.97	C_3HF_7	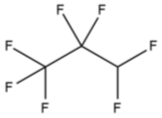
1.14	C_4HF_9	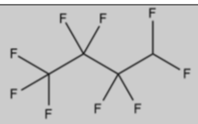

The position of H atoms in the molecules was derived from the EI-fragmentation pattern in the mass spectra.

Table S3. Properties and chemical composition of filtered groundwater sample from Leuna, Germany.

pH	**DO** [a] **mg L^{-1}**	**EC** [b] **µS cm^{-1}**	**TOC** [c] **mg L^{-1}**	**Cl^-** **mg L^{-1}**	**NO_3^-** **mg L^{-1}**	**SO_4^{2-}** **mg L^{-1}**	**MTBE** **mg L^{-1}**	**Benzene** **mg L^{-1}**
7.6	0.2	2579	67	281	48	538	1.9	3.5

[a] DO: dissolved oxygen.

[b] EC: electrical conductivity.

[c] TOC: total organic carbon content

Figures S1 to S10 Referred in the Main Text

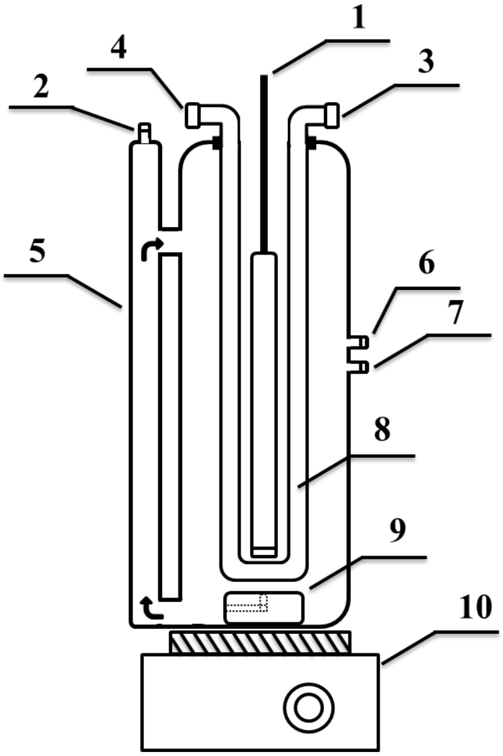

Figure S1. Scheme of the experimental setup for photochemical experiments. (1) low-pressure mercury UV lamp, (2) sampling port, (3) inlet water port, (4) outlet water port, (5) bypass, (6) inlet gas port, (7) outlet gas port, (8) quartz cooling tube, (9) magnetic drive circulation bar, (10) magnetic stirrer.

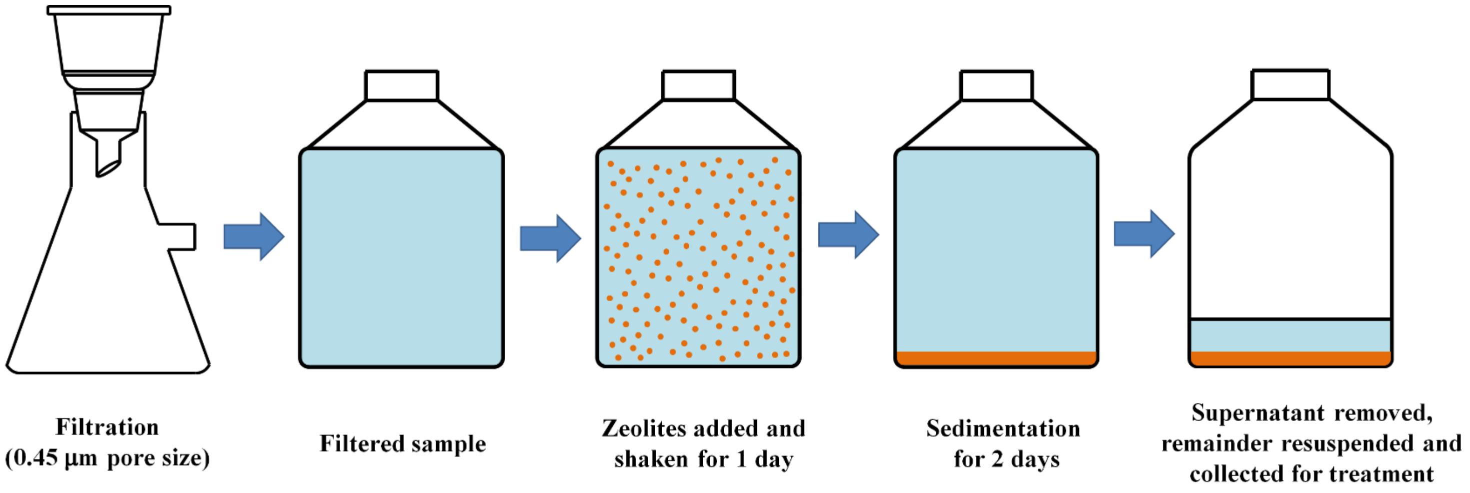

Figure S2. Diagram of groundwater treatment prior to irradiation.

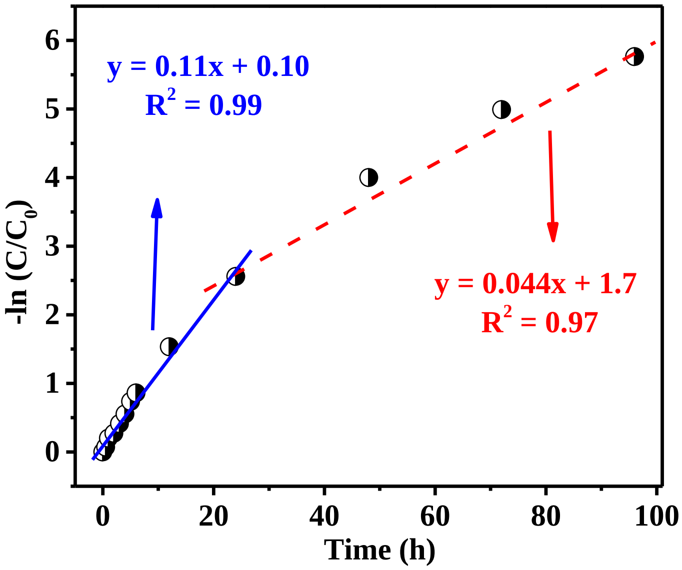

Figure S3. PFOS degradation first-order-kinetics plot, ln(C/C$_0$) versus reaction time. 0.5 g L^{-1} Fe-BEA35, C$_{0,\text{PFOS}}$ = 20 µM, pH$_0$ = 3.0, oxygen atmosphere. Pseudo-first-order kinetics can fit well PFOS photochemical degradation within the period of 0-24 h (blue curve) corresponding to ≤92% turnover. The rate coefficient decreases slightly at higher turnover.

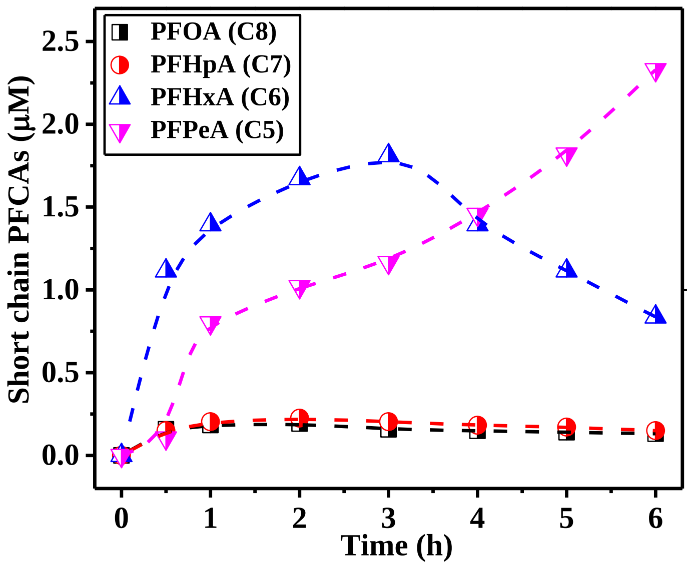

Figure S4. Formation of short-chain intermediates during photochemical degradation of PFOS in the early reaction stages (0 to 6 h). 0.5 g L^{-1} Fe-BEA35, $C_{0,PFOS}$ = 20 μM, pH_0 = 3.0 and oxygen atmosphere. Lines serve as guides for the eye.

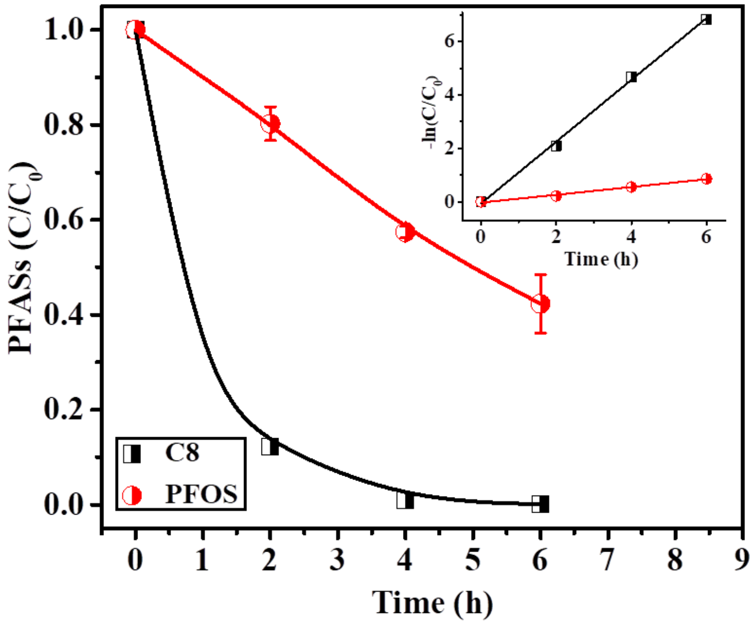

Figure S5. Comparison of photochemical degradation of PFOS and PFOA (C8). 0.5 g L^{-1} Fe-BEA35, $C_{0,PFOS}$ = 20 μM, $C_{0,PFOA}$ = 20 μM, pH_0 = 3.0 and oxygen atmosphere. Lines serve as guides for the eye.

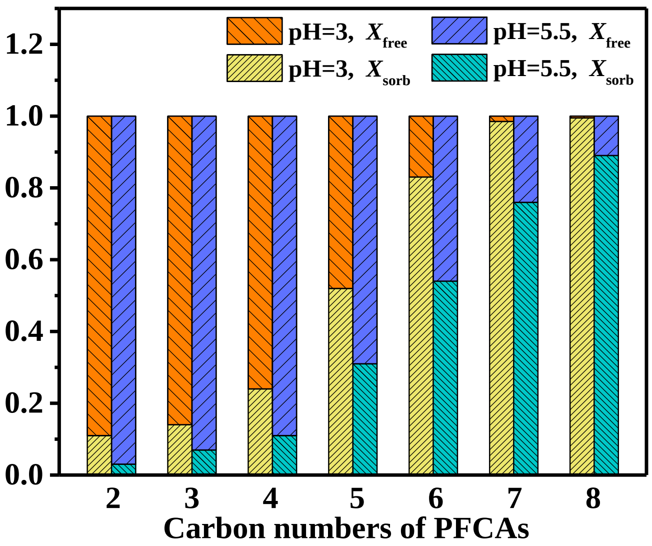

Figure S6. Partitioning of PFCAs with various chain lengths and at different initial pH values between zeolite Fe-BEA35 (X_{sorb}) and the aqueous phase (X_{free}) after 1 day shaking. 0.5 g L^{-1} Fe-BEA35, $C_{0,PFCAs}$ = 2.4 µM.

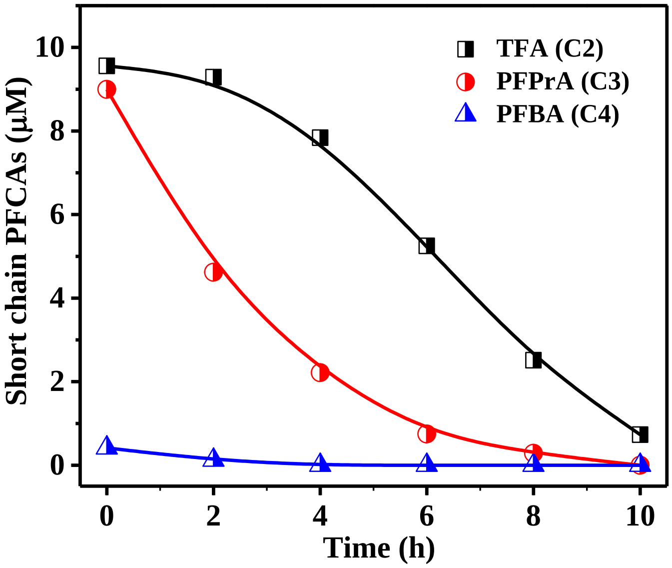

Figure S7. Short-chain PFCA degradation by UV/$Na_2S_2O_8$. $Na_2S_2O_8$ was added in five steps (8.4 mM each) every two hours. The start solution was the aqueous phase of the PFOS/Fe-zeolite suspension after 96 h irradiation. The procedure to obtain this solution is described in Experimental Section in SI. Lines serve as guides for the eye.

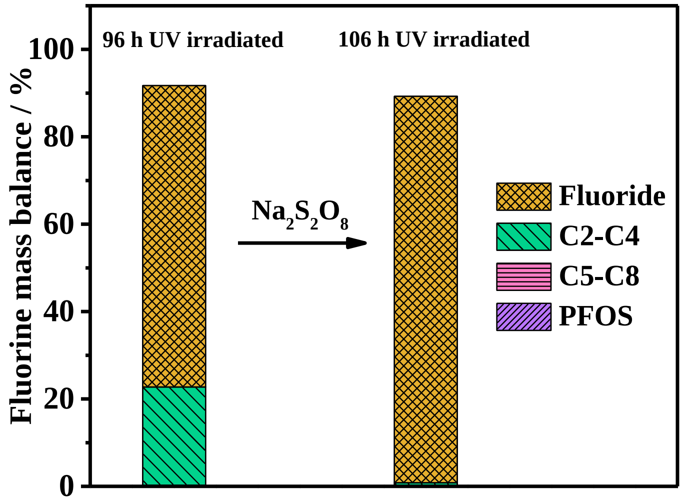

Figure S8. Fluorine mass balance before and after $Na_2S_2O_8$ treatment of PFOS degradation products solution. The start solution was the aqueous phase of the PFOS/Fe-zeolite suspension after 96 h irradiation. The procedure to obtain this solution is described in Experimental Section in SI.

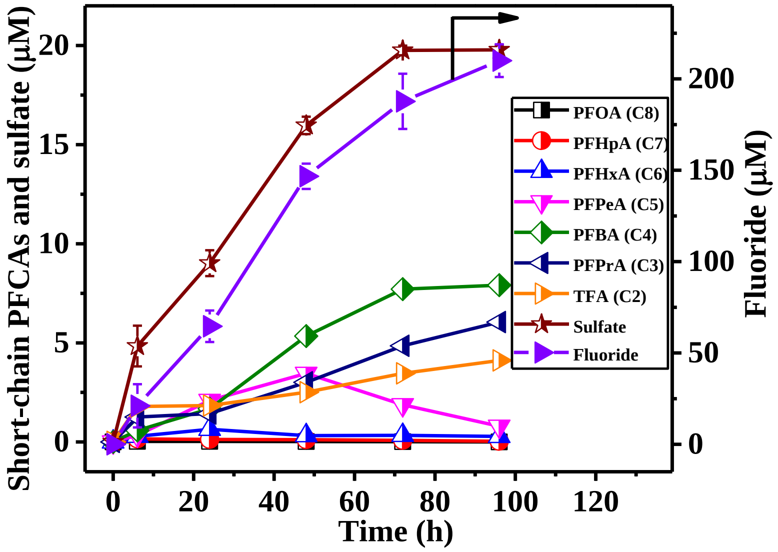

Figure S9. Formation of short-chain intermediates, fluoride and sulfate during photochemical degradation of PFOS. 0.5 g L^{-1} Fe-BEA35, $C_{0,PFOS}$ = 20 µM, pH_0 = 5.5, oxygen atmosphere. Error ranges stand for the standard deviations of the results from triplicate assays. Lines serve as guides for the eye.

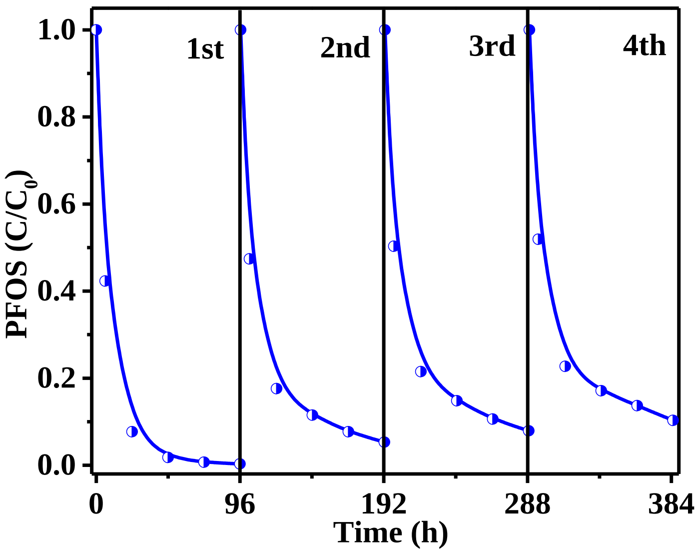

Figure S10. PFOS degradation and defluorination in reusability test with Fe-BEA35 (0.5 g L^{-1}) under UV irradiation. $C_{0,PFOS}$ = 48 µM each, pH_0 = 3.0, oxygen atmosphere. Lines serve as guides for the eye.

Considerations of Energy Demand and Practical Application

As discussed in Section 3.7., the Fe-zeolites system without an enrichment step is a high energy demanding PFOS treatment technology. Nevertheless, an efficient enrichment of highly diluted PFOS in water can be achieved with Fe-zeolites thanks to their high adsorption affinity towards PFOS. This is a “concentrate-and-destroy” strategy for degradation of PFOS in water using adsorptive photocatalyst Fe-zeolite particles. For instance, when the desired PFOS depletion in water is achieved by mixing the PFOS-contaminated water with a certain amount of Fe-zeolites, 90% or even 99% of water can be discharged after separation of the Fe-zeolite particles. This means, only 10% or even 1% of the contaminated water volume has to be treated photochemically. This would reduce the SEC by two orders of magnitude, i.e. from ca. 470 to 4.7 kWh m^{-3} of cleaned water (calculated based on the fluence rate of the photochemical reactor with a 1.1 cm optical path length). Then, the PFOS-loaded Fe-zeolites can be re-suspended and further treated in a small water volume. As discussed in Section 3.3., the overall PFOS degradation rate will not differ a lot when the zeolite concentration is in an applicable range after the enrichment step. In this way, the corresponding energy demand per m³ of cleaned water can be decreased by several orders of magnitudes.

In fact, we conducted a PFOS enrichment and photochemical treatment process for a real groundwater sample in Section 3.5 with the detailed procedures presented in Photochemical Procedures Section in SI. It is worth noting that the enrichment factor in the current study was restricted due to the limited volume of PFOS containing groundwater sample. A higher enrichment factor is realizable in principle. It can be for example enlarged by applying a cascade of batch adsorption reactors for achieving higher PFOS removal degree with a minimum amount of Fe-zeolite than in a single batch. Another technological approach could be the development of a flow-through system with immobilized Fe-zeolites e.g. in the form of photoactive coatings.

Overall, the main purpose of this study is to show the working principle of a novel PFOS degradation technology, comprising first a zeolite-based adsorption step followed by a step for photochemical regeneration of the adsorbent. This can be done by on-site and utilizing e.g., regenerative energy for lamp operation. In comparison, the currently prevailing large-scale technologies for PFAS removal (activated carbon or ion-exchange adsorption and membrane separation) do not degrade the target pollutant PFOS but require transportation and off-site treatment of large amounts of solids or liquids. Nevertheless, further optimization on improving photochemical activity of Fe-zeolites, and designing suitable treatment processes and reactors still needs to be done before a final evaluation of process and energy costs can be provided.

Reaction Scheme for PFOS Decomposition

The upper circle in Scheme 1 (main part) shows the proposed degradation pathway from PFOS to PFOA. After electron transfer from the sulfonate anion to the Fe^{3+} site and the SO_3-elimination of the $C_8F_{17}SO_3\cdot$ (eq. 1), the perfluoroalkyl radical $\bullet C_8F_{17}$ is formed.

$$C_8F_{17}SO_3\cdot + H_2O \longrightarrow C_8F_{17}\cdot + SO_4^{2-} + 2\,H^+ \qquad (1)$$

In the presence of molecular oxygen, $\bullet C_8F_{17}$ probably reacts with O_2 to produce the peroxyl radical $C_8F_{17}OO\cdot$. $C_nF_{2n+1}OO\cdot$ as intermediates and their subsequent further decomposition steps were proposed in previous studies on perfluoroalkyl acid degradation [1]. Thus, subsequent radical reactions are proposed here according to the literature, and $C_8F_{17}OH$ will be finally produced (eqs. 2-5) [4-5].

$$C_8F_{17}\cdot + O_2 \longrightarrow C_8F_{17}OO\cdot \quad (2)$$

$$2\ C_8F_{17}OO\cdot \longrightarrow C_8F_{17}OOOOC_8F_{17} \quad (3)$$

$$C_8F_{17}OOOOC_8F_{17} \longrightarrow 2\ C_8F_{17}O\cdot + O_2 \quad (4)$$

$$C_8F_{17}O\cdot + H_2O \longrightarrow C_8F_{17}OH + \cdot OH \quad (5)$$

Alternatively, $\bullet C_8F_{17}$ is also able to react with hydroxyl radicals ($\cdot OH$) to produce $C_8F_{17}OH$ (eq. 6).

$$C_8F_{17}\cdot + \cdot OH \longrightarrow C_8F_{17}OH \quad (6)$$

The following hydrolysis reactions take place rapidly, and PFOA is generated (eqs. 9-10).

$$C_8F_{17}OH \longrightarrow C_8F_{15}OF + HF \quad (7)$$

$$C_8F_{15}OF + H_2O \longrightarrow C_7F_{15}COOH + HF \quad (8)$$

The lower circle in Scheme 1 illustrates the proposed degradation pathway from PFOA to shorter-chain perfluorinated carboxylic acids (PFCAs). The produced PFCAs will continue to be adsorbed and complexed with Fe^{3+} ions on zeolites (eq. 9).

$$C_nF_{2n+1}COO^- + Fe^{3+}\text{-zeolite} \longleftrightarrow [C_nF_{2n+1}COO\text{-}Fe]^{2+}\text{-zeolite} \quad (9)$$

The PFCAs-Fe^{3+} complexes are oxidized upon irradiation via a carboxylate-to-metal electron-transfer process to produce carboxyl radicals ($C_nF_{2n+1}COO\cdot$) (eq. 10) [6].

$$[C_nF_{2n+1}COO\text{-}Fe]^{2+}\text{-zeolite} \xrightarrow{\text{UV-C}} C_nF_{2n+1}COO\cdot + Fe^{2+}\text{-zeolite} \quad (10)$$

This reaction is faster than the analogous e-transfer from the sulfonate group, as suggested by the comparison experiment shown in Figure S3. The resulting $C_nF_{2n+1}COO\cdot$ decarboxylates and yields perfluorinated alkyl radicals ($\cdot C_nF_{2n+1}$) (eq. 11).

$$C_nF_{2n+1}COO\cdot \longrightarrow C_nF_{2n+1}\cdot + CO_2 \quad (11)$$

A similar cascade of reactions will then take place as described above. Nevertheless, the low sorption affinity towards short-chain perfluorinated carboxylic acids (Figure S6), which are formed in the course of the reaction sequence, have some consequences: although the treated zeolite is fully regenerated, these acids are enriched in the aqueous phase of the regeneration suspension, they have to be mineralized by a complementary treatment step, as discussed in Section 3.1., e.g., by persulfate oxidation.

In addition, the influence of the reaction atmosphere (N_2 or O_2) has been investigated in our previous work with PFOA as the target contaminant. Oxygen was shown to be essential for the catalytic reaction cycle, as the photochemical degradation of PFOA was inhibited in nitrogen atmosphere [1]. Oxygen closes the catalytic cycle by re-oxidation of Fe^{2+} to Fe^{3+} and thus acts as the terminal oxidant (eq. 12).

$$Fe^{2+}\text{-zeolite} + O_2 \xrightarrow{\qquad} Fe^{3+}\text{-zeolite} + \cdot O_2^- \tag{12}$$

References

[1] Qian, L.; Georgi, A.; Gonzalez-Olmos, R.; Kopinke, F.-D., Degradation of perfluorooctanoic acid adsorbed on Fe-zeolites with molecular oxygen as oxidant under UV-A irradiation. Appl. Cat. B: Environ. 2020, 278, 119283.

[2] Gonzalez-Olmos, R.; Roland, U.; Toufar, H.; Kopinke, F. D.; Georgi, A., Fe-zeolites as catalysts for chemical oxidation of MTBE in water with H_2O_2. Appl. Cat. B: Environ. 2009, 89, (3), 356-364.

[3] Demas, J.; Bowman, W.; Zalewski, E.; Velapoldi, R., Determination of the quantum yield of the ferrioxalate actinometer with electrically calibrated radiometers. J. Phys. Chem. 1981, 85, (19), 2766-2771.

[4] Lutze, H. V.; Brekenfeld, J.; Naumov, S.; von Sonntag, C.; Schmidt, T. C., Degradation of perfluorinated compounds by sulfate radicals–New mechanistic aspects and economical considerations. Water Res. 2018, 129, 509-519.

[5] Kutsuna, S.; Hori, H., Rate constants for aqueous-phase reactions of SO_4^- with $C2F5C(O)O^-$ and $C3F7C(O)O^-$ at 298 K. Int. J. Chem. Kinet. 2007, 39, (5), 276-288.

[6] Hori, H.; Yamamoto, A.; Koike, K.; Kutsuna, S.; Osaka, I.; Arakawa, R., Photochemical decomposition of environmentally persistent short-chain perfluorocarboxylic acids in water mediated by iron (II)/(III) redox reactions. Chemosphere 2007, 68, (3), 572-578.

3.3 Enhanced degradation of perfluorooctanoic acid by heat-activated persulfate in the presence of zeolite

Lin Qian[a], *Frank-Dieter Kopinke*[a], *Tom Scherzer*[b], *Jan Griebel*[b] *and Anett Georgi**[a]

[a] Helmholtz Centre for Environmental Research – UFZ, Department of Environmental
Engineering, Permoserstr. 15, D-04318, Leipzig, Germany

[b] Leibniz Institute of Surface Engineering (IOM), Material Characterization and Analytics,
Permoserstr. 15, D-04318, Leipzig, Germany

ABSTRACT

The treatment of contaminations with perfluorooctanoic acid (PFOA) is a huge challenge due to its environmental persistence and global distribution. To remove PFOA traces from water, a combination of adsorption and degradation processes is considered as a promising approach. In the present study, we developed a novel treatment strategy for PFOA using heat-activated persulfate in the presence of BEA35 - a BEA-structure type zeolite. Our experimental results show for the first time that BEA35 does not only remove PFOA by adsorption, but also accelerates its degradation by means of heat-activated persulfate until complete mineralization. The presence of zeolite (50 g L^{-1}) increases PFOA degradation to 99.8% compared with 58% in homogeneous solution under the same reaction conditions ($C_{0,\text{persulfate}}$ = 100 mM, 90 min, 70°C). The influence of reaction conditions such as pH value, zeolite dosage and type were investigated. Possible reaction mechanisms were considered. The applicability of the zeolite-based treatment system was verified with real groundwater samples. A first cost estimation was provided for the application case of a zeolite fixed-bed adsorber with intermittent regeneration by heat-activated persulfate. The presented approach has the potential to overcome several shortcomings of the existing PFOA degradation technologies, such as high energy demands, vulnerability in complex water matrices, and inefficiency at trace concentration level. Our findings provide an effective and efficient strategy for treatment of water containing traces of PFOA, which can also inspire the development of remediation technologies for water contaminated by other micropollutants.

1. Introduction

Per- and polyfluoroalkyl substances (PFAS) are emerging persistent organic pollutants (POPs), which cause environmental problems as they are reported to be not eliminated in wastewater treatment plants [1]. Recent studies show that the exposure of PFAS at certain levels may cause adverse effects on human health [2, 3]. Although the production and application of PFAS is currently restricted, the possible risk of human exposure due to their accumulation in the environment will exist over a long period of time [4]. Even worse, the treatment of PFAS in the environment is a huge challenge. Firstly, PFAS concentration in natural water bodies are rather low, i.e., usually at or even below the ng L^{-1} level [5]. Chemical treatment of such low concentrations is usually not efficient, so a pre-enrichment process is necessary. Secondly, PFAS are rather resistant to most conventional oxidation, reduction and biological degradation processes mainly due to the very strong carbon-fluorine bonds ($D_{\text{C-F}} \approx 485$ kJ mol^{-1}) [6]. Among various PFAS, perfluorooctanoic acid (PFOA) is one representative perfluorinated carboxylic acid (PFCA), which has drawn much attention recently due to its frequent detection in the environment. PFOA and its most important pre-cursors have been banned by Stockholm convention in 2019, however, with exceptions for various industries such as in semiconductor manufacturing or polytetrafluoroethylene (PTFE) production for various purposes. Thus, efficient and cost-effective PFOA degradation techniques are urgently needed for treating e.g., wastewaters and contaminated natural waters.

Several current technologies can remove PFOA from water, e.g. activated carbon adsorption, reverse osmosis and ion exchange [7]. In these cases, PFOA-enriched solutions or solids are produced and need to be further treated. Taking the activated carbon as an example, the common way to treat exhausted activated carbon is incineration or, if possible, high-temperature regeneration in specialized treatment plants with suitable off-gas treatment.

Beside the PFOA removal technologies, several PFOA degradation technologies have been studied recently, e.g. oxidation by activated persulfate or peroxymonosulfate, electrochemical, sonochemical, photochemical, and photocatalytic treatment [8]. These technologies can degrade or even fully mineralize PFOA within acceptable time; however, the relatively high energy demands and operation costs have been limiting their practical application.

In PFOA degradation by activated persulfate (S2O82-) or peroxymonosulfate (SO52-), sulfate radicals are considered as the main reactive species. Hori et al. [9] first reported an efficient degradation of PFOA and shorter-chain perfluorocarboxylic acids (PFCAs) using persulfate as a photochemically activated oxidant (eq.1).

$$S_2O_8^{2-} \xrightarrow{h\upsilon} 2SO_4^{-}\cdot \qquad (1)$$

The produced sulfate radicals attack PFOA by a one-electron transfer step. Similarly, persulfate can also be thermally activated at elevated temperatures (T $\geqslant$ 50 ° C) (eq.2) [10]. In addition, it can be chemically activated in homogeneous or in heterogeneous media upon use of activators such as dissolved transition metals [11] and metallic materials [12-15].

$$S_2O_8^{2-} \xrightarrow{\Delta} 2SO_4^{-}\cdot \qquad (2)$$

The persulfate-based processes were also widely used in environmental remediation for treating other kinds of contaminants, e.g. pesticides, pharmaceuticals and personal care products [16]. In several cases, high reaction stoichiometric efficiency (%RSE) was observed [17-19], which is the molar ratio of target compound degraded per oxidant consumed. However, in case of PFCAs the efficiency of persulfate-based processes is strongly limited by the low reaction rate constant of the primary single-electron transfer step, which is about ($k_{SO_4^{-}\cdot} = (1.7\text{-}4.4) \times 10^4\ \mathrm{M^{-1}s^{-1}}$) [11]. This implies low radical utilization rates in the presence of coexisting radical consumers such as certain inorganic anions (e.g. chloride and carbonate) and organic compounds [20]. Thus, a preceding selective enrichment of PFOA by adsorption to an inert adsorbent material is a promising option for improved efficiency of persulfate-based processes.

Zeolites are microporous minerals with certain framework structures, which are commonly applied as catalysts and adsorbents. PFAS adsorption by zeolites has been investigated by various researchers. Van den Bergh et al. [21] recently investigated the performance of an all-silica BEA type zeolite for selective removal of PFOA and perfluorooctanesulfonic acid (PFOS). They claimed the adsorption of PFOA and PFOS to be driven by favorable steric factors and negative adsorption enthalpy. Qian et al. established an adsorption-degradation approach for removal of PFOA and PFOS from a real groundwater sample using Fe-doped zeolites (Fe-BEA35) [22, 23]. In this process, Fe-BEA35 not only shows a high adsorption affinity toward PFOA and PFOS, but also acts as a photocatalyst, which can be regenerated by photochemical degradation of PFOA and

PFOS under UV irradiation. Since sulfate radicals are known to degrade PFOA, it is of great interest whether a combined process, i.e. heat-activated persulfate for degradation of PFOA adsorbed to zeolites, can be used to effectively treat PFOA contaminations in water.

In the current study, we chose one synthetic, commercial BEA framework type zeolite, BEA35, which presents high PFOA adsorption affinity, for detailed studies, but also included further BEA and FAU zeolites for comparison. For the first time, PFOA adsorption and zeolite regeneration with heat-activated persulfate were combined. Our experimental results show that BEA35 accelerates PFOA degradation in the adsorbed state. Several aspects were investigated: I) effects of reaction pH and zeolite dosage on the removal/degradation performances; II) %RSE evaluation under different persulfate dosages and activation temperatures; III) possible mechanisms explaining the promoted PFOA degradation process; and IV) stability of the system and tests with real groundwater. These findings contribute to a promising strategy for treatment of water containing trace PFOA by combined adsorption and oxidation.

2. Materials and methods

2.1. Chemicals and materials

All chemicals were in reagent grade or higher and used as received, where not otherwise stated. Deionized (DI) water was used for solution and suspension preparation in this work. Methanol was acquired from (Th. Geyer, Chemsolute). Sodium persulfate (99% purity, $Na_2S_2O_8$), perfluorobutyric acid (98% purity, PFBA, C_3F_7COOH) and perfluorooctanoic acid (96% purity, PFOA, $C_7F_{15}COOH$) were acquired from Sigma Aldrich. Perfluoropropionic acid (97% purity, PFPrA, C_2F_5COOH), perfluoropentanoic acid (97% purity, PFPeA, C_4F_9COOH) and perfluorohexanoic acid (98% purity, PFHeA, $C_5F_{11}COOH$) were acquired from J&K Scientific. Trifluoroacetic acid (99% purity, TFA, CF_3COOH) was acquired from Fluka. Perfluoroheptanoic acid (97% purity, PFHpA, $C_6F_{13}COOH$) was acquired from Alfa Aesar. In addition, the technical PFOA that contains a higher proportion of branched PFOA isomers was acquired from Haihang Industry (China). The PFOA isomer standards were acquired from Wellington Laboratories (Canada).

The zeolites BEA24 and BEA35 were acquired from Clariant Produkte GmbH (Germany). The zeolites BEA28, BEA40, BEA100 and FAU15 were acquired from Tosoh Corporation (Japan). The BEA framework contains two types of channels with 12 Si or Al atoms, i.e., with openings of a diameter (Ø) of 6.6 – 6.7 Å for the straight and Ø 5.6 – 5.7 Å for the zig-zag form channels, respectively, whereas the pore volume of the FAU framework consists mainly of big cages with Ø of 8 – 11.9 Å. The numbers in the zeolite type names represent SiO_2/Al_2O_3 molar ratios. The XRD pattern of BEA35 was measured, which was in good agreement with the BEA framework type as shown in Figure S1. More detailed information about these zeolites including morphology, particle size and BET surface areas are presented in the SI.

2.2. PFOA degradation experiments

Degradation of PFOA by heat-activated persulfate in the presence and absence of zeolites were conducted in sealed 40 mL glass flasks. For most experiments, an aqueous PFOA solution (30 mL, 240 μM) was mixed with 1.5 g zeolite in the flask followed by 2 h shaking to achieve adsorption equilibrium. About 99.9% of PFOA was in the adsorbed state. Before start of reaction, the flasks containing PFOA solutions or zeolite suspensions were preheated in a water bath, where a reaction temperature of 70 °C was maintained. When the temperature of the PFOA solutions or zeolite suspensions was stabilized, the reaction was initiated by introducing certain amounts of sodium persulfate.

The real groundwater samples had very low PFOA concentrations, ranging from 35 to 82 ng L^{-1}. The PFOA was enriched from groundwater samples by the zeolite thanks to its high adsorption affinity towards PFOA. Figure S2 shows in a scheme how the PFOA-containing groundwater samples were treated before the reaction. 1 L of groundwater was filtered through a 0.45 μm paper filter for removal of large particles. The chemical composition of groundwater samples after filtration is shown in Table S1. The filtered groundwater sample was then mixed with 0.5 g BEA35 zeolite and shaken for 1 day. The majority of PFOA was adsorbed by the zeolite after 1 day. For determination of very low PFOA concentrations, aqueous samples were concentrated by evaporation. The concentration of dissolved PFOA after adsorption was below the detection limit of the LC-MS measurement (50 ng L^{-1}) even after evaporative concentration by two orders of magnitude. The suspension was kept standing for 2 days, after which the supernatant was discarded completely. The PFOA-loaded zeolite particles were then washed once by 50 mL DI water, and the supernatant was removed by centrifugation at 2500 rpm for 5 min. After that, the washed PFOA-loaded zeolite particles were re-suspended with 10 mL DI water and collected for the further treatment. Almost no inorganic ions (e.g. sulfate, chloride and carbonate) were detected in the resulting zeolite suspension. After this, an enrichment factor of 10^2 for PFOA was achieved (from 1 L to 10 mL) and the final zeolite concentration was 50 g L^{-1}.

For zeolite reusability tests, the supernatant was removed after each reaction period (90 min) by centrifugation at 2500 rpm for 5 min. The remaining zeolite particles were re-suspended in the fresh aqueous PFOA solution. The suspension was prepared for the next reaction run after shaking for 2 h for adsorption equilibration.

2.3. Extraction of PFOA and intermediates from zeolites

After sampling of zeolite suspensions, methanol was added to the sample both to scavenge radicals and to extract PFOA and intermediates from zeolites as previously described [24]. 2 mL of methanol was added to a 100 μL zeolite suspension aliquot in a 4 mL tube. After shaking overnight, the mixture was centrifuged at 2500 rpm for 5 min. The supernatant was taken and analysed by LC-MS to determine the total PFOA and intermediate concentrations (adsorbed and freely dissolved fractions). This extraction procedure can achieve almost a complete recovery ((94 ± 2) %) of PFOA from a sample after 2-h adsorption. Most of the produced fluoride during the reaction was released into the aqueous phase. The remaining fluoride in the zeolites was extracted by adjusting suspension pH to 12. After the centrifugation, the supernatant was subjected to analysis by ion chromatography (IC, DX500, Thermo Fisher).

2.4. Chemical analysis

Quantitative analysis of PFOA and its degradation intermediates, i.e. PFHpA, PFHeA, PFPeA, and PFBA were performed with LC/MS (LCMS-2020, SHIMADZU Corp.). The detailed procedure for LC/MS was described in a previous work [23]. The correlation coefficients (R^2) of the calibration curves for PFOA, PFHpA, PFHeA, PFPeA and PFBA were $\geqslant 0.99$ for concentration ranges of 1 μg L^{-1} - 1 mg L^{-1}. The limit of detection for PFOA was around 50 ng L^{-1}. The standard deviations of single values were obtained from triplicate assay results. For the technical PFOA containing higher proportions of branched PFOA isomers, an isocratic LC/MS method with 45% solvent A (20 mM ammonium acetate in 90 vol-% DI water and 10 vol-% methanol) and 55% solvent B (20 mM ammonium acetate in 90 vol-% methanol and 10 vol-% DI water) was performed to separate the branched PFOA isomers. The running time for each measurement was 38 min. Quantitative analysis of PFPrA, TFA and fluoride was performed with

IC. The analysis of octanol was performed on a GC/MS device (GCMS-QP2020, SHIMADZU Corp.). The determination of persulfate concentration was conducted with spectrophotometric method by measuring the absorbance of I_3^- at 352 nm [25]. The 2θ/ω XRD pattern was measured with a diffractometer (ULTIMA IV, Rigaku) in out-of-plane geometry with parallel beam optics. Cu Kα radiation with λ= 0.15406 nm was used for the measurements. The diffractometer was equipped with a scintillation detector.

3. Results and discussion

3.1. Degradation of PFOA by heat-activated persulfate in the presence and in the absence of BEA35 zeolite.

Previous studies reported that sulfate radicals are able to react with PFCAs leading to stepwise chain-shortening [20, 24, 26]. Based on these studies the generally accepted perspective is that sulfate radicals attack the carboxylic head group of PFCAs by a one-electron transfer to generate carboxylic radicals (eq. 3) followed by decarboxylation and yielding perfluorinated alkyl radicals ($\bullet C_nF_{2n+1}$) and CO_2 (eq. 4). The $\bullet C_7F_{15}$ radicals react preferentially with dissolved O_2 to produce the peroxyl radical ($C_7F_{15}OO\bullet$) (eq.5). Through several radical reactions and hydrolysis processes, a PFCA with one CF_2 unit less will be produced (eqs. 6 - 10). The produced shorter-chain PFCAs continue to be attacked by sulfate radicals and finally a complete mineralization of PFCAs can be achieved.

$$C_7F_{15}COO^- + SO_4^-\bullet \longrightarrow C_7F_{15}COO\bullet + SO_4^{2-} \qquad (3)$$

$$C_7F_{15}COO\bullet \longrightarrow C_7F_{15}\cdot + CO_2 \qquad (4)$$

$$C_7F_{15}\bullet + O_2 \rightarrow C_7F_{15}OO\bullet \qquad (5)$$

$$2C_7F_{15}OO\bullet \rightarrow C_7F_{15}OO\text{-}OOC_7F_{15} \qquad (6)$$

$$C_7F_{15}OO\text{-}OOC_7F_{15} \rightarrow 2C_7F_{15}O\bullet + O_2 \qquad (7)$$

$$C_7F_{15}O\bullet + HSO_4^- \rightarrow C_7F_{15}OH + SO_4^-\bullet \qquad (8)$$

$$C_7F_{15}OH \rightarrow C_7F_{13}OF + HF \qquad (9)$$

$$C_7F_{13}OF + H_2O \rightarrow C_6F_{13}COOH + HF \qquad (10)$$

In this section, we compare PFOA degradation by heat-activated persulfate in the homogeneous and heterogeneous system, where zeolite functions as an adsorbent of PFOA. A typical homogeneous system contained 100 mM persulfate and $C_{0,\mathrm{PFOA}}$ = 240 μM. A heterogeneous system contained in addition 50 g L^{-1} BEA35 zeolite, where PFOA exists predominantly in the adsorbed state (99.9%) after 2 h equilibration. The initial pH values of both systems were adjusted to $pH_0 = 3.0$. The total concentration of PFOA in zeolite suspension (including freely dissolved and adsorbed fractions) was obtained via a solvent extraction step (as described in Section 2.3). As shown in Figure 1(a), 99.8% degradation and 71% defluorination of the initial 240 μM PFOA was achieved in the presence of zeolite within 90 min compared to 58% degradation in the absence of zeolites under identical conditions. That is, PFOA degradation by heat-activated persulfate was significantly promoted in the presence of zeolite. When describing the PFOA degradation kinetics with a pseudo-first-order kinetics the acceleration effect is a factor of about 7 (= ln(100/0.2)/ln(100/42), see below).

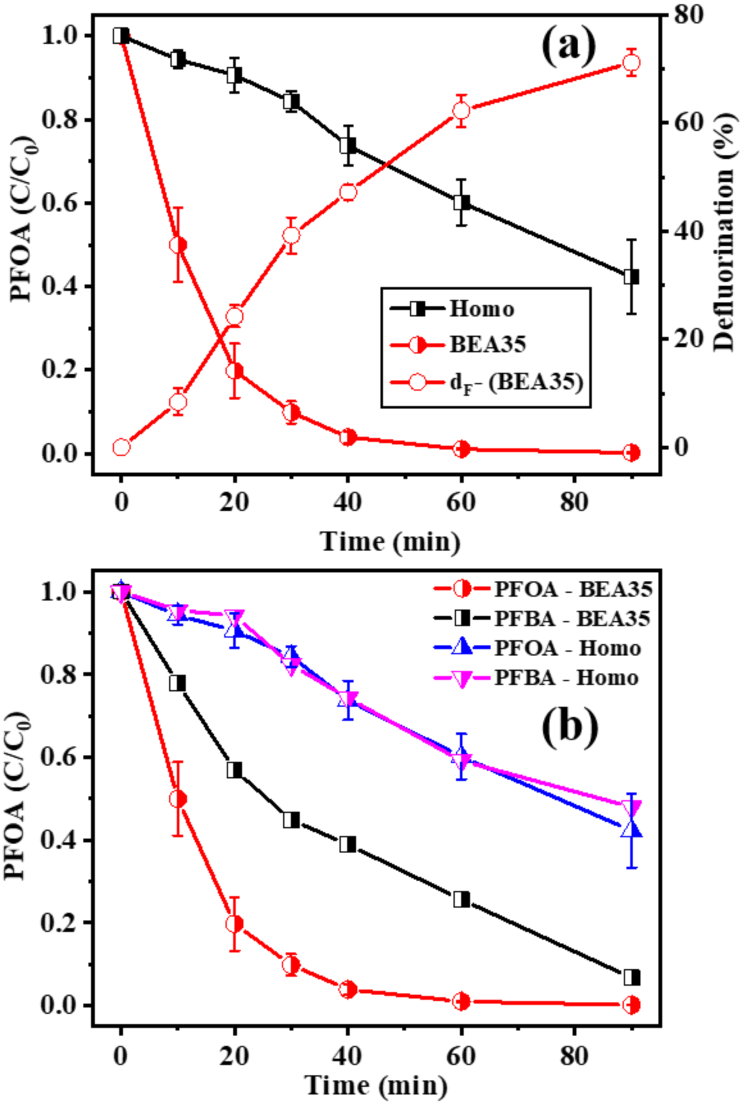

Figure 1. Comparison of heat-activated persulfate processes: (a) PFOA degradation with and without zeolite; (b) PFOA and PFBA degradation with and without zeolite. $C_{0,\mathrm{PFCAs}}$ = 240 µM, $C_{0,\mathrm{persulfate}}$ = 100 mM, pH_0 = 3.0, T = 70 °C, and C_{zeolite} = 50 g L^{-1} where applied. Error ranges represent mean deviations of single values from the mean of at least two experiments. Lines in plots of relative concentrations are added as guides for the eye.

In general, two types of reactions in the presence of zeolite should be considered, i.e., homogeneous reaction in the solution phase and heterogeneous reaction, i.e., reaction of adsorbed PFOA inside the zeolite. The fractions of adsorbed PFOA (X_{sorb}) and freely dissolved PFOA (X_{free}) can be described as follows:

$$X_{\mathrm{sorb}} = 1 - X_{\mathrm{free}} \tag{11}$$

$$X_{\mathrm{free}} = C_{\mathrm{PFOA,free}} / C_{\mathrm{PFOA}} \tag{12}$$

Based on eq. 3, a rate eq. 13 can be derived:

$$-\frac{\mathrm{d}C_{\mathrm{PFOA}}}{\mathrm{d}t} = k_1 \cdot C_{\mathrm{PFOA}} \cdot X_{\mathrm{sorb}} \cdot C_{\mathrm{zeolite,\,SO_4^{-}\cdot}} + k_2 \cdot C_{\mathrm{PFOA}} \cdot X_{\mathrm{free}} \cdot C_{\mathrm{bulk,\,SO_4^{-}\cdot}} \tag{13}$$

where k_1 and k_2 are the rate constants for reaction of adsorbed and freely dissolved PFOA with sulfate radicals, respectively and $C_{\mathrm{zeolite,\,SO_4^{-}\cdot}}$ and $C_{\mathrm{bulk,\,SO_4^{-}\cdot}}$ are the concentrations of sulfate radicals (per total water volume) produced by thermal activation of persulfate inside the zeolite and in the bulk phase, respectively. However, the values of $C_{\mathrm{zeolite,\,SO_4^{-}\cdot}}$ and $C_{\mathrm{bulk,\,SO_4^{-}\cdot}}$ cannot be easily determined. The fractions of X_{sorb} and X_{free} can be experimentally obtained. For instance, under the condition of $C_{\mathrm{zeolite}} = 50$ g L^{-1} and $C_{0,\mathrm{PFOA}} = 240$ µM, $X_{\mathrm{free}} = 0.002$ was much smaller than $X_{\mathrm{sorb}} = 0.998$. In this case, the homogeneous reaction in bulk phase can be ignored, and eq. 13 results in the simplified rate eq. 14:

$$-\frac{\mathrm{d}C_{\mathrm{PFOA}}}{\mathrm{d}t} = k_1 \cdot \mathrm{C}_{\mathrm{PFOA}} \cdot X_{\mathrm{sorb}} \cdot C_{\mathrm{zeolite,\,SO_4^{-}\cdot}} \tag{14}$$

It is worth noting that under the described conditions the initial period of PFOA degradation (0 – 60 min) in the presence of zeolite can be well fitted by pseudo-first-order kinetics ($R^2 = 0.998$, Figure S3), which is in accordance with reaction kinetics described by eq. 14 considering that persulfate turnover is still very low and thus $C_{\mathrm{zeolite,\,SO_4^{-}\cdot}} \approx$ constant. The apparent rate constant decreases slightly at high PFOA turnover (> 99% at t > 60 min).

To further confirm that a heterogeneous reaction dominates the PFOA degradation in the presence of zeolite, we compared the degradation of PFOA with a shorter-chain PFCA, i.e., PFBA. It has the same carboxylic group as PFOA but with a shorter carbon chain length. As a consequence, zeolites have much weaker adsorption affinity for PFBA due to weaker hydrophobic interactions, as reported in our previous work [22, 23]. Under these conditions ($C_{\mathrm{zeolite}} = 50$ g L^{-1} and $C_{0,\mathrm{PFBA}} = 240$ µM), only 23% of PFBA was adsorbed after 2 h equilibration. As shown in Figure 1(b), the degradation rates of PFOA and PFBA were almost identical in the homogeneous systems. This is not surprising because the sulfate radicals attack PFCAs at the carboxylic head group, which is the same for PFOA and PFBA [20]. The different carbon chain lengths are not decisive in the initial reaction step. However, in the presence of zeolite, the degradation of PFOA was much faster than that of PFBA, where the majority of PFOA was adsorbed onto the zeolite but PFBA was dominantly present in the aqueous phase. This is clear evidence that in the presence of zeolites, PFOA degradation takes place via a heterogeneous reaction inside the zeolite. Since the PFOA degradation was significantly increased after its adsorption to BEA35, it can be supposed that BEA35 zeolite may not only be an adsorbent of PFOA but also a catalyst for its degradation. More detailed investigation of this promotion effect is discussed in the following sections.

In order to elucidate the PFOA degradation mechanism, the concentrations of the intermediates produced during the reaction were analyzed. Six shorter-chain PFCAs were identified and quantified by means of IC (C2 and C3) and LC/MS (C4 to C7) analysis. Their concentration profiles along the reaction time are displayed in Figure 2(a). The PFCAs with longer chains, e.g. C5 to C7, reached their maximal concentrations at earlier stages (< 60 min) and then diminished gradually, while shorter-chain PFCAs were increasingly detected. This indicates that longer-chain PFCAs are degraded stepwise towards shorter-chain PFCAs. Additionally, the degradation of shorter-chain PFCAs is slower, most likely due to their lower adsorption affinities to zeolite. In fact, the degradation of shorter-chain PFCAs, e.g. C2 and C3, probably took place outside the zeolite in the water bulk phase.

The fluorine mass balance during PFOA degradation in the heat-activated persulfate/zeolite system is shown in Figure 2(b). The fluorine in the system is classified into four groups: fluoride, C2 to C4 PFCAs, C5 to C7 PFCAs and the remaining PFOA. The initial fluorine (i.e. PFOA) recovery of (94 ± 2)% was obtained by methanol extraction (see experimental part). After 3 h of reaction, a final fluorine recovery of (84 ± 3)% was obtained, which consisted mainly of fluoride and minor contributions of C2 and C3 PFCAs. In addition, the GC/MS headspace analysis did not reveal volatile fluorinated and non-fluorinated compounds produced during the process. The incomplete fluorine mass balance may be due to the formation of some undetected fluorine-containing compounds, which may be strongly bound in the zeolite and could not be extracted.

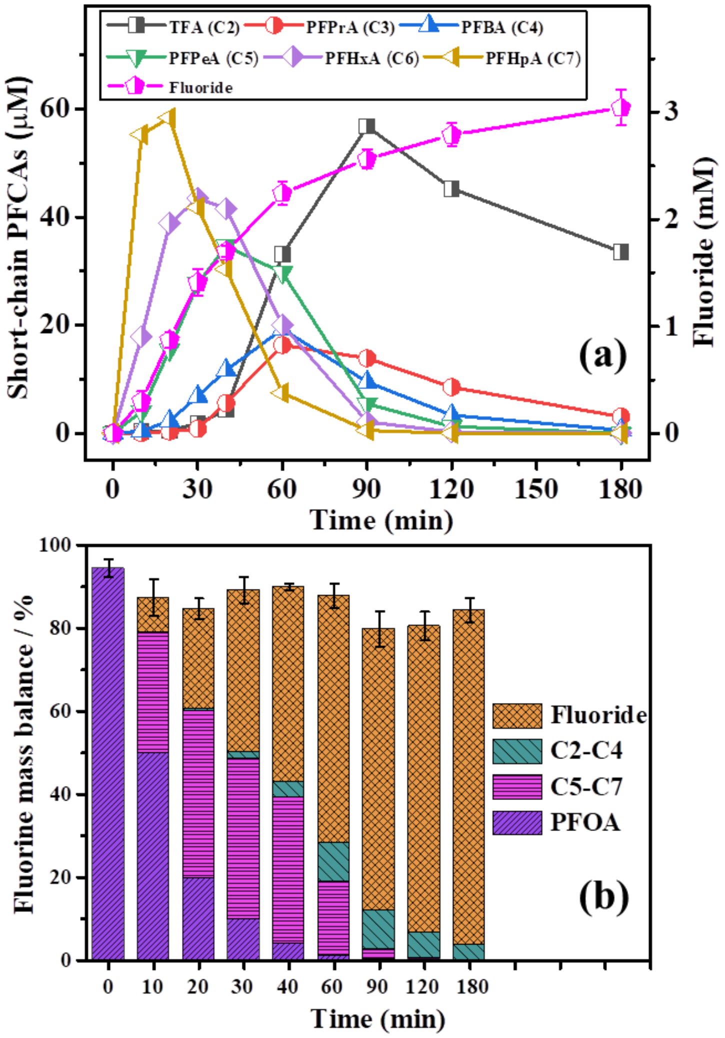

Figure 2. (a) Formation of short-chain PFCAs and fluoride during PFOA degradation by heat-activated persulfate; (b) Fluorine mass balance. The 0 min mass balance represents fluorine detected as PFOA in zeolite suspension determined by methanol extraction before start of reaction. The 180 min mass balance represents fluorine detected as C2 to C4 PFCAs and fluoride in the aqueous phase. $C_{\text{zeolite}} = 50$ g L^{-1} and $C_{0,\text{PFOA}} = 240$ µM, $C_{0,\text{persulfate}} = 100$ mM, $\text{pH}_0 = 3.0$, and $T = 70$ °C. Error ranges represent mean deviations of single values from the mean of at least two experiments in Figure 2(a). The cumulative error is shown in Figure 2 (b). Lines in plots of relative concentrations are added as guides for the eye.

3.2. Effect of pH

We tried to fit degradation curves under both conditions (with and without zeolite) according to eq. 14 in section 3.1 and discuss the pH effect on reaction kinetics in this section. The initial reaction period (0 – 60 min) in the presence of zeolite can be well fitted by first-order kinetics, while this is not the case in the absence of zeolite where an apparent zero-order kinetics is more appropriate. The thermal decomposition of persulfate causes a decrease in solution pH due to the reaction stoichiometry given by eq. 15 [27]:

$$S_2O_8^{2-} + H_2O \xrightarrow{\Delta} 2SO_4^{2-} + 2H^+ + \frac{1}{2}O_2 \tag{15}$$

In unbuffered systems applying 100 mM persulfate with initial pH0 = 3.0, the final solution pH after 90-min reaction decreased to around 1.5 with and without zeolites (Figure S4). The decreasing pH may have an effect on the rate of PFOA degradation. Therefore, we tried to maintain the pH between 2.5 and 3.0 in both cases by manually adding NaOH solution. As seen in Figure 3(a) and (b), PFOA degradation in the presence of zeolite with buffered reaction pH showed almost identical degradation rates compared with the unbuffered conditions. However, in the absence of zeolite, PFOA degradation slowed down with buffered reaction pH. Interestingly, under buffered conditions, the PFOA degradation in the absence of zeolite can now also be fitted by a first-order kinetics ($R^2 = 0.99$). Hence, deviations from first-order kinetics in the unbuffered solution were due to the superimposed pH effect. This effect has also been observed by other researchers [27]. However, the pH effect was largely attenuated in the presence of zeolite.

Furthermore, we investigated PFOA degradation by heat-activated persulfate in the presence of zeolite at various initial pH values, i.e. pH0 = 3.0, 5.0, and 7.0. As shown in Table S2, the initial adsorbed fractions of PFOA (X_{sorb}) on BEA35 zeolite are $\geqslant$ 0.998 under all tested conditions. Comparing with the rate at $pH_0 = 3.0$, the PFOA degradation slowed down somewhat at $pH_0 = 5.0$ and 7.0, resulting in 1.2 and 1.6 times higher PFOA half-life, respectively (Figure 3(c)). Overall, the pH effect is much less pronounced in the presence of the zeolite (i.e. with PFOA predominantly adsorbed) than in the homogeneous heat-activated persulfate system. Further discussion on the mechanistic basis of the pH effect is presented below.

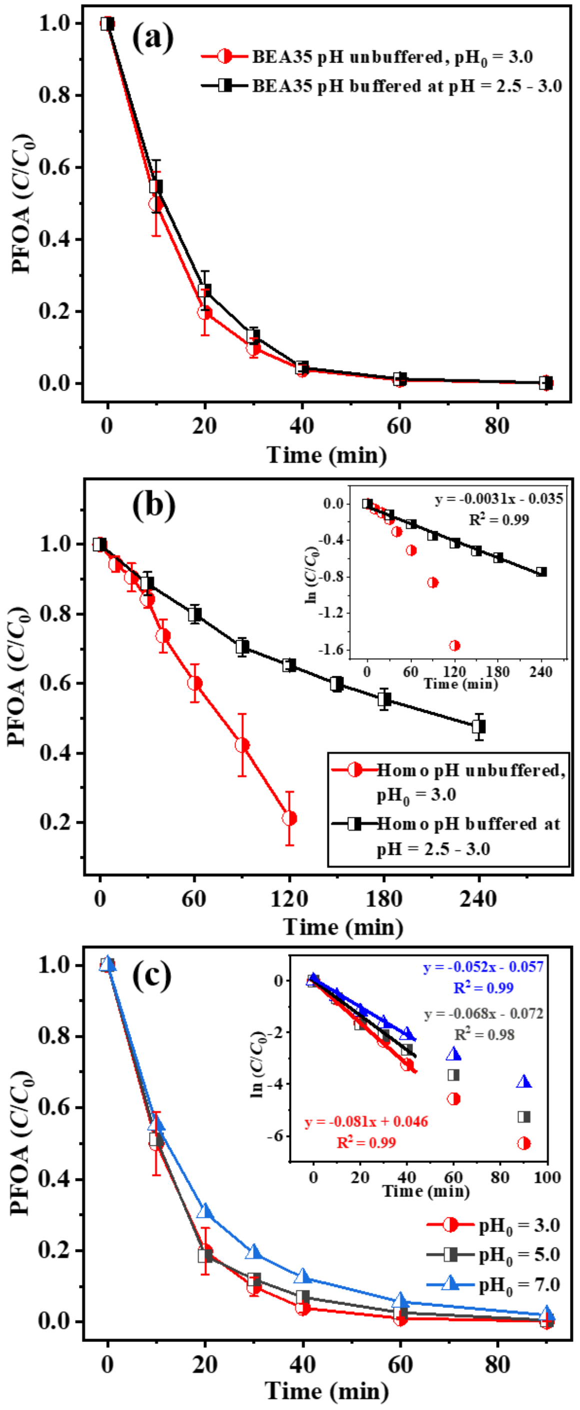

Figure 3. PFOA degradation by heat-activated persulfate: (a) effect of pH control in the presence of zeolite; (b) Effect of pH control in the absence of zeolite; (c) At various initial pH values in the presence of zeolite (no pH control). $C_{0,\text{PFOA}}$ = 240 µM, $C_{0,\text{persulfate}}$ = 100 mM, T = 70 °C, and C_{zeolite} = 50 g L^{-1} where applied. Error ranges represent mean deviations of single values from the mean

of at least two experiments. Lines in plots of relative concentrations are added as guides for the eye. Insets show fitting to pseudo-first order kinetics.

3.3. Role of internal vs. external zeolite surface

In Section 3.1, it is mentioned that the zeolite may promote PFOA degradation by heat-activated persulfate. In fact, both linear and branched PFOA isomers are formed during the production of PFOA using electrochemical fluorination [28]. Our preliminary experiments indicate that BEA35 has a stronger adsorption affinity towards linear PFOA than towards some branched isomers due to the steric effect, i.e. size exclusion by the zeolite pore structure with channel openings of 0.56 – 0.67 nm. It is interesting to know whether the internal surface or the external surface of the zeolite particles promotes the PFOA degradation. [29]. The adsorption of linear and branched PFOA isomers would be nearly identical on the external surface, yet only linear PFOA and certain branched PFOA isomers can access the internal surface. In order to provide comparable conditions in the experiments, the branched PFOA isomers were enriched to a similar concentration range as for linear PFOA by means of selective adsorption onto zeolites (for details, see Experimental Part in SI). Some LC/MS chromatograms from degradation of PFOA mixtures with and without zeolites are shown in Figure 4. PFOA isomer standards were used for peak assignment (Figure S5). As can be seen, the degradation rates of linear PFOA and branched isomers are almost identical in the homogeneous system. This is not surprising as the PFOA degradation by sulfate radicals starts at the carboxylate group (eq. 3), which is identical in all PFOA isomers. In the presence of zeolite, the linear PFOA and certain mono-branched PFOA isomers, i.e. 5m-PFOA and 6m-PFOA, exhibit higher degradation rates than those of di-branched PFOA isomers, i.e. 5,5m-PFOA and 4,5m-PFOA. The symbol ‘m’ stands for branching by one or two CF_3 groups in the respective positions in the PFOA molecule. These findings are a clear indication that the promotion of PFOA degradation by heat-activated persulfate takes place on the internal surfaces in the pores rather than the external surfaces of the zeolite.

3.4. Variation of substrate, zeolite dosages or types and activation temperatures

To elucidate possible reasons for the promoting effect of zeolite on PFOA degradation, several comparison experiments were conducted. Our first hypothesis suggested that persulfate decomposition rate might be enhanced in the presence of zeolite, which responds for promoted

PFOA degradation. We monitored the concentration of persulfate during thermal activation with and without zeolites. As shown in Figure S6, the persulfate decomposition kinetics are almost identical in both cases. It seems that the presence of zeolite is irrelevant for the overall persulfate decomposition rate. However, with a concentration of 50 g L^{-1} BEA35, the zeolite pore volume only contributes to less than 3% of the total volume. 97% is bulk water phase. This means, even with a factor of 3 increase in persulfate decomposition rate constant inside the zeolite, the overall enhancement of persulfate decomposition will still be within the error range (<10%) as the observable rate constant $k_{\text{obs,persulfate}}$ would be equal to the summed products of internal/external rate constants and fractions of persulfate. Therefore, this test cannot clarify whether persulfate

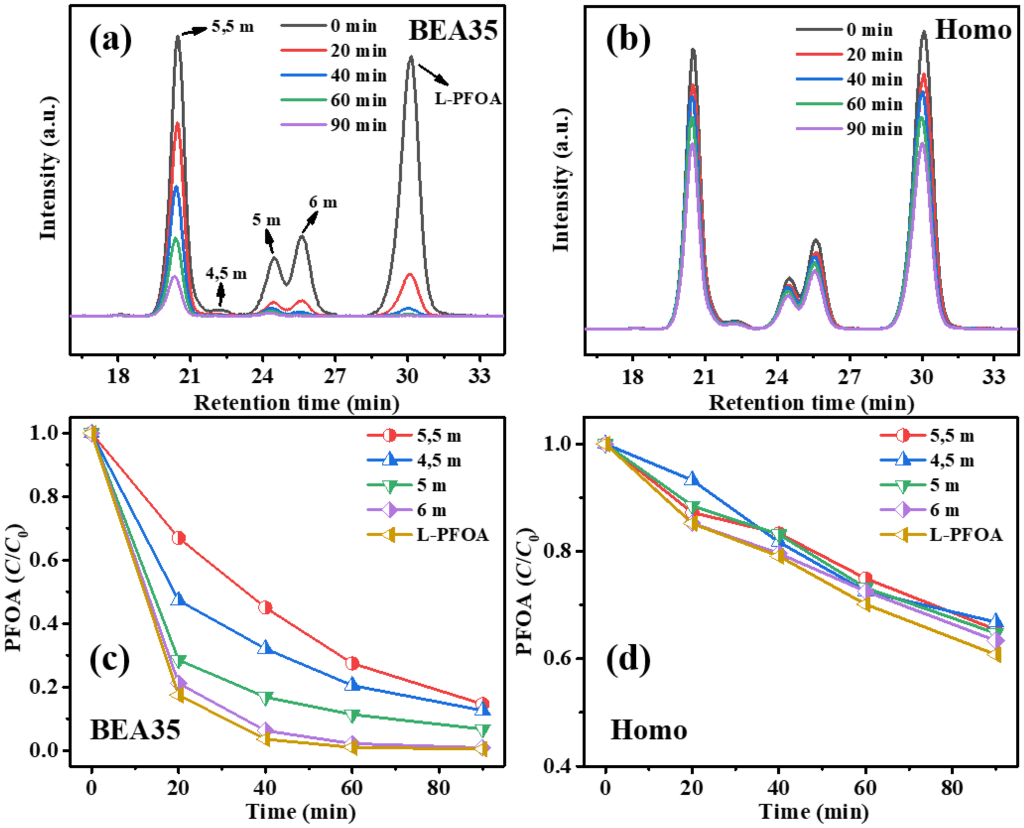

Figure 4. Some LC/MS chromatograms of samples from degradation of technical PFOA mixtures in the presence (a) and in the absence (b) of zeolite. Kinetics of degradation of technical PFOA mixtures in the presence (c) and absence (d) of zeolite. $C_{0,\text{persulfate}}$ = 100 mM, T = 70 °C, and C_{zeolite} = 50 g L^{-1} where applied. Lines in plots of relative concentrations are added as guides for the eye.

decomposition rate inside the zeolite was enhanced or not. Thus, another experiment was designed in which we replaced PFOA by n-octanol. Similar to PFOA, n-octanol can be well adsorbed on BEA35 zeolite. Unlike PFOA, n-octanol is attacked by sulfate radicals through hydrogen abstraction [30]. Nevertheless, we used here n-octanol oxidation as a probe reaction for sulfate radicals in the zeolite pores. As seen in Figure S6, the presence of zeolite suppressed the octanol degradation. This indicates that the accelerating effect is rather related to the substrate PFOA than the enhancement of persulfate decomposition into free sulfate radicals.

Table 1. Adsorption and kinetic data on PFOA degradation with different BEA35 zeolite dosages (at $pH_0 = 3.0$, $C_{0,\ PFOA} = 240$ μM, $C_{persulfate} = 100$ mM, and $T = 70$ °C)

Zeolite dosages (g L^{-1})	**100**	**50**	**5**	**0.5**
$X_{Sorb,\ PFOA}$	0.999	0.998	0.985	0.58
q_{PFOA} (g kg^{-1}) [a]	1.0	2.0	19	120
K_d (L kg^{-1}) [b]	2.1×10^4	1.9×10^4	1.3×10^4	2.8×10^3
$k_{obs,PFOA}$ (min^{-1}) [c]	0.098±0.007	0.077±0.004	0.063±0.012	0.030±0.001
PFOA $t_{1/2}$ (min)	6.6±0.5	8.5±0.4	9.2±1.8	22.0±1.0

[a] Sorbent loading.

[b] Single point adsorption coefficient K_d (L kg^{-1}) = q_{PFOA} (g kg^{-1}) / $C_{PFOA,free}$ (g L^{-1}).

[c] $k_{obs,PFOA}$ is obtained by first-order kinetics fitting within initial period of PFOA degradation (0 – 60 min). The error ranges are derived from the regression analysis of the data.

We tested various dosages of zeolites (from 0.5 to 100 g L^{-1}) with the same initially dissolved PFOA concentration, as shown in Figure 5 and Table 1. In general, the presence of zeolites promotes PFOA degradation even at the lowest zeolite dosage (0.5 g L^{-1}), where due to $X_{sorb,PFOA} = 0.58$ the PFOA degradation reaction occurred in both compartments, i.e. inside the zeolite and in the aqueous bulk phase. A much lower PFOA degradation rate constant was observed at $C_{zeolite} = 0.5$ g L^{-1} than in other cases with higher zeolite dosages. Note that the diffusion of persulfate between bulk phase and pore volume is relatively fast, i.e. with a characteristic diffusion time in the order of 10^{-4} s for 0.5 μm distance (= average BEA35 zeolite particle diameter).

Therefore, the lower PFOA degradation rate constant cannot be explained by persulfate depletion in the zeolite pores. When we kept the initial PFOA concentration constant and increased the zeolite dosages to 5 - 100 g L^{-1}, the PFOA was predominantly adsorbed on zeolites ($X_{\mathrm{free}} < 0.015$, see Table 1). Under these conditions, the PFOA degradation rate constants were significantly enhanced. The acceleration of PFOA degradation by heat-activated persulfate is more pronounced when higher zeolite dosages are applied. Additionally, when the zeolite dosage was kept constant at 50 g L^{-1} and the initial PFOA concentration was decreased from 240 to 2.4 µM, the PFOA degradation rate constants were almost identical under both sets of conditions (Figure S8), i.e. the same accelerating effect was observed from 100-fold different PFOA loadings on zeolite.

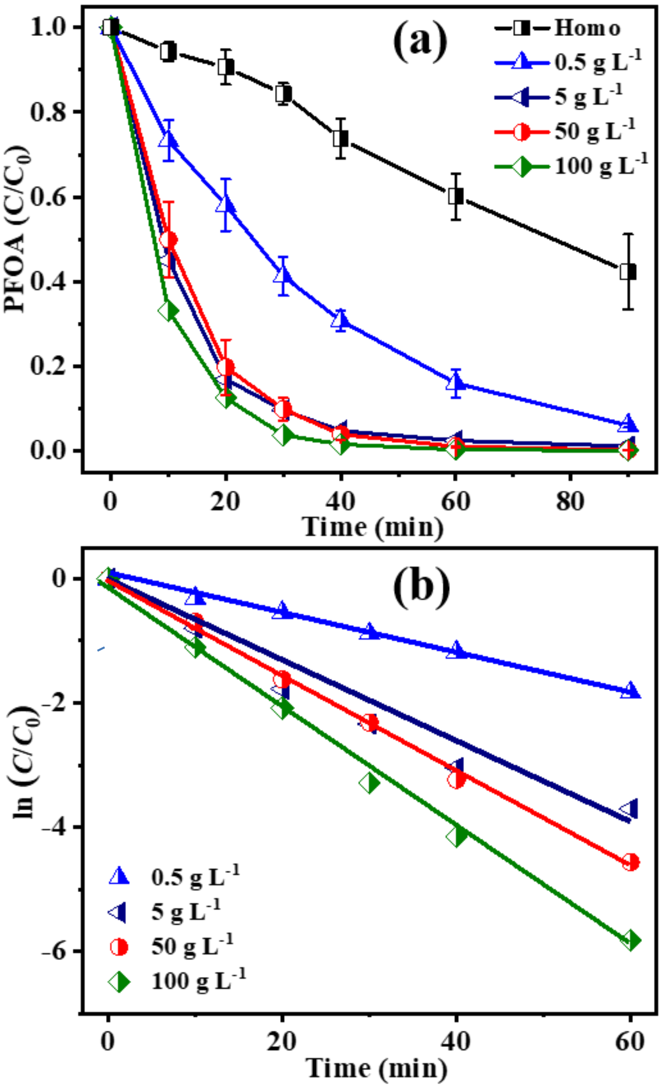

Figure 5. PFOA degradation by heat-activated persulfate with various zeolite dosages. $C_{0,\text{PFOA}}$ = 240 µM, $C_{0,\text{persulfate}}$ = 100 mM, pH$_0$ = 3.0, and T = 70 °C. (a) Residual concentrations over time and (b) pseudo-first order kinetics plots for initial reaction period (60 min). Error ranges represent mean deviations of single values from the mean of at least two experiments. Lines in (a) are added as guides for the eye.

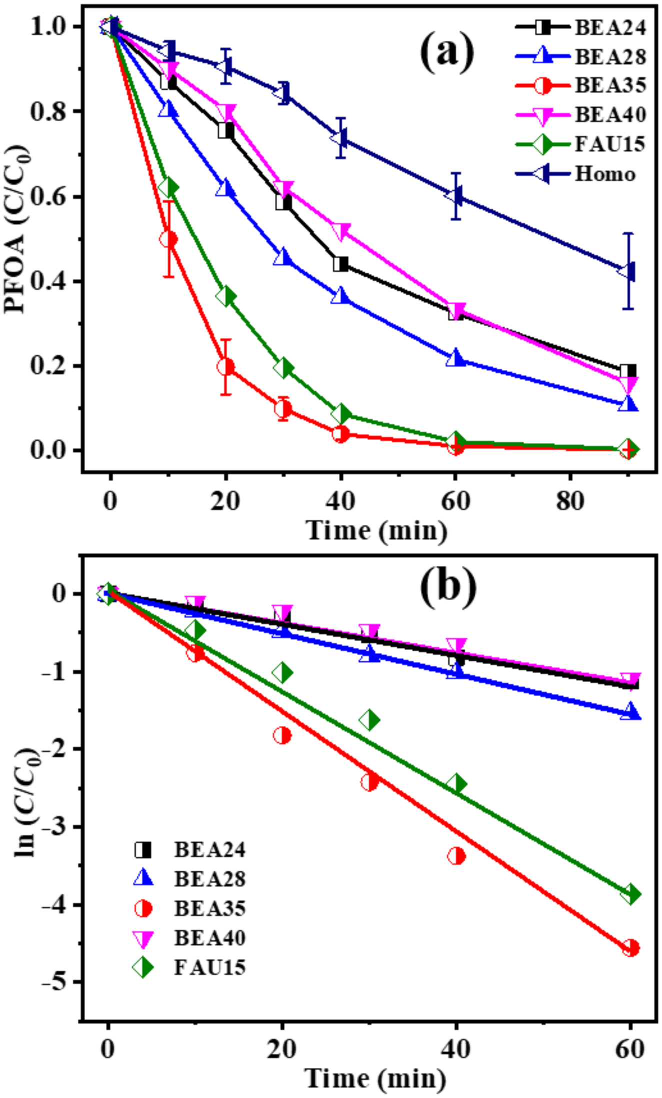

Figure 6. PFOA degradation by heat-activated persulfate with various types of zeolite. C_{zeolite} = 50 g L^{-1}, $C_{0,\text{PFOA}}$ = 240 µM, $C_{0,\text{persulfate}}$ = 100 mM, pH$_0$ = 3.0, and T = 70 °C. (a) Residual concentrations over time and (b) pseudo-first order kinetics plots. Error ranges represent mean deviations of single values from the mean of at least two experiments. Lines in (a) are added as guides for the eye.

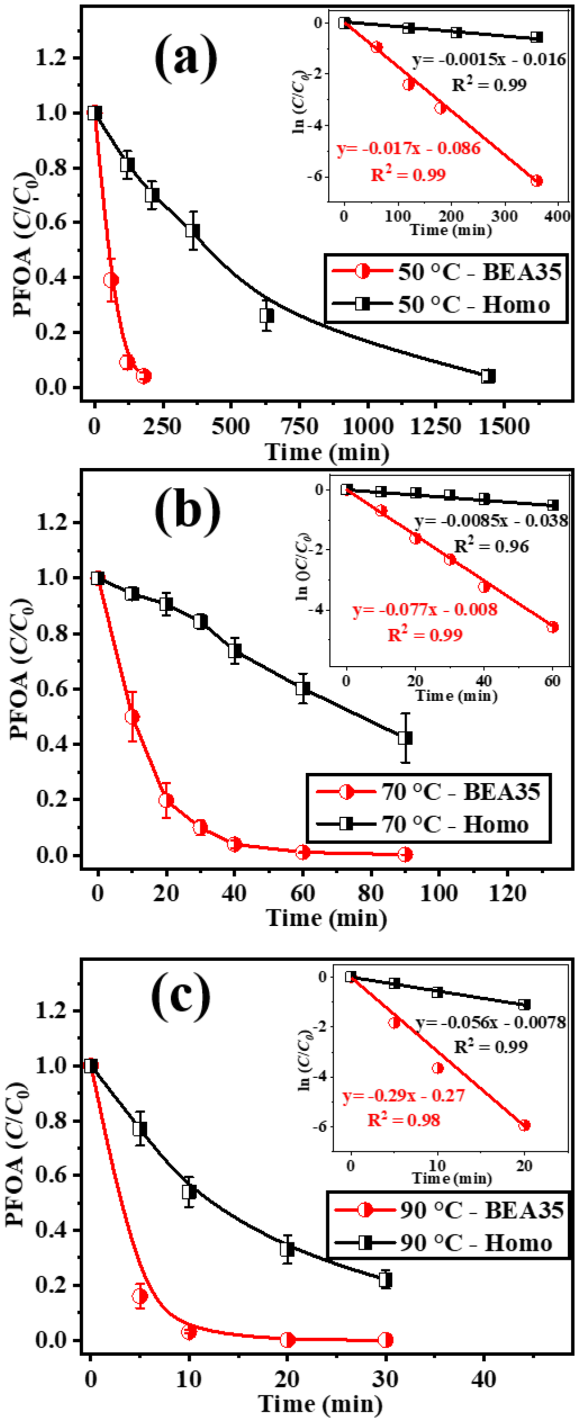

Figure 7. PFOA degradation by heat-activated persulfate at various activation temperatures. $C_{0,\mathrm{PFOA}}$ = 240 μM, $C_{0,\mathrm{persulfate}}$ = 100 mM, pH_0 = 3.0, and C_{zeolite} = 50 g L^{-1} where applied. Error ranges represent mean deviations of single values from the mean of at least two experiments. Lines in plots of relative concentrations are added as guides for the eye. Insets show fitting to pseudo-first order kinetics.

In addition to BEA35, other BEA type zeolites with various SiO_2/Al_2O_3 ratios, i.e. BEA24, BEA28, BEA40, and a zeolite of another framework type (faujasite), i.e. FAU15, were chosen in order to compare their effects on PFOA degradation by heat-activated persulfate. In general, in the presence of all types of zeolites, PFOA was predominantly adsorbed (> 99%), indicating that the heterogeneous degradation reaction should be dominant in all cases. In addition, as shown in Figure 6, all types of zeolites can promote PFOA degradation in comparison with the homogeneous system when identical conditions (including initial pH) are applied. The ranking in the PFOA degradation rate constants is BEA35 > FAU15 > BEA28 > BEA24 > BEA40, with a factor of 4 between the highest (BEA35) and lowest (BEA40) rate constant, as shown in Table S3. SEM images of zeolite particle morphology are shown in Figure S9, while information on primary particle sizes (between 125 and 540 nm) and BET surface areas (between 510 and 660 $m^2\ g^{-1}$) is presented in Table S3. No clear correlation between any one of these parameters and the catalytic effect of the zeolites is obvious. Additionally, the contents of Brønsted acid sites (BAS) and Lewis acid sites (LAS) were determined by means of IR measurements after pyridine adsorption (detailed procedures are described in SI, Experimental Section). The IR spectra and the calculated LAS and BAS contents of the zeolites are presented in Figure S10 and Table S4, respectively. As expected, the number of BAS in BEA zeolites increases with increasing Al content (decreasing SiO_2/Al_2O_3 ratio), as each Al in the structure creates a negatively charged site which is protonated in dry H-form zeolites and attracts protons or other cations when suspended in water. A higher number of BAS in BEA zeolites also corresponds to a lower native suspension pH (Table S4). In contrast, the number of LAS seems not to correlate to the SiO_2/Al_2O_3 ratio. LAS are mainly assigned to coordinatively unsaturated (extra-framework) Al^{3+} species in zeolites, and thus could also play a role for interacting with PFOA anions. However, no significant correlation between either BAS or LAS numbers of the zeolites and their promoting effect on PFOA degradation was found.

In addition, we tested the effect of temperature on PFOA degradation by heat-activated persulfate in the presence of zeolite. As seen in Figure 7, PFOA degradation rates increased by raising the activation temperature from 50 to 90 °C. Increased temperature not only enhanced the rate of persulfate decomposition, but also facilitated the PFOA degradation, so that an overall improved PFOA degradation rate was achieved. The presence of zeolite promoted the PFOA degradation over the investigated temperature range from 50 to 90 °C. We fitted the degradation curves at various activation temperatures according to Eq. 14 in Section 3.1. using the initial reaction period for fitting. As seen in Figure 7 and Table S5, the initial observable rate constant $k_{\mathrm{obs,PFOA}}$ increased due to the presence of zeolite by factors of 11, 9 and 5, at activation temperatures of 50, 70 and 90 °C, respectively. In addition, reaction stoichiometric efficiency (% RSE) of the system was calculated for PFOA degradation of 80 to 90% at different activation temperatures. A higher %RSE (7.6%) at 50 °C activation temperature in the presence of zeolite was observed comparing with RSE of 3.6% and 3.4% at 70 and 90 °C, respectively (Table S5). Overall, acceleration of PFOA degradation ($k_{\mathrm{PFOA,zeolite}}/k_{\mathrm{PFOA,homo}}$) and persulfate utilization efficiency (% RSE) by the zeolite become most significant at the lowest temperature (50 °C). In further work, even lower temperatures (≤ 25°C) will be tested to provide relevant suggestions for *in-situ* PFCA remediation techniques.

3.5. Mechanistic consideration of accelerated PFOA degradation by heat-activated persulfate in the presence of zeolite

From the observations described above we conclude that: I) all zeolites that were able to adsorb PFOA accelerated its degradation by heat-activated persulfate, with some differences which, however, could not be assigned to specific structural parameters; II) if certain catalytic sites were to be relevant, their number does not appear to be significantly limited, as the accelerating effect was the same for 100-fold different PFOA loadings on zeolite and also did not vary significantly with increasing zeolite concentration after PFOA adsorption degree ≥ 90% was reached; III) the conditions for persulfate decomposition into free radicals inside the zeolite pores are not necessarily beneficial in general, as another substrate, i.e. n-octanol, was inhibited in its degradation when adsorbed to zeolite; and IV) the pH effect, i.e. decreasing PFOA degradation rates with increasing pH, was much less pronounced for the heterogeneous compared to the homogeneous reaction.

Sulfate radical attack by electron transfer from the carboxylic head group of PFOA is considered to be the main initial reaction step in PFOA degradation by heat-activated persulfate [10, 20, 26]. It is interesting to consider the findings and hypotheses of Bruton and Sedlak [27] in terms of the pH-effect in PFOA degradation in the homogeneous heat-activated persulfate system. In their system, consumption of sulfate radicals by OH^- became relevant only at alkaline pH. An impact of OH^- is also not expected for the homogeneous reaction under the conditions applied in this study. In addition, Bruton and Sedlak noted that persulfate decomposition rates are nearly independent of pH in the range of 8 to 2 and only slightly affected by acid catalysis below pH 2. Thus, they suggested three hypotheses for the acceleration of PFOA degradation by heat-activated persulfate with decreasing pH: I) protonation of the PFOA anion improves its reactivity towards sulfate radicals, as the reaction of two negatively charged species could be detrimental; II) protonation of sulfate radicals improves their reactivity with PFOA anions; and III) acid catalysis occurs in the reaction between PFOA and sulfate radical. The pK_a values of PFOA (-0.5 to 1 [31, 32]) and sulfate radicals (estimated below 2) are uncertain, which makes differentiation between these hypotheses difficult. Nevertheless, it is hard to accept one of these hypotheses for aqueous solutions when the applied pH value is several units above the relevant range, i.e. pH ≥ 4.

In a similar manner, one could propose the following hypotheses for the zeolite systems: firstly, acid/base equilibria of PFOA and/or sulfate radicals could be shifted to higher protonation degrees inside the zeolite pores than in the aqueous bulk phase. Van den Bergh et al. [11] suggested that PFOA adsorption in Al-free BEA zeolite may occur in the protonated form with specifically beneficial head-to-head interactions of PFOA molecules inside the zeolite. This hypothesis was mainly derived from DFT calculations (which however cannot take into account solvation/dissociation effects) and solid-state NMR results for dried PFOA-loaded zeolites. Alternatively, acid catalysis by the zeolite surface could play a role, but cannot be assigned clearly to the content of acidic sites in zeolites due to the superposition of various effects.

Recently, Suehnholz et al. [33] described a heterogeneous activation of persulfate by FeS for oxidation of various organic compounds at ambient temperature. They suggest a surface-assisted homolytic bond cleavage of the O-O-bond in the peroxydisulfate dianion ($^-O_3S\text{-}O\cdots O\text{-}SO_3^-$) which proceeds with a low activation energy of $E_A = (31 \pm 1)$ kJ mol^{-1}. In a forthcoming study [34], these authors apply the system persulfate + FeS for the degradation of PFOA. Transferring this hypothesis to the system PFOA + persulfate + zeolite (instead of FeS), one could also postulate a surface-assisted persulfate activation in this case. This activation may promote the one-electron transfer from the PFOA carboxylate group to persulfate without attack of free sulfate radicals.

$$[C_7F_{15}COO^-]_{\text{adsorbed}} + [S_2O_8^{2-}]_{\text{surface activated}} \xrightarrow{e^-\text{ transfer}} C_7F_{15}COO\bullet + SO_4^{2-} + SO_4^{-}\bullet \qquad (16)$$

Such a hypothesis is in conformity with our observations: I) inhibition of n-octanol oxidation, which cannot be converted by electron transfer; II) absence of strong pH effects known for free sulfate radical-driven homogenous PFOA degradation by heat-activated persulfate; and III) insignificant acceleration of persulfate decomposition in the presence of zeolites. Based on the experimental results and mechanistic considerations, the proposed possible reaction pathways for PFOA degradation are further discussed in SI. Clearly, more research is needed in order to clarify the role of the zeolite in the accelerated PFOA degradation by heat-activated persulfate. The benefits of its combined role as adsorbent for PFOA removal and catalyst for subsequent degradation justify further detailed studies.

3.5. Stability and reusability test

As elucidated in chapter 3.2, PFOA degradation by heat-activated persulfate in the presence of zeolite is feasible under acidic to neutral conditions. Nevertheless, the decomposition of persulfate inevitably decreases the pH value of the system, which could challenge the stability and reusability of the zeolites. Although decreasing the initial persulfate dosage could still ensure a complete PFOA degradation without a strong pH decrease, this would extend the reaction time. Controlling or buffering the system pH during the reaction would be another solution, with some additional efforts needed. However, Figure 8(c) shows that the zeolites maintained constant catalytic activities in PFOA degradation by heat-activated persulfate even after 6 runs without controlling the reaction pH during each cycle (detailed procedures are described in SI, Experimental Section). This shows that BEA35 indeed acts as a catalyst, and also indicates a good stability of the zeolite even under temporarily strongly acidic conditions (pH 1.5).

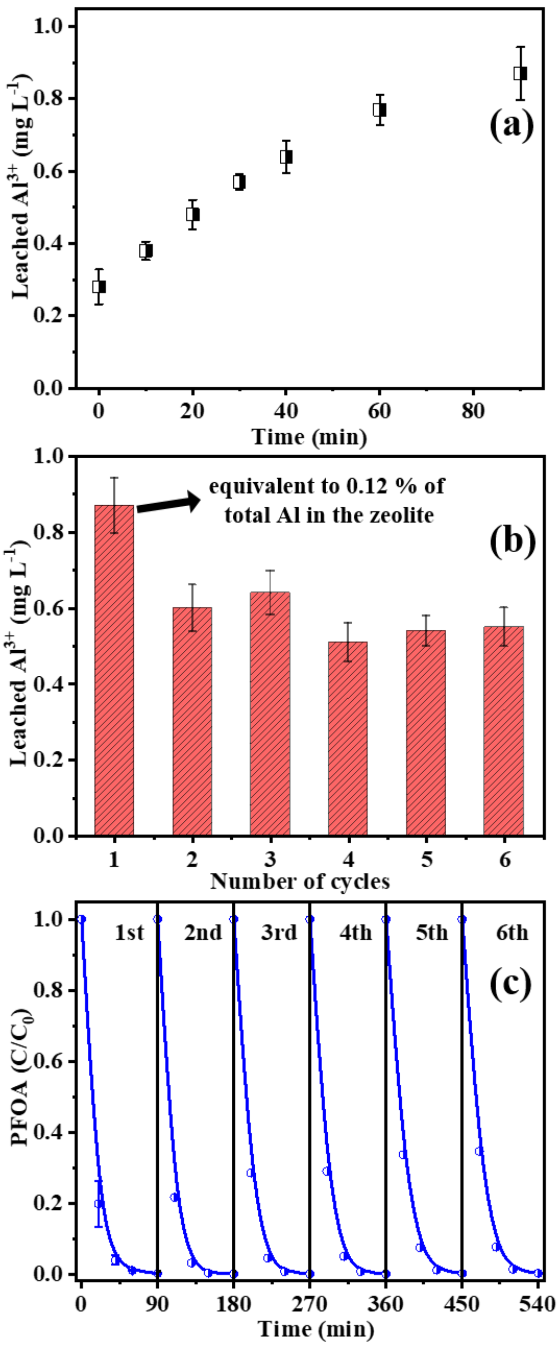

Figure 8. Aluminum leaching from zeolite BEA35 during PFOA degradation by heat-activated persulfate in the presence of zeolite: (a) in one cycle experiment; (b) in 6 consecutive batch runs. (c) The reusability of BEA35 in 6 consecutive batch runs. $C_{\text{zeolite}} = 50$ g L^{-1} and $C_{0,\text{PFOA}} = 240$ µM each, $C_{0,\text{persulfate}} = 100$ mM each, $pH_0 = 3.0$, and $T = 70$ °C. Error ranges represent mean deviations of single values from the mean of at least two experiments. Lines in plots of relative concentrations are added as guides for the eye.

As shown in Figure 8 (a), a small amount of Al^{3+} (0.28 mg L^{-1} from 50 g L^{-1} zeolite) was leached out after 2 h adsorption. The Al^{3+} leaching increased with decreasing pH to 0.87 mg L^{-1} after 90-min reaction. After one reaction cycle, the leached Al^{3+} amount is approximately 0.12% of the total Al in the zeolite. The Al^{3+} leaching is strongest in the first run and then declines, becoming stable after the 3rd run with 0.09% of total Al per cycle. For practical application, a two-step process is most promising, whereby the zeolite is first used as adsorbent e.g. in a fixed-bed for treating contaminated water by safe and fast adsorption. Heat-activated persulfate would then be used only for regeneration of the fixed-bed, e.g., by in-circuit flushing with persulfate solution and heating of the bed. This low-volume regeneration solution can be post-treated by neutralization, whereby any leached Al^{3+} is precipitated as $Al(OH)_3$, and by adding Ca^{2+} to precipitate F^- as CaF_2.

3.6. Application to real water matrices and considerations for practical application

We have thus shown an efficient PFOA degradation by heat-activated persulfate in synthetic water in the presence of zeolites. In reality, ground and surface waters usually contain trace PFOA concentrations and complex water matrices, e.g. with coexisting organic compounds and inorganic ions. For instance, chloride is reported to be a strong competitor for sulfate radicals [35]. As shown in Figure S11, we compared the PFOA degradation behavior by heat-activated persulfate in the presence of zeolites with and without addition of chloride. The addition of 5 mM chloride strongly inhibited the PFOA degradation, although its complete degradation can still be achieved after longer reaction times (> 6 h). Therefore, when dealing with real waters, a pretreatment (see Section 2.2) should be performed in order to: I) eliminate inorganic matrix components; and II) enrich the trace amount of PFOA from water. In this study, three groundwater samples were taken from three wells located in Leuna, a former refinery site in Germany. These groundwater samples contain trace amounts of PFOA, ranging from 35 to 82 ng L^{-1}. Detailed chemical composition of these groundwater samples, i.e. electrical conductivity, pH values, total organic carbon content and inorganic ions content, is presented in Table S1. Briefly, zeolite was added to groundwater samples for PFOA adsorption, precipitated by centrifugation and then the solid zeolite was transferred into DI water. In this way, most of the inorganic matrix components were excluded. The results in Figure 9(a) show that PFOA degradation by heat-activated persulfate is still applicable (PFOA degradation > 90% at t > 180 min) when dealing with trace PFOA in groundwater samples. Compared with PFOA in clean solution (Table 1), a decrease in $k_{\mathrm{obs,PFOA}}$ was observed when PFOA had been previously extracted and concentrated on zeolite from groundwater. This was possibly due to competing degradation reactions of some organic compounds co-adsorbed in the zeolite (e.g. methyl *tert*-butyl ether and benzene), as the groundwater sample with the lowest DOC content showed the fastest PFOA degradation. In short, PFOA enrichment from a real groundwater sample can be achieved using zeolite, and combined with a subsequent heat-activated-persulfate PFOA degradation process.

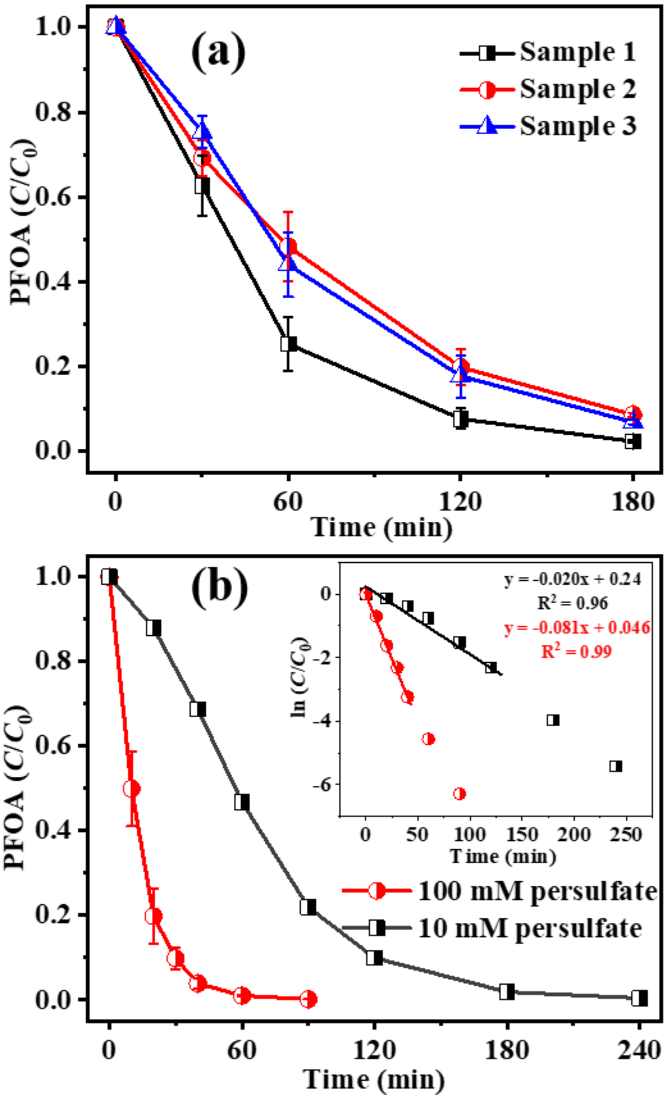

Figure 9. PFOA degradation by heat-activated persulfate in the presence of zeolite (a) with various groundwater samples, $C_{0,\text{persulfate}}$ = 100 mM; (b) with various initial persulfate dosages. C_{zeolite} = 50 g L^{-1}, pH$_0$ = 3.0, and T = 70 °C. Error ranges represent mean deviations of single values from the

mean of at least two experiments. Lines in plots of relative concentrations are added as guides for the eye. Inset shows fitting to pseudo-first order kinetics.

Besides testing the degradation principle with real water, the economical consideration of this approach is also an important aspect that needs to be considered. Here we provide an initial estimate of the costs for treatment of PFOA-contaminated water in a realistic application scenario, i.e. using a zeolite fixed-bed adsorber, which is periodically regenerated by heat-activated persulfate (detailed cost estimate in SI). We estimated the total treatment costs, for zeolite, persulfate, and bed heating, to be in the range of 0.02–0.25 € m^{-3}. In addition, site-specific operational costs for groundwater pumping and reactor installation must be considered. The estimated operation cost is comparable to the prevailing large-scale PFAS *removal* technologies, i.e. ion exchange, activated carbon adsorption and reverse osmosis, with the groundwater pump-and-treat units operation costs of 0.8–1.7 € m^{-3}, 0.5–0.9 € m^{-3}, and 1.7-2.2 € m^{-3}, respectively [7].

In addition, it was also interesting to evaluate the reaction stoichiometric efficiency (% RSE) of the system. In the case where the system contained 100 mM persulfate, $C_{0,\mathrm{PFOA}}$ = 240 mM, and C_{zeolite} = 50 g L^{-1}, the RSE was calculated to be 3.6% when 90% PFOA degradation was achieved after 30 min. This value is higher than the RSE of 0.6% obtained in the homogenous heat-activated persulfate PFOA degradation at the same conditions. In this work, we designed the experiments with a high initial persulfate concentration in order to enable a fast degradation process while providing a proof-of-principle for a novel PFOA treatment approach. Accordingly, a relatively low RSE was obtained, which can certainly be improved at lower initial persulfate concentrations or step-wise dosing of persulfate as the oxidant itself acts as a consumer of sulfate radicals ($SO_4^- \cdot + S_2O_8^{2-} \longrightarrow SO_4^{2-} + S_2O_8^{-}\cdot$).

When we conducted the reaction at a 10-times lower initial persulfate dosage, the overall PFOA degradation rate declined (Figure 9(b)), but it still gave an adequate PFOA degradation efficiency (99.5%) at an extended reaction time of 4 h. The %RSE was calculated to be 12% when 90% PFOA degradation was achieved after 2 h. Considering the rather low second-order rate constants ($k_{SO_4^-\cdot} = (1.7\text{-}4.4) \times 10^4\ M^{-1}s^{-1}$) for reactions between PFCAs and sulfate radicals in aqueous solution [20], comparably low RSE values are expected. The relatively high RSE obtained in the presence of zeolite point to an additional reaction mechanism (in addition to the $SO_4^- \cdot$ attack) which may include $S_2O_8^{-}\cdot$. The role of this transient species needs to be explored in future studies.

Nevertheless, in real applications, one can optimize the initial persulfate dosage and the corresponding reaction time such as to achieve a minimized chemicals and/or energy demand.

Although the BEA35 zeolite showed good performance not only in removing PFOA by adsorption, but also in accelerating its degradation by persulfate, thermal activation was still required to initiate this process. This is one limitation of the established approach. For *in situ* remediation of contaminated sites, it is desired to have an absorbent/catalyst able to adsorb traces of PFOA from e.g. contaminated aquifers, and activate injected persulfate at *in situ* relevant temperatures (about 12 °C). Thus, more investigations still needs to be done regarding the PFOA degradation under *in situ* relevant conditions in future studies.

4. Conclusion

This study presents an approach for a novel PFOA treatment technology, where PFOA can be firstly removed from water by zeolite adsorption, and then degraded directly in the adsorbed state by heat-activated persulfate. Overall, the major findings are summarized as follows:

I. Degradation by heat-activated persulfate is effective for PFOA adsorbed to a BEA-type zeolite, and a significant rate-enhancement was observed compared to the sulfate radical-based homogeneous system.

II. PFOA degradation by heat-activated persulfate in the presence of zeolite showed an adequate performance at initially neutral pH.

III. Zeolite internal surface promoted PFOA degradation by heat-activated persulfate. Further studies are needed in order to elucidate this catalytic effect, which may be due to reactive sites inside the zeolite.

IV. The stability and reusability of the zeolite were evaluated. After six adsorption/degradation cycles, BEA35 showed no significant decline in PFOA degradation performance.

V. Real groundwater samples containing PFOA in the ng L^{-1} range were found to be still effectively treated by the combination of zeolite adsorption and heat-activated persulfate.

VI. The costs for PFOA-contaminated water treatment were evaluated by applying a realistic scenario, i.e. a zeolite-based fixed-bed adsorber with intermittent regeneration by in-circuit flushing with persulfate solution at elevated temperature (70 °C). This preliminary estimation suggests that the approach can be cost-competitive to state-of-the-art processes, and deserves further research.

Acknowledgments

We thank Jieying Zhou for useful discussion and proof reading and Silke Woszidlo for technical support in conducting experiments. Lin Qian acknowledges financial support by China Scholarship Council.

Reference

[1] F. Xiao, T.R. Halbach, M.F. Simcik, J.S. Gulliver, Input characterization of perfluoroalkyl substances in wastewater treatment plants: Source discrimination by exploratory data analysis, Water Res. 46 (2012) 3101-3109. https://doi.org/10.1016/j.watres.2012.03.027
[2] V. Gallo, G. Leonardi, B. Genser, M.-J. Lopez-Espinosa, S.J. Frisbee, L. Karlsson, A.M. Ducatman, T. Fletcher, Serum perfluorooctanoate (PFOA) and perfluorooctane sulfonate (PFOS) concentrations and liver function biomarkers in a population with elevated PFOA exposure, Environ. Health Perspect. 120 (2012) 655-660. https://doi.org/doi:10.1289/ehp.1104436
[3] K. Steenland, S. Tinker, A. Shankar, A. Ducatman, Association of perfluorooctanoic acid (PFOA) and perfluorooctane sulfonate (PFOS) with uric acid among adults with elevated community exposure to PFOA, Environ. Health Perspect. 118 (2010) 229-233. https://doi.org/doi:10.1289/ehp.0900940
[4] A.G. Paul, K.C. Jones, A.J. Sweetman, A first global production, emission, and environmental inventory for perfluorooctane sulfonate, Environ. Sci. Technol. 43 (2009) 386-392. https://doi.org/10.1021/es802216n
[5] N. Yamashita, K. Kannan, S. Taniyasu, Y. Horii, G. Petrick, T. Gamo, A global survey of perfluorinated acids in oceans, Mar. Pollut. Bull. 51 (2005) 658-668. https://doi.org/10.1016/j.marpolbul.2005.04.026
[6] D. Huang, L. Yin, J. Niu, Photoinduced hydrodefluorination mechanisms of perfluorooctanoic acid by the SiC/Graphene catalyst, Environ. Sci. Technol. 50 (2016) 5857-5863. https://doi.org/10.1021/acs.est.6b00652
[7] H.-G. Edel, D.-I.D. Klopp, B.E.J. Drubel, B.E.D. Korte, D.-I.C. Kellner, D.-I.U. Rehnig, PFAS Groundwater remediation: State of the art technology and comparison of costs - English translation of reprint from Handbuch Altlastensanierung und Flachenmanagement (HdA).
[8] M. Trojanowicz, A. Bojanowska-Czajka, I. Bartosiewicz, K. Kulisa, Advanced oxidation/reduction processes treatment for aqueous perfluorooctanoate (PFOA) and perfluorooctanesulfonate (PFOS) – a review of recent advances, Chem. Eng. J. 336 (2018) 170-199. https://doi.org/10.1016/j.cej.2017.10.153
[9] H. Hori, A. Yamamoto, E. Hayakawa, S. Taniyasu, N. Yamashita, S. Kutsuna, H. Kiatagawa, R. Arakawa, Efficient decomposition of environmentally persistent perfluorocarboxylic acids by use of persulfate as a photochemical oxidant, Environ. Sci. Technol. 39 (2005) 2383-2388. https://doi.org/10.1021/es0484754
[10] H. Hori, Y. Nagaoka, M. Murayama, S. Kutsuna, Efficient decomposition of perfluorocarboxylic acids and alternative fluorochemical surfactants in hot water, Environ. Sci. Technol. 42 (2008) 7438-7443. https://doi.org/10.1021/es800832p
[11] S. Naim, A. Ghauch, Ranitidine abatement in chemically activated persulfate systems: Assessment of industrial iron waste for sustainable applications, Chem. Eng. J. 288 (2016) 276-288. https://doi.org/10.1016/j.cej.2015.11.101
[12] A. Ghauch, G. Ayoub, S. Naim, Degradation of sulfamethoxazole by persulfate assisted micrometric Fe0 in aqueous solution, Chem. Eng. J. 228 (2013) 1168-1181. https://doi.org/10.1016/j.cej.2013.05.045
[13] G. Ayoub, A. Ghauch, Assessment of bimetallic and trimetallic iron-based systems for persulfate activation: Application to sulfamethoxazole degradation, Chem. Eng. J. 256 (2014) 280-292. https://doi.org/10.1016/j.cej.2014.07.002

[14] S.X. Liang, Z. Jia, W.C. Zhang, X.F. Li, W.M. Wang, H.C. Lin, L.C. Zhang, Ultrafast activation efficiency of three peroxides by Fe78Si9B13 metallic glass under photo-enhanced catalytic oxidation: A comparative study, Appl. Cat. B: Environ. 221 (2018) 108-118. https://doi.org/10.1016/j.apcatb.2017.09.007

[15] S.-X. Liang, X. Wang, W. Zhang, Y.-J. Liu, W. Wang, L.-C. Zhang, Selective laser melting manufactured porous Fe-based metallic glass matrix composite with remarkable catalytic activity and reusability, Appl. Mater. Today 19 (2020) 100543. https://doi.org/10.1016/j.apmt.2019.100543

[16] J. Wu, B. Wang, G. Cagnetta, J. Huang, Y. Wang, S. Deng, G. Yu, Nanoscale zero valent iron-activated persulfate coupled with Fenton oxidation process for typical pharmaceuticals and personal care products degradation, Sep. Purif. Technol. 239 (2020) 116534. https://doi.org/10.1016/j.seppur.2020.116534

[17] A. Baalbaki, N. Zein Eddine, S. Jaber, M. Amasha, A. Ghauch, Rapid quantification of persulfate in aqueous systems using a modified HPLC unit, Talanta 178 (2018) 237-245. https://doi.org/10.1016/j.talanta.2017.09.036

[18] O. Tantawi, A. Baalbaki, R. El Asmar, A. Ghauch, A rapid and economical method for the quantification of hydrogen peroxide (H2O2) using a modified HPLC apparatus, Sci. Total Environ. 654 (2019) 107-117. https://doi.org/10.1016/j.scitotenv.2018.10.372

[19] R. El Asmar, A. Baalbaki, Z. Abou Khalil, S. Naim, A. Bejjani, A. Ghauch, Iron-based metal organic framework MIL-88-A for the degradation of naproxen in water through persulfate activation, Chem. Eng. J. 405 (2021) 126701. https://doi.org/10.1016/j.cej.2020.126701

[20] H.V. Lutze, J. Brekenfeld, S. Naumov, C. von Sonntag, T.C. Schmidt, Degradation of perfluorinated compounds by sulfate radicals – New mechanistic aspects and economical considerations, Water Res. 129 (2018) 509-519. https://doi.org/10.1016/j.watres.2017.10.067

[21] M. Van den Bergh, A. Krajnc, S. Voorspoels, S.R. Tavares, S. Mullens, I. Beurroies, G. Maurin, G. Mali, D.E. De Vos, Highly selective removal of perfluorinated contaminants by adsorption on all-silica zeolite beta, Angew. Chem. Int. Ed. 59 (2020) 14086-14090. https://doi.org/10.1002/anie.202002953

[22] L. Qian, F.-D. Kopinke, A. Georgi, Photodegradation of perfluorooctanesulfonic acid on Fe-zeolites in water, Environ. Sci. Technol. 55 (2021) 614-622. https://doi.org/10.1021/acs.est.0c04558

[23] L. Qian, A. Georgi, R. Gonzalez-Olmos, F.-D. Kopinke, Degradation of perfluorooctanoic acid adsorbed on Fe-zeolites with molecular oxygen as oxidant under UV-A irradiation, Appl. Cat. B: Environ. 278 (2020) 119283. https://doi.org/10.1016/j.apcatb.2020.119283

[24] B. Sun, J. Ma, D.L. Sedlak, Chemisorption of perfluorooctanoic acid on powdered activated carbon initiated by persulfate in aqueous solution, Environ. Sci. Technol. 50 (2016) 7618-7624. https://doi.org/10.1021/acs.est.6b00411

[25] C. Liang, C.-F. Huang, N. Mohanty, R.M. Kurakalva, A rapid spectrophotometric determination of persulfate anion in ISCO, Chemosphere 73 (2008) 1540-1543. https://doi.org/10.1016/j.chemosphere.2008.08.043

[26] S. Kutsuna, H. Hori, Rate constants for aqueous-phase reactions of SO4− with C2F5C(O)O− and C3F7C(O)O− at 298 K, Int. J. Chem. Kinet. 39 (2007) 276-288. https://doi.org/10.1002/kin.20239

[27] T.A. Bruton, D.L. Sedlak, Treatment of perfluoroalkyl acids by heat-activated persulfate under conditions representative of in situ chemical oxidation, Chemosphere 206 (2018) 457-464. https://doi.org/10.1016/j.chemosphere.2018.04.128

[28] R.C. Buck, J. Franklin, U. Berger, J.M. Conder, I.T. Cousins, P. de Voogt, A.A. Jensen, K. Kannan, S.A. Mabury, S.P. van Leeuwen, Perfluoroalkyl and polyfluoroalkyl substances in the environment: Terminology, classification, and origins, Integr. Environ. Assess. Manag. 7 (2011) 513-541. https://doi.org/10.1002/ieam.258

[29] W. Kim, J.-C. Kim, J. Kim, Y. Seo, R. Ryoo, External surface catalytic sites of surfactant-tailored nanomorphic zeolites for benzene isopropylation to cumene, ACS Catal. 3 (2013) 192-195. https://doi.org/10.1021/cs300678n
[30] C.L. Clifton, R.E. Huie, Rate constants for hydrogen abstraction reactions of the sulfate radical, SO4−. alcohols, Int. J. Chem. Kinet. 21 (1989) 677-687. https://doi.org/10.1002/kin.550210807
[31] K.-U. Goss, The pKa values of PFOA and other highly fluorinated carboxylic acids, Environ. Sci. Technol. 42 (2008) 456-458. https://doi.org/10.1021/es702192c
[32] A. Baggioli, M. Sansotera, W. Navarrini, Thermodynamics of aqueous perfluorooctanoic acid (PFOA) and 4,8-dioxa-3H-perfluorononanoic acid (DONA) from DFT calculations: Insights into degradation initiation, Chemosphere 193 (2018) 1063-1070. https://doi.org/10.1016/j.chemosphere.2017.11.115
[33] S. Sühnholz, F.-D. Kopinke, K. Mackenzie, Reagent or catalyst? – FeS as activator for persulfate in water, Chem. Eng. J. 387 (2020) 123804. https://doi.org/10.1016/j.cej.2019.123804
[34] S. Sühnholz, A. Gawel, F.-D. Kopinke, K. Mackenzie, Evidence of heterogeneous degradation of PFOA by activated persulfate – FeS as adsorber and activator, Chem. Eng. J. (2021) 130102. https://doi.org/10.1016/j.cej.2021.130102
[35] H.V. Lutze, N. Kerlin, T.C. Schmidt, Sulfate radical-based water treatment in presence of chloride: Formation of chlorate, inter-conversion of sulfate radicals into hydroxyl radicals and influence of bicarbonate, Water Res. 72 (2015) 349-360. https://doi.org/10.1016/j.watres.2014.10.006

Supporting information

Detailed information on Experimental Section

Identification of various PFOA isomers

The PFOA isomer standards were measured by means of LC/MS in order to assign the peak of each PFOA isomer as shown in Figure S4. In addition, one PFOA isomer standard containing both 4,5 m and 3,5 m PFOA isomers was further analyzed with UPLC/MS/MS (Waters Acquity Xevo-TQS). Under the conditions with three different LC columns (reversed-phase C18 column, fluoro phenyl column and reversed-phase octyl column), the 4,5 m PFOA isomer elutes earlier than the 3,5 m PFOA isomer.

Preparation of technical PFOA

The technical PFOA sample contains 20 to 30% branched isomers of the total PFOA. While, the concentration of some branched PFOA isomers is still quite small. Our preliminary experiments showed that BEA35 has a stronger adsorption affinity towards linear PFOA compared with the branched isomers due to steric effect (size exclusion). The selective adsorption by BEA35 was used to remove most of linear PFOA from the technical PFOA mixture. After zeolite adsorption and centrifugation, the supernatant containing higher proportion of branched PFOA isomers could be used for further experiments as described in Section 3.3.

Estimation of relative contributions of adsorbent and regeneration costs to the total treatment costs

Here, we try to provide a first estimation of the costs for treatment of PFOA-contaminated water in a realistic application scenario, i.e. using a zeolite-based fixed-bed adsorber which is periodically regenerated by heat-activated persulfate. We exemplarily consider the case of treatment of 10 m^3 h^{-1} flux of contaminated water with an inflow concentration of 10 µg L^{-1} PFOA. In the regeneration step, persulfate is pumped through the fixed bed in circuit using a reservoir with additional pH control/re-adjustment while the bed is heated to 70 °C.

(1) Zeolite fixed bed cost estimation.

In order to allow for a residence time of the water in the adsorber fixed bed of t_R = 6 min, an adsorber volume of 2 m^3 has to be provided (at a total porosity of the bed of pelletized zeolite of

50%). A 2 m^3 volume zeolite bed requires 1800 kg zeolite according to a bed density of 0.9 kg L^{-1} [1]. Thus, at an approximate price of 20-60 € kg^{-1} for industrial BEA-type zeolites (depending on specific product and ordered amount), the investment cost for the zeolite material alone would be 36,000 - 108,000 €.

Assuming a step-function breakthrough curve, at an inflow PFOA concentration of 10 μg L^{-1} and a K_d of 30,000 L kg^{-1} (pH 7, Table S2), a PFOA equilibrium loading of 300 mg kg^{-1} is obtained. Considering 1800 kg zeolite in one unit bed, this PFOA loading is aquired from $V_{\text{step-funct}}$ = 54,000 m^3 inflow water, i.e. elution of 54,000 unit bed volumes is needed to reach this status. In reality, the breakthrough curve is rather of S-shape than a step-function (due to dispersion effects) and regeneration should be performed after e.g. 10% PFOA breakthrough ($C_{\text{out}}/C_{\text{in}}$ = 0.1) is achieved. Nevertheless, the volume of treated water in this case can be assumed to be within 70-90% of $V_{\text{step-funct}}$, i.e. roughly 43,000 m^3.

(2) Sodium persulfate costs estimation.

For each regeneration cycle, at maximum 540 g adsorbed PFOA needs to be mineralized (a loading of ≤ 300 mg kg^{-1} with 1800 kg zeolite). When a 100-fold molar demand of sodium persulfate is suggested, the required amount of sodium persulfate for each regeneration step is 130 mol or 31 kg. This amount could be supplied e.g. in form of 1.2 m^3 regeneration solution with 25 g L^{-1} sodium persulfate pumped through the fixed bed in circuit using a reservoir with additional pH control/re-adjustment. The costs for sodium persulfate are 25 € (the cost of industrial grade sodium persulfate is about 800 € per ton) for each regeneration step.

(3) Heat energy costs estimation.

Calculation of the heat energy required for heating the fixed bed to 70°C can be done as follows:

$$Q = m\, c_p\, \Delta T$$

where Q = heat energy (J), m = mass of water (suspension) (kg), c_p = specific heat capacity (J K^{-1} kg^{-1}), and ΔT = change in temperature (K).

The specific heat capacity of water (c_p) is 4180 J K^{-1} kg^{-1}. The c_p of zeolite is estimated to be 1400 J K^{-1} kg^{-1} [2]. For each regeneration cycle, the energy for heating 2 m^3 zeolite bed (containing 1.2 m^3 regeneration solution) from 15 to 70 °C can be calculated as:

$$Q = (2000\text{ L} \times 0.9\text{ kg L}^{-1} \times 1400\text{ J K}^{-1}\text{ kg}^{-1} + 1200\text{ kg} \times 4180\text{ J K}^{-1}\text{ kg}^{-1}) \times (70 - 15)\text{ K}$$

$$= 4.14 \times 10^8\text{ J}$$

If a safety factor of 1.3 can be considered for thermal losses, it can be assumed that the required energy to hold the temperature at 70 °C in a closed water circuit for the reaction time of 3 h is considered with this safety factor thanks to appropriate thermal insulation. The required electricity can be calculated as:

$$4.14\times10^{8}\ \mathrm{J}\times 1.3\times\frac{\mathrm{kWh}}{3.6\times10^{6}\ \mathrm{J}} = 150\ \mathrm{kWh}$$

Based on the average industrial electricity cost in Germany of 0.23 € kWh^{-1}, the cost of heat energy for each regeneration step is 35 €. In case of an appropriate industrial infrastructure at the site of water treatment, low-temperature heat would be available to even much lower costs.

(4) Overall

If the zeolite fixed bed can be used for the treatment of 430,000 – 2150,000 m^3 PFOA-containing water (i.e. re-used within 10 – 50 adsorption/regeneration cycles), the costs contributed by zeolite, persulfate and bed heating) per m^3 treated water can be estimated as:

for 10 cycles: [36,000 to 108,000 € (for zeolite) + 25 € × 10 (for persulfate) + 35 € × 10 (for heating)] ÷ 430,000 m^3 = 0.08 – 0.25 € m^{-3}.

For 50 cycles: [36,000 to 108,000 € + 25 € × 50 + 35 € × 50] ÷ 2,150,000 m^3 = 0.02 – 0.05 € m^{-3}.

Thus, the total treatment costs will be in the range of 0.02 – 0.25 € m^{-3} plus certain operation (electricity for pumps, base for neutralization) and investment costs (reactor + installations). It can be derived that the cost of PFOA-contaminated water treatment in the zeolite fixed bed is determined mainly by the investment costs for the zeolite depending on its long-term stability. Note, that only the small amount of regeneration solution has to be heated. The large amount of contaminated water remains at its ambient temperature.

Another aspect relates to the number of adsorber beds that might be necessary for a continuous operation. Due to the large treatment capacity of the adsorber (43,000 m^3 contaminated water in the considered example) and the fast regeneration (a few hours) one can possibly work with only one adsorber bed. On the other hand, the fast chemical regeneration of the loaded adsorber bed offers a cost reduction potential: smaller adsorber bed + more frequent bed regeneration reduces the overall treatment costs significantly.

Zeolite acidity determination

Sample preparation.

Before the preparation of zeolite discs for IR measurements, the zeolite powders were dried in vacuum at 150 °C overnight. Compacted pellets of zeolite powders were prepared just after the end of the drying process using a hydraulic press (Perkin Elmer). About 12 mg of the zeolite were put into a compression mold with a diameter of 13 mm. A compaction load of 2 t was chosen for the present investigations. Samples prepared in this way still have a limited mechanic stability, but they can be readily modified with pyridine and measured by IR spectroscopy without disintegration [3]. Pyridine adsorption was performed at 150 °C according to the procedures described in literature. The compacted zeolite pellets were introduced into a 150 mL vial with a silicon cap. After the vacuum drying at 150 °C overnight, 0.75 mL of pyridine (Merck) was slowly injected to assure a complete volatilization of pyridine. After 4 h, the compacted zeolite pellets were saturated with pyridine. The silicon cap was opened and the temperature was maintained at 150 °C for 2 h to desorb the physically adsorbed pyridine.

Analytical Methods.

IR were recorded in transmission with a Tensor II IR spectrometer equipped with a DTGS detector (Bruker Optics, Ettlingen, Germany). For each spectrum, 32 scans were accumulated. The spectra were recorded and analyzed using the OPUS software version 8.1. Thickness and weight measurements of the compacted discs were carried out with a thickness gauge (Garant, Hoffmann Group) and an analytical balance, respectively.

Calculation of the concentration of acid sites.

The concentration of Brønsted and Lewis acid sites (BAS, LAS) in moles per mass of zeolite ($n_{\text{py}}/m_{\text{z}}$) is shown in Table S4. They were calculated from the IR bands at 1547 cm^{-1} (BAS) and 1455 cm^{-1} (LAS) according to the approaches and using the corresponding extinction coefficients described by Zholobenko et al. [3]. The $n_{\text{py}}/m_{\text{z}}$ was calculated from

$$n_{\text{py-x}} / m_{\text{z}} = (S \times A) / (\varepsilon_{\text{py-x}} \times m_{\text{z}}) \qquad \text{(eq. S1)}$$

where S and m_z are the area (cm²) and the mass of the zeolite disc (g), respectively. A is the integrated absorption (cm^{-1}) and $\varepsilon_{\text{py-x}}$ is the molar extinction coefficient (x = H$^+$ for BAS or L for LAS, respectively). The value of $\varepsilon_{\text{py-H}^+}$ was found to depend on the specific zeolite. It was reported to be (1.12 ± 0.16) cm µmol^{-1} for zeolites of the BEA type and (1.54 ± 0.15) cm µmol^{-1} for FAU. In contrast, $\varepsilon_{\text{py-L}}$ did not depend on the zeolite type, and its value was given to be (1.71 ± 0.1) cm µmol^{-1} [3].

Tables S1 to S5 referred in the main text and supporting information

Table S1. Properties and chemical composition of three filtered groundwater samples.

Sample	EC[a] mS cm^{-1}	pH	TOC[b] mg L^{-1}	PFOA ng L^{-1}	K^+ mg L^{-1}	Na^+ mg L^{-1}	Ca^{2+} mg L^{-1}	Mg^{2+} mg L^{-1}	SO_4^{2-} mg L^{-1}	NO_3^- mg L^{-1}	Cl^- mg L^{-1}
1	2.1	7.2	8.4	82	16	212	205	61	333	121	237
2	2.2	7.3	37.3	35	18	196	157	52	315	181	231
3	2.5	7.3	38.8	47	14	196	154	53	572	369	297

[a] EC: electrical conductivity.

[b] TOC: total organic carbon content.

Table S2. PFOA adsorption, pseudo-first-order degradation rate constants ($k_{\mathrm{obs,PFOA}}$) and half-lives of PFOA at different initial pH values (C_{zeolite} = 50 g L^{-1}, $C_{0,\mathrm{PFOA}}$ = 240 μM, $C_{0,\mathrm{persulfate}}$ = 100 mM, and T = 70 °C).

	pH = 3.0	**pH = 5.0**	**pH = 7.0**
$X_{\mathrm{Sorb,PFOA}}$ (%)	0.998	0.999	0.999
q_{PFOA} (g kg^{-1}) [a]	2.0	2.0	2.0
K_d (L kg^{-1}) [b]	1.9×10^4	2.7×10^4	3.1×10^4
$k_{\mathrm{obs,PFOA}}$ (min^{-1}) [c]	0.077 ± 0.004	0.061 ± 0.001	0.048 ± 0.005
PFOA $t_{1/2}$ (min)	8.5 ± 0.4	10.0 ± 1.5	13 ± 1

[a] Sorbent loading.

[b] Single point adsorption coefficient K_d (L kg^{-1}) = q_{PFOA} (μmol kg^{-1}) / $C_{\mathrm{PFOA,free}}$ (μmol L^{-1})

[c] $k_{\mathrm{obs,PFOA}}$ is obtained by first-order kinetics fitting within the initial period of PFOA degradation (0 – 60 min). The error ranges are derived from regression analysis of the data.

Table S3. Physical-chemical properties and PFOA degradation kinetics of various types of zeolites.

	BEA24	**BEA28**	**BEA35**	**BEA40**	**FAU15**
BET surface (m^2 g^{-1})	660	510	656	530	550
Particle size (nm) [a]	125	400	500	540	450
Initial pH values [b]	2.7	2.9	3.0	3.7	4.2
X_{sorb}	0.995	0.999	0.998	0.999	0.997
$k_{\mathrm{obs,PFOA}}$ (min^{-1}) [c]	0.020 ± 0.002	0.026 ± 0.001	0.077 ± 0.004	0.019 ± 0.003	0.065 ± 0.006
PFOA $t_{1/2}$ (min)	31 ± 4	26 ± 1	8.5 ± 0.4	33 ± 4	10 ± 1

[a] The particle size is determined by SEM.

[b] The initial pH values were determined after mixing of 240 μM PFOA solution with 50 g L^{-1} zeolites and shaking for 2 h.

[c] $k_{\mathrm{obs,PFOA}}$ is obtained by first-order kinetics fitting within the initial period of PFOA degradation (0 – 60 min). The error ranges are derived from the regression analysis of the data.

Table S4. Determination of the concentration of acid sites inside the zeolites with pyridine as a probe molecule.

Sample	Mass [mg]	Disk thickness [μm]	Area (Py-H$^+$) 1547 cm^{-1}	Area (Py-L) 1455 cm^{-1}	$n_{\text{py-H}^+}/m_z$ [μmol g^{-1}]	$n_{\text{py-L}}/m_z$ [μmol g^{-1}]
BEA 24	12.5	118	1.29	0.50	31	122
BEA 28	12.4	120	0.63	0.33	21	61
BEA 35	14.4	127	0.32	0.36	20	26
BEA 40	12.3	123	0.29	0.54	34	28
FAU 15	9.8	108	0.51	0.22	17	45

Table S5. Pseudo-first-order degradation rate constants ($k_{\text{obs,PFOA}}$) of PFOA and reaction stoichiometric efficiency (% RSE) at various activation temperatures.

	50 °C	70 °C	90 °C
$k_{\text{obs,PFOA}}$ with zeolites (min^{-1}) [a]	0.017 ± 0.002	0.077 ± 0.004	0.29 ± 0.05
$k_{\text{obs,PFOA}}$ without zeolites (min^{-1}) [a]	0.0015 ± 0.0002	0.0085 ± 0.002	0.056 ± 0.006
RSE with zeolites (%) [b]	7.6 ± 0.7	3.6 ± 0.4	3.4 ± 0.3
RSE without zeolites (%) [b]	0.75 ± 0.07	0.60 ± 0.06	0.63 ± 0.06

[a] $k_{\text{obs,PFOA}}$ is obtained by first-order kinetics fitting within the initial period of PFOA degradation. The error ranges are derived from the regression analysis of the data.

[b] RSE values are calculated when 80 to 90% PFOA degradation is achieved.

Figures S1 to S11 referred in the main text and supporting information.

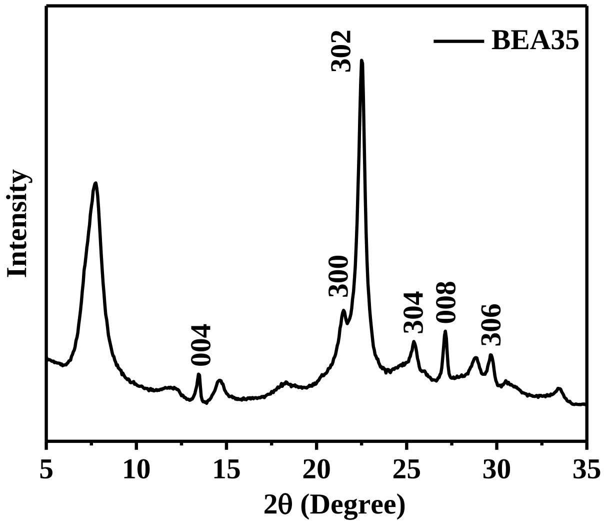

Figure S1. The X-ray powder diffraction pattern of BEA35.

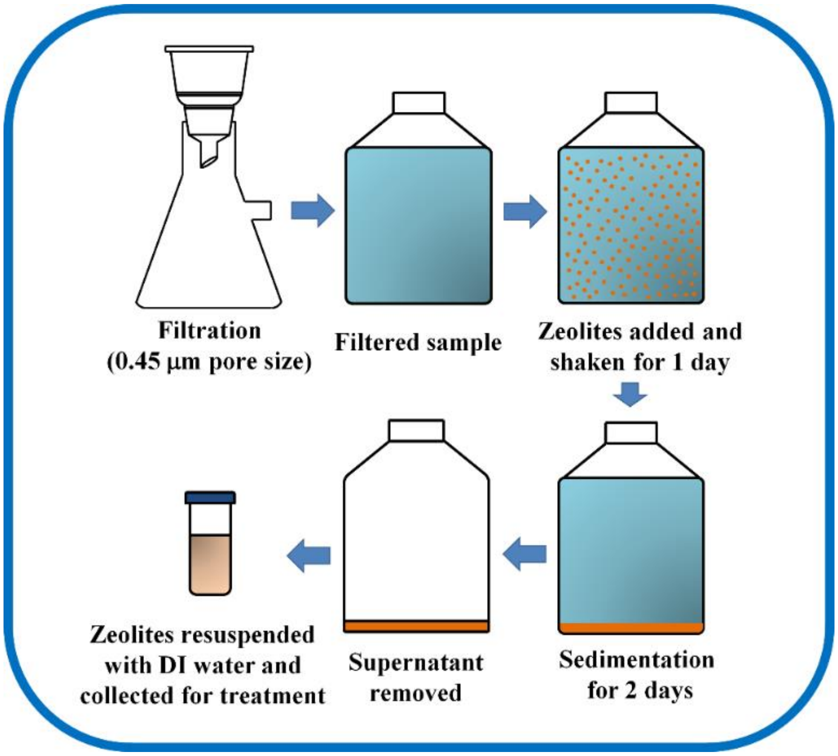

Figure S2. Scheme of groundwater samples treatment prior to reaction.

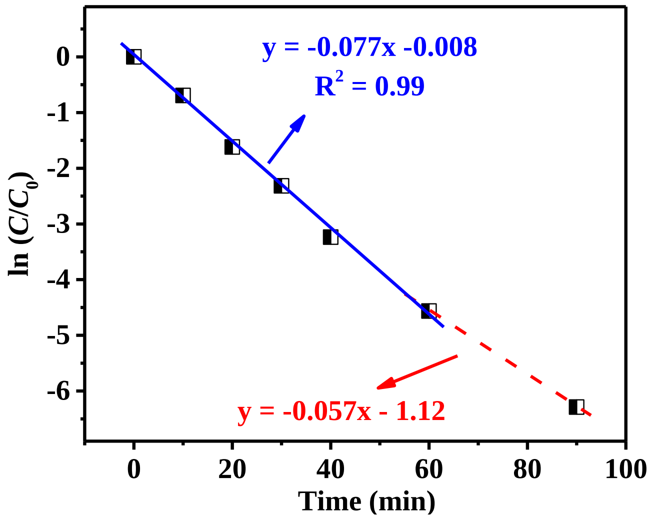

Figure S3. PFOA degradation first-order-kinetics plot, ln(C/C_0) versus reaction time. C_{zeolite} = 50 g L^{-1} and $C_{0,\mathrm{PFOA}}$ = 240 µM, $C_{0,\mathrm{persulfate}}$ = 100 mM, pH_0 = 3.0, and T = 70 °C. Pseudo-first-order kinetics can fit PFOA degradation well within the period of 0 - 60 min (blue curve) corresponding to ≤99% turnover. The rate coefficient decreases slightly at higher turnover.

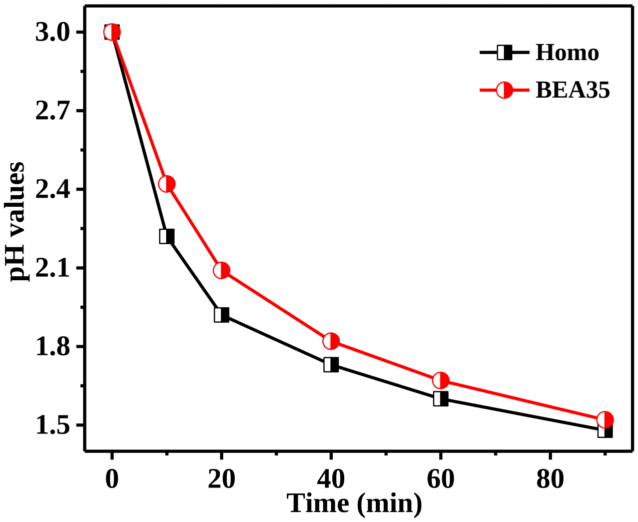

Figure S4. pH variation with and without BEA35 zeolite during persulfate driven PFOA degradation. $C_{0,\mathrm{PFOA}}$ = 240 µM, C_{PS} = 100 mM, pH_0 = 3.0, T = 70 °C, and C_{zeolite} = 50 g L^{-1} where applied. Lines are added as guides for the eye.

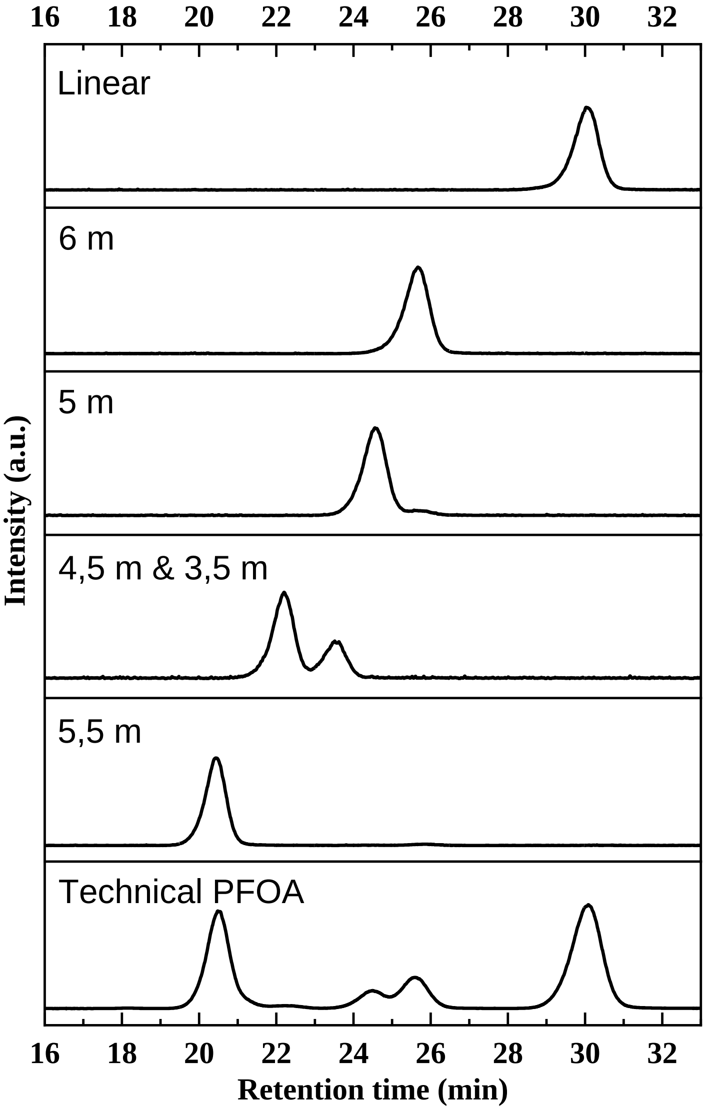

Figure S5. Assignment of PFOA isomer standards to LC/MS chromatograms from technical PFOA. The annotations in chromatograms represent the structure of each isomer according to the position of CF_3-substituents in the chain, e.g., 4,5 m-PFOA = CF_3-CF(CF_3)-CF(CF_3)-CF_2-CF_2-COOH.

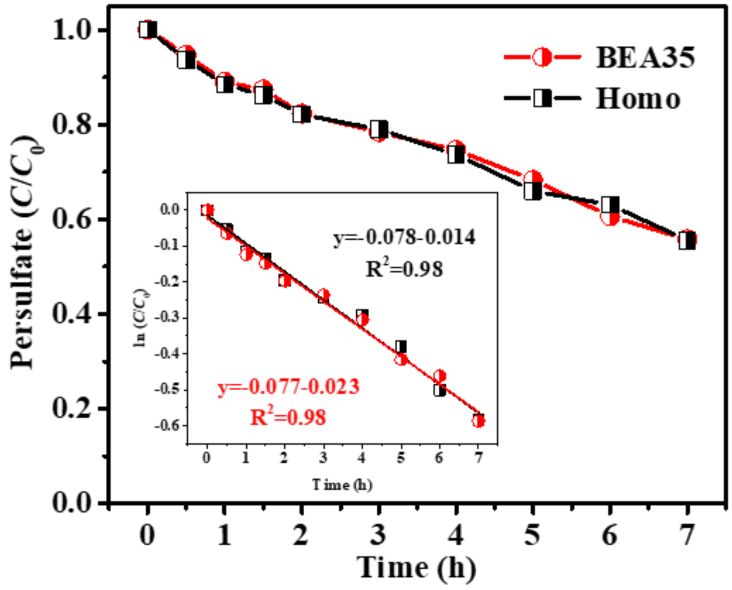

Figure S6. Persulfate thermal decomposition with and without BEA35 zeolite. $C_{0,\mathrm{PFOA}}$ = 240 µM, $C_{0,\mathrm{persulfate}}$ = 100 mM, pH_0 = 3.0, T = 70 °C, and C_{zeolite} = 50 g L^{-1} where applied. Lines are added as guides for the eye.

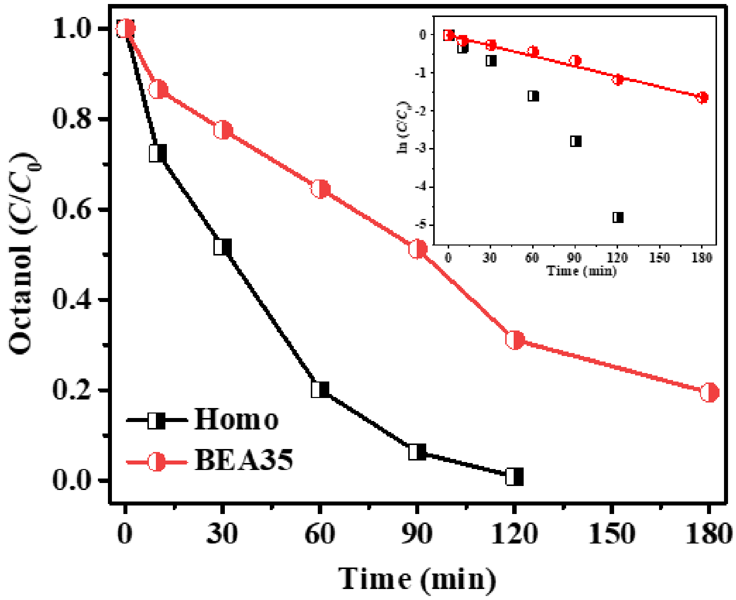

Figure S7. Comparison of persulfate driven n-octanol degradation with and without zeolite. $C_{0,\mathrm{octanol}}$ = 240 µM, $C_{0,\mathrm{persulfate}}$ = 100 mM, pH_0 = 3.0, T = 60 °C, and C_{zeolite} = 50 g L^{-1} where applied. Lines are added as guides for the eye.

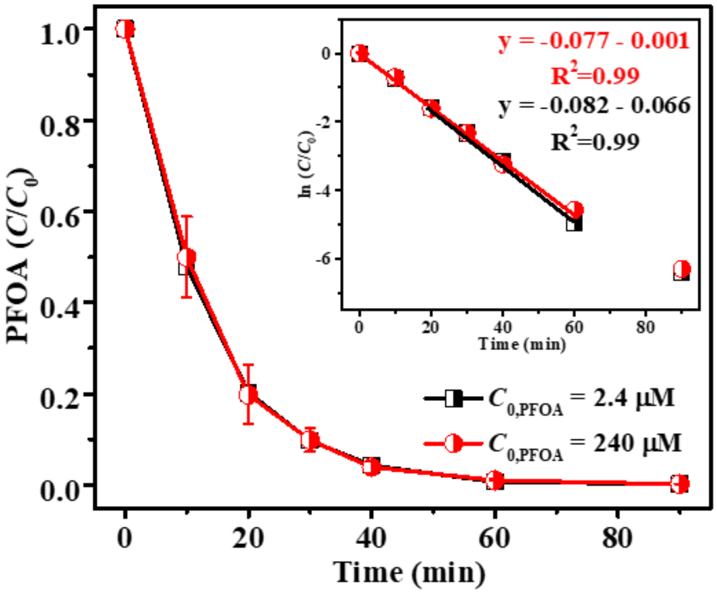

Figure S8. PFOA degradation by heat-activated persulfate in the presence of zeolite with different initial PFOA concentrations. $C_{0,\text{persulfate}}$ = 100 mM, T = 70 °C, and C_{zeolite} = 50 g L^{-1}. Error ranges represent the standard deviations of triplicate assays results. Lines are added as guides for the eye.

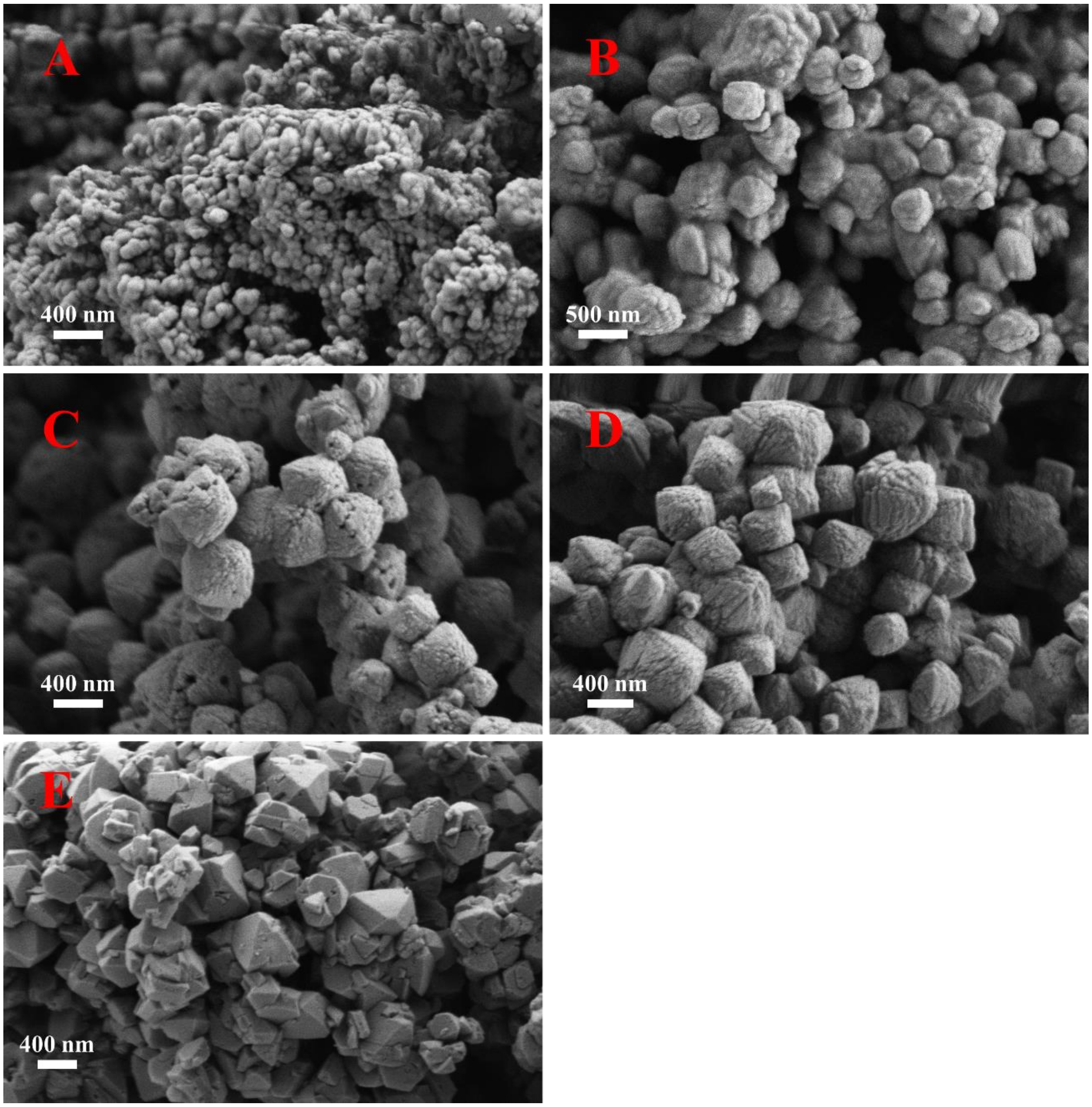

Figure S9. Scanning electron microscope (SEM) images of various types of zeolites. (A) BEA24, (B) BEA28, (C) BEA35, (D) BEA40, and (E) FAU15.

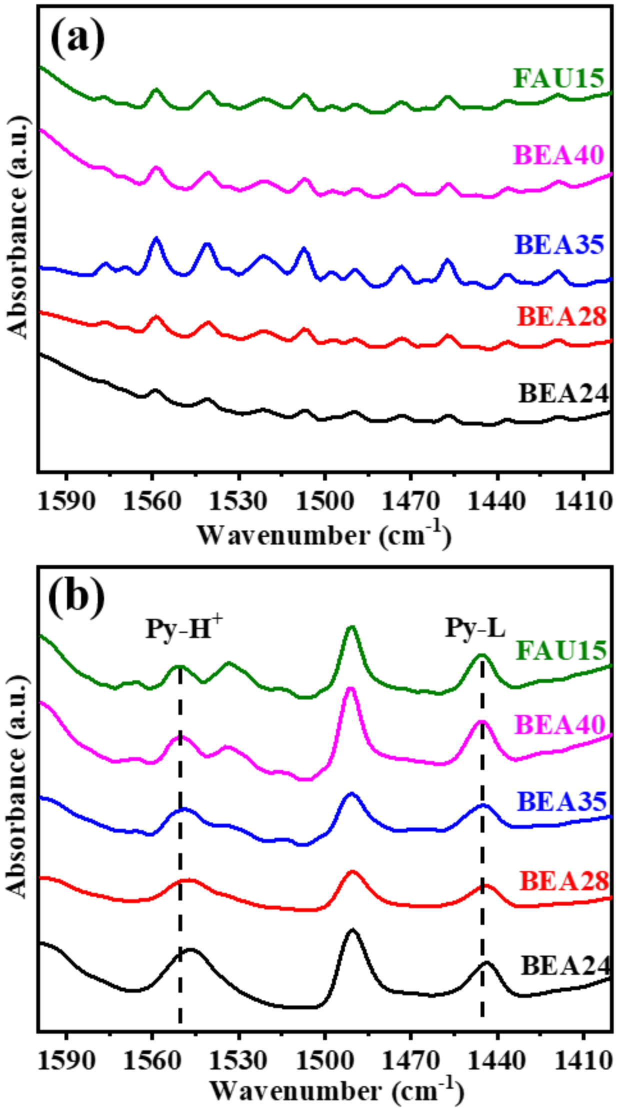

Figure S10. IR spectra of (a) dried zeolite pellets before pyridine loading; (b) Zeolite pellets after pyridine loading: using pyridine as probe molecule for the BAS and LAS sites determination. Py-H$^+$ is protonated pyridine on Brönsted acid sites and Py-L is pyridine coordinated to Lewis acid sites. The spectra recorded at ambient temperature.

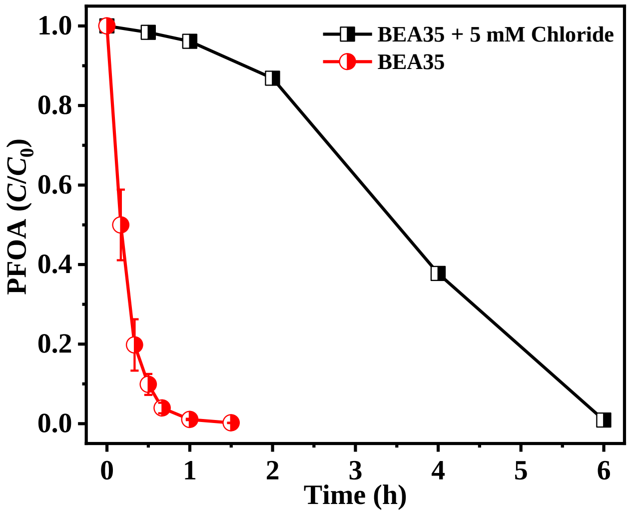

Figure S11. Effect of chloride (C_0 = 5mM) during PFOA degradation by heat-activated persulfate in the presence of zeolite. $C_{zeolite}$ = 50 g L^{-1} and $C_{0,PFOA}$ = 240 µM, $C_{0,persulfate}$ = 100 mM, pH_0 = 3.0, and T = 70 °C. Error ranges represent the standard deviations of triplicate assays results. Lines are added as guides for the eye.

Possible reaction pathways for PFOA degradation

Based on our experimental results and literature studies [4-6], the possible PFOA degradation pathway is proposed in Scheme S1. The generally accepted mechanism for the first step is that sulfate radicals attack the carboxylic head group of PFOA by a one-electron transfer to generate carboxylic radicals (eq. S2). Another possible pathway for the first step as already discussed in Section 3.5 is that a surface-assisted persulfate activation may occur in the zeolite system. This activation may promote the one-electron transfer from the PFOA carboxylate group to persulfate without attack of free sulfate radicals (eq. S3). Alternatively, the persulfate radical $S_2O_8^-$• may be involved in the primary electron transfer step. The produced carboxylic radicals from both possible pathways will decarboxylate and yield perfluorinated alkyl radicals (•C_7F_{15}) and CO_2 (eq. S4). The •C_7F_{15} radicals react preferentially with dissolved O_2 to produce the peroxyl radical ($C_7F_{15}OO$•) (eq. S5). Through several radical reactions and hydrolysis steps, a PFCA with one CF_2 unit less will be produced (eqs. S6 – S10). The produced shorter-chain PFCAs continue to be attacked by sulfate radicals or persulfate species and finally a complete mineralization of PFCAs can be achieved.

$$C_7F_{15}COO^- + SO_4^-\bullet \longrightarrow C_7F_{15}COO\bullet + SO_4^{2-} \tag{S2}$$

$$[C_7F_{15}COO^-]_{\text{adsorbed}} + [S_2O_8^{2-}]_{\text{surface activated}} \xrightarrow{e^-\ \text{transfer}} C_7F_{15}COO\bullet + SO_4^{2-} + SO_4^-\bullet \tag{S3}$$

$$C_7F_{15}COO\bullet \longrightarrow C_7F_{15}\bullet + CO_2 \tag{S4}$$

$$C_7F_{15}\bullet + O_2 \longrightarrow C_7F_{15}OO\bullet \tag{S5}$$

$$2C_7F_{15}OO\bullet \longrightarrow C_7F_{15}OO\text{-}OOC_7F_{15} \tag{S6}$$

$$C_7F_{15}OO\text{-}OOC_7F_{15} \longrightarrow 2C_7F_{15}O\bullet + O_2 \tag{S7}$$

$$C_7F_{15}O\bullet + HSO_4^- \longrightarrow C_7F_{15}OH + SO_4^-\bullet \tag{S8}$$

$$C_7F_{15}OH \longrightarrow C_7F_{13}OF + HF \tag{S9}$$

$$C_7F_{13}OF + H_2O \longrightarrow C_6F_{13}COOH + HF \tag{S10}$$

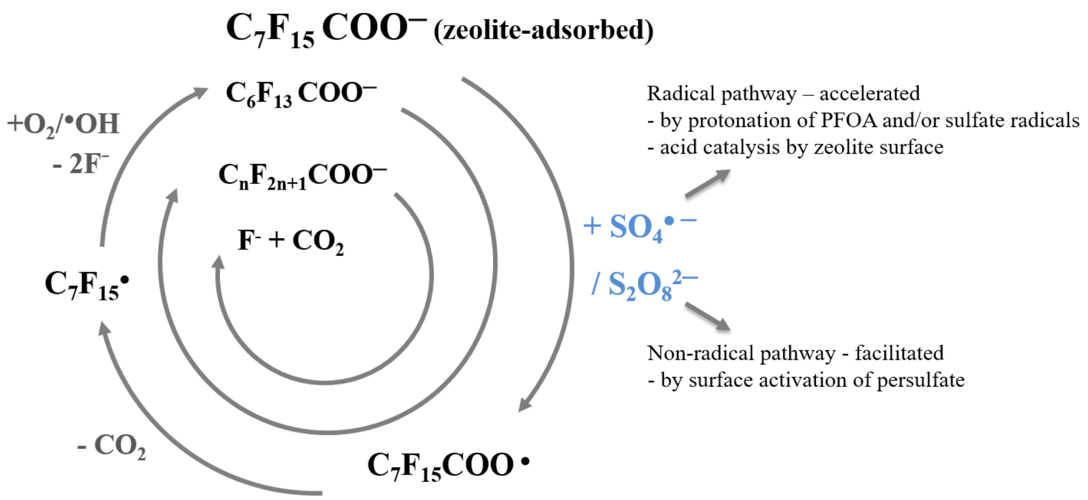

Scheme S1. Hypothetical PFOA degradation pathway by heat-activated persulfate in the presence of zeolite and possible mechanisms for catalytic effect of the zeolite.

Reference

[1] R. Gonzalez-Olmos, F.-D. Kopinke, K. Mackenzie, A. Georgi, Hydrophobic Fe-zeolites for removal of MTBE from water by combination of adsorption and oxidation, Environ. Sci. Technol. 47 (2013) 2353-2360. https://doi.org/10.1021/es303885y

[2] X. Lu, Y. Wang, L. Estel, N. Kumar, H. Grénman, S. Leveneur, Evolution of specific heat capacity with temperature for typical supports used for heterogeneous catalysts, Processes 8 (2020) 911. https://www.mdpi.com/2227-9717/8/8/911

[3] V. Zholobenko, C. Freitas, M. Jendrlin, P. Bazin, A. Travert, F. Thibault-Starzyk, Probing the acid sites of zeolites with pyridine: Quantitative AGIR measurements of the molar absorption coefficients, J. Catal. 385 (2020) 52-60. https://doi.org/10.1016/j.jcat.2020.03.003

[4] S. Kutsuna, H. Hori, Rate constants for aqueous-phase reactions of SO4− with C2F5C(O)O− and C3F7C(O)O− at 298 K, Int. J. Chem. Kinet. 39 (2007) 276-288. https://doi.org/10.1002/kin.20239

[5] H.V. Lutze, J. Brekenfeld, S. Naumov, C. von Sonntag, T.C. Schmidt, Degradation of perfluorinated compounds by sulfate radicals – New mechanistic aspects and economical considerations, Water Res. 129 (2018) 509-519. https://doi.org/10.1016/j.watres.2017.10.067

[6] S. Sühnholz, A. Gawel, F.-D. Kopinke, K. Mackenzie, Evidence of heterogeneous degradation of PFOA by activated persulfate – FeS as adsorber and activator, Chem. Eng. J. 423 (2021) 130102. https://doi.org/10.1016/j.cej.2021.130102

4 Summary

In the present thesis, we use zeolite as both adsorbent and catalyst, which opens up the design of new technological approaches for PFAAs treatment. A feasible process scheme consists of the following steps: in the first step, PFAAs are removed from water by adsorption to a zeolite fixed bed or suspended zeolite that can then be separated by microfiltration. In the second step, the loaded zeolite particles can be regenerated *in situ* by various techniques: i) under UV-A irradiation (300 nm $< \lambda <$ 400 nm), i.e., a solar light fraction, for PFOA degradation (Fe-zeolite); ii) under UV-C irradiation ($\lambda = 254$ nm) for PFOS degradation (Fe-zeolite); iii) heat-activated persulfate for PFOA degradation. Zeolites of BEA framework type were successfully applied in all three processes. Overall, a combination of PFAAs adsorptive enrichment and degradation by applying related types of zeolites can be realized. These findings of the thesis provide efficient strategies for treatment of water containing highly recalcitrant trace amounts of PFAAs, which will contribute to the field of PFAAs removal/degradation. The main objectives of the thesis are: (i) developing adsorptive PFAAs removal technologies combined with onsite adsorbent regeneration; (ii) inspiring PFAAs removal approaches based on zeolite and other adsorptive catalysts; (iii) providing suggestions for adsorptive remediation technologies for water contaminated by other micropollutants.

In the first manuscript “Degradation of perfluorooctanoic acid adsorbed on Fe-zeolites with molecular oxygen as oxidant under UV-A irradiation” published in *Applied Catalysis B: Environmental*, a novel, efficient degradation approach of PFOA under UV-A irradiation after adsorption on Fe-zeolites with molecular oxygen being the terminal oxidant was established. Experimental results show:

(i) The Fe-zeolite-based photochemical system using suspended zeolite particles of about 1 µm diameter exhibit a better PFOA degradation performance under irradiation (a wider range from UV-C to UV-A) compared to the homogeneous system based on dissolved ferric ions.

(ii) Slightly acidic conditions are optimal in terms of PFOA adsorption and complexation.

(iii) Molecular oxygen works as the terminal oxidant and is involved in re-oxidization of ferrous ions to ferric ions, producing reactive species and facilitating further mineralization of PFOA.

(iv) Except for sulfate, the presence of other commonly present inorganic anions has a negligible impact on PFOA degradation.

(v) The isolated Fe^{3+} ions in octahedral coordination are involved in the carboxylate-to-metal charge transfer, which plays the major role in the process of PFOA degradation.

In the second manuscript "Photodegradation of perfluorooctanesulfonic acid on Fe-zeolites in water" published in *Environmental Science & Technology*, we demonstrate for the first time a successful photochemical PFOS degradation under UV-C irradiation after adsorption on Fe-zeolites, again with molecular oxygen as the terminal oxidant. The Fe-zeolite, as a separable adsorbent, is able to catalyze not only PFOA but also PFOS degradation in the adsorbed state which is even more challenging. Thus, our findings are relevant for the development of adsorptive PFAAs removal technologies combined with on-site adsorbent regeneration. Based on our experimental results, we can draw the following conclusions:

(i) The Fe-zeolite-based photochemical system shows a better PFOS degradation and defluorination performance under UV-C irradiation compared to a homogeneous system based on ferric ions. A complete mineralization of PFOS can be achieved by combination with UV activation of sodium persulfate.

(ii) The Fe-zeolite-based photochemical system favors acidic conditions in terms of better adsorption and higher fraction of complexed PFOS. However, different from dissolved ferric iron the zeolite-based catalyst is active also at moderately acidic conditions, e.g., at pH = 5.5.

(iii) The photochemical degradation of PFOS is not affected when Fe-zeolites concentration increased to a certain extent, which makes the Fe-BEA35 system qualified for modifiable zeolite concentrations in application.

(iv) The Fe-zeolite-based photochemical system is applicable to real groundwater containing PFOS at a trace level only, showing adequate PFOS degradation performance.

(v) Sulfonate-to-metal electron transfer plays a key role in PFOS degradation under UV irradiation. The excitation and decomposition of PFOS-Fe^{3+} complexes may be the rate-limiting step in the PFOS degradation process.

In the third manuscript "Enhanced degradation of perfluorooctanoic acid by heat-activated persulfate in the presence of zeolites" submitted to *Chemical Engineering Journal*, we present a novel PFOA treatment technology, where PFOA can be firstly removed from water by zeolite adsorption, and then be degraded by heat-activated persulfate in the presence of zeolite. Overall, the major findings are summarized as follows:

(i) The PFOA degradation by heat-activated persulfate is effective in the presence of zeolite, and a significant PFOA degradation promotion was observed comparing with the sulfate radical-based homogeneous system.

(ii) The PFOA degradation by heat-activated persulfate in the presence of zeolite showed an adequate performance at initially neutral pH.

(iii) Zeolite internal surface promoted PFOA degradation by heat-activated persulfate. It might be contributed by reactive sites inside the zeolites, whereby the nature of these sites is still unknown.

(iv) The stability and reusability of the zeolite were evaluated. After six adsorption/degradation cycles, the BEA35 showed no significant decline in PFOA degradation performance.

(v) Real groundwater samples containing PFOA in the ng L^{-1} range were tested to be still effectively degradable with heat-activated persulfate in the presence of zeolite. The cost for PFOA-contaminated water treatment was estimated by assuming a realistic scenario, i.e., zeolite-based fixed-bed adsorber/reactor.

Declaration of authorship contribution

In the manuscript 3.1 “Degradation of perfluorooctanoic acid adsorbed on Fe-zeolites with molecular oxygen as oxidant under UV-A irradiation” published in *Applied Catalysis B: Environmental* 278 (2020): 119283, I served as the first author. I carried out the experiments, analyzed and evaluated the data, and prepared the original draft. Dr. Rafael Gonzalez-Olmos was involved in manuscript review and editing. Dr. Anett Georgi and Prof. Dr. Frank-Dieter Kopinke supervised this work and were involved in manuscript review and editing.

In the manuscript 3.2 “Photodegradation of perfluorooctanesulfonic acid on Fe-zeolites in water” published in *Environmental Science & Technology* 55 (2021) 614-622, I served as the first author. I carried out the experiments, analyzed and evaluated the data, prepared the original draft. Dr. Anett Georgi and Prof. Dr. Frank-Dieter Kopinke supervised this work and were involved in manuscript review and editing.

In the manuscript 3.3 “Enhanced degradation of perfluorooctanoic acid by heat-activated persulfate in the presence of zeolite” submitted to *Chemical Engineering Journal*, I served as the first author. I carried out the experiments, analyzed and evaluated the data, prepared the original draft. Dr. Tom Scherzer and Dr. Jan Griebel was involved in sample analysis and manuscript review and editing. Dr. Anett Georgi and Prof. Dr. Frank-Dieter Kopinke supervised this work and were involved in manuscript review and editing.

Acknowledgements

Firstly, I would like to thank the China Scholarship Council (CSC) for financial support during my PhD.

I would like to express my sincere gratitude to my supervisor Prof. Dr. Frank-Dieter Kopinke for providing me the opportunity to work in his group. I was always impressed by his enthusiasm on science as well as his scientific expertise, which was very helpful whenever I needed support. I would like to thank my supervisor Dr. Anett Georgi for her great guidance and support. She was very friendly and easy to approach, and she always provided me manageable ideas and solutions with her scientific experience and insights. I also want to thank Dr. Katrin Mackenzie who was all the time warmhearted and helpful.

My PhD career in Germany was not very smooth at the beginning. I also need to thank myself that I made that decision and decided to continue my PhD here in UFZ, Leipzig. I can say it was a right decision for me, as I am working now in the field I like, particularly with nice supervisors and good team.

Many thanks to my great colleagues Lisa-Marie Frenzel, Kerstin Lehmann, Sarah Sühnholz, Ali Shee, Alina Gawel, Maria Balda, Evelyn Becker, Jonas Jörns, Jieying Zhou, Navid Saeidi, Silke Woszidlo, Dr. Frank Holzer, Dr. Lars Krause, Dr. Gang Yan. Additionally, I need to thank Jieying Zhou for useful discussion and proof reading of my manuscripts, and for German assistance whenever I needed help.

Lastly, I want to thank my parents, my sister and friends for their unconditional support and encouragement in all aspects of my life.

Curriculum vitae

Name: Lin Qian
Date of Birth: 21st December 1990
Place of Birth: Shengzhou, China
Nationality: China
Email: lin.qian@ufz.de; qianlinw@gmail.com

Education

01/2018 – present	**Doctoral candidate in Chemistry**
	Faculty of Chemistry and Mineralogy, University of Leipzig.
	“Degradation of Perfluoroalkyl Acids using Zeolites”
	conducted at Department of Environmental Engineering,
	Helmholtz Centre for Environmental Research - UFZ, Leipzig
09/2013 – 06/2016	**Master of Science - Physical Chemistry**
	Tongji University, Shanghai, China
09/2009 – 06/2013	**Bachelor of Engineer - Chemical Engineering**
	Zhejiang University of Technology, Hangzhou, China

Scientific activities

Publications

Qian, L., Georgi, A., Gonzalez-Olmos, R. and Kopinke, F.D. Degradation of perfluorooctanoic acid adsorbed on Fe-zeolites with molecular oxygen as oxidant under UV-A irradiation. *Applied Catalysis B: Environmental* 278 (2020): 119283.

Qian, L., Kopinke, F.-D., Georgi, A. "Photodegradation of perfluorooctanesulfonic acid on Fe-zeolites in water." *Environmental science & technology*, 55.1 (2020), 614 – 622.

Qian, L., Kopinke, F. D., Scherzer, T, Griebel, J, and Georgi, A. Enhanced degradation of perfluorooctanoic acid by heat-activated persulfate in the presence of zeolite. *Submitted to Chemical Engineering Journal* 429 (2022):132500.

Conference contributions

- Oral presentation at first joint IP-day of the Integrated Projects "Controlling Chemicals' Fate" and "Sustainable Biotechnology & Bioeconomy", Leipzig, Germany, 25 October 2018.
- Oral presentation at the 5th International Conference on Photocatalytic and Advanced Oxidation Technologies for the Treatment of Water, Air, Soil and Surfaces, Antwerp, Belgium, 23-25 April 2019.
- Poster presentation at Symposium Strategien zur Boden- und Grundwassersanierung, Frankfurt, Germany, 11 October 2020.
- Poster presentation at Industrial Water 2020 (virtually), Germany, 17-20 October 2020.
- Oral presentation at International Conference on Characterization and Remediation of Per and Polyfluoroalkyl Substances and Other Emerging Contaminants (virtually), Germany, 10-12 May 2021.

PHD DISSERTATION 12|2021

ISSN 1860-0387

Lin Qian | Degradation of Perfluoroalkyl Acids using Zeolite

Helmholtz Centre for
Environmental Research – UFZ
Permoserstraße 15
04318 Leipzig I Germany
www.ufz.de